Electronic Thesis and Dissertation Repository

3-14-2014 12:00 AM

Isotopic Fingerprinting of Shallow and Deep Groundwaters in Southwestern Ontario and its Applications to Abandoned Well Remediation

Mitchell E. Skuce
The University of Western Ontario

Supervisor
Fred Longstaffe
The University of Western Ontario

Graduate Program in Geology
A thesis submitted in partial fulfillment of the requirements for the degree in Master of Science
© Mitchell E. Skuce 2014

Follow this and additional works at: https://ir.lib.uwo.ca/etd

Part of the Geochemistry Commons, and the Hydrology Commons

Recommended Citation
Skuce, Mitchell E., "Isotopic Fingerprinting of Shallow and Deep Groundwaters in Southwestern Ontario and its Applications to Abandoned Well Remediation" (2014). *Electronic Thesis and Dissertation Repository*. 1926.
https://ir.lib.uwo.ca/etd/1926

Isotopic Fingerprinting of Shallow and Deep Groundwaters in Southwestern Ontario and its Applications to Abandoned Well Remediation

(Thesis format: Monograph)

by

Mitchell E. Skuce

Department of Earth Sciences
Graduate Program in Geology

A thesis submitted in partial fulfillment
of the requirements for the degree of
Master of Science

The School of Graduate and Postdoctoral Studies
The University of Western Ontario
London, Ontario, Canada

Abstract

Abandoned hydrocarbon wells in southwestern Ontario can act as conduits for sulphur water, brines, and hydrocarbons from deep Paleozoic bedrock aquifers. Such leakage may pose a threat to shallow groundwater and the environment. Cost-effective plugging of these wells requires knowledge of the sources of the leaking fluids. This study characterizes the isotopic compositions ($\delta^{18}O_{H2O}$, $\delta^{2}H_{H2O}$, $\delta^{34}S_{SO4}$, $\delta^{18}O_{SO4}$, $\delta^{13}C_{DIC}$, $^{87}Sr/^{86}Sr$) of groundwaters in the region, which are distinct in different bedrock formations. A Bayesian mixing model was applied to these data to develop a tool for identifying the source(s) of leaking fluids. The geochemical data also improve our understanding of groundwater origin and evolution. Shallow (~<350m) aquifers are recharged by recent meteoric water. At greater depths, brine aquifers contain residual evaporated Paleozoic seawater, modified by rock-water interaction and mixing with meteoric water. These brines are likely related to long-distance fluid migration from deeper portions of the adjacent Michigan and Appalachian basins.

Keywords

Acknowledgements

I wish to thank a number of individuals whose guidance, support and encouragement over the past few years has made this thesis possible. First and foremost, I would like to express my great appreciation for my supervisor Dr. Fred Longstaffe, who has been enormously supportive throughout this project. Fred, you have been a great help and our conversations were always interesting and invaluable for guiding this thesis. Through your expert knowledge and guidance, you have immensely helped to improve my understanding and appreciation of stable isotopes and research in general. You were always available if I had a question, and your advice and patience were most appreciated. I am deeply honoured to have had the opportunity to work with you on such an interesting project and wish you all the best in the future.

In addition, my project colleague Joanne Potter and the project leader at the Ontario Ministry of Natural Resources, Terry Carter, have also provided important advice and expertise to this project. Terry, our discussions of the geology and hydrology of southwestern Ontario provided an essential foundational understanding for this work, and your enthusiasm and passion for geology has helped nurture my own. I would also like to thank Terry as well as Lee Fortner, from the Ontario Oil, Gas and Salt Resource library, for their hard work in arranging sampling opportunities.

I am also indebted and grateful to the tremendously dedicated and hard-working staff at the Laboratory for Stable Isotope Science (LSIS), particularly Li Huang whose expertise and guidance was indispensable during the numerous analytical runs required during this project. Similarly, I would like to thank Paul Middlestead at the University of Ottawa's G. G. Hatch Stable Isotope Laboratory for his assistance in the analysis of sulphur isotopes, and also the staff at SGS Laboratories and Isotope Tracer Technologies for their help in analyzing the ion concentrations and strontium isotopes, respectively.

I would also like to extend my gratitude to all the well operators, quarry personnel, drillers, MNR staff, and others who have helped, directly or indirectly, with sample

Table of Contents

List of Tables

List of Figures

List of Appendices

Chapter 1

1   Introduction

1.1   Problem Overview

Southwestern Ontario has a long history of hydrocarbon production. The first commercial oil well in North America was dug in 1858 in Oil Springs, Lambton County. Although production has been steadily declining for the past several decades, with peak oil in 1985 and peak gas in 1995 (OGSR, 2009), there are currently about 2,400 commercial oil and gas wells still operating in the region. Records are available for about 27,000 petroleum wells in southwestern Ontario but several thousand additional wells are believed to have been drilled before reporting was required (T. Carter, personal communication, 2013). Most of the wells in Ontario are concentrated in the southwest and southeast portions of the southwestern Ontario peninsula, around Essex, Kent, Lambton, Elgin, Haldimand and Norfolk Counties (Figure 1.1). Many of these wells were completed before the advent of well design and decommissioning regulations, which were first enacted in the early 20th century (OEB, 2014) and initially had no regulatory oversight. The issue of poor well construction is compounded by the presence of a regional zone of sulphur water at shallow to intermediate depths, such that, today, the metal casings of many of these wells are highly corroded or absent altogether. The majority also have no cement behind the casing, and many do not have intact wellheads. Thousands of these older wells now lie abandoned, mostly in farmers' fields, in poor condition and not properly plugged (OMNR, 2013). The wells provide potential conduits for surface contaminants, such as fertilizers, herbicides, pesticides and manure, to enter shallow potable groundwater aquifers, as well as upward flow of deep formation fluids into shallow aquifers and to the surface. Many of the deep bedrock formations contain oil, natural gas, brines, and/or sulphur water, the latter of which contains high levels of dissolved hydrogen sulphide (H_2S), and in some places certain formations are known to exhibit artesian flow to the surface. Venting natural gas can cause explosive build-ups in houses and other structures. H_2S is harmful to aquatic ecosystems, and is also toxic to humans, with concentrations

above 750 ppm causing immediate unconsciousness and can lead to cardiac arrest (Henderson, 2011).

The Ontario Ministry of Natural Resources (OMNR) initiated the Abandoned Works Program (AWP) in 2006 with the objective of plugging these abandoned oil and gas wells in order to protect public health and drinking water resources. Candidate wells for plugging are ranked according to their risk to public safety and potential for environmental damage. As many of the wells are more than 50 years old, Ministry records are often incomplete or non-existent (OMNR, 2013). Often there is also uncertainty as to whether a well was a water well or a hydrocarbon well. Accordingly, there is significant uncertainty as to how deep the wells were originally drilled, and from which geological formation(s) the leaking fluids originate. This makes the plugging process very challenging, and results in inflated quotes from well plugging contractors who cover the uncertainty by quoting high. Many wells also have debris obstructing the borehole, making it prohibitively expensive to attempt to reach the bottom of such wells.
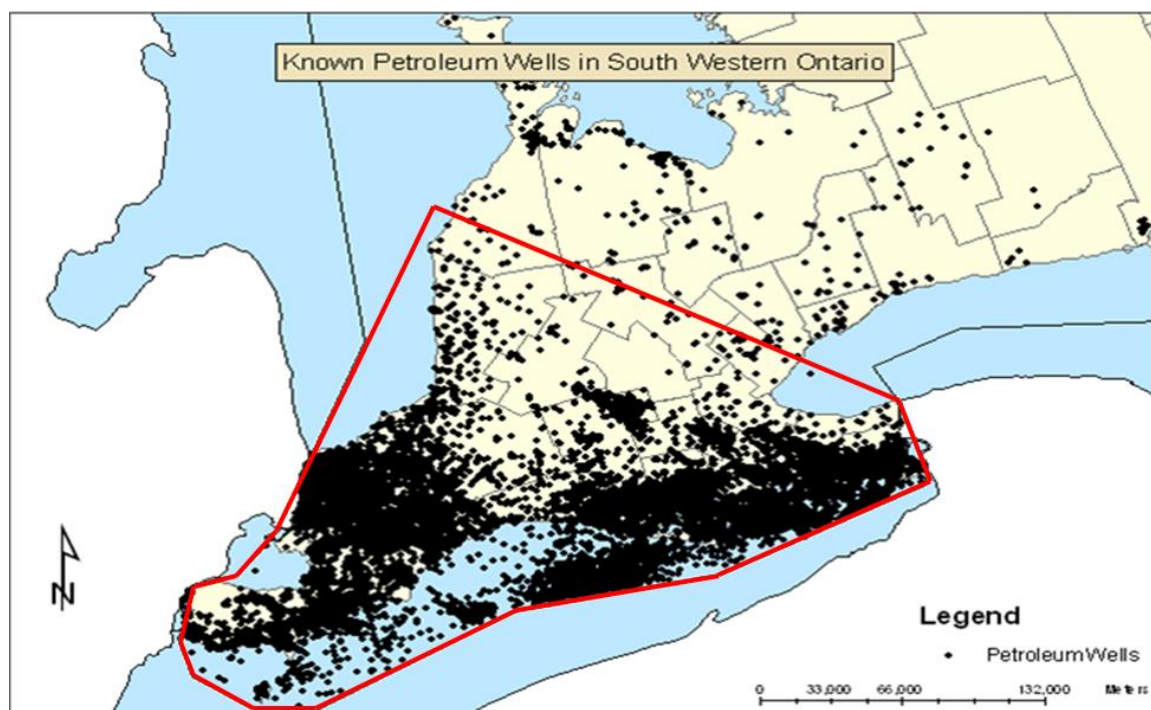
Figure 1.0: Map of southwestern Ontario with locations of known petroleum wells (modified from Carter, 2012). The approximate boundaries of the study area for this project are outlined in red.

1.2   Research Objectives

This paper represents half of a greater, two-part project to characterize the geochemical compositions of groundwaters and natural gases from the various geological formations in the subsurface of southwestern Ontario. This study presents and interprets the results for the groundwaters, while a second study focuses on the gases. The primary goal of the project is to use the improved geochemical characterization to devise a tool or method that will facilitate the process of plugging of abandoned wells by identifying the source(s) of leaking fluids. In cases where the well bottom is uncertain, or where it is impossible or prohibitively expensive to reach the bottom due to obstructions or other difficulties, the geochemistry of the leaking fluids can be used to identify leaking horizons, providing a target depth for the plugging crews. Discrimination between formations is sought through the identification of unique 'fingerprints' for each formation based on the isotope geochemistry of their groundwaters, while the same is in progress in the companion study for natural gases. Results from both groundwaters and gases are to be integrated into the final geochemical tool.

The Petroleum Operations Section of the Ministry of Natural Resources is nearing completion of a project to map confined aquifers in the subsurface Paleozoic bedrock formations of southern Ontario. The geologic/hydrogeologic model resulting from that study (Carter, 2012; Carter and Fortner, 2012; Sharpe et al., 2014) is used in this project to identify target aquifers and geologic intervals for sampling of water and gases.

Previous authors (McNutt et al., 1987; Dollar et al., 1991) have reported significant isotopic differences between waters from various stratigraphic units in Ontario. The present research builds on these findings, adding results for new samples and providing data from further geochemical parameters in order to better define each formation's fingerprint. It is hypothesized that the geochemical differences between formations will be sufficiently significant to allow their use for determining the origins of unknown fluid samples. To this end, over 125 groundwater samples were collected from a range of formations and locations throughout southwestern Ontario. These samples have been

analysed for a wide suite of geochemical parameters – the oxygen and hydrogen isotopes of water ($\delta^{18}O$ and δ^2H), the oxygen and sulphur isotopes of dissolve sulphate ions ($\delta^{18}O_{SO4}$ and $\delta^{34}S_{SO4}$), the carbon isotopes of dissolved inorganic carbon ($\delta^{13}C_{DIC}$), strontium isotopic ratios ($^{87}Sr/^{86}Sr$), and major and minor ion chemistry.

A Bayesian mixing model program known as SIAR (Stable Isotope Analysis in R; Parnell et al., 2010) has been applied to this large, multidimensional dataset in order to assess the possibility that a given unknown leaking fluid sample represents a mixture of waters originating from multiple source formations, and, if so, estimate the probable amounts contributed by each source. Hence, the leaky formations can be identified and their relative importance assessed. This information, combined with existing knowledge of the geology and formation depths at a given location, will give Abandoned Works crews a much improved target depth for their plugging efforts. The current plugging strategy, which may overestimate the plugging depth required, can be very expensive, on the order of hundreds of thousands of dollars per well; a more targeted approach is expected to considerably reduce the cost and time required to plug these wells.

In addition to its main application to the AWP, a secondary goal of this project is to use this new dataset to improve our current understanding regarding the nature of the bedrock groundwater regimes in southwestern Ontario, and sedimentary basins in general, helping to better resolve questions about the origins and evolution of fluids and their solutes, and the nature of present or historical fluid movement. Brines are present in the deeper formations, and the current understanding of brine formation is still a matter of some debate. Several theories have been proposed to explain the isotopic and geochemical characteristics of the brines in the study region, including seawater evaporation (Dollar et al., 1991) and diagenetic modification of meteoric waters (Clayton et al., 1966). With the additional samples and geochemical parameters provided by this project, a more detailed analysis of these groundwaters is made possible.

1.3   Thesis Structure

Chapter 2 provides a summary of the important background information relevant to this study, including an overview of the regional geology, descriptions of the geological formations, the hydrogeological framework, a discussion of the nature of saline waters and associated isotopic considerations, and an overview of previous research concerning the geochemistry of groundwaters in southwestern Ontario and the surrounding area. Chapter 3 provides a description of the methodology used in this study, including sample collection, processing, analysis, and an introduction to mixing models and SIAR. Chapter 4 presents the results of all the geochemical analyses. Chapter 5 discusses the formulation of the SIAR geochemical tool, and also interprets the data in terms of groundwater origins and evolution. Chapter 6 summarizes the major findings of the project, and provides suggestions for future work.

Chapter 2

2　Background Information

The primary aim of this chapter aims to provide an overview of the geological and hydrogeological context in southwestern Ontario for this project. It also summarizes the current understanding of groundwater geochemistry and evolution in the area, and briefly discusses isotopic considerations relating to saline waters.

2.1　Geology

This section introduces essential information regarding the geology of the study area, which roughly encompasses the peninsula of southwestern Ontario, from Essex County to the south, through to Bruce County in the north and the Niagara Peninsula region to the east (see area outlined in Figure 1.1).

2.1.1　　Regional Geological Overview

The bedrock of southwestern Ontario consists of an extensive sequence of Paleozoic clastic and carbonate sedimentary rocks, deposited between the upper Cambrian through early Mississippian in the warm, shallow seas that covered much of eastern North America at the time. This sequence reaches a maximum thickness of nearly 1,400 m, and consists predominantly of limestones, dolostones, shales, sandstones, anhydrite and halite (Armstrong and Carter, 2010).

This sedimentary sequence unconformably overlies the complexly deformed crystalline metamorphic rocks of the Grenville Province, part of the Canadian Shield. These rocks were formed during the Grenville orogeny about 1.1 billion years ago, and represent the roots of a great mountain range that was eroded to an undulating peneplain by Cambrian time. A marine transgression then occurred and the Paleozoic sediments were deposited overtop the Precambrian basement (Johnson et al, 1992; Frizzell et al., 2011). Another major unconformity, representing at least 250 Ma of exposure and erosion (Johnson et al,

1992), is marked by the upper boundary of the sequence, where the sedimentary bedrock is overlain by a thick layer of recent glacial sediments, deposited during the Wisconsinan glaciation, which ended approximately 10,000 years ago (Gillespie et al, 2008).

The southwestern Ontario peninsula lies at the boundary between two major Paleozoic sedimentary basins, the Michigan Basin to the west and the Appalachian Basin to the east. The peninsula straddles a broad northeast-trending topographic high in the underlying Precambrian basement, known as the Algonquin Arch. At the southern tip of the peninsula, the southwest-plunging Algonquin Arch meets its American extension, the northeast-plunging Findlay Arch, at a structural low known as the Chatham Sag. These two arches are the structural features that separate the Michigan and Appalachian basins (Armstrong and Carter, 2010) (Figure 2.1).

The Michigan Basin is a semi-circular intracratonic basin, one of several in North America and of uncertain origin (Howell and van der Pluijm, 1999). It is carbonate-dominated, and also contains considerable thicknesses of evaporite units (Armstrong and Carter, 2010). The Michigan basin covers an area of ~316,000 km^2 over northern Michigan (Friedman and Kopaska-Merkel, 1991), and has a maximum sedimentary sequence thickness of ~4,800 m in its center (Frizzell et al., 2011). In contrast, the Appalachian Basin is an elongate foreland basin which developed as a result of tectonic loading during orogenic events on the east coast of North America during the Paleozoic. While it also contains carbonate units, it is dominated by siliciclastic sedimentary rocks (Armstrong and Carter, 2010). The Appalachian Basin strata reach a maximum thickness of approximately 7,000 m towards its eastern margin (Frizzell et al., 2011).

The sedimentary formations in southwestern Ontario are generally correlative to equivalent formations in the adjacent basins, although there are some differences in nomenclature. Unit thicknesses increase away from the Algonquin Arch, towards the basin depocenters. The lithological characteristics of the rocks in southwestern Ontario vary geographically with respect to their position relative to the adjoining basins. Units extending into Ontario on the Appalachian Basin side tend to be more siliciclastic, while the strata become increasingly carbonate- and evaporite-dominated with proximity to the Michigan basin (Armstrong and Carter, 2010; Frizzell et al., 2011).

Sedimentation in southwestern Ontario and the adjoining basins continued until at least the Mississippian, but was interspersed with periods of tectonic uplift and erosion, marked by regional unconformities. Tectonic uplift and subsidence of the Algonquin Arch, in response to epeirogenic movements and horizontal tectonic forces, acted as the dominant structural control on these depositional patterns (Leighton, 1996, Howell and van der Pluijm, 1999; Frizzell et al., 2011). Karstification of carbonate and evaporite rocks during these periods of exposure and erosion greatly enhanced porosity and permeability. These paleokarst horizons are the principal geologic control on the location of aquifers in the Paleozoic bedrock formations (Carter, 2012; Carter and Fortner, 2012; Sharpe et al., 2014).

The sedimentary units in southwestern Ontario are almost flat-lying, dipping at a very slight angle regionally, controlled mainly by the topography of the Algonquin Arch. Along the crest of the arch, the strata dip at 3 to 6 m/km southwestwards towards the Chatham Sag; on its flanks, they dip westward towards the Michigan Basin depocenter and southwards into the Appalachian Basin, at 3.5 to 12 m/km. Along the flanks, regional dip tends to increase with depth and distance away from the crest of the arch (Armstrong and Carter, 2010). The regional bedrock dip controls the distribution of the formations at the surface, with the effect that progressively older units subcrop towards the northeast, in belts that run roughly perpendicular to the crest of the arch (Figure 2.1).

While relatively undisturbed, the Paleozoic sedimentary sequence is cut by several normal and strike-slip faults, the most prominent being the Electric Fault (~100 m vertical displacement) and the Dawn Fault (~50 m vertical displacement) (Armstrong and Carter, 2010). These faults are thought to have been formed by propagation of older faults in the underlying Precambrian basement (Boyce and Morris, 2002). Many of these faults have been important in the development of hydrocarbon reservoirs in the region. They were also important conduits for fluid movement in the geologic past, creating hydrothermal dolomite reservoirs in Ordovician carbonate units (Lazorek and Carter, 2008), influencing dolomitization of Silurian carbonates (Coniglio et al., 2003; Carter, 1991), as well as locally enhancing the dissolution of Silurian evaporites (Armstrong and Carter, 2010).

Several of the sedimentary units of southwestern Ontario host significant economic oil and natural gas reservoirs (Lazorek and Carter, 2008). The majority of the hydrocarbons discovered to date lie towards the southwestern tip of the peninsula, in Essex, Elgin, Lambton and Kent counties, and along the northeastern shore of Lake Erie, near Norfolk and Haldimand counties. There are a number of different styles of hydrocarbon trap found in the region, each associated with different stratigraphic units. Oil is found in structural traps in the Devonian carbonates, in anticlines formed by collapse from differential dissolution of underlying evaporite units. Upper Silurian carbonates host oil and gas in reefal traps, most notably the so-called Guelph pinnacle reefs. Natural gas is found in Lower Silurian sandstone lenses surrounded by shale. Ordovician carbonates host oil and gas in fault-controlled hydrothermal dolomite reservoirs, surrounded by impermeable limestones. Finally, there are a few oil and gas reservoirs within the Cambrian sandstones, both in normal fault-bounded traps or in pinch-out traps towards the crest of the Algonquin Arch (Lazorek and Carter, 2008).
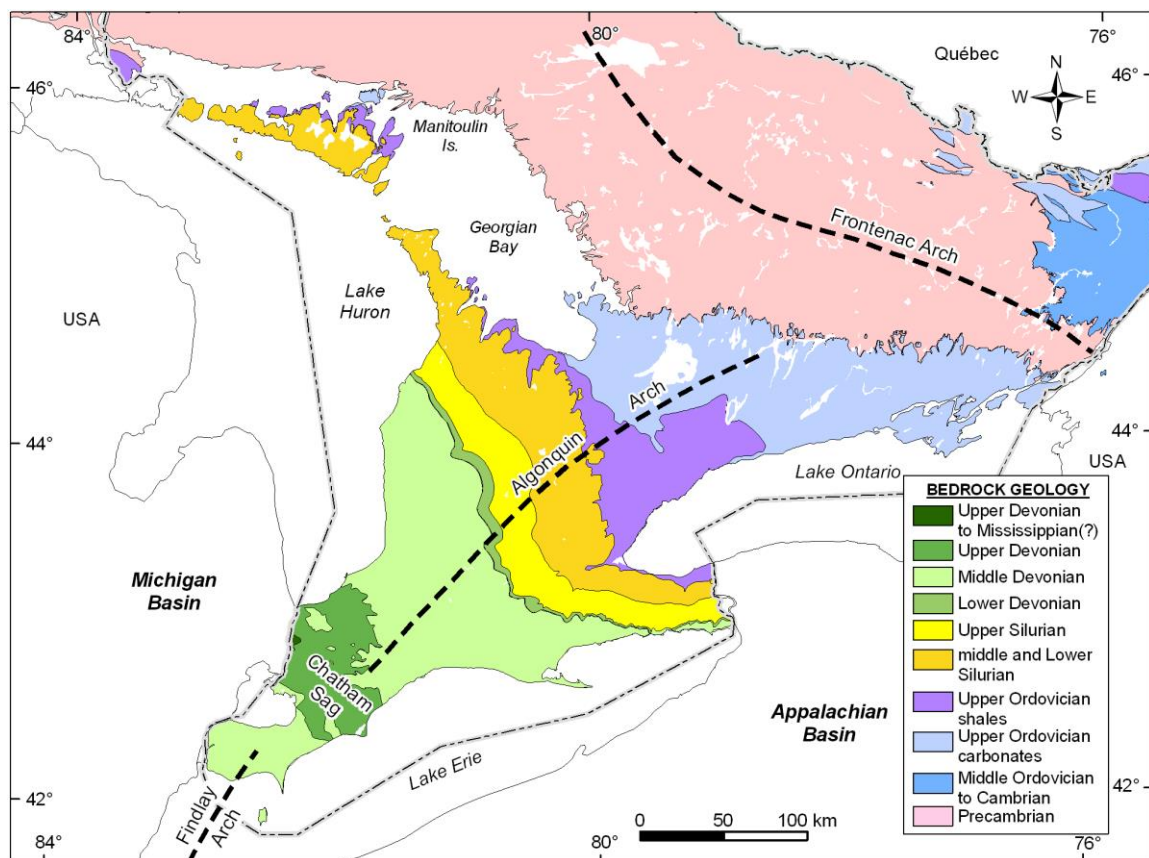
Figure 2.1: Map of the subcrop belts of the bedrock units by age in southwestern Ontario, as well the locations of major structural arches (Armstrong and Carter, 2010).

2.1.2   Geological unit descriptions

This section describes the major units of the southwestern Ontario Paleozoic sedimentary sequence, as well as the Quaternary overburden and Precambrian basement. Lithological characteristics and other details such as thickness and distribution for each unit are presented in descending stratigraphic order, from youngest to oldest. The stratigraphy and distribution of units across the southwestern Ontario region is illustrated in Figure 2.2, from Armstrong and Carter (2010). There are a number of differences in the formation nomenclature reported in the literature; here, the terminology used follows that of Armstrong and Carter (2010).
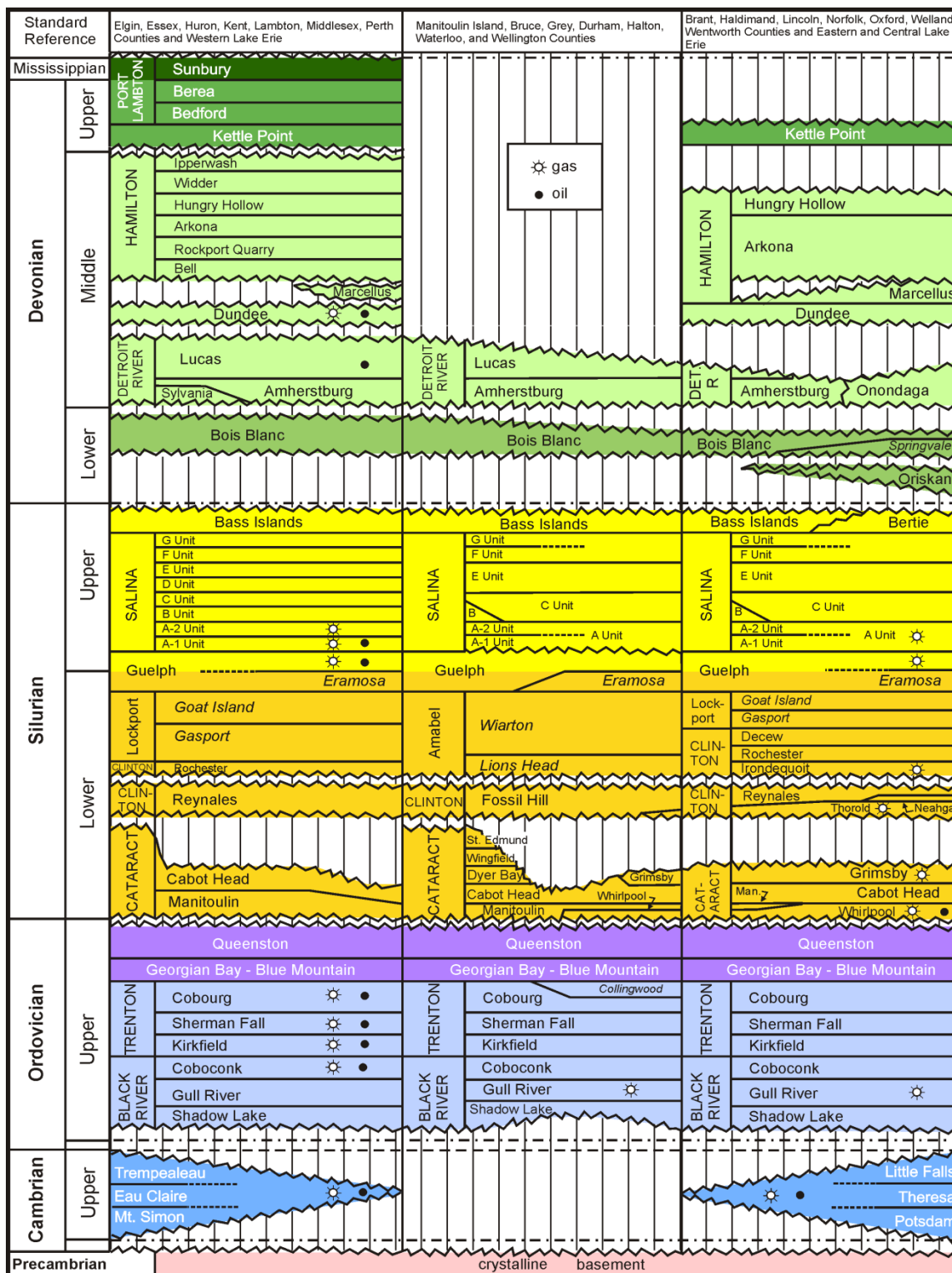
Figure 2.2: The Paleozoic stratigraphy of southwestern Ontario. The three columns show the distribution of units in different counties. Oil- and gas-bearing zones are indicated, and unconformities are shown as broken lines (from Armstrong and Carter, 2010).

2.1.2.0   Quaternary sediments

While not a particular focus of this study, the Quaternary unconsolidated sediment overburden is a geologically and hydrologically important feature in southwestern Ontario. The Wisconsinan glaciation during the Pleistocene caused significant erosion of the bedrock surface and buried much of the bedrock under thick till, clay, silt, sand and gravel deposits (Barnett, 1992). Significant heterogeneity exists in the lithology of the overburden; fluctuations in the extents of the various glacial ice lobes in the area created a complex sequence of interfingering till sheets (Karrow, 1974). The distribution of quaternary soil types have been mapped by the Ontario Geological Survey (Figure 2.3; Barnett et al., 1991). Overburden thicknesses vary considerably across the area, exceeding 250 m in places, such as the Oak Ridges Moraine; the thickest areas often coincide with buried bedrock valleys (Gao et al., 2006).
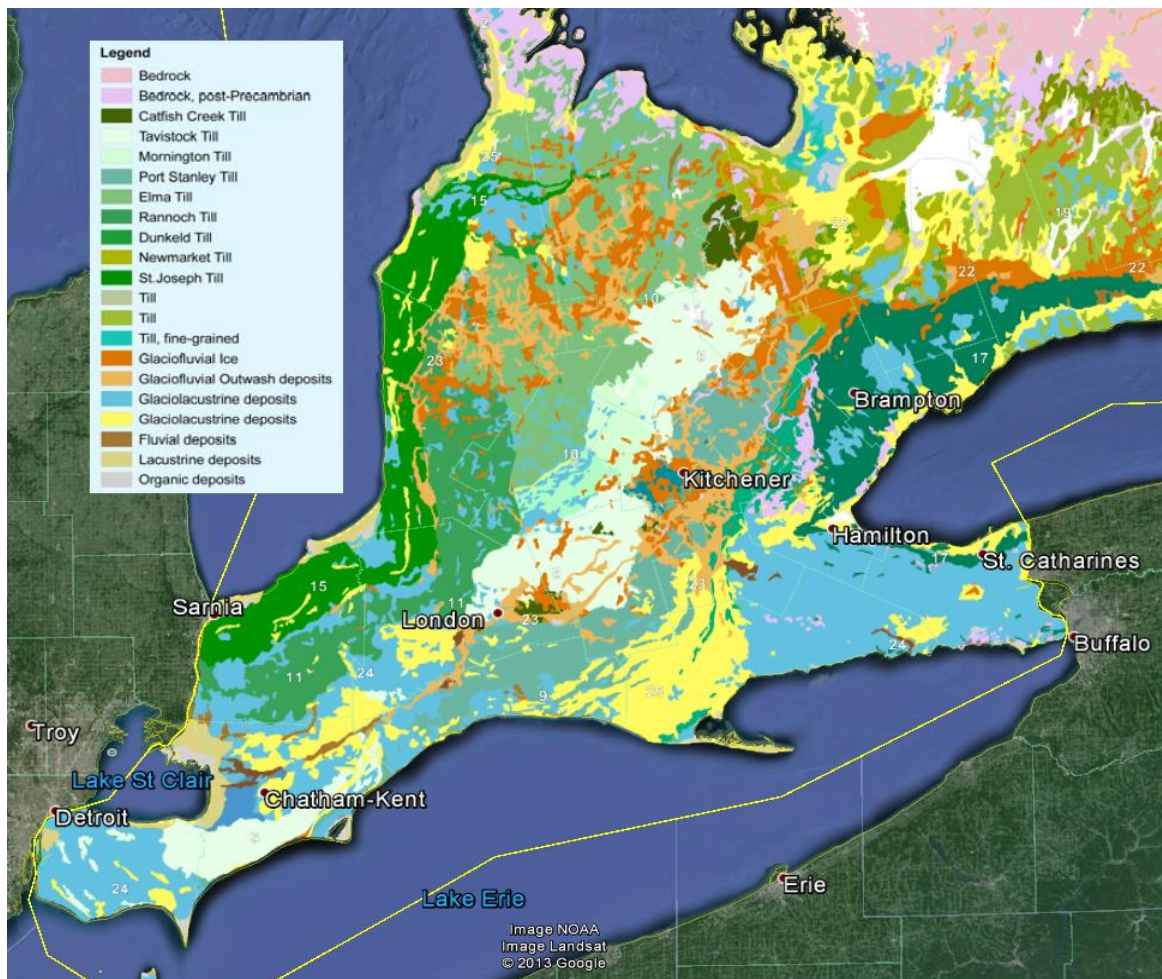
Figure 2.3: Quaternary sediment lithologies of southwestern Ontario (Barnett et al., 1991).

2.1.2.1   Port Lambton Group

The Port Lambton Group, Late Devonian to Mississippian in age, is the youngest Paleozoic unit in southwestern Ontario. It has no surface exposures in the area, but subcrops in western Lambton County (Armstrong and Dodge, 2007). It is subdivided into the Sunbury, Berea and Bedford formations. The Sunbury Formation, the only Mississippian unit in Ontario and restricted to a small area in Lambton county, consists of black, organic-rich shale, up to 20 m thick. Sharply and unconformably underlying it is the Berea Formation, consisting of grey, fine- to medium-grained sandstone with interbeds of shale and siltstone. It occasionally includes sandstone channels up to 60 m thick that are cut into underlying units (Sanford, 1968). Outside these channels, the Berea Formation has a gradational contact with the Bedford Formation. The lowermost unit of the Port Lambton Group, the Bedford Formation consists of light grey shale, with silty and sandy interbeds towards the top of the unit. It is approximately 30 m thick and disconformably overlies the Kettle Point Formation (Armstrong and Carter, 2010).

2.1.2.2   Kettle Point Formation

The Kettle Point Formation is an Upper Devonian unit that subcrops throughout Lambton and Kent counties (Armstrong and Dodge, 2007). The formation consists of up to 105 m of dark brown to black, laminated, fossiliferous and organic-rich shale, silty shale and siltstone, with minor organic-poor, grey-green bioturbated shales and siltstones. Large carbonate concretions known as 'kettles' occur in the lower part of the unit. Coalified plant matter, pyrite and marcasite are also locally abundant. The basal contact with the underlying Hamilton Group is sharp, and commonly marked by a pyritic lag bed containing abundant black, phosphatized fossil fragments (Armstrong and Carter, 2010).

2.1.2.3   Hamilton Group

The Hamilton Group is a widespread, Middle Devonian calcareous shale unit, up to 90 m thick. Over much of its distribution, it disconformably overlies the Dundee Formation, although southeast of St. Thomas, it overlies the black shales of the Marcellus Formation.

In Ontario, the Hamilton Group is subdivided into six formations; in descending order, they are the Ipperwash, Widder, Hungry Hollow, Arkona, Rockport Quarry, and Bell formations, although some may be locally absent. The Ipperwash Formation is a unit of grey-brown, argillaceous, fossiliferous bioclastic limestone with shaley interbeds, with a thickness of up to 13 m. Sharply but conformably underlying it is the Widder Formation, which consists of up to 21 m of grey to grey-brown, fossiliferous, calcareous or argillaceous, nodular limestone and coarse-grained bioclastic limestone (Tsujita et al., 2001; Armstrong and Carter, 2010). It conformably overlies the roughly 2 m-thick Hungry Hollow Formation, which is divided into two parts. The upper section is coral-rich, calcareous, and shaley, while the lower interval is predominantly composed of fossiliferous, bioclastic limestones. The unit contains sharp pyritized internal contacts, and disconformably overlies the Arkona Formation. The Arkona Formation is composed of up to 37 m of blue-grey calcareous shale, interbedded with argillaceous limestone. It has a gradational contact with the Rockport Quarry Formation, which consists of up to 6 m of grey to brown, fine-grained, argillaceous limestone (Sanford, 1968). Sharply underlying it is the Bell Formation, consisting of about 14.5 m of blue-grey, calcareous shale with abundant brachiopods (Johnson et al., 1992; Armstrong and Carter, 2010). It contains thin, organic-rich limestone interbeds towards the sharp basal contact with the Dundee Formation, which is also commonly marked by pyrite occurrences. On the southeast side of the Algonquin Arch, the Bell Formation disconformably overlies the black Marcellus Formation shales, which are not exposed and have a very limited extent in Ontario (Armstrong and Carter, 2010).

2.1.2.4   Dundee Formation

The Middle Devonian Dundee Formation consists of 35 to 45 m of limestone, occurs across much of southwestern Ontario, and disconformably overlies carbonates of the Detroit River Group (Johnson et al., 1992; Armstrong and Carter, 2010). Limestones of this unit are grey to brown, fossiliferous, and medium- to thickly-bedded, and contain minor dolostone. Bituminous partings, microstylolites and chert nodules are common. Fractures and the more porous fossiliferous beds commonly contain oil (Armstrong and Carter, 2010).

2.1.2.5   Detroit River Group

The Detroit River Group, another Middle Devonian carbonate package, is subdivided into 3 formations: in descending order, the Lucas, Amherstburg and Sylvania formations.

The Lucas Formation consists predominantly of dolostone and limestone, with lesser amounts of sandstone and anhydrite. The upper part of this formation is a high-purity limestone lithofacies known as the Anderdon Member, consisting of light to dark grey-brown, fine-grained and sparsely fossiliferous limestones, alternating with coarser bioclastic limestones. Fossil occurrences are mainly stromatoporids and amphipora, with corals being less abundant. It also locally contains a sandy lithofacies commonly termed the "Columbus Sandstone". The Anderdon Member occurs in Essex, Elgin, Norfolk and Oxford counties and beneath central Lake Erie. Below it lies the undifferentiated Lucas Formation, which consists of light to grey-brown, fine-crystalline, poorly fossiliferous, laminated dolostones and limestones. Locally, this unit contains needle-like porosity, anhydrite and gypsum beds, and dissolution breccias. The Lucas Formation has a maximum thickness of 96 m in Ontario, but thickens and becomes more evaporite-dominated towards the Michigan Basin (Sanford, 1968; Armstrong and Carter, 2010).

Conformably underlying the Lucas Formation, the Amherstburg Formation consists of grey to brown, fossiliferous, bioclastic, bituminous, and commonly cherty limestones and dolostones, up to 60 m in thickness. In Essex County, the Amherstburg Formation has a gradational, conformable contact with the underlying Sylvania Formation; throughout the rest of its distribution in Ontario, it disconformably overlies the Bois Blanc Formation (Armstrong and Carter, 2010).

The Sylvania Formation is a Lower to Middle Devonian orthoquartzitic sandstone unit, occurring only in Essex County. It also contains dolomitic quartz arenites and minor cherty dolostone beds, forming cycles of upward-decreasing carbonate content (Russell, 1993). It is up to 30 m thick and has a disconformable contact with the underlying Bois Blanc Formation (Birchard et al., 2004; Armstrong and Carter, 2010).

2.1.2.6 Bois Blanc Formation

The Lower Devonian Bois Blanc Formation consists of greenish grey to grey-brown, fine- to medium-grained, fossiliferous, bioturbated and cherty limestones and dolostones. It contains a 3 to 10 m-thick basal unit of green-brown, commonly glauconitic, quartzitic sandstones with minor sandy carbonates, known as the Springvale Member (Sanford, 1968; Armstrong and Carter, 2010). The Bois Blanc Formation ranges from 3 to 50 m thick in Ontario, thickening towards the Michigan Basin (Sanford, 1968; Johnson et al., 1992). It disconformably overlies Silurian strata or the Oriskany Formation, where present (Armstrong and Carter, 2010).

2.1.2.7 Oriskany Formation

The Oriskany Formation is a Lower Devonian unit consisting of grey to yellowish white, coarse-grained, calcareous, fossiliferous, quartzose sandstones. Locally, the base of this unit is conglomeratic, with clasts of dolostone, glauconitic shale and sandstone. Both the upper and lower contacts are unconformable (Armstrong and Carter, 2010).

2.1.2.8 Bass Islands and Bertie Formations

The Bass Islands and Bertie formations are the youngest Silurian strata preserved in southwestern Ontario. The latter is an Appalachian Basin unit, found in Ontario only near the Niagara Peninsula area, while the former is a Michigan Basin unit that is more widespread. While they are not quite age-equivalent (Haynes and Parkins, 1992), the two formations occupy the same stratigraphic position, conformably overlying the Salina Group, and often are treated as a single formation or equivalent due to the difficulty in reliable identification in drill core and cuttings (Armstrong and Carter, 2010).

These strata consist of brownish, mottled, argillaceous, bituminous, sparsely fossiliferous, finely-crystalline dolostone, with minor shales. Locally they contains intraclastic breccias, evaporite mineral molds, and minor anhydrite and sandstone beds (Sanford, 1969; Liberty and Bolton, 1971; Armstrong and Carter, 2010). The Bass Islands and Bertie formations generally range in thickness from 10 to 90 m, but locally thicken up to 150 m in features

thought to be related to syndepositional subsidence resulting from dissolution of underlying salt layers in the Salina Group (Sanford, 1969; Armstrong and Carter, 2010).

2.1.2.9   *Salina Group*

The Salina Group is a major succession of evaporite and evaporite-related sediments, consisting of up to 420 m of interbedded carbonates, shales, anhydrite and halite; equivalent strata reach 750 m thick in the Michigan Basin (Catacosinos et al., 1990). The Salina Group conformably underlies the Bass Islands and Bertie formations, and all units within the group were deposited conformably, with the exception of some small-scale disconformities resulting from post-depositional dissolution of evaporite units (Sanford, 1977; Armstrong and Carter, 2010). Unit lithologies vary cyclically according to salinification-upwards cycles, grading upwards from carbonates to anhydrites to halite. The predominantly evaporitic lithologies of Salina Group units become increasingly shaley upwards, as well as laterally towards the Appalachian Basin. The halite beds rapidly become thinner, less numerous, and eventually disappear altogether eastward from the Michigan Basin, as a result of onlap thinning, dissolution and facies changes. The zero thickness edge of the halite beds is often very abrupt, interpreted as a dissolution front. East of this edge, there is a rapid lateral shift to a significantly thinner sequence of dolomite, anhydrite, shale, and intraformational breccias left behind after halite dissolution (Armstrong and Carter, 2010).

Determining the timing of salt dissolution is difficult, although isopach mapping by Bailey Geological Services Ltd. and Cochrane (1985) identified at least one major dissolution event, during deposition of the Bass Islands Formation. Linear trends in the thickness of this formation and the Salina B salt coincide with major faults, suggesting that the latter acted as conduits for water to dissolve the salt. Differential timing of post-depositional dissolution of the Salina salt beds and subsequent collapse of younger strata greatly impacted thicknesses, distribution, structure, and fracture patterns in the overlying strata. Structural domes created subsidence fracturing also formed large hydrocarbons traps in the Dundee and Lucas formations, and also contributed to aquifer development (Bailey Geological Services Ltd. and Cochrane, 1985; Armstrong and Carter, 2010).

In Michigan and Ontario, a lettering system is used to subdivide the Salina Group into units A through G. The uppermost, the Salina G unit, consists of up to 12 m of dolomite or anhydrite grading upwards into shaley dolomite. It becomes progressively thinner to the southeast, and may be absent in the Appalachian Basin (Armstrong and Carter, 2010).

The F unit consists of halite, anhydrite, shales and dolostones, divided into six sub-units in the Michigan Basin, each containing a halite bed (Lilienthal, 1978). The salt beds decrease in thickness and in number eastward towards the basin margins, eventually pinching out, such that the F unit salts in Ontario are restricted to a belt along the shore of Lake Huron, from Goderich to Sarnia (Sanford, 1969). Beyond the salt pinch-out, the F unit consists of a lower package of dolostones, shales and anhydrite, and an upper section of dark green shales with pink or blue anhydrite nodules. In Ontario, the salts can reach over 110 m thick, but elsewhere in the region, where the salts are absent, the F unit has a thickness of about 30 m (Armstrong and Carter, 2010).

The E unit is an approximately 25 m-thick package of interbedded tan, laminated to massive dolostones, light grey-green argillaceous dolostones, and green shales with anhydrite nodules and beds. The E unit usually has a distinctive upper bed of shaley dolomite up to a few meters thick, and in Michigan, also contains thick halite beds (Lilienthal, 1978; Armstrong and Carter, 2010).

The D unit generally consists of two halite beds, several meters thick, separated by a thin (<1 m), occasionally shaley dolostone bed, with a combined thickness of up to 16 m in Ontario. Its Ontario distribution is restricted to the northern two-thirds of Lambton County, and a narrow belt along the shoreline of Lake Huron to just north of Goderich (Sanford, 1969), with a thin package of non-salt equivalent strata occasionally found further east (Armstrong and Carter, 2010).

The C unit consists of a lower bed of shaley anhydrite or dolostone transitioning upwards to anhydritic shale, interspersed with thin dolostone and shale beds. It is lithologically uniform and widespread throughout southwestern Ontario (Armstrong and Carter, 2010).

The B unit is typically sub-divided into the upper B unit, the B salt (or the "B equivalent" where salt has been dissolved, leaving behind insoluble components), and the lower B anhydrite. The upper B unit consists of occasionally anhydritic to argillaceous dolostone, anhydrite and anhydritic shale. The B salt consists of white to dark brown, coarsely crystalline halite, with thin partings and interbeds of yellowish to light green-grey shale and dolostone. It is the thickest and most widespread halite unit in Ontario, reaching up to 90 m near Sarnia. Where the salt is absent, the B equivalent is lithologically similar to the upper B unit. Marking the base of the B unit is an anhydrite-rich zone known as the B anhydrite, which, while anhydrite-dominated, also contains dolostone and shale. The B unit reaches up to 92 m thick where the B salt is present; elsewhere, over the Algonquin Arch and in the Niagara region, it is only 15-20 m thick (Armstrong and Carter, 2010).

The A unit is generally divided into two sub-units, the A-1 and A-2; occasionally an A-0 unit is mapped as well.

The uppermost unit, the A-2, is further subdivided into an upper A-2 carbonate, a lower A-2 evaporite, which are separated by a thin, dark grey-green shale unit known as the A-2 shale. The A-2 carbonate consists of grey-brown, fine-grained dolostone and limestone, containing anhydrite nodules, patches of microsucrosic dolostone, minor argillaceous dolostone, and small intraclastic breccia zones. The A-2 evaporite consists of a combination of light blue-grey, nodular anhydrite, anhydritic dolostone, and thick beds of coarse white halite (Armstrong and Carter, 2010). The A-2 salt occurs in a curved belt along the shore of Lake Huron, from north of Lake St. Clair up to southwest Bruce County (Sanford, 1969); east of this area, the A-2 evaporite consists only of anhydrite or is absent altogether. The A-2 unit ranges from 12 m thick over the underlying Guelph barrier reefs, to 85 m thick in the Sarnia area (Armstrong and Carter, 2010).

The A-1 unit is also subdivided into an upper A-1 carbonate and a lower A-1 evaporite. The A-1 carbonate is composed of very fine- to medium-grained, tan-grey to black, bituminous dolostones and limestones, locally containing thin anhydritic beds (Armstrong and Carter, 2010). In Michigan, the A-1 carbonate is mostly limestone, while in Ontario it is regionally dolomitized east of, and over the crest of the Algonquin Arch. West of the arch, the A-1 carbonate shows a complex dolomitization pattern related to faults and

underlying reefs (Carter, 1991). The A-1 evaporite consists of anhydrite with minor dolostone and halite, with the anhydrite transitioning to halite and sylvite towards the Michigan Basin (Lilienthal, 1978). The total thickness of the A-1 unit ranges from 49 m near Lake Huron to less than 6 m over the Algonquin Arch (Sanford, 1969).

The A-0 unit, which is not well-mapped in Ontario and averages 2 m thick, consists of dark brown to black, thinly laminated, bituminous limestone or dolostone, gradational with the overlying A-1 evaporite and the underlying Guelph Formation (Carter et al., 1994). As the lowermost unit in the Salina Group, it represents the first evaporitic cycle and the onset of the salinification of the epicontinental sea covering the Michigan Basin (Armstrong and Carter, 2010).

2.1.2.10   Guelph Formation

The Guelph Formation consists of platformal and reefal dolostones and limestones, forming a basin-rimming carbonate complex, the nature of which is still a matter of some debate. It has been subdivided into numerous facies belts, including barrier reef, lagoonal, patch reef and pinnacle reef (Sanford, 1969; Bailey, 1986). Recent models (Carter et al., 1994; Coniglio et al., 2003) group the patch reef belt and reef bank complexes into the "Ontario platform", with the pinnacle reefs in a basin slope setting. The Guelph regional intrareef facies averages 4-8 m thick on the basin slope; dolomudstones of the Salina A-0 unit are commonly mapped as the uppermost few meters of this unit (Carter et al., 1994). The lower 2-6 m consists of porous, sucrosic, dark brown to black dolomudstone, siltstone, and fragments of grey dolowackestone that are similar to the underlying Goat Island Member of the Lockport Formation. Carter et al. (1994) interpreted this unusual rock as a paleosol breccia – the karstic debris resulting from two or more episodes of exposure. A thin (<1 m), lithologically similar, layer of grey dolomitic wackestone separates these breccias into two beds. This intrareef Guelph facies thickens by up to 1 m near pinnacle reefs. Within these pinnacles, which commonly host hydrocarbons, the Guelph Formation thickens considerably, exceeding 100 m in places. The Guelph's reefal facies is characterized by brownish, fine- or medium-crystalline, sucrosic, fossiliferous and commonly biostromal to biohermal dolostones. Bituminous dolostones and

limestones near the base of, or underlying, the Guelph Formation are known as the Eramosa Member; Armstrong and Carter (2010) consider it part of the Guelph Formation although previously authors (e.g., Bolton, 1957; Johnson et al., 1992; Brett et al., 1995) have given it different assignations. It consists of tan to black, fine- to medium-crystalline, variably fossiliferous, bituminous, commonly microstylolitic dolostone, which locally can be argillaceous or cherty (Armstrong and Carter, 2010).

Recently, Brintnell (2012) reinterpreted the classic Guelph pinnacle reef model as karst towers that formed in a paleokarst basin. She found that the 'pinnacles' largely consist of stacked tabular beds, as opposed to thick carbonate accretions with reefal affinities. Rather than being biohermal, the pinnacle-like topography appeared to be entirely a consequence of post-depositional erosion associated with karst development. She also proposed that the Guelph Formation was deposited on an easterly-dipping carbonate ramp, rather than a basin centered on central Michigan, as the Guelph facies with more open, deep marine character and least subaerial exposure were found in the eastern portion of the Michigan Basin, while facies indicative of more restricted marine conditions and greater subaerial exposure occurred towards the central to western portions of the Michigan Basin.

2.1.2.11   *Lockport Formation*

Underlying the Guelph Formation is the Lower Silurian Lockport Formation. It is sub-divided into the Goat Island and Gasport members.

The Goat Island Member is a package of grey-brown, finely crystalline, irregularly bedded, moderately fossiliferous, variably argillaceous dolostones, locally containing abundant chert and vugs filled with gypsum, calcite and/or fluorite. In the Hamilton area, it contains basal beds of nodular or lenticular chert, informally called the Ancaster chert beds, as well as an upper shaley section known as the Vinemount shale (Bolton, 1957; Armstrong and Carter, 2010).

The Gasport Member consists of thickly-bedded, blue-grey, white, or pinkish-grey dolostone, dolomitic limestone, and minor argillaceous dolostone. It is characteristically a

crinoidal grainstone, and commonly shows horizontal planar lamination, ripple cross-lamination and cross-bedding. It also locally contains small bryozoan and coral bioherms developed above crinoidal shoals (Crowley, 1973; Armstrong and Carter, 2010).

2.1.2.12   Clinton and Cataract Groups

The Lower Silurian Clinton and Cataract groups, generally regarded as Appalachian Basin units, consist of a series of thin sandstone, shale and carbonate units, many of which thin and pinch out or are cut by regional unconformities on the northern flank of the basin in Ontario. In southwestern Ontario, the Clinton Group is generally subdivided into several formations, which, in descending order, are the Decew, Rochester, Irondequoit, Reynales, Neahga and Thorold. The underlying Cataract Group consists of the Grimsby, Cabot Head, Manitoulin and Whirlpool formations (Bolton, 1957; Armstrong and Carter, 2010).

The Decew Formation consists of up to 4 m of finely-crystalline, argillaceous to arenaceous dolostone, with minor shale (Johnson et al., 1992). It distinctively contains large soft-sediment deformation structures, interpreted as the product of synsedimentary seismic activity (Brett et al., 2004). The Decew Formation's upper contact with the Gasport Member is sharp, possibly disconformable (Bolton, 1957), while its basal contact with the Rochester Formation is gradational (Armstrong and Carter, 2010).

The Rochester Formation consists of dark, calcareous shale, with variably abundant, thin interbeds of fine- to medium-grained calcareous to dolomitic calcisiltite to bioclastic calcarenite (Bolton, 1957; Brett et al., 1995). Its thickness decreases from 24 m under eastern Lake Ontario to its pinch-out between Hamilton and Goderich (Sanford, 1969).

The Irondequoit Formation consists of thickly bedded, light to pinkish grey, medium- to coarse-grained, crinoid- and brachiopod-rich limestone (Johnson et al., 1992; Brett et al., 1995). It contains small bryozoan bioherms, especially near its top. It ranges from up to 3 m thick in its outcrop belt, to over 10 m in the subsurface, and pinches out in an irregular line from central Lake Erie to northern Waterloo County (Sanford, 1969).

Sharply and disconformably underlying the Irondequoit Formation is the Reynales Formation, a unit of grey, thin- to medium-bedded, finely crystalline, sparsely fossiliferous dolostone and argillaceous dolostone, with thin shaley interbeds and partings. This unit can be divided into an upper section of non-fossiliferous, fine-grained dolostone, and a more argillaceous and fossiliferous lower section containing abundant brachiopods (Armstrong and Carter, 2010). The upper Reynales Formation has a sharp, disconformable base, characterized by a phosphatic and/or green shaley bed. The basal contact of the lower Reynales Formation with the underlying Neagha Formation is also disconformable (Brett et al., 1995), although in some places it may be gradational. In Ontario, the Reynales Formation reaches a maximum thickness of roughly 6 m (Sanford, 1969; Armstrong and Carter, 2010).

The Neagha Formation consists of dark to greenish grey, sparsely fossiliferous shale, thinly interbedded with limestone. This unit has a maximum thickness of about 2 m and has a relatively limited distribution in Ontario, in Niagara and Haldimand counties (Sanford, 1969). A basal phosphatic pebble lag bed suggests that the contact with the underlying Thorold Formation is disconformable (Brett et al., 1995).

The Thorold Formation is a grey-green to white, quartzitic sandstone unit, with minor thin partings of grey-green shale or siltstone and shale intraclasts (Armstrong and Carter, 2010). The sandstones contain numerous marine fossils (Pemberton, 1987) and various current-related sedimentary features (Johnson et al., 1992). The Thorold Formation has a maximum thickness of about 4 m in outcrop and 6.5 m in the subsurface, and pinches out in an irregular southwestwardly line from Hamilton to central Lake Erie (Bolton, 1957; Sanford, 1969). The nature of its basal contact is uncertain, and has been previously interpreted both as conformable and disconformable (Armstrong and Carter, 2010).

The Grimsby Formation, the uppermost unit of the Cataract Group, is a package of interbedded red shales and sandstones. The upper half of the formation is predominantly composed of red, green, or white, mottled, channelized, cross-stratified, fine-grained quartzitic sandstones. The lower section consists of red to green shales with interbeds of red, planar laminated to hummocky cross-stratified sandstones (Armstrong and Carter, 2010). The Grimsby Formation has a maximum thickness of about 15 m in outcrop and

24 m in the subsurface, and has an irregular pinch-out and/or erosional edge extending from Hamilton to west-central Lake Erie (Bolton, 1957; Sanford, 1969).

The Cabot Head Formation consists of grey, green, or red noncalcareous shales, with sandstone and carbonate interbeds (Johnson et al., 1992). Its thickness in Ontario varies from ~40 m under west-central Lake Erie to ~12 m over the Algonquin Arch (Sanford, 1969). Towards the crest of the arch, its top appears to be cut by a regional angular unconformity at the base of the Reynales Formation (Armstrong and Carter, 2010).

The Manitoulin Formation is considered a Michigan Basin unit, part of a shallow south-dipping carbonate ramp. It consists of grey, fine- to medium-crystalline, moderately fossiliferous dolostone, argillaceous dolostone with minor grey-green shale (Armstrong and Carter, 2010). The Manitoulin Formation commonly contains chert nodules, lenses and silicified fossils (Johnson et al., 1992). Thickening towards the Michigan Basin, it has a maximum thickness of 25 m in Ontario, and pinches out to the southeast along a line from eastern Niagara Peninsula and western Lake Erie (Sanford 1969). The Manitoulin Formation gradationally overlies the Whirlpool Formation, where present, otherwise it unconformably overlies the Queenston Formation (Armstrong and Carter, 2010).

The Whirlpool Formation is composed of white, grey or maroon, fine-grained, orthoquartzitic sandstone (Johnson et al., 1992). This unit has an upper section consisting of interbedded sandstones and shales which have shallow marine sedimentary features, including symmetrical ripple marks and hummocky cross-stratification, and contain marine fossils. A lower section is more massive, unfossiliferous, contains features indicative of deposition in a braided fluvial environment, such as trough cross-bedding (Rutka et al., 1991), and its basal surface is commonly mud-cracked. The Whirlpool Formation is up to 9 m thick, and pinches out in an irregular line extending from near Collingwood to central Lake Erie (Sanford, 1969; Rutka et al., 1991). As the lowermost Silurian unit, it unconformably overlies the Ordovician Queenston Formation (Armstrong and Carter, 2010).

2.1.2.13   Queenston Formation

The distinctive red shales of the Upper Ordovician Queenston Formation underlie all of southwestern Ontario, and are exposed along the Niagara Escarpment. They are part of a large package of terrestrial to marginal marine, predominantly siliciclastic sediments deposited in response to the Taconic orogeny. The Queenston Formation has a maximum thickness of over 275 m beneath eastern Lake Erie, thinning to less than 50 m in northwestern Bruce Peninsula (Sanford, 1961). While the Queenston Formation consists mostly of reddish, variably calcareous shale, it also contains lesser amounts of green shale, siltstone, sandstone and limestone (Donaldson, 1989; Johnson et al., 1992; Brogly et al., 1998), commonly with a thin grey-green interval along the upper contact. Gypsum also occurs as locally abundant nodules and fracture fillings. Carbonate content tends to increase regionally to the northwest (Armstrong and Carter, 2010).

2.1.2.14   Georgian Bay and Blue Mountain Formations

The Upper Ordovician Georgian Bay and Blue Mountain formations are lithologically similar, both consisting predominantly of shales, interbedded with limestones, siltstones and sandstones (Byerley and Conigilio, 1989; Kerr and Eyles, 1991; Johnson et al., 1992). The thickness and abundance of the interbeds generally decrease stratigraphically downwards, as well as from north to south. Shales are generally noncalcareous, and vary in colour from greenish to bluish to brownish-grey, while the sandstones and siltstones commonly contain calcareous cement and bioclastic material. The Georgian Bay Formation is between 125-200 m thick, while the Blue Mountain Formation is up to 60 m thick. Because of their similar natures and the gradational contact between them, these two formations are generally mapped together in the subsurface (Johnson et al., 1992; Armstrong and Carter, 2010).

2.1.2.15   Trenton and Black River Groups

The Upper Ordovician Trenton and Black River groups are another lithologically similar package of rocks, consisting of transgressional marine carbonates deposited on a

shallowly dipping ramp northwest of the Taconic foreland basin. They form a deepening-upward sequence, transitioning from basal clastics to tidal/supratidal carbonates, to lagoonal/shoal carbonates and finally deep shelf carbonates (Kobluk and Brookfield, 1982; Armstrong and Carter, 2010). They sit unconformably above the Cambrian clastic and carbonate rocks, or directly above the Precambrian basement, towards the crest of the Algonquin Arch beyond the Cambrian pinch-out. In descending order, the Trenton Group is subdivided into the Cobourg, Sherman Fall, and Kirkfield Formations, while the Black River Group consists of the Coboconk, Gull River and Shadow Lake Formations (Armstrong and Carter, 2010). The Trenton Group reaches over 170 m in thickness, while the Black River Group ranges from 10 m thick near its erosional edge in eastern Ontario, thickening to the southwest to nearly 150 m at the Detroit River (Bailey Geological Services Ltd. and Cochrane 1984a; Trevail et al., 2004). These units are locally dolomitized near vertical wrench fault zones, enhancing porosity and resulting in the development of important hydrocarbon reservoirs (Armstrong and Carter, 2010).

The Cobourg Formation consists of blue-grey to grey-brown fossiliferous limestones and argillaceous limestones, with shaley interbeds and partings. Various bedding styles are present, including nodular, irregular tabular and planar tabular. There is a general downward-coarsening gradation in grain size. Under Essex, Kent and part of Lambton counties, the uppermost few meters of the Cobourg Formation is dolomitized (Sanford, 1961; Armstrong and Carter, 2010).

The Sherman Fall Formation is subdivided into a lower "argillaceous" unit and an upper, "fragmental" unit. The lower subunit consists of up to 60 m of interbedded limestone and calcareous shale. The limestone beds are grey-brown and fossiliferous, highly variable in grain size, thickness and bedding style, and include lime mudstones, bioclastic and intraclastic wackestones and grainstones (Melchin et al., 1994; Armstrong and Carter, 2010). The upper subunit consists entirely of limestones, predominantly cross-stratified, tan to light grey, fossiliferous bioclastic and intraclastic grainstones (Armstrong and Carter, 2010). It is up to 10 m thick and may be laterally discontinuous (Armstrong, 2000; Melchin et al., 1994).

The lowermost unit of the Trenton Group, the Kirkfield Formation consists of thin- to thick-bedded fossiliferous limestones interbedded with shales. It is also subdivided into two subunits, which have a gradational contact. The lower subunit consists of fine-grained, thin- to medium-bedded, peloidal to bioclastic limetones interbedded with green shales, which have been interpreted as storm beds (Melchin et al., 1994; Armstrong and Carter, 2010). The upper subunit contains storm beds as well, but also includes other types of limestone, and its shale content is limited to thin partings. Limestones in the upper unit include fine- to medium-grained, bioturbated, bioclastic wackestones, packstones and grainstones, containing fossils such as crinoids, trilobites, bryozoans and brachiopods. The total thickness of the Kirkfield Formation ranges from about 55 m in Middlesex County to less than 15 m on Manitoulin Island (Armstrong and Carter, 2010).

The Coboconk Formation consists of brownish-grey, medium- to very thickly-bedded, fine- or medium-grained, bioturbated, laminated or locally cross-stratified, bioclastic limestones, mostly wackestones, packstones and grainstones, containing fossils that are indicative of deposition in a shallow shoal environment. The Coboconk Formation ranges in thickness from about 33 m under Kent County to less than 2 m east of Toronto (Melchin et al., 1994; Armstrong and Carter, 2010).

The Gull River Formation is characterized by very fine-grained, light grey to dark brown limestones, also containing minor dolostone, shale and argillaceous sandstone, reaching up to 135 m thick in southwestern Ontario (Johnson et al., 1992; Armstrong and Carter, 2010). Liberty (1969) divided it into three members. The uppermost consists of thin- to very thickly bedded, bioturbated, fossiliferous limestones, predominantly wackestones, with lime mudstone interbeds common towards the base, and coarser-grained packstone and grainstone interbeds towards the top. The middle unit is composed mainly of sparsely fossiliferous lime mudstones, commonly laminated and containing intraclasts. The lower unit is lithologically variable, containing fine-grained dolostones, very fine-grained, variably fossiliferous limestones, argillaceous sandy dolostones, and minor argillaceous dolomitic sandstones and shales. The basal contact with the underlying Shadow Lake Formation is generally gradational (Armstrong and Carter, 2010).

The Shadow Lake Formation is the oldest Ordovician unit in southwestern Ontario, forming the base of the Black River Group, and unconformably overlying Cambrian strata or Precambrian basement. It consists of poorly sorted, red and green sandy shales, argillaceous and arkose sandstones, and lesser proportions of sandy argillaceous dolostones and arkose conglomerates. There is a gradation from clastic lithologies towards the base to carbonates at the top. Sand grains in all rock types are commonly frosted, suggesting aeolian sediment input (Armstrong and Carter, 2010). The Shadow Lake Formation is generally only 2-3 m thick, but can thicken up to 15 m where it directly overlies the Precambrian basement (Sanford, 1969; Johnson et al., 1992).

2.1.2.15   *Cambrian Strata*

The base of the Paleozoic sedimentary sequence in southwestern Ontario is composed of Upper Cambrian strata, considered here as undivided. These strata consist predominantly of sandstones, and there is an upwards succession of quartzose sandstones, interbedded sandstones and dolostones, and dolostones (Armstrong and Carter, 2010). Sanford and Quillian (1959) applied formational names to these three lithological groups, using different nomenclatures from the adjacent basins. However, Bailey Geological Services Ltd. and Cochrane (1984b) noted that the character of these individual units becomes less distinct towards their pinch-out near the Algonquin Arch, and therefore treated the entire Cambrian section as one undivided unit, an approach used today by the petroleum industry. The lower part of the Cambrian strata consists of white to light grey, well-sorted, coarse-grained sandstones, with an arkose sandstone base. Above these lies an interval of fine- to medium-grained sandstone, interbedded with grey, fine-crystalline dolostone, grey shaley dolostone and minor amounts of glauconite. The upper section consists mainly of fine- or medium-crystalline dolostone (Sanford and Quillian, 1959). These lithologies represent the transgressive on-lapping of the Cambrian sea over the Algonquin Arch. Post-depositional uplift of the Arch has resulted in erosion of the Cambrian strata such that their present distribution is limited to the fringes of the southwestern Ontario peninsula (Sanford and Quillian, 1959; Trevail, 1990). Thus, both the upper and lower boundaries of the Cambrian are unconformable.

2.1.2.16   Precambrian Shield

While not part of the Paleozoic sedimentary sequence which is the focus of this study, the Precambrian basement rocks had a strong influence on the evolution of the overlying strata and possibly on fluid movement therein, and thus will be briefly described here.

Crystalline metamorphic rocks of the Precambrian Grenville Province unconformably underlie the Paleozoic sedimentary succession. All except the easternmost basement rocks in the study area have been affected by several episodes of deformation and high-grade metamorphism during the Grenville Orogeny, which ended around 1,050 to 1,070 Ma ago (Easton, 1992; Easton and Carter 1994, 1995; Armstrong and Carter, 2010).

Most of the study area is underlain by the Central Gneiss Belt, a broad zone of granitic, monzonitic and tonalitic gneisses. It is bounded to the west by the Grenville Front Tectonic Zone, and to the east by the Central Metasedimentary Belt Boundary Zone. Rocks in the Central Gneiss Belt show well-developed, northeast-trending and southwest-dipping gneissing layering. They contain variable proportions of quartz, K-feldspar, and plagioclase, with accessory biotite and hornblende (Armstrong and Carter, 2010).

An alteration zone occurs along the Precambrian-Paleozoic contact; it is widely distributed and has been attributed to long-distance westward movement of warm basinal brines along the unconformity, in response to orogenic events (e.g., Ziegler and Longstaffe, 2000). Several alteration episodes have been identified – Harper et al. (1995) dated secondary feldspars at 453 to 412 Ma, and Ziegler and Longstaffe (2000) reported ages of 365 to 321 Ma for secondary illites; more detail is provided in Section 5.2.2.9.

2.1.3   Hydrogeology

This section provides an overview of the hydrogeology of southwestern Ontario, discussing different water types, aquifers, aquitards, and flow paths. As described in the previous section, the stratigraphy of southwestern Ontario consists of units of limestone, dolostone, shale, evaporites and sandstone. Aquifers are generally found in the more permeable carbonate and sandstone units, while shales and evaporites act as aquitards. Karst, produced by partial dissolution of more soluble rocks such as carbonates and evaporites, is an important factor for increasing porosity in these rocks. Both modern and ancient karst are present in the region, with recent karst developing along the subcrop belts of many units, while paleokarst is commonly associated with unconformities in the deeper subsurface (Armstrong and Carter, 2010; Freckelton, 2013). However, where unaffected by karsting or other porosity-enhancing processes, carbonates generally have very low porosity and permeability, and act as aquitards.

2.1.3.1   Hydrogeochemical stratification

Geochemically, groundwaters in southwestern Ontario can be broadly classified into three, largely depth-controlled, stratified water horizons, present in all major water-bearing units.

The uppermost horizon is an interval of fresh water, upon which a large portion of Ontario's residents rely for drinking water. Fresh water is found within the Quaternary overburden and in a regional contact aquifer comprising the lowermost few metres of the drift and the uppermost few metres of jointed, fractured, and/or karsted bedrock immediately underneath (Armstrong and Carter, 2010; Carter, 2012). Fresh water can also extend deeper into bedrock in places, up to 200 m below the top of bedrock, but only in areas with karst. The Dundee-Lucas, Bois Blanc-Bass Islands, and Salina-Guelph-Lockport formations contain important karstic fresh water aquifers at relatively shallow depths (OPI, 2012).

The fresh water zone transitions down-dip into a region of sulphurous and commonly brackish or saline (as defined in Table 2.1, Section 2.3) water at shallow to intermediate depths. The nature of the fresh-sulphur water interface is not well understood and the depths at which sulphur water is found are quite variable, from near-surface down to approximately 500 m (T. Carter, personal communication, 2013). In generally, however, it is found at greater depths than fresh water. This sulphur water is characterized by high levels of dissolved hydrogen sulphide (H_2S), believe to have been produced by sulphur-reducing bacteria, which use sulphate to oxidize organic matter under anoxic conditions (Dyer, 2003; Matheson, 2010). The presence of H_2S represents an important hazard, not only because it is highly poisonous to humans and aquatic ecosystems, but also since it corrodes metal well casings, and thus is a major factor leading to the deterioration of the leaky wells that are the main subject of this study. Sulphur water is most notably found in the shallow Devonian Dundee and Lucas formations, but is also present in the Silurian Bass Islands, Salina, and Guelph formations. Well records from the Ontario Oil, Gas and Salt Resources Library (OGSR) for all of these formations show a strong down-dip zonation, from fresh water near where the units subcrop beneath the drift, to sulphur water deeper in the basin (Figure 2.4).

The deepest water horizon is a system of highly saline brines, with total dissolved solids (TDS) commonly in excess of 200,000 mg/L and locally exceeding 400,000 mg/L. The depth of the transition zone between the brine system and the less saline aquifers above it is estimated at between ~350-450 m, based on isotopic depth profiles from boreholes at the Nuclear Waste Management Organization (NWMO)'s Deep Geological Repository (DGR) site (Clark et al., 2010a,b; Clark et al., 2011), located near the northwestern edge of the study area. While this transition depth may not be the same everywhere in the region, it is consistent with the data from this project and from a previous study of the southwestern Ontario brines by Dollar et al. (1991). While some saline waters have been reported in driller logs in the deepest parts of the Dundee, Lucas and Bass Islands Formations, only one sample from these units was found in the present study to be concentrated enough to be considered a brine. Brines in southwestern Ontario are typically found in units stratigraphically within or below the Salina Group, although these

same units also contain fresh or sulphur water at shallower depths, where not overlain by evaporites. The high salt contents of the brines are believed to be partially due to dissolution of the Salina Group halite beds, whereas the water itself is thought to primarily be remnant seawater from the time of the formations' deposition, which has since undergone chemical alteration (Dollar et al., 1991), although other theories have been proposed (e.g. Clayton et al., 1966; see Section 5.2.2.1).
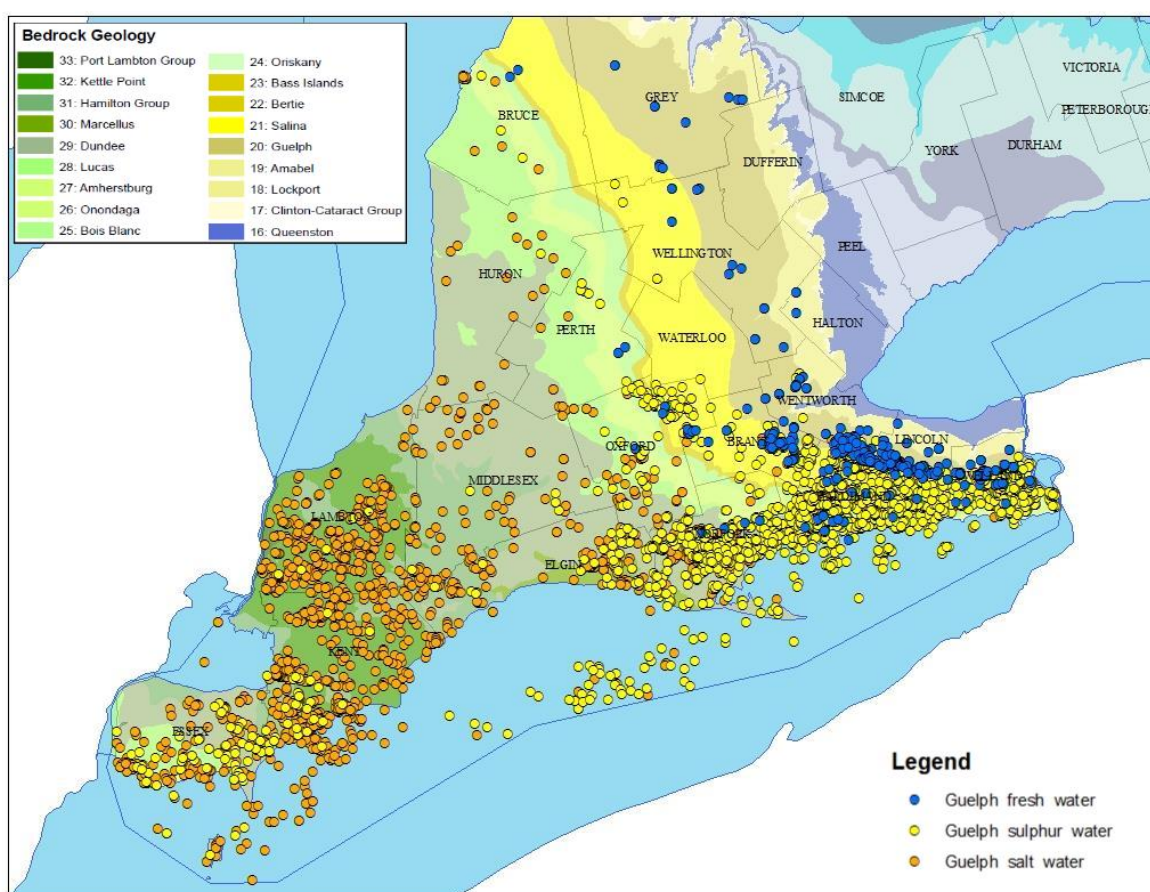
Figure 2.4: Occurrences of fresh, sulphur(/brackish), and salt waters (brines) reported in Ontario Petroleum Institute well records for hydrocarbon wells penetrating the Guelph Formation. Depth increases down-dip to the southwest, towards the Chatham Sag. Fresh water is found at the shallowest depths, along and near the outcrop belt, progressing to sulphur water at intermediate depths, and finally brines are found in the deepest parts of the basin. All other formations show similar down-dip zonation of water types. Map constructed in ArcGIS by L. Fortner (2013).

2.1.3.2 Groundwater flow patterns

This section discusses the main features of the groundwater flow systems in southwestern Ontario, based largely on ongoing studies by T. Carter and L. Fortner. Figure 2.6 illustrates the current understanding of groundwater flow and occurrence, from Carter (2012) and Sharpe et al. (2014).

Most modern groundwater flow in the region is restricted to within the unconsolidated Quaternary glacial drift, forming a shallow, topographically-driven flow system. Much of the groundwater in the drift is contained within a large number of relatively small, separate, confined and unconfined aquifers with limited lateral extent, reflecting the complexity and rapid lateral facies changes in the overburden (Carter, 2012). The flow system in the drift also includes the aforementioned, regionally-extensive 'contact aquifer'. These drift aquifers are recharged by precipitation, generally at topographic highs, such as glacial moraines, along the spine of the Algonquin Arch, and the Niagara Escarpment. The latter two features form important hydrological divides in the regional flow systems. As well as being heavily exploited for human use, the overburden aquifers naturally discharge to topographic lows such as streams and the Great Lakes (McIntosh and Walter, 2006; Sykes et al., 2011; Hobbs et al., 2011).

While most of the groundwater in the overburden flow system discharges into the Great Lakes catchment, a small amount, thought to be less than 2% (Eberts and George, 2000), penetrates the underlying shallow bedrock aquifer system. This groundwater enters into bedrock units that have sufficient porosity and permeability, generally recharging only along their subcrop belts. The bedrock flow system occurs primarily in the Devonian and Silurian formations. While flow in this shallow bedrock aquifer system is mainly intraformational, karst features such as solution-widened joints and sinkholes locally allow cross-formational flow of water through the Dundee Formation directly into the underlying Lucas Formation. Extensive shallow karsting in reefal facies of the Guelph, Gasport and Goat Island formations also allows deep penetration of fresh water into these units (Sharpe et al., 2014; Freckelton, 2013). Flow in both the drift and the bedrock aquifers is gravity-driven and is controlled by the dip of the bedrock units, with flow

southwest along the crest of the Algonquin Arch towards the Chatham Sag, or down the flanks of the arch towards the adjacent basins (Vugrinovich, 1987; Sykes et al., 2011; Carter, 2012; Sharpe et al, 2014); Figure 2.5 presents the potentiometric surface map for the Lucas Formation aquifer. In Silurian formations, down-dip penetration of meteoric waters beyond a few hundred meters below the surface is inhibited by the strong density gradient associated with the brines at depth, compounded by the low regional topographic gradients and lack of discharge pathways for the deep groundwaters, and so flow deeper in these units is expected to have a major component parallel to the strike of the formations (McIntosh and Walter, 2005; Sykes et al., 2011; Hobbs et al., 2011). In the shallow bedrock flow system, discharge occurs through artesian springs, household water wells, quarries, road-cuts, and unplugged wells in topographic lows. The bedrock system also likely discharges into the Great Lakes; Cartwright et al. (1979) and Hoaglund et al. (2004) found upward hydrologic gradients under Lake Michigan, and noted that gradients were higher in areas underlain by more permeable bedrock units.
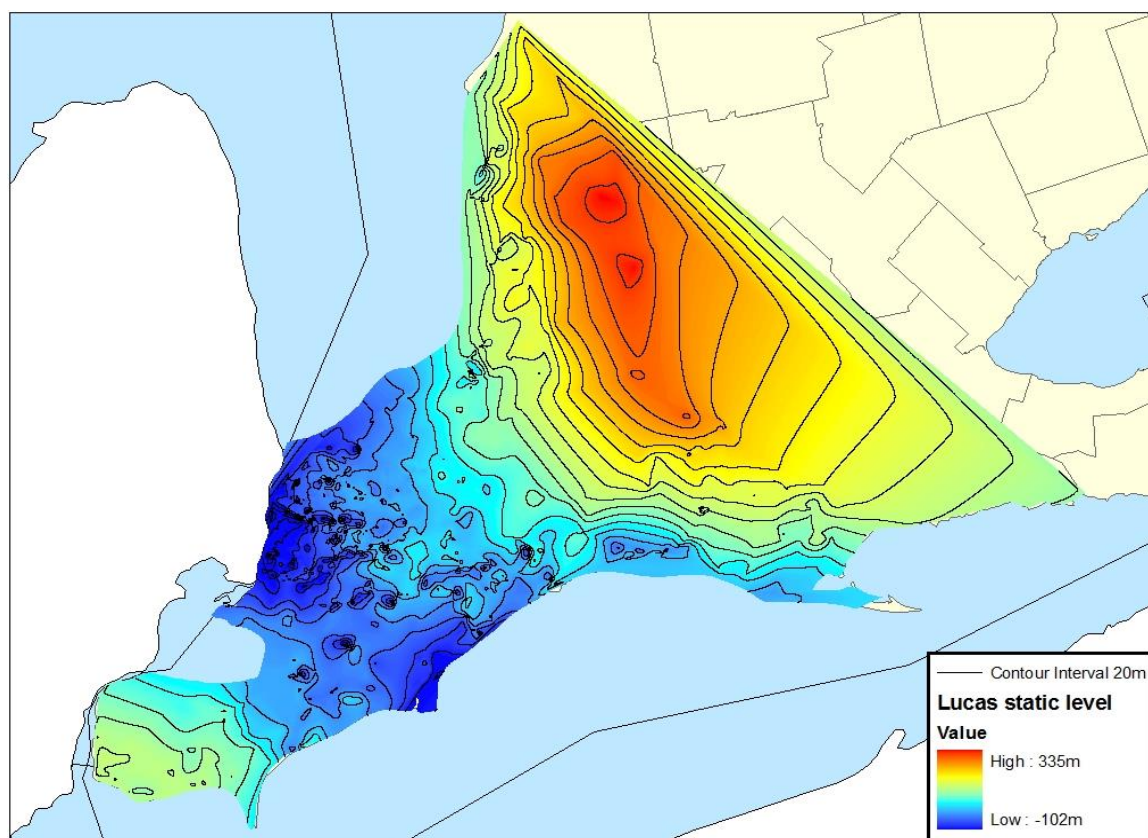
Figure 2.5: Lucas Formation static levels (generated from MNR well database).

Beneath the shallow meteoric flow systems are a series of brine aquifers in the deep Cambrian through Silurian units. The isotopic compositions of these brines tend to be more ^{2}H- and ^{18}O-enriched than modern precipitation, plotting to the right of the meteoric water line (Hobbs et al., 2011), suggesting that they have been relatively unaffected by meteoric recharge. These aquifers are thus generally viewed as a largely isolated hydrologic system, relatively undisturbed over geological timescales, with recent groundwater velocities being essentially stagnant and solute transport diffusion-dominated (e.g., Mazurek, 2004); hydrological modelling by Sykes et al. (2011) supports this conclusion. The isotopic compositions also differ between these deeper units, suggesting they are also to some degree hydrologically separate from each other (Dollar et al., 1991). Such separation is facilitated by the extensive shale, carbonate, and evaporite aquitard units that lie between the various water-bearing formations. Cross-formational fluid flow from these deep formations to the surface has not been reported, and there are no other known discharge pathways (Hobbs et al., 2011). However, as discussed later in this report, there is some evidence for mixing between the shallow aquifers and some Silurian brines. While this may be due to anthropogenic activities, coincidence between fault locations and areas of salt dissolution suggests that fresh water has locally penetrated at some point at least as deep as the lower units of the Salina Group (Bailey Geological Services Ltd. and Cochrane, 1985), although interpretations of the timing of salt dissolution suggest that most if not all salt dissolution took place before Late Devonian time (e.g., Grieve, 1955; Brigham, 1971). Where the evaporites remain, they are expected to seal against cross-formational flow between the shallower waters and these brines. The strong density contrast between these systems, combined with the low topographic gradients in the region, is also believed to inhibit down-dip intraformational mixing between these systems (Hobbs et al., 2011; Sharpe et al., 2014).
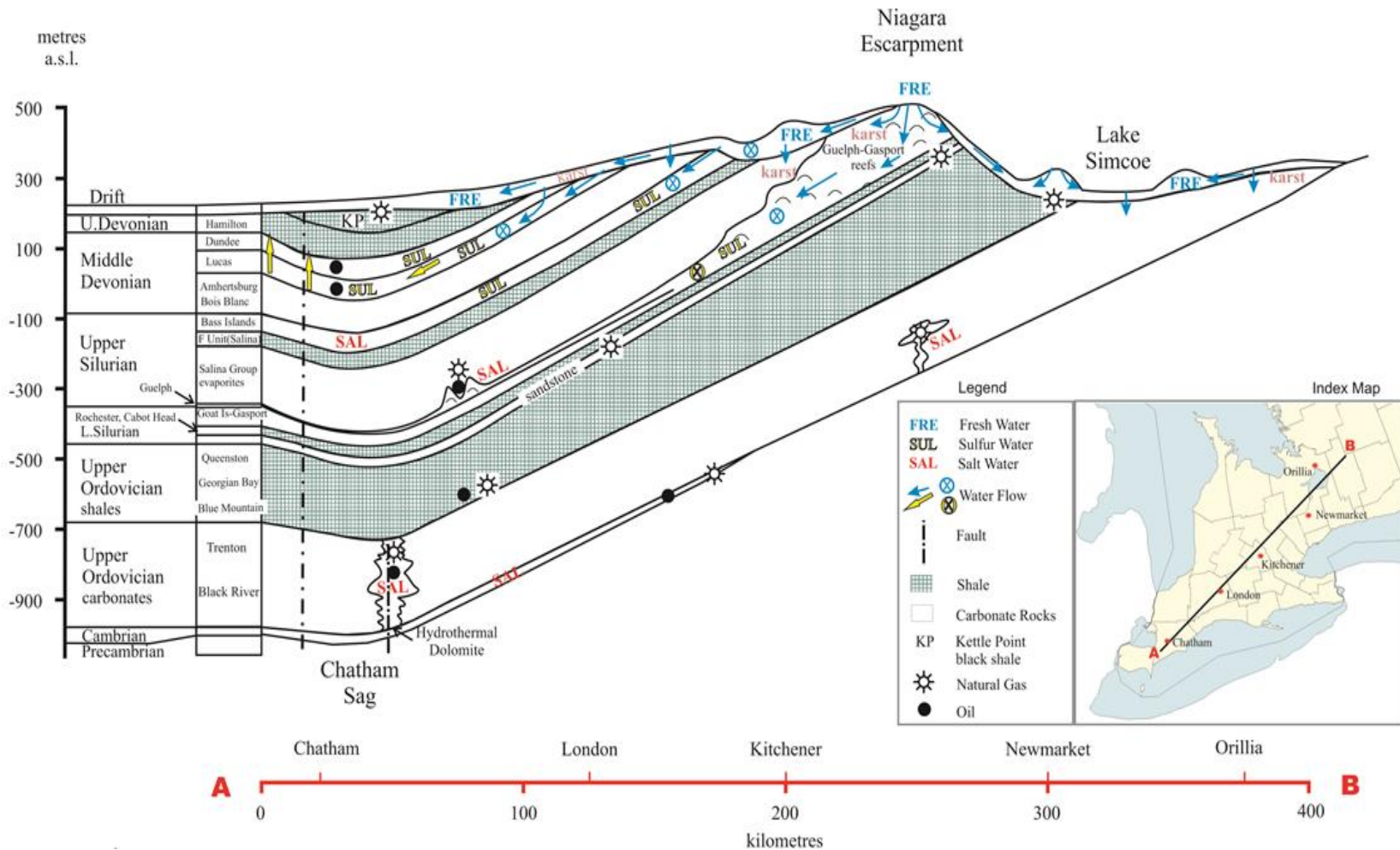
Figure 2.6: Hydrogeological cross-section along the crest of the Algonquin Arch, depicting water type zonation, occurrence of aquifers, and general flow directions. The occurrence of faults and major hydrocarbon reservoirs are also illustrated (Carter, 2012).

2.1.3.3   Hydrologic effects of glaciation

Approximately 14,000 years ago, southwestern Ontario was covered by the Laurentide Ice Sheet (LIS) (Person et al., 2007). During and immediately following this glaciation, increased hydraulic gradients from LIS meltwater significantly impacted groundwater flow systems in the region. Pleistocene meteoric waters and glacial meltwaters penetrated down-dip deep into all permeable formations, significantly supressing the fluid salinities in the Cambrian, Ordovician and Silurian units (e.g., Siegel and Mandle, 1984; McIntosh et al., 2002; 2011). It appears that today, these Pleistocene waters have not yet been completely flushed from the hydrologic system. For instance, Husain et al. (2004) reported a large zone of stagnant water in western Lambton County with very low isotopic signatures typical of Pleistocene recharge, trapped in a contact aquifer between the bedrock and a clayey aquitard layer in the drift. McIntosh and Walter (2006) report similar waters in drift and shallow bedrock aquifers along the margins of the Michigan Basin, and Dollar et al. (1991) note their occurrence in the shallow Devonian aquifers throughout southwestern Ontario. In southwestern Ontario, the maximum depth at which glacial waters have been found is 130 m, in shallow bedrock wells (Aravena et al. 1995).

2.1.3.4   Hydrogeological characterization of the bedrock units

This section provides more detailed hydrogeological descriptions for each of the main bedrock units, and is based largely on work by Carter (2012), Carter and Fortner (2012), and Sharpe et al. (2014).

Aside from the contact aquifer, the stratigraphically highest regional bedrock aquifer in southwestern Ontario is found in the Dundee and Lucas formations. This aquifer commonly contains fresh water in the recharge areas near the subcrop belt, and exhibits down-dip zonation to sulphurous/brackish to saline water as described in Section 2.1.3.1, and commonly displays artesian flow at the surface in topographically-low discharge areas such as along the north shore of Lake Erie and in stream valleys. Except for along their subcrop belts, these units are isolated from the drift aquifers by the Port Lambton,

Kettle Point and Hamilton shales. While primary porosity and permeability in the Dundee Formation is generally low and thus this formation regionally acts more like an aquitard, locally it is water-bearing due to solution-widened fractures, relating to collapse of underlying strata from differential salt dissolution in the Salina Group. The Lucas Formation forms the major regional aquifer. It contains regionally-extensive paleokarst, which is particularly pronounced in a 1,400 km^2 region in Huron, Middlesex and Perth Counties known as the Breathing Well Zone, where it contains large open vugs (T. Carter, personal communication, 2013; Freckelton, 2013). The Lucas Formation also has a facies with 30% microporosity, and the sandy Columbus Member also has high intergranular porosity (Carter and Armstrong, 2010).

The Bois Blanc Formation is not generally considered a major bedrock aquifer, and samples show little or no visible porosity. However, fresh water is sometimes found near the subcrop belt, and sulphur water is present at depth in the lower parts of the Bois Blanc, especially in the Springvale and Oriskany sandstones. The Bass Islands/Bertie Formation has similarly low porosity, although the upper few meters contain sand-filled joints, open fractures and paleokarst resulting from weathering along an unconformity. This higher-porosity interval is water-bearing, and forms a continuous aquifer with the overlying Springvale, Oriskany and lower Bois Blanc formations, and shows typical gradation from fresh water along the sub-crop belt, through a regional sulphur water aquifer, to saline water at depth, similar to the zonation illustrated in Figure 2.5. (Armstrong and Carter, 2010; T. Carter and L. Fortner, personal communications, 2013).

In the deep subsurface, Salina Group forms a barrier to groundwater flow, separating the shallow Devonian aquifers from the deeper saline brines below (Vugrinovich, 1986; Carter, 2012). However, near the subcrop belt dissolution of evaporites, carbonates, and erosion of shales in the Salina Group has led to the formation of buried bedrock valleys and gorges in the Niagara and Waterloo areas (Gao et al., 2006). Fresh water has collected in these valleys, although it contains relatively elevated levels of dissolved solids (Hamilton, 2011). In the deeper subsurface, brines are associated with hydrocarbon reservoirs in the Salina A-1 and A-2 carbonate units.

The Guelph Formation forms an important regional aquifer. In the subcrop belt it contains fresh water to depths of up to 250 m due to near-surface karstification and primary porosity in the reefal facies, transitioning down-dip to sulphur water (T. Carter, personal communication, 2013). At greater depths (>300-500 m), the Guelph Formation contains a major brine aquifer. Brines are found in both the thick reefal facies and the thin, inter-reef regional facies, which is a paleokarst breccia formed by a prolonged period of subaerial exposure in the geologic past (Carter et al., 1994, Armstrong and Carter, 2010). The reefal facies also hosts significant hydrocarbon reservoirs. Locally, the underlying Lockport Formation is also reefal (Armstrong and Carter, 2010), and so the Guelph aquifers may be continuous down into the Lockport strata.

The shaley Clinton and Cataract Groups do not usually contain significant aquifers, given their generally low permeability. Small amounts of brine are sometimes produced from the more porous Thorold, Grimsby, and Whirlpool sandstones and some carbonate units, believed to have infiltrated after extraction of natural gas from pore spaces (Armstrong and Carter, 2010).

The Ordovician units are regionally considered major aquitards. The Queenston, Georgian Bay and Blue Mountains formations are largely impermeable shales, while the Trenton and Black River groups also have extremely low porosity and permeability (Mazurek, 2004). However, where the Trenton and Black River limestones have locally been dolomitized along vertical wrench vaults, these altered zones have greatly increased porosity and permeability, forming oil reservoirs which contain associated brines (Armstrong and Carter, 2010).

The Cambrian strata, particularly the sandier facies, are regionally porous and permeable, and also contain hydrocarbon-associated brines (Armstrong and Carter, 2010). Most of the water reported in Cambrian well records in Ontario is on the eastern side of the Algonquin Arch (L. Fortner, personal communication, 2013), although this is may be a sampling bias resulting from current well distribution.

2.2   Previous Research

Several researchers have previously investigated the geochemistry of groundwaters in southwestern Ontario, and their work acts as a foundation for the present study. This section briefly summarizes some of the most relevant studies.

Clayton et al. (1966) were among the first to conduct a comprehensive isotopic study of sedimentary basin formation waters, including samples from the Michigan Basin. They found brines that plotted below and to the right of the Global Meteoric Water Line (GMWL) – the linear trend (approximated by $\delta^2H = 8[\delta^{18}O] + 10$) on which lie the isotopic compositions of all global precipitation – yet had compositions different from seawater, which could be extrapolated back to the local meteoric intercept on the GMWL (Figure 2.7). They concluded that all waters originally present in the formations had been flushed from the system, replaced with recent meteoric waters. They postulated that the enrichment in ^{18}O relative to meteoric waters was the result of rock-water interaction, and that δ^2H variations were due to differences in original precipitation compositions.
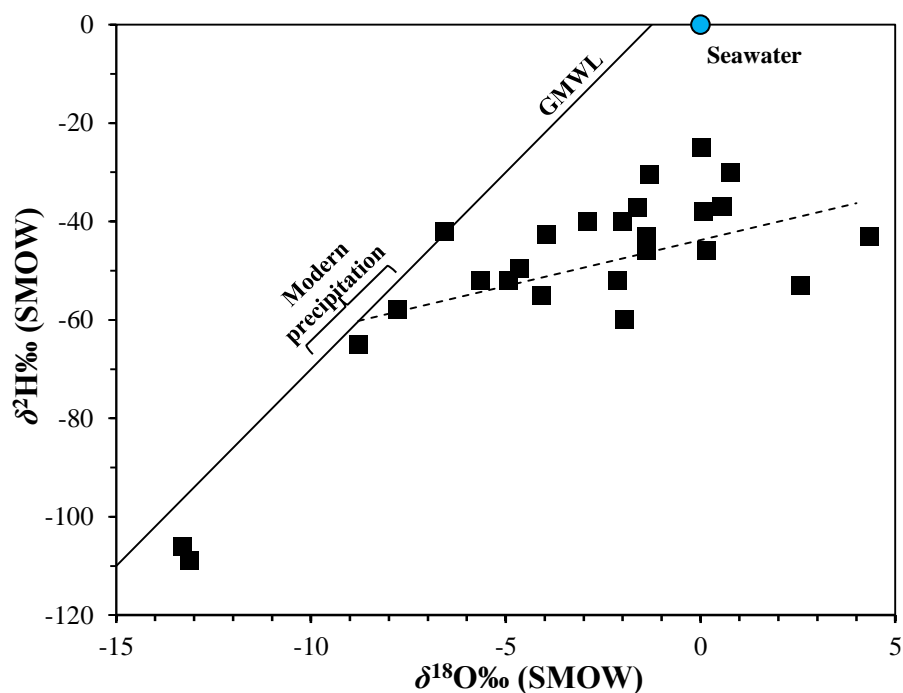
Figure 2.7: Oxygen and hydrogen isotope data from Michigan Basin groundwaters analysed by Clayton et al. (1966). The dashed linear trend shown was interpreted to indicate alteration of modern meteoric water by rock-water interaction.

Dollar et al. (1991) conducted another major study, in which they collected brine samples from a large number of hydrocarbon wells from various formations, and measured oxygen and hydrogen isotope ratios, tritium contents, strontium isotope ratios, and major ion chemistries. Their samples were almost exclusively from deeper formations, while Clayton et al. (1966) focused mainly on shallow Devonian units. Dollar et al. (1991) were the first to note isotopic differences between brines from different formations (Figures 2.8-2.9), and postulated the existence of several independent hydrological systems. They theorized that the brines were evaporated seawaters, generated by hooked isotopic evolution pathways described by Holser (1979) and Knauth and Beeunas (1986).
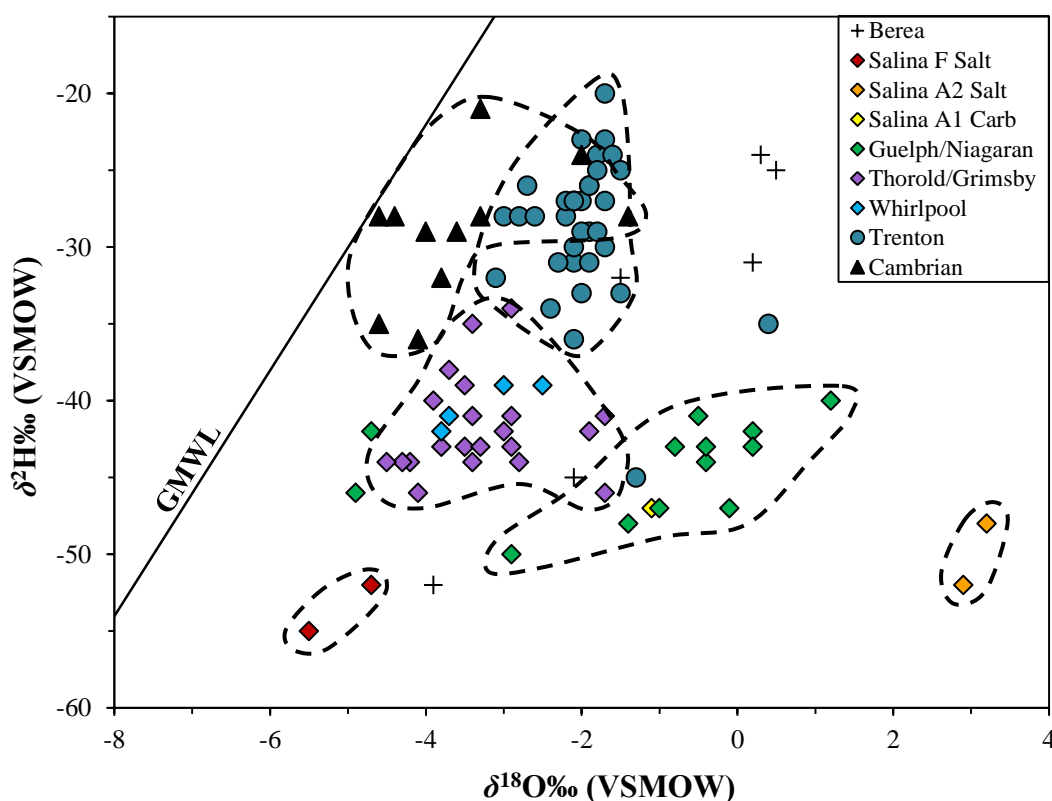
Figure 2.8: Oxygen and hydrogen isotope data for various groundwaters from the Michigan Basin and southwestern Ontario analysed by Dollar et al. (1991). Different formations have different although somewhat overlapping ranges.

Enrichments in ^{2}H in the Cambrian-Ordovician units relative to the Silurian units were explained as either the product of membrane filtration or mixing with a meteoric water component enriched in ^{2}H relative to modern precipitation. Oxygen isotope differences between the Cambrian and Ordovician units were attributed to interaction with carbonate

reservoir rocks. The ^{18}O enrichments and ^{2}H depletions relative to seawater observed in the Salina A-2 salt were attributed to gypsum dehydration water; similar water was expected in the Salina F, however the isotopic signatures found were different, suggesting that the gypsum dehydration water had since migrated elsewhere, and been replaced with brine from a different unit. Waters from the Silurian carbonates were interpreted as mixtures between expelled gypsum dehydration water and concentrated seawater brines. A direct correlation between TDS and δ^{18}O observed in the Silurian and Mississippian sandstones was attributed to mixing between concentrated brine and a more ^{18}O-depleted, presumably meteoric, end-member. Finally, a few Devonian samples collected in Ontario were found to have highly negative δ^{18}O and δ^{2}H signatures, interpreted as glacial water. Some Devonian samples were also collected towards the center of the Michigan basin, and these waters closely matched the Ontario brine compositions.

Dollar et al. (1991) also found that, in general, the ^{87}Sr/^{86}Sr ratios for the groundwaters sampled were higher than expected for seawaters of the same age, attributed to rock-water interaction with Rb-bearing phases. Similar to the observed groupings with the water isotopes, it was noted that when the reciprocal of total Sr^{2+} was plotted against ^{87}Sr/^{86}Sr, the compositions for different formations plotted in fairly distinct fields (Figure 2.9).
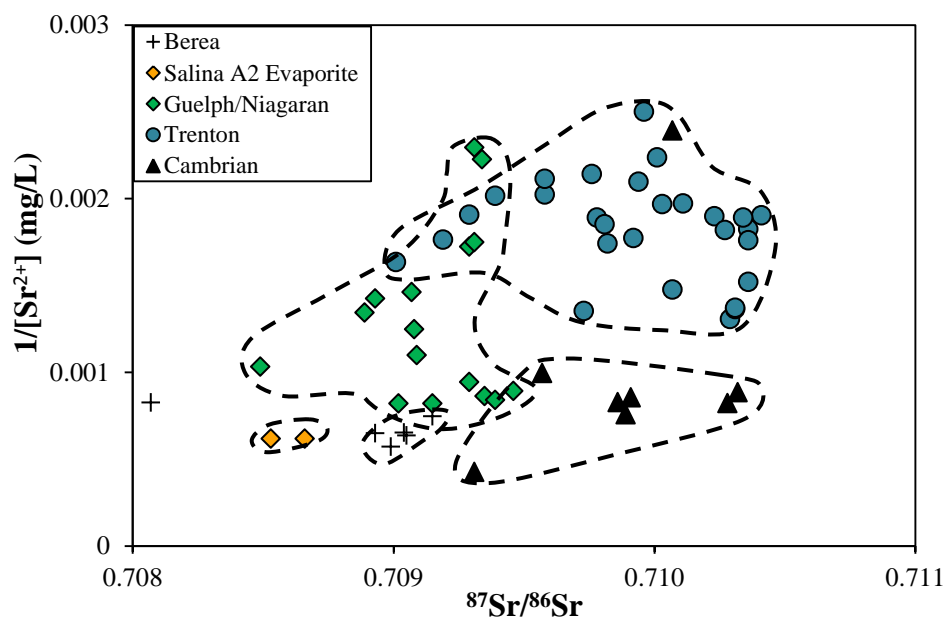
Figure 2.9: Strontium isotope data for groundwaters analysed by Dollar et al. (1991). Different formations again have different although overlapping ranges.

Wilson and Long (1993a,b) studied the geochemistry of Devonian and Silurian brines in central Michigan Basin, focusing mainly on ion compositions but also analysing oxygen, hydrogen and strontium isotopes for some samples. In the Devonian formations, they found stratigraphic chemical differences, with predominantly Na-Ca-Cl brines in upper formations, and Ca-Na-Cl brines in lower formations. Ion ratios indicated an evaporated seawater source for these brines, modified by rock-water interactions, most importantly dolomitization and reactions with aluminosilicate minerals. Wilson and Long (1993a,b) also found that the δ^{18}O and δ^{2}H compositions (Figure 2.10) were consistent with evolved seawaters, as well as fluids from gypsum dehydration. They proposed that the Devonian brines originated either from *in situ* porewater, or migrated upward from deeper formations, and near basin margins had since been diluted with meteoric water. The Silurian brines were also Ca-Na-Cl type, with Br concentrations suggestive of a seawater origin, concentrated into the MgSO$_4$ or KCl facies.
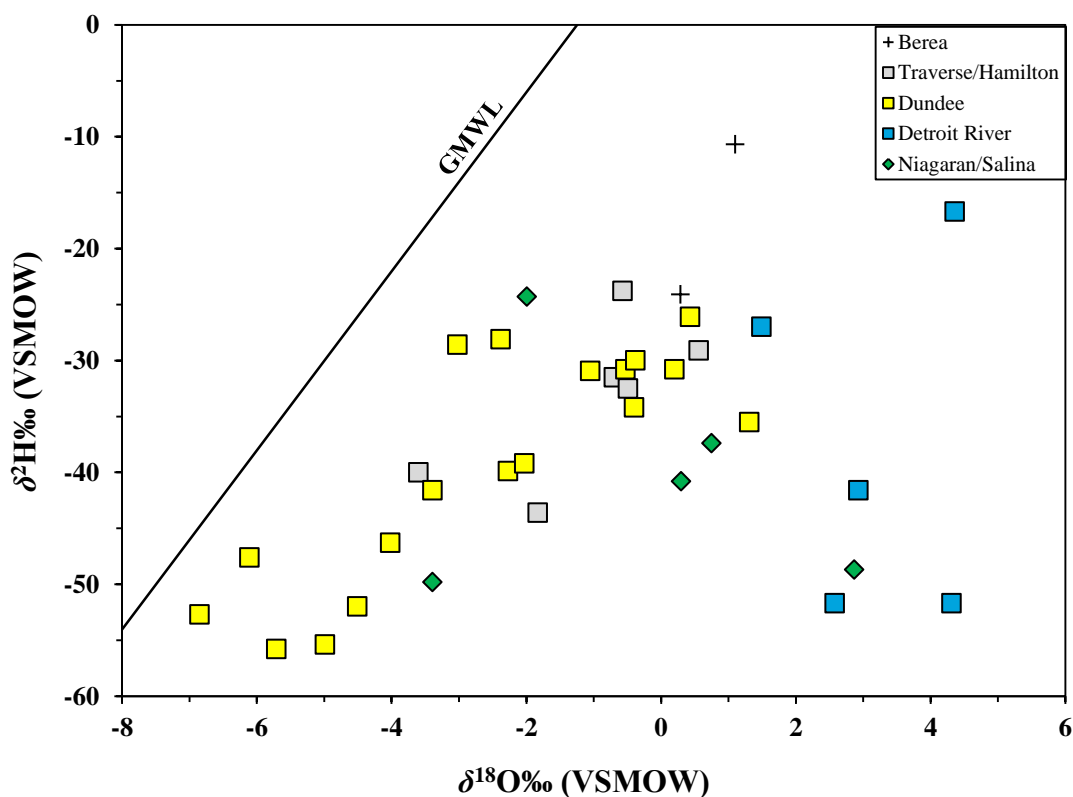
Figure 2.10: Oxygen and hydrogen isotopic compositions of brines from various formations in the Michigan Basin, reported by Wilson and Long (1993a,b).

Weaver et al. (1995) investigated the sources of saline waters in several Ontario Devonian oil reservoirs (Bothwell, Oil Springs and Petrolia). As well as analysing ion compositions and water isotopes, they were the first in Ontario to present sulphate isotopes (both $\delta^{18}O$ and $\delta^{34}S$). Most of their samples had similar ion chemistries, and the water isotope compositions were close to the GMWL. However, in southern Oil Springs, waters had elevated chloride contents, a narrow range of $\delta^{18}O$ and a wide range of $\delta^{2}H$. Weaver et al. (1995) explained these characteristics using a multi-stage mixing scenario (Figure 2.11).
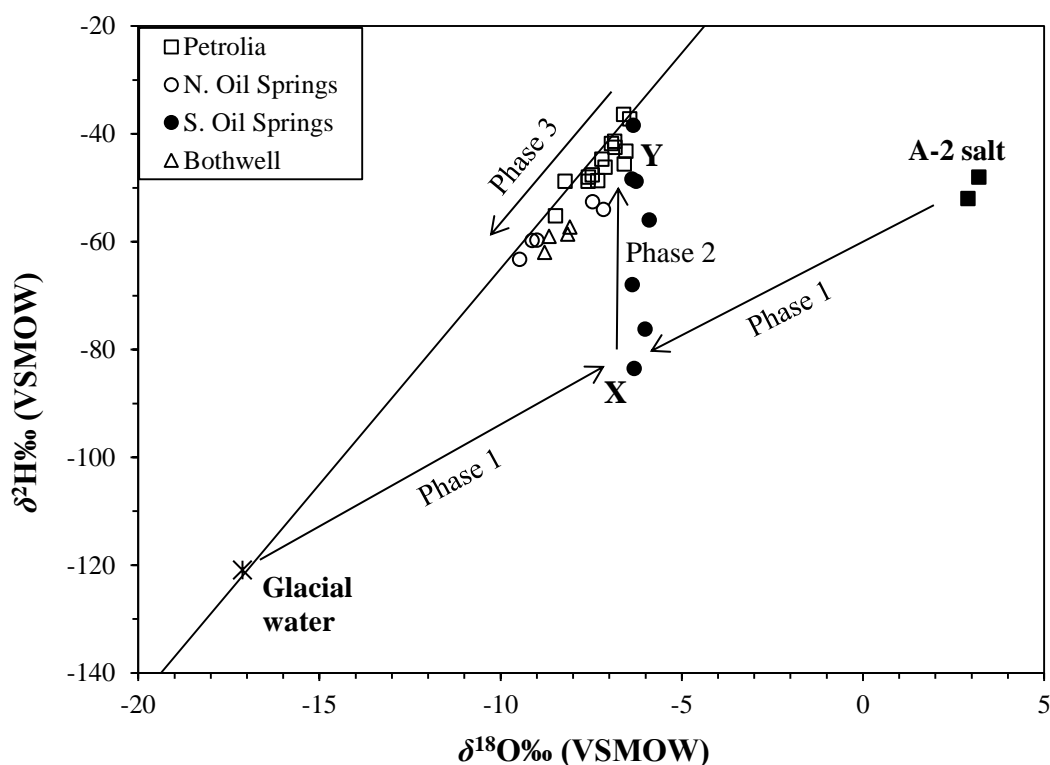
Figure 2.11: Oxygen and hydrogen isotope data from several Devonian oilfield waters, analysed by Weaver et al. (1995). A three-phase mixing model was proposed to explain the data, as described in text.

Initial mixing (Phase 1) between an ^{18}O- and ^{2}H-depleted glacial water end-member and ^{18}O- and ^{2}H-enriched brines from the Salina A-2 salt produced the sample with the lowest measured $\delta^{2}H$ value (composition X), which then mixed (Phase 2) with shallower, more ^{2}H-enriched waters in the Dundee Formation (composition Y), which then mixed (Phase 3) with more negative meteoric waters to produce the spread of samples along the GMWL. This model also showed close agreement between observed and predicted ion

data. Sulphate isotope compositions ranged from +26.0 to +33.7‰ for δ^{34}S, and +15.2 to +18.4‰ for δ^{18}O. The Bothwell, Petrolia and northern Oil Springs sulphate isotope compositions were consistent with dissolution of Devonian marine sulphate minerals and bacterial reduction, while the samples from southern Oil Springs had slightly lower δ-values, and were interpreted to have been derived from Silurian sulphates, consistent with cross-formational flow.

Recently, Freckelton (2013) measured a range of geochemical parameters for a number of shallow water samples from the Lucas Formation in Huron and Perth Counties. She found that the groundwaters had δ^2H and δ^{18}O values that plot along or near the local meteoric water line, indicating an aquifer dominated by recent recharge, primarily during the winter. Samples fell into two groups for sulphate isotopes – one group with low values (δ^{34}S = −1.5 to +4.3 ‰; δ^{18}O = −1.0 to +5.6 ‰), and one with higher values (δ^{34}S = +14.8 to +27.1 ‰; δ^{18}O = +11.1 to +16.8 ‰). The former group was attributed to sulphide oxidation (which was corroborated by ion chemistry data), while the latter was interpreted as dissolution of marine sulphates. No influence of mixing with deeper brines was observed. Similarly, Matheson (2012) investigated shallow groundwaters in the Niagara region, and found comparable results with water isotopes, although some samples showed signs of mixing with brines, thought to be upwelling through abandoned wells. He also identified sulphate originating from sulphide oxidation and marine sulphate dissolution, but had a larger range of values, with δ^{34}S up to +44‰. This was attributed to subsequent bacterial sulphate reduction, which enriches the residual sulphate phase in ^{34}S; both sources of sulphate were interpreted to be affected by such bacterial activity.

Very few other hydrogeochemical studies have been conducted in the Ontario region, with most work having been focused on shallow groundwaters, either in the drift or very shallow bedrock aquifers. Hobbs et al. (2011) provide a more comprehensive review of all previous work. There is also a large body of similar work regarding brines in the Illinois Basin, located southwest of the Michigan Basin, mostly developed in the 1980s-1990s. However, these waters are sufficiently separated from Ontario that direct comparisons are not considered here.

2.3   Saline Waters

Given that a significant proportion of the groundwaters in deep subsurface of southwestern Ontario are highly concentrated brines, and other waters of varying salinities are also present, this section briefly discusses the nature of saline waters, with a particular focus on isotopic considerations related to them, including the so-called 'salt-effect'. The widely-used classification system for saline waters by Davis (1974) is presented in Table 2.1 and will be used throughout the paper.

Water type	Total Dissolved Solids (TDS) range (mg/L)
Fresh water	< 1,000
Brackish water	1,000 – 10,000
Saline water	10,000 – 100,000
Brine	> 100,000

Table 2.1: Salinity classification scheme for waters (Davis, 1974). By comparison, seawater has about 35,000 mg/L TDS.

Saline waters are found in a wide range of geological environments throughout the world, including sedimentary basins. They are geologically and economically significant in the sense that they are often associated with hydrocarbon reservoirs, and petrologic and isotopic evidence shows that they have been involved in large-scale fluid and solute transport, water–rock interactions, and formation of ore deposits. The sources of solutes in saline waters are often of interest, and can range widely, including surficially-weathered salts, seawater, metamorphic–magmatic fluids, products of subsurface water–rock interaction, and evaporite dissolution (Carpenter, 1978; Horita, 2005).

An important requirement for the formation of saline water is a closed or at least semi-closed hydrologic system, so that solutes can accumulate without being flushed by dilute waters. Subaerially, this generally takes the form of a restricted water body such as a lake, sabkha or marginal sea. In colder regions, freezing can also produce brines. Subsurface brine production mechanisms are more complex, and include evaporite dissolution, diagenetic/metamorphic reactions, and membrane filtration by shales (Horita, 2005).

2.3.1 Isotopic evolution during saline water formation

There is currently a reasonably good understanding of the behaviour of the oxygen and hydrogen isotope ratios in water during the major brine-forming hydrogeochemical processes (Figure 2.12).
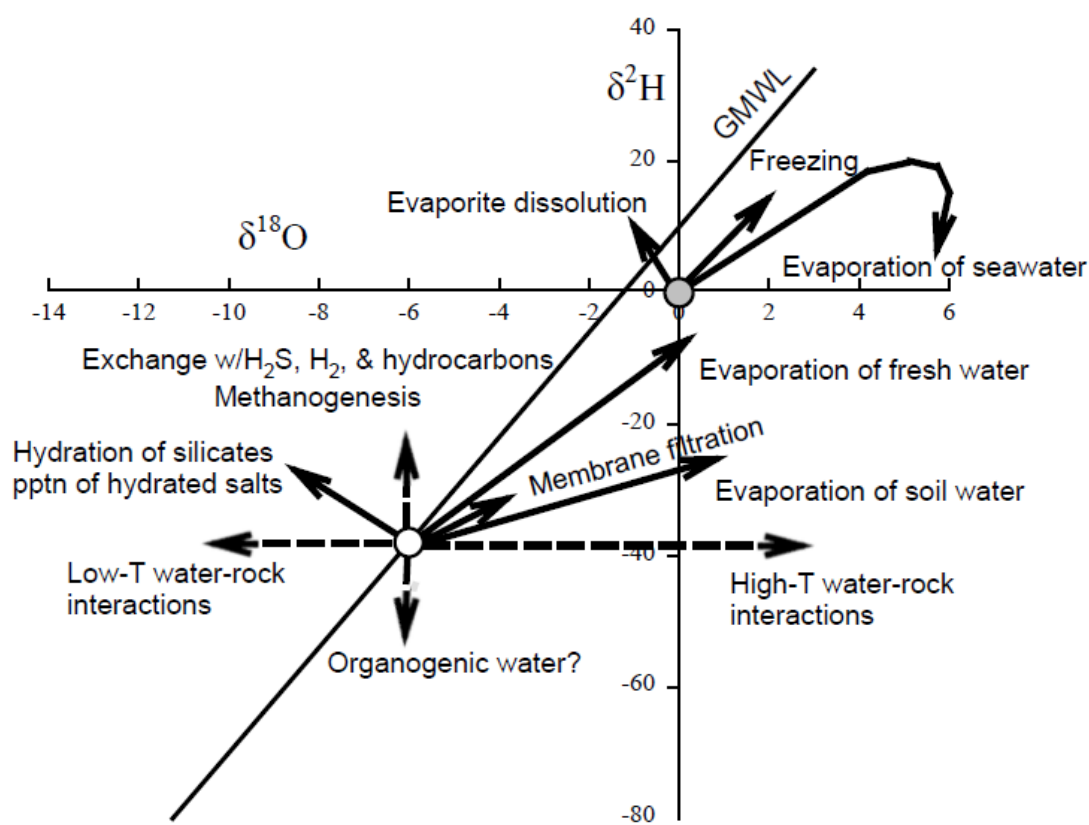
Figure 2.12: Isotopic evolution pathways of water for primary brine-forming processes (solid lines), as well as secondary, modifying processes (dashed lines). Line lengths reflect the relative potential impact of each process on water composition. Isotope ratios are expressed on the activity scale (see Sectoin 2.3.2). Modified from Horita (2005).

Subaerially, the most important brine-forming process is the evaporation of surface water, during which, both lighter isotopes are fractionated into the vapour phase, leaving the remaining water enriched in ^{2}H and ^{18}O. In δ^2H/δ^{18}O space, the trajectory of evaporating water bodies has a slope of 4–6. The variation in this slope is influenced by several physical (temperature, relative humidity, salinity) and hydrologic (inflow, outflow, fraction of remaining water) factors (Horita, 2005).

During extended evaporation of water in restricted basins, δ^2H and $\delta^{18}O$ values show a complex, hook-shaped pattern, initially both increasing during the early stages of evaporation, then reaching maxima, and finally decreasing during extreme desiccation stages. The reversal in the earlier isotopic enrichment trend is due to precipitation of hydrous minerals such as gypsum, as they preferentially incorporate the heavier isotopes in their mineral structure (Lloyd, 1966; Fontes and Gonfiantini, 1967; Sofer and Gat, 1975; Holser, 1979; Pierre et al., 1984; Knauth and Beeunas, 1986; Chacko et al., 2001). The exact shape of this curved trajectory depends on several parameters, including the initial chemical and isotopic compositions of the water, relative humidity, and the isotopic composition of atmospheric water vapour (Sofer and Gat, 1975); several paths are illustrated in Figure 2.13.
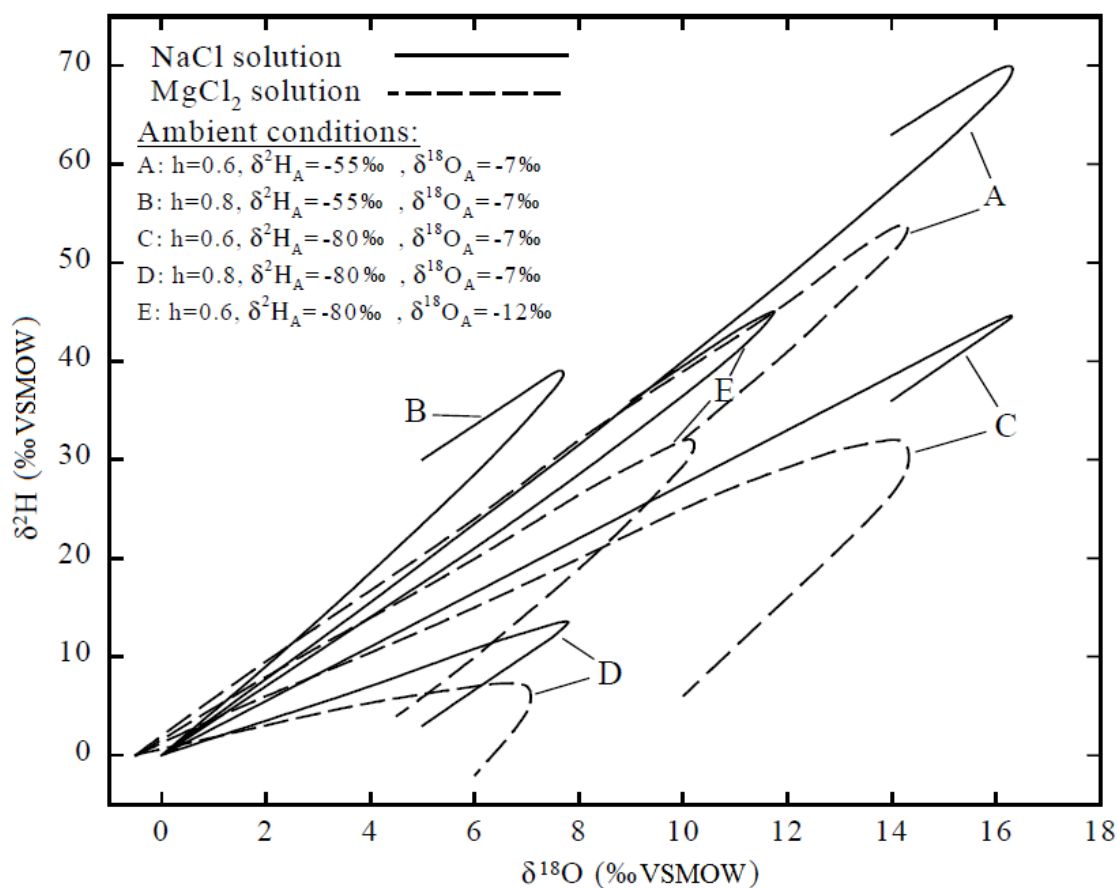
Figure 2.13: Numerically-modelled trends for δ^2H concentration and $\delta^{18}O$ activity values during evaporation of 0.5 molal NaCl and MgCl$_2$ solutions under different conditions (h=humidity; $\delta^{18}O/^2H_A$ = isotopic composition of ambient vapour). The "loop" occurs only in very late stages of evaporation (Sofer and Gat, 1975).

In the subsurface, numerous reactions affect the isotopic composition of groundwaters. Dissolution of anhydrous evaporite deposits, such as halite or anhydrite, does not change the isotopic composition ratio of water, but it may change the isotopic activity ratios, as explained in the following section. Dissolution or diagenesis of hydrated minerals, however, affects the water's isotopic composition, since the hydration waters are typically of a different composition. Shale ultrafiltration – the forcing of water through a shale layer under pressure – is also known to have a small isotopic effect, leaving both the heavier isotopes and salts behind (Coplen and Hanshaw, 1973). Over geologic timescales, isotopic exchange between water and carbonate rocks at elevated temperatures generally enriches the waters in ^{18}O, but does not have a significant effect on hydrogen, since the volume of water is usually much greater than that of hydrogen-bearing minerals. There are numerous other subsurface processes that can modify the isotopic compositions of brines, including other diagenetic reactions, exchange with other liquid or gaseous species, and mixing between different water types (Horita, 2005).

2.3.2 Isotopic salt effect and analytical considerations for saline waters

One fundamental aspect of hydrogen and oxygen isotopic compositions of saline waters is that their isotope activity ratios differ from their concentration ratios, a behaviour known as the "isotope salt effect". The isotope concentration ratio refers to the actual ratio of the abundance of the heavy and light isotopes, while the activity ratio is the "effective" ratio in terms of the participation of the isotopes in chemical reactions. The difference between the isotope activity and concentration ratios in saline waters is caused by interaction between water molecules and salt ions, forming hydration spheres that preferentially incorporate one of the isotopes over the other. This salt effect was first discovered by Taube (1954), but was not systematically investigated and quantified until the 1970's (Sofer and Gat, 1972, 1975; Stewart and Friedman, 1975). The isotope salt effect, Γ, can be thermodynamically defined as follows (Horita et al., 1993):

$$\Gamma = \frac{R_{activity}}{R_{concentration}} = \frac{a(^1H^2HO)/a(H_2O)}{X(^1H^2HO)/X(H_2O)} \text{ or } \frac{a(H_2^{18}O)/a(H_2^{16}O)}{X(H_2^{18}O)/X(H_2^{16}O)} = \frac{\gamma(^1H^2HO)}{\gamma(H_2O)} \text{ or } \frac{\gamma(H_2^{18}O)}{\gamma(H_2^{16}O)} \quad (2.1)$$

where *a*, *X*, and *γ* denote the activity, mole fraction, and activity coefficient of isotopic water molecules, respectively. R represents the $^{18}O/^{16}O$ or $^{2}H/^{1}H$ ratio, and since R = $1+10^{-3}\delta$, the *δ* value for the salt effect can be given as (Horita, 2005):

$$10^{3}\ln \Gamma \approx \delta_{activity} - \delta_{concentration} \tag{2.2}$$

The magnitude of the salt effect varies by isotope and by ion content. For oxygen, the effect is such that the measured (activity) values are less enriched in ^{18}O than the true (concentration) values. Magnesium salts induce the largest effect, with no significant difference between $MgSO_4$ and $MgCl_2$, while the impact of $CaCl_2$ is about half that of magnesium, and KCl shows a slight effect in the opposite direction, i.e., making the brine appear more enriched in ^{18}O than it actually is. NaCl seems to have no effect (Sofer and Gat, 1972). Conversely, the salt effect on hydrogen isotopes is the opposite of that observed for oxygen, with activity values more ^{2}H-enriched than concentration values. $CaCl_2$ shows the greatest effect, slightly greater than $MgCl_2$, and about twice that of KCl; NaCl shows only a very small effect (Sofer and Gat, 1975).

In mixed salt solutions, the salt effects of the individual ions are simply additive, with no apparent interference effects between salts. The salt effect from each salt increases in a predictable, linear fashion according to molality. Experimentally-derived equations from Sofer and Gat (1972, 1975) can be used to predict the salt effect in mixed salt solutions:

$$for\ oxygen: \quad 10^{3}\ln \Gamma = -1.11m_{Mg} - 0.47m_{Ca} + 0.16m_{K} \tag{2.3}$$

$$for\ hydrogen: \quad 10^{3}\ln \Gamma = 6.1m_{CaCl2} + 5.1m_{MgCl2} + 2.4m_{KCl2} + 0.4m_{NaCl} \tag{2.4}$$

When working with saline waters, it is important to be mindful of these effects, and report and interpret data using proper scales. Different analytical techniques produce data on different scales. Equilibration techniques yield isotopic activity data, while distillation/ quantitative extraction methods, such as U- or Zn-reduction (Bigeleisen et al., 1952; Friedman, 1953; Coleman et al., 1982), yield concentration data. However, it should be noted that the latter type of technique is fraught with challenges when analyzing saline waters, as hydrated salts are left behind from which it is extremely difficult to fully extract all sample water, and thus considerable isotopic fractionations can occur (Horita,

1989). Horita and Gat (1988) developed an azeotropic distillation procedure that removed the cations prior to distillation, which reportedly gave acceptable results for hydrogen. Horita and Gat (1989) compared this method with equilibration techniques, illustrating the salt effect for δ^2H for a suite of Dead Sea brines. Figure 2.14 compares this work with erroneous traditionally-generated δ^2H data reported in the literature (Gat, 1984).
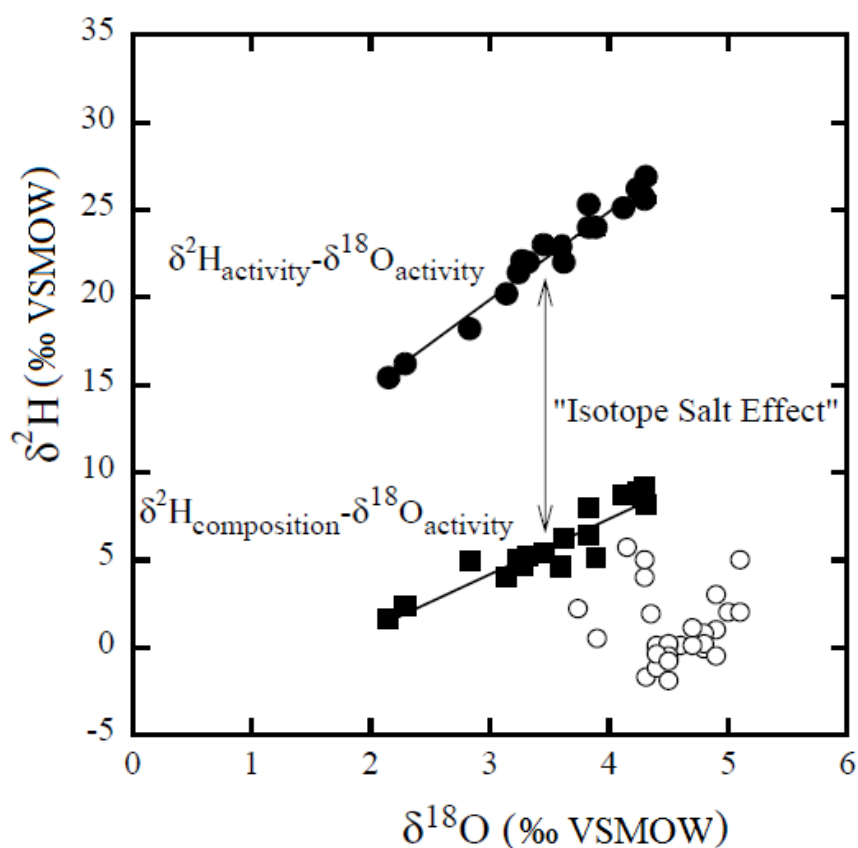
Figure 2.14: Plot of δ^2H activity and concentration values vs. $\delta^{18}O$ activity values for Dead Sea brines (modified from Horita, 2005). Black symbols are from Horita and Gat (1989) using equilibration techniques (activity values) and a modified distillation technique (hydrogen composition values), and show the expected positive linear relationship between the two isotopes, while previously reported concentration values (open circles, from Gat, 1984) using distillation techniques show large systematic errors.

Chapter 3

3 Methodology

The following chapter describes the methods used throughout this project, including the collection and treatment of water samples, the different techniques used to analyse them in the laboratory, and the mixing model program used to develop the geochemical tool.

3.1 Sample Collection

Water samples were collected between winter 2011 and summer 2013 from a variety of sites throughout southwestern Ontario. Sample sites were selected with the help of the MNR, with the goal of achieving a good geographical distribution and representation of all major water-producing formations, although ultimately sampling opportunities were dependant on site operator cooperation. The majority of sampling sites were active oil and gas wells with known producing intervals and good casing records. From these sites, water was sampled whenever possible directly from the wellhead or flow-lines from the wellhead to production batteries, but in some cases water was also collected from separator tanks and brine storage tanks. Other sampling sites included artesian springs, quarries, abandoned wells, and new wells being drilled by cable-tool rig. The latter provided an opportunity to sample multiple water zones from a single well, with (hopefully) minimal contamination, as these rigs do not use drilling fluids. Some samples from hydrocarbon well sites are also expected to have some contaminated or modified as a result of production-related factors such as injection of fresh water and/or reinjection of brine, potentially modified by evaporation while in surface tanks, and hot water treatment to remove wax build-up. Such contaminated can often be detected in the isotope results, as discussed in later sections, and during sampling, the well operators were questioned regarding such production activities that might modify water compositions. Samples thusly affected are noted in Appendix B. While such samples differ from the original natural baseline, their existence should be considered when interpreting results of our geochemical tool for identifying sources of leaking well fluids, particularly in areas with extensive production histories.

At each sampling site, five bottles were collected, when possible – two 500 mL HDPE bottles, for cation and anion analysis; one 250 mL HDPE bottle for analysis of sulphate isotopes (δ^{34}S and δ^{18}O); one 60 mL HDPE bottle for analysis of water isotopes (δ^2H and δ^{18}O); and one 40 mL sepia glass vial with a septa cap for analysis of dissolved inorganic carbon isotopes (δ^{13}C). The anion aliquot was also used for analysis of strontium isotopes (^{87}Sr/^{86}Sr).

At active well sites, water samples were ideally collected directly from the wellhead, to ensure the most representative, uncontaminated sample possible. Sometimes this was not possible, however, and on occasion, water was collected from other points, such as separator tanks and brine tanks. While some sample collection procedures reported in the literature (e.g., Kharaka et al., 1987) involve complex line systems to prevent atmospheric exposure, with in-line filtration and geochemical parameter monitoring equipment and a N_2-sparging system, such was not deemed feasible in our situation and a simpler approach was used, described in the following paragraph. In many cases, the brine samples were quite dirty and oily, and would quickly clog any in-line filter, possibly damage the equipment, and render the line very difficult to clean and reuse. Brines coming up from wells were also generally under high pressure, frequently associated with methane, and had sporadic flow. Also, with the possible exception of direct wellhead collection, water from many sampling sites would have already been exposed to the atmosphere to some extent, rendering an in-line system irrelevant. Finally, several samples were also collected by drillers, well inspectors and site operators, and thus it was decided that adoption of a complex sampling apparatus was not ideal.

To deal with this unusual and challenging sampling environment, a simpler system was devised and used for all sampling situations. Sample water was first transferred into a plastic container, which had been cleaned with soap and rinsed with deionized water and then ultra-pure Millipore water in the laboratory, and rinsed in the field with sample water. Water was then filtered into the sample bottles using a large-volume-capacity polypropylene filtering apparatus (similarly cleaned) from Cole Parmer, equipped with 47 mm-diameter 0.4 μm glass fibre filters, coupled to a 60 mL disposable syringe. Water was preferentially collected from the bottom of the container, and the processing was done as

quickly as reasonably possible to reduce atmospheric exposure; the DIC and sulphate bottles, being more sensitive to exposure, were filtered before the other bottles. Following filtration, the cation and sulphate aliquots were acidified with 0.5M HCl to pH ≤3, for preservation purposes, and in the latter case, to also eliminate carbonate from the sample, which is necessary for later processing steps. All bottles were filled to a high meniscus, leaving little to no headspace, capped tightly and finally, the join between cap and bottle was sealed with Parafilm™ tape to reduce the potential for atmospheric exchange. While in the field, samples were stored in an insulated cooler box with freezer packs, and then kept in a refrigerated room at 4^0C upon returning to the university.

At several sites, basic water chemistry parameters, including temperature, pH, TDS, salinity and conductivity were measured in field with a PCSTestr 35 multiparameter meter (Oakton Instruments). However, this step was not always conducted, for several reasons, including the nature of the sampling sites often being unconducive to reliable temperature and pH measurements, and the latter three parameters were analyzed in the laboratory, and also because these parameters were not considered directly important for the primary goal of the project, being unsuitable as tracers for discriminating between formations.

3.2   Sample analysis

A number of geochemical parameters were analysed over the course of this study: the oxygen and hydrogen isotopes of water (δ^{18}O and δ^{2}H), the oxygen and sulphur isotopes of dissolved sulphate ions (δ^{18}O$_{SO4}$ and δ^{34}S$_{SO4}$), carbon isotopes of dissolved inorganic carbon (δ^{13}C$_{DIC}$), strontium isotopic ratios (^{87}Sr/^{86}Sr), and major and minor ion chemistry.

This section describes the procedures used for the analysis of these geochemical parameters in further detail, including instrumentation, sample preparation procedures, standardization, and reproducibility of the data.

Stable isotope data is reported in the standard delta notation (Coplen, 2011):

$$\delta \text{ (in per mil, ‰)} = \left(\frac{R_{sample}}{R_{standard}} - 1 \right) \qquad (3.1)$$

where R is the ratio of heavy to light isotopes (e.g., $^{18}O/^{16}O$) and standard refers to the international reference material for the isotope in question - oxygen and hydrogen: Vienna Standard Mean Ocean Water (VMOW); carbon: Vienna Pee Dee Belemnite (VPDB); sulphur: Canyon Diablo Troilite (CDT).

3.2.1　　　Water isotopes analysis

The oxygen and hydrogen isotopic ratios ($\delta^{18}O$ and δ^2H) of water were analysed at the Laboratory for Stable Isotope Studies (LSIS), The University of Western Ontario, London, Ontario, Canada, using equilibration methods (see below) and a Thermo Finnigan GasBench II connected to a Thermo Finnigan Delta^{plus} XL continuous-flow isotope ratio mass spectrometer (CF-IRMS). Both oxygen and hydrogen isotope methods yield data on the activity scale for brines; accordingly, the salt effect corrections by Sofer and Gat (1972, 1975) (equations 2.3, 2.4) were used to convert the data to the isotopic concentration scale. Results on both scales are reported in Section 4.1 and in Appendix B.

3.2.1.1　　　Oxygen isotopes

Water oxygen isotopes ($\delta^{18}O$) were analysed by the traditional CO_2-equilibration method (e.g., Epstein and Mayeda, 1953). One (1) mL volumes of sample water were pipetted into septum-sealed glass vials, and placed in the heated GasBench block. The atmosphere inside the vials was then flushed and replaced with 0.3% CO_2 in He. Samples were equilibrated at 35ºC for at least 3-4 days; the GasBench did not have shaking capability but this equilibration time was deemed adequate, given that Fritz et al. (1986) for similar brines reported a maximum equilibration time of 20h, with shaking.

Four in-house laboratory standards calibrated to VSMOW were placed regularly throughout each analytical run: LSD (–22.57‰), MID (–13.08‰), EDT (–7.27‰) and Heaven (–0.27‰). These standards were calibrated against the international standards VSMOW and SLAP as described by Coplen (1994). LSD and Heaven were used to generate a two-point calibration curve to correct the raw isotopic ratios to their true isotopic ratios, and both had overall reproducibilities of ±0.07‰ (n=32 and n=27,

respectively). MID and EDT were omitted from the curve and were used to verify the accuracy of the calibration; their average $\delta^{18}O$ values over all runs were -12.94 ± 0.14‰ (n=28) and -7.32 ± 0.12‰ (n=29), respectively. Sample duplicates were analyzed approximately every 5 samples to verify reproducibility, and samples were occasionally rerun in later analytical sessions to check inter-run reproducibility and sample preservation. Overall reproducibility of sample duplicates averaged ± 0.10‰.

3.2.1.2   *Hydrogen isotopes*

Water hydrogen isotopes (δ^2H) were analysed with a H_2-equilibration method described by Horita (1988). Equlibration was chosen over other more traditional techniques such as distillation and reduction over hot metal, in order to avoid difficulties associated with such techniques (see Section 2.3.2), and also because the LSIS Zn-reduction line had been dismantled. The comparability of data generated by these two methodology types is discussed in Appendix F.

Similar to the oxygen isotope equilibration technique, 1 mL sample volumes were used, in the same type of vials. A re-usable platinum catalyst known as a 'Hokko stick' (Shoko Co. Ltd, Japan), similar to the 'Hokko beads' described by Horita (1988), was also added to each vial. The catalyst consists of a thin rectangular stick composed of hydrophobic styrene divinyl benzene copolymer infused with 3 wt% Pt (Horita, 1988). The catalyst stick rests on the bottom of the vial, and about half its length lies above the water surface. Samples with high levels of H_2S were pre-treated by addition of copper wire, since H_2S may poison the catalyst (Révész and Coplen, 2008). Waters were equilibrated with 2% H_2 in He at 35ºC in the GasBench for approximately 2 hours, as recommended by Horita (1988) for a Dead Sea brine. The Hokko sticks were cleaned between uses by rinsing with deionized water in a sonic bath, dried overnight in an oven at ~60ºC, and then stored in a desiccator. Equilibration tests with deionized water following the final analysis demonstrated that the catalytic ability of the Hokko sticks had not been impaired by H_2S poisoning, other reactions with the samples, or cleaning.

The same internal standards were used as for with oxygen: LSD (-161.8‰), MID (-108.1‰), EDT (-56.0‰) and Heaven ($+88.7$‰). LSD and Heaven were again used for

calibration, and had overall reproducibilities of ±1.99‰ (n=56) and ±2.05‰ (n=50), respectively. Accuracy was assessed using MID and EDT, which had average δ^2H values over all analytical runs of −107.74 ± 2.39‰ (n=47) and −55.56 ± 2.08‰ (n=45), respectively. Sample duplicates were analyzed about every 5 samples, and replicates of samples analyzed in previous runs were occasionally included. Overall reproducibility of sample duplicates averaged ±1.63‰.

3.2.2 DIC carbon isotopes

Stable carbon isotopes ($\delta^{13}C$) of dissolved inorganic carbon (DIC) in the water samples were also analysed at LSIS, also on the GasBench II coupled with the Delta[plus] XL CF-IRMS, using a method similar to that of Torres et al. (2005). Depending on DIC concentrations, between 1-7 mL of sample were injected into a septum-sealed glass vial, the atmosphere within which having been previously replaced by He. Roughly 5 drops of 104% orthophosphoric acid were added to the vials prior to flushing with He. The acid reacts with the DIC to release CO_2 gas. The vials were placed in the GasBench to react for at least 3 hours at 35ºC.

Four solid carbonate internal reference standards, calibrated to the international VPDB standard, were used: NBS-19 (+1.95‰), NBS-18 (−5.0‰), Suprapur (−35.28‰) and WS-1 (+0.76‰). These were weighed into the bottom of glass vials, which were then placed in a rack in a horizontal position, such that acid could be added to the upper section of the vial (closest to the opening), in order for the acid to remain separate from the standard at the opposite end. The septum caps were then attached and the atmosphere in the vials replaced with He; after flushing, the vials were turned upright so the acid could flow down and react with the standard. These standards were placed in the GasBench prior to the samples, and left to react until there no more visible standard material remained. An aqueous standard of reagent-grade $NaHCO_3$ was also prepared, treated in the same manner as the samples; a solid version of this standard was also prepared in the same way as the other standards, to verify that there was no fractionation involved in the reaction of the acid with the samples.

These standards were interspersed throughout each run. NBS-19 and Suprapur were used to calibrate the raw $\delta^{13}C$ values to VPDB, and had reproducibilities of $\pm0.09‰$ (n=18) and $\pm0.10‰$ (n=20), respectively. NBS-18 and WS-1 were used to check the accuracy of the measurements, and had average $\delta^{13}C$ values over all runs of $-4.99 \pm 0.09‰$ (n=19) and $+0.76 \pm 0.12‰$ (n=18), respectively. The solid and liquid $NaHCO_3$ standards had values of $-2.78 \pm 0.07‰$ (n=7) and $-2.68 \pm 0.39‰$ (n=5), respectively. Duplicate samples were placed every 8-10 samples, and their overall reproducibility averaged $\pm0.20‰$.

3.2.3 Sulphate isotopes

3.2.3.1 Sample preparation

Prior to isotopic analysis of sulphate, the dissolved sulphate ions in each water sample had to be converted to a stable solid form. The traditional method for doing so is to precipitate the sulphate as barium sulphate ($BaSO_4$) (Carmody et al., 1998). An amended version of this approach was used in this project, as described below.

3.2.3.1.1 H_2S sparging

Some samples, particularly those from shallower formations, contained elevated levels of hydrogen sulphide (H_2S). There was concern that this H_2S might oxidize to sulphate, and thus affect the isotopic results. While it was logistically unfeasible to remove this H_2S in the field, an apparatus was designed to sparge the H_2S from samples in the laboratory, minimizing exposure to the atmosphere, prior to the precipitation of $BaSO_4$. This procedure is described below and the apparatus used is illustrated in Figure 3.1.

A 250 mL Erlenmeyer flask with a side-arm outlet port served as the sparging chamber. A rubber stopper sealed the main (top) opening of the flask, and was pierced by two glass tubes - a longer one reaching to the bottom of the flask, and a shorter one terminating shortly below the rubber stopper. The external ends of these glass tubes were attached to two rubber lines carrying pure N_2 gas. A short length of tubing was attached to the flask's side outlet, and a funnel was attached to the other end. A lid from a spare sample bottle was attached to the funnel, and a hole drilled through its center. The nitrogen flow was

turned on, thus flushing the atmosphere in the flask out through the funnel port. After about five minutes, the flask was considered to be adequately flushed with nitrogen, and the rubber tubing was unattached from the shorter glass tube, allowing the nitrogen flow to escape the flask from this port rather than the funnel. The sample bottle to be sparged was positioned directly beneath the funnel, and the cap on the bottle was then unscrewed and the bottle quickly attached to the cap on the funnel. The contents of the sample bottle were then upended into the funnel, thus flowing into the flask, while the constant nitrogen flow vented through the upper port. Nitrogen, flowing through the longer glass tube into the bottom of the flask would bubble through the sample water, sparging out the H_2S. Once emptied, the sample bottle could then be detached from the funnel, and the second nitrogen line reattached to the shorter glass tube, flushing the gas above the water out through the funnel port. The samples were left for about 10 minutes, deemed sufficient to complete the sparging; Carmody et al. (1998) suggested 10-20 minutes for a much larger volume (8-10 L). The Erlenmeyer flask was not quite large enough to hold the full 250mL sample volume without bubbling liquid out through the funnel port, so a small un-sparged aliquot was left over. This was precipitated independently from the main sparged sample, and allowed for assessment of the process' effectiveness. While only a few samples had noticeable levels of H_2S, all samples were sparged for the sake of consistency.
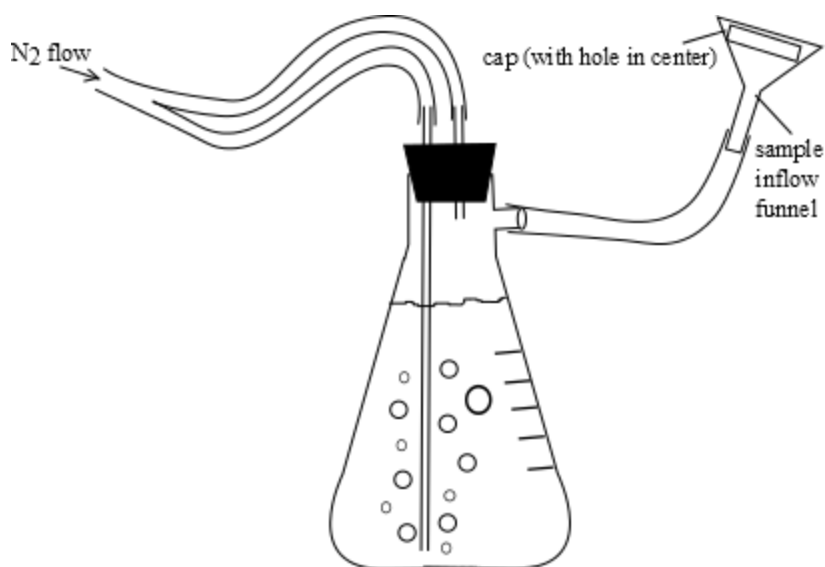
Figure 3.1: H_2S sparging apparatus, as described in text.

3.2.3.1.2 $BaSO_4$ precipitation

Following sparging, samples were checked to ensure that pH was ≤3, and more acid was added if necessary. The goal of acidification is to convert any dissolved inorganic carbon species to $CO_{2(aq)}$; at higher pH, $CO_3^{2-}{}_{(aq)}$ is present, which would be precipitated as $BaCO_3$ alongside $BaSO_4$ and thus affect the oxygen isotope results. Also, any samples that still had visible traces of oil, other particulate matter, or were strongly coloured were re-filtered, at 0.45 μm.

Approximately 60 mL of sample was then transferred into a clean glass beaker along with a magnetic stir bar, and placed on a combination hot plate/magnetic stir plate. Samples were heated to approximately 70-90°C. The main goals of heating are to help drive off dissolved CO_2 prior to $BaSO_4$ precipitation, and to facilitate growth of coarser-grained $BaSO_4$ crystals (Carmody et al., 1998). After heating to the target temperature, about 5 mL of 0.2 M $BaCl_2$ solution was added (representing a strong excess of barium), causing precipitation of sulphate as $BaSO_4$; $BaCl_2$ solutions were prepared fresh daily using acidified Millipore water and reagent-grade $BaCl_2$ from Fisher Scientific. The samples were stirred and heated for 10 minutes to ensure reaction completeness.

After the reaction was complete, the precipitate and sample liquid were transferred into clean centrifuge tubes, and centrifuged for 12 minutes at 12,000 RPM, to separate the precipitate from the liquid. The liquid was then transferred back into its original beaker, and further $BaCl_2$ solution was added to verify that all sulphate had been precipitated. If new precipitate formed, or if some of the original precipitate had escaped with the liquid into the beaker, the first centrifuge step was repeated. Otherwise, the precipitate remaining at the bottom of the centrifuge tube was rinsed and re-centrifuged three times, to remove any remaining original sample water. The first two rinses were made using Millipore water acidified to about pH 2.5, to inhibit dissolution of atmospheric CO_2 that might react with any barium left in the small amount of liquid not decanted. The final rinse was made using normal, un-acidified Millipore water. After the third rinsing and centrifugation step, the precipitate was transferred with more Millipore water into a cylindrical glass vial, and placed in an oven at ~60^{0}C to evaporate to dryness. Once dried,

the clean precipitate was removed from the vial, weighed, and transferred into a small glass vial for storage. All equipment used during this process, as well as the sparging process, was washed thoroughly with Sparkleen soap, rinsed with de-ionised water, and rinsed again with Millipore water before drying overnight.

A stock solution of reagent-grade $NaSO_4$ was prepared to serve as a standard for experimental reproducibility. Aliquots of this solution were periodically precipitated alongside samples. As a further check on reproducibility, duplicates of several samples were precipitated, sometimes simultaneously, and sometimes on a different day, to ensure consistency of the precipitation process.

3.2.3.2   Sulphur isotope analysis

Sulphur isotope ratios ($\delta^{34}S_{SO4}$) of the $BaSO_4$ precipitates were measured at the G. G. Hatch laboratory at the University of Ottawa, Ottawa, Ontario, Canada. About 0.7 mg of each sample was weighed into tin capsules along with about 2.1 mg of V_2O_5 as a combustion agent. Samples were combusted in an Elementar Vario Micro Cube Elemental Analyser (EA) coupled to a Thermo Finnigan Delta^{plus} XP CF-IRMS. The sulphur in the samples was combusted to SO_2 gas at 1,800°C, which was trapped in a special molecular sorption column in the EA. Once all other combustion gases had passed through the system, the sorption column was heated to 230ºC to release the SO_2, which was then carried by helium into the IRMS for isotopic measurement. The EA was also used to measure the amount of sulphur (wt% S) in each sample, as a further check on sample purity and completeness of combustion. The amount of sulphur measured averaged 14.5 ± 0.6‰, relatively close to the theoretical value of 13.7‰.

Three different in-house standards were interspersed through the analytical session - NBS 127 (+20.3‰), T123-1 (−0.22‰) and HAS-1 (+24.4‰). A solid Na_2SO_4 material as well as $BaSO_4$ precipitates prepared from a solution composed of the same Na_2SO_4 were also analyzed. The former had an average $\delta^{34}S$ composition of −2.06 ± 0.74‰ (n=5) and the latter had an average composition of −2.14 ± 1.37‰ (n=8), indicating that no significant fractionating effects occurred during precipitation. Sample duplicates were placed every 10 samples; precipitation method duplicates were also included as part of this

examination of reproducibility. Overall average sample reproducibility was ±0.35‰. Several precipitates generated from non-sparged aliquots were also analysed. These samples generally had $\delta^{34}S$ values 1-3‰ higher than their sparged versions.

3.2.3.3 *Oxygen isotope analysis*

The oxygen isotope ratios ($\delta^{18}O_{SO4}$) of the $BaSO_4$ precipitates were analysed at LSIS. About 0.2 mg of each sample was weighed into silver capsules, combusted to carbon monoxide in a Thermo Finnigan High-Temperature Conversion Elemental Analyzer (TC/EA) and analysed on a Thermo Finnigan Delta^{Plus} XL CF-IRMS. A liquid nitrogen trap placed between the reactor and the gas chromatograph (GC) removed unwanted volatiles. Two international standards, IAEA-CH-6 and NBS 127, were used to calibrate the raw data to VSMOW. Their accepted $\delta^{18}O$ values are +36.4‰ (Kornexl et al., 1999) and +9.3‰ (IAEA, 1995), respectively; both had reproducibilities over all runs of ±0.42‰ (n=72 and n=67, respectively). Two in-house laboratory standards, Barite 1 and Barite 2, were used to assess accuracy. The $\delta^{18}O$ values for Barite 1 averaged +18.54 ± 0.71‰ (n=19), compared to its accepted value of +18.67 ± 0.28‰. Values for Barite 2 averaged +13.12 ± 0.37‰ (n=20), compared to its accepted value of +13.16 ± 0.31‰. Sample duplicates were placed every 5 samples, and again wet chemistry method duplicates were also analysed. Overall average sample reproducibility was ±0.25‰.

3.2.4 **Strontium isotope analysis**

The $^{87}Sr/^{86}Sr$ ratios of dissolved strontium ions in the water samples were analysed by Isotope Tracer Technologies Inc. (ITT), Waterloo, Ontario, Canada. After analysing the samples' ion chemistry, 60 mL of the filtered but otherwise untreated anion aliquot was used for the strontium isotope analysis.

3.2.4.1 *Preparation*

A few micrograms of Sr^{2+} can be analyzed using the analytical method utilized, although the ideal amount is between 25-100 μg. Samples were refiltered by ITT through a 0.2 μm

filter. Oil-field samples were heated to 65-75°C and treated with paraffin flakes to absorb any residual oil residue prior to filtration. Samples were then evaporated to dryness. Based on the method of Horowitz et al. (1992), Sr^{2+} was separated using a Sr^{2+}-specific ion-exchange resin from Eichrom (1.0M 4,4'(5')-ditbutylcyclohexano 18-crown-6 (crown ether) in 1-octanol); the resin was loaded onto an inert chromatographic support (40% w/w) with the Sr^{2+} resin bed density at approximately 0.35 g/mL. Prior to transferring to the column, about 160-165 mg of resin was slurried in a few mL of 0.05M HNO_3. The column length used varied from 2-4 cm, depending on sample Sr^{2+} content. The resin columns were preconditioned with at least 1 mL of 7M HNO_3, for optimal Sr^{2+} retention. Dried samples were dissolved in 1.5-3 mL of 7-8M HNO_3 and transferred into the resin columns. The columns were washed with 5 free column volumes (FCV; the volume of the empty column) of 5M HNO_3 to remove all other alkali and alkaline earth metals, and then rinsed with 1 FCV of ultra-pure water. Finally, Sr^{2+} was then eluted with 5-6 FCV of ultra-pure water, collected in a Teflon container and evaporated to dryness and the columns washed thoroughly with ultra-pure water (~50 FCV).

3.2.4.2 *Analysis*

The strontium isotopic ratios were determined on a Thermo Finnigan Triton Thermal Ionization Mass Spectrometer (TIMS). Once the eluted samples were dry, they were re-dissolved in a few microliters of 0.3M H_3PO_4. They were then placed on a filament, dried in a positive laminar flow air chamber, and then mounted onto the Triton analysis magazine and ionized. Each magazine typically consisted of 16 samples, 3 standards (NIST 987) and 2 duplicates. Each sample measurement consisted of 200 readings to determine the $^{87}Sr/^{86}Sr$ ratio. The analytical sessions were monitored to ensure that standards remained within the working limits of $^{87}Sr/^{86}Sr = 0.71025 \pm 0.00004$; the consistency and uniformity of the ion beam was also monitored during the analytical session. If the internal precision expressed absolute standard error of a sample exceeded 0.00002, or if significant deformation or instability of the ion beam was observed, then the sample was repeated within the same run or with a new run. 2σ reproducibility for samples reported by the laboratory was between 0.00002-0.00003. Overall reproducibility of sample duplicates averaged ± 0.0000108.

3.2.5   Ion geochemistry

The major and minor cation and anion compositions of the water samples were analysed by SGS Canada Inc., Lakefield, Ontario, Canada. While this paper focuses on the major ions Na^+, Ca^{2+}, K^+, Mg^{2+}, Sr^{2+}, Cl^-, Br^-, SO_4^{2-}, HCO_3^-, the minor and trace elements Al, Ag, As, B, Ba, Be, Cd, Co, Cr, Cu, Fe, Li, Mn, Mo, Ni, Pb, Sb, Se, Sn, Ti, Tl, U, V, and Zn were also analyzed by SGS; these data are available in Appendix E. Concentrations of CO_3^{2-}, OH^-, dissolved H_2S, total alkalinity, pH, relative density, resistivity, and salinity were also measured.

Ca^{2+}, Fe^{2+}, K^+, Mg^{2+}, Na^+, B and Si were analyzed using inductively coupled plasma optical emission spectrometry (ICP-OES), based on EPA method 200.7 (EPA, 2001). Other trace elements were analyzed by inductively coupled plasma mass spectrometry (ICP-MS) and ICP-OES, based on EPA method 200.8 (EPA, 1994). The main anions, Cl^-, Br^-, and SO_4^{2-}, were measured using ion chromatography, based on EPA method 300.1 (EPA, 1997). The concentrations of HCO_3^-, CO_3^{2-}, OH^-, and total alkalinity were measured by titration, based on method SM 2310 B (APHA, 1998). pH was measured electrometrically with a glass electrode probe (SM 4500-H-B; APHA, 1998), resistivity was calculated based on conductivity, as measured by electrodes (SM 2510-B; APHA, 1998), relative density was determined gravimetrically, salinity was measured indirectly based on other physical properties (SM 2520-A; APHA, 1998), and dissolved H_2S was measured by the methylene blue method (SM 4500- S^{2-} E; APHA, 1998).

3.3   SIAR modelling

Isotope-based statistical mixing models are commonly used by ecologists to estimate food source proportions in complex ecosystems, but can be also used for a wide range of applications. In this study, a mixing model known as SIAR was used to estimate water source proportions in unknown samples from abandoned wells, which are potentially mixtures of water from multiple formations. This section introduces the fundamentals of mixing models in general and discusses the SIAR model.

3.3.1 Mixing models – background

Mixing models use tracers, such as isotopes or elemental abundances, to determine the proportions of sources contributing to a mixture. They rely on the various sources having different compositions, such that the composition of the mixture is intermediate between that of its sources.

In an isotopic mixing model, the proportional contributions of $n+1$ different sources can be uniquely determined by using n different isotopes, based on mass balance equations, given no variability/uncertainty in source or mixture compositions. For example, in a system with 2 isotopes and 3 sources, the mixing model can be formulated with the following equations (Phillips, 2001):

$$\delta J_M = f_A \delta J_A + f_B \delta J_B + f_C \delta J_C$$

$$\delta K_M = f_A \delta K_A + f_B \delta K_B + f_C \delta K_C$$

$$f_A + f_B + f_C = 1 \tag{3.2}$$

where δJ and δK represent the isotope ratios of two elements (e.g., $\delta^2 H$ and $\delta^{18}O$). The subscripts A, B, C, and M represent three sources and the mixture, respectively, and f represents the fractional contribution of each source in the mixture. The three unknowns (f_A, f_B, and f_C) can then be determined as follows:

$$f_A = \frac{(\delta K_C - \delta K_B)(\delta J_M - \delta J_B) - (\delta J_C - \delta J_B)(\delta K_M - \delta K_B)}{(\delta K_C - \delta K_B)(\delta J_A - \delta J_B) - (\delta J_C - \delta J_B)(\delta K_A - \delta K_B)}$$

$$f_B = \frac{(\delta J_M - \delta J_C) - (\delta J_A - \delta J_C)f_A}{\delta J_B - \delta J_C}$$

$$f_C = 1 - f_A - f_B \tag{3.3}$$

However, many systems have too many sources or variability to use such simple linear mixing models. When the number of potential sources exceeds $n+1$, finding unique solutions is not possible - the model is mathematically underdetermined. Nonetheless,

even in such cases, the requirement for mass balance conservation can still be used to find multiple combinations of source proportions that give feasible solutions (Phillips, 2001).

IsoSource (Phillips and Gregg, 2003) is one model commonly used to evaluate these underdetermined problems, providing a suite of possible or feasible solutions. It does so by iteratively evaluating all possible combinations of each source contribution (0–100%) in small increments (e.g., 1%). Combinations that sum to the observed isotopic composition of the mixture, within a small tolerance (e.g., 0.1‰), are considered as feasible solutions, from which the frequency and range of potential source contributions is determined (Phillips and Gregg, 2003). The summary information provided for this range of solutions includes means, error estimates, and minimum and maximum values. However, the use of this information is not easily understood, and many authors often erroneously report the statistical mean solutions as seemingly the 'most likely', despite the fact that the frequency distribution does not actually reflect probability - the frequency simply reflects the number of possible solutions using a given proportion; in IsoSource, all solutions are equally likely. Thus it is recommended that the full range of solutions should be reported (Phillips and Gregg, 2003; Fry et al., 2013).

Mixing models such as described above have several major limitations. None take into account natural variations in source compositions, or variability in the mixture, in cases such as where the 'mixture' represents a group of samples, such as a population of organisms. In systems where isotopes are fractionated between source and mixture, such as diet, many models also do not account for uncertainty in the fractionation factor. Most also ignore differences in elemental concentrations between sources and variability therein. Finally, solutions for undetermined problems, such as provided by IsoSource, do not include a true indication of which solutions are most probable.

3.3.2 Bayesian mixing models

Recently, two programs – MixSIR by Moore and Semmens (2008) and SIAR by Parnell et al. (2010) – have been developed which use a Bayesian statistical approach to overcome the abovementioned limitations of previous mixing models; these models are

able to incorporate variability in the source and mixture compostions, and provide true probability distributions for source proportions. SIAR is the model used in this study, and so its functioning is explained below. However, MixSIR is fundamentally very similar.

SIAR (Stable Isotope Analysis in R) is an open source software package that runs in the free statistical computing environment "R" (http://www.r-project.org/). The model uses Markov Chain Monte Carlo (MCMC) methods to produce simulations of possible source proportions consistent with the data using a Dirichlet prior distribution. The resulting posterior probability density distributions of the feasible source proportions allow direct identification of the most likely solution, and upper and lower credibility intervals describe the possible range of source proportions. It is similar to IsoSource in that it gives a range of feasible solutions, but with the key difference that these ranges represent true probability distributions, through the incorporation of uncertainties regarding source and mixture compositions; it can also account for concentration differences between sources, source-mixture fractionation factors, and allows users to include prior information regarding proportions, if available. For a set of N mixture measurements on J isotopes with K sources, the mixing model can be expressed as follows (Parnell et al., 2010):

$$X_{ij} = \frac{\sum_{k=1}^{K} p_k q_{jk}(s_{jk} + c_{jk})}{\sum_{k=1}^{K} p_k q_{jk}} + \varepsilon_{ij}$$

$$s_{jk} \sim N(\mu_{jk}, \omega_{jk}^2)$$

$$c_{jk} \sim N(\lambda_{jk}, \tau_{jk}^2)$$

$$\varepsilon_{jk} \sim N(0, \sigma_j^2) \tag{3.4}$$

where:
X_{ij} = observed isotopic composition j of the mixture i
s_{jk} = source value k on isotope j; normally distributed with mean μ_{jk} and variance ω_{jk}^2
c_{jk} = source-mixture enrichment factor for isotope j on source k; normally distributed with mean λ_{jk} and variance τ_{jk}^2
p_k = mixing proportion of source k; to be estimated by the model
q_{jk} = element concentration of isotope j in source k
ε_{jk} = residual error, describing additional inter-observation variance not described by the model, σ_j^2 estimated by the model.

In short, SIAR accounts for variation and uncertainty in source and mixture compositions, incorporates concentration dependence and isotopic enrichment factors, and provides a true probability distribution of the solutions. SIAR also has the advantage of allowing the user to include prior information about source proportions, if available from separate lines of evidence. This provides a further constraint on the model and can limit the source proportions distribution. For a full description of the model, see Parnell et al. (2010).

While SIAR is a robust program that works well on a variety of datasets and produces precise proportion estimates, Parnell et al. (2010) recommend a number of caveats to consider when using it and other Bayesian mixing models:

(1)   The underlying system is undetermined, and thus outputs only represent probable solutions, rather than definitive ones. Single-summary values (such as the mean) should be used with care, and there is no reason to expect that the mean proportions of each source sum to unity.

(2)   The variability in the various parameters that SIAR takes into account (e.g., sources, enrichment factors) is assumed to be normally distributed. If there is reason to suspect that these distributions are not normal, it is possible (with some recoding) to change the likelihood function.

(3)   In ecological systems, SIAR assumes that there are no isotopic routing effects within the body of the consumer, and that all isotopes are assimilated equally.

(4)   SIAR will always attempt to fit a model, even if mixture data lie outside the mixing polygon defined by the sources. It is thus important to verify that mixtures lie within this polygon.

Chapter 4

4   Results

This chapter summarizes the isotopic and geochemical data collected in this study, organized by parameter and by formation.

4.1   Stable Isotope Geochemistry

This section presents the isotope results for the water samples collected in this study. A summary of the compositions for each unit is provided in Table 4.2 at the end of the chapter, and a full list of the data is found in Appendix C.

4.1.1   Oxygen and hydrogen isotopes of water

The oxygen and hydrogen isotope compositions (δ^{18}O and δ^2H) of the water samples are reported here both on the original activity scale, as well as corrected to the concentration scale, as per Sofer and Gat's (1972, 1975) equations (Section 2.3.2). For some samples where ion data was not collected, chemical data from nearby wells was used in the calculation of the salt effect correction. The data for all formations are illustrated in Figures 4.1a+b (activity and concentration scale, respectively) relative to the Great Lakes Meteoric Water Line (GLMWL) (δ^2H = 7.1[δ^{18}O] + 1.0; Longstaffe et al., 2011). A number of samples in Figure 4.1 marked as "unknown" do not have source formations that are precisely known; they are not explicitly described in the following sections, but their isotopic compositions are similar to the shallow groundwaters, and accordingly are presumed to have shallow origins.

Appendix A presents the locations of all samples along with the distribution of oxygen isotopes within each formation.
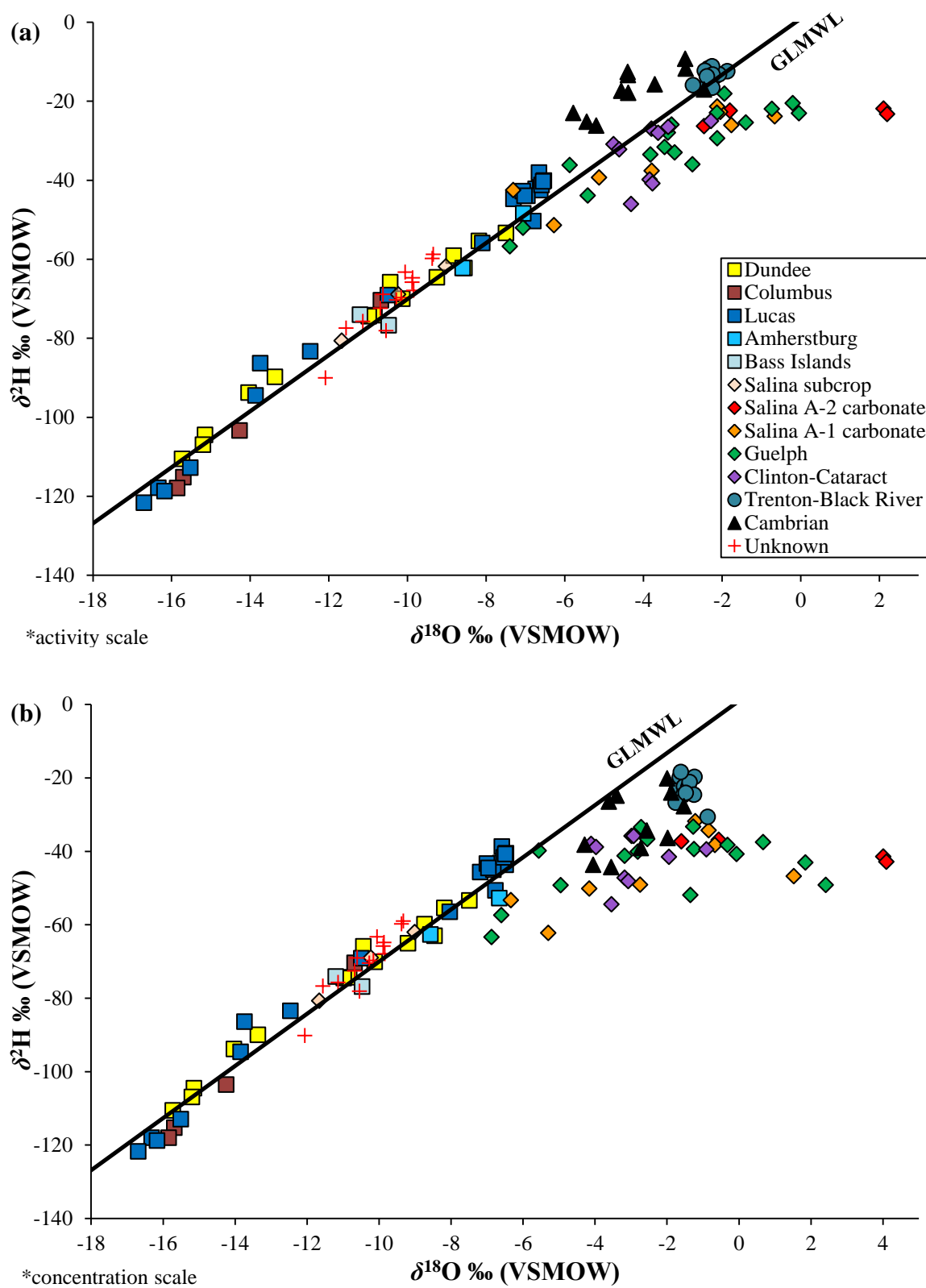
Figure 4.1: Oxygen and hydrogen isotopic compositions for all groundwaters collected in this study, reported on **(a)** the activity scale and **(b)** and the concentration scale.

Dundee Formation

Fourteen water samples were collected from the Dundee Formation, from wells in 8 different fields, plus the Port Dover quarry, giving a good geographical coverage across the region. There was no strong geographical pattern observed in the isotope compositions. Given the low salinity of these waters, the isotope activity and concentration values were essentially equivalent; $\delta^{18}O$ and δ^2H values ranged from -15.7 to $-7.5‰$ and -111 to $-53‰$, respectively. While in most cases only one sample was collected from a given pool, three samples were collected from the Bothwell-Thamesville Pool; the $\delta^{18}O$ values varied from -9.2 to $-8.5‰$ across the pool.

Detroit River Group

Of the twenty-six samples collected from within the Detroit River Group, twenty were from the Lucas Formation, four from the Columbus Member, and two from the Amherstburg Formation. Reasonably good geographical coverage of the region was achieved, although most samples were from Lambton and Elgin Counties. Samples from Lambton County tended to be more ^{18}O-rich than elsewhere in the region. The Lucas Formation samples were from seven separate pools plus two quarries, the Columbus Member samples came from two pools, and the Amherstburg Formation samples were both from different pools. While the Detroit River Group waters were generally more saline than the Dundee Formation waters, they were still dilute enough that the isotope activity and concentration values were largely comparable. For the Lucas Formation, $\delta^{18}O$ and δ^2H compositions ranged from -16.7 to $-6.5‰$ and -122 to $-39‰$, respectively. The Columbus Member waters range from -15.7 to $-10.7‰$ and -118 to $-70‰$ for $\delta^{18}O$ and δ^2H, respectively. Three of the four Columbus samples were from a field undergoing water flooding to boost production, and thus they are likely not truly representative of the regional composition. The flooding water was pumped from the drift aquifer with $\delta^{18}O$ of $-16.5‰$; the affected samples range from -15.7 to $-14.3‰$, with the well furthest from the injection site having the least negative values. The two Amherstburg Formation samples have compositions of $-8.6‰$ and $-6.7‰$ $\delta^{18}O$, and $-63‰$ and $-53‰$ δ^2H. Local variability in the Detroit River Group samples was similar to the Dundee Bothwell-Thamesville pool; there was a 0.5‰ variation in $\delta^{18}O$ between seeps in the McGregor

quarry, a 1.5‰ variation across the Petrolia Pool, and a 0.7‰ variation within the Oil Springs pool.

Salina Group

Four samples were collected from the Salina A-2 carbonate and eight samples from the A-1 carbonate, from the deeper parts of the basin. Also, two samples from the Salina E unit, and one from the A-2 carbonate, were collected from the subcrop belt. Most of the deep samples were collected from wells in Lambton and Kent Counties. Two of the A-2 samples were collected from opposite ends of the Goderich salt mine, and were the most ^{18}O-enriched waters measured in this study; the other two A-2 samples were from separate pools in Kent County. The A-1 samples were from five different pools, mostly in Lambton. With the exception of the subcrop samples, these waters are all highly saline and salt effect corrections were applied, on the order of 1.0-2.2‰ for oxygen, and 9-19‰ for hydrogen. On the activity scale, the A-2 samples range from –2.5 to +2.2‰ δ^{18}O, and –27 to –22‰ δ^2H; on the concentration scale, the range is from –1.6 to +4.1‰ δ^{18}O, and –43 to –37‰ δ^2H. For A-1 samples, the isotopic activity values range from –7.3 to –0.7‰ δ^{18}O and –51 to –21‰ δ^2H; on the concentration scale, values range from –6.3 to +1.5‰ δ^{18}O and –62 to –32‰ δ^2H. Finally, the subcrop samples are more comparable with the shallower Devonian waters, with compositions ranging from –11.7 to –9.0‰ δ^{18}O and –81 to –62‰ δ^2H. While the two A-2 samples from the salt mine were very close in isotopic composition, several A-1 samples taken from the same pools showed considerable variation, on the order of 2-3‰ δ^{18}O.

Guelph Formation

Eighteen samples were collected from the Guelph Formation, all from active oil, gas, or brine production wells in fifteen different pools. There is a fairly good geographical spread in the samples, but they are more concentrated in the western and central parts of the region, particularly Huron, Lambton, Elgin and Essex Counties. There does not seem to be any strong geographical trends in the data, although many of the most ^{18}O-rich samples are from northwest Lambton County. The samples are also highly saline, although to quite varying degrees, and salt effect corrections range from 0.3-2.4‰ δ^{18}O

and 3-26‰ δ^2H. One outlier from Huron County is significantly less saline and has much lower isotopic compositions than the other samples (–11.1‰ δ^{18}O), and has likely been substantially contaminated with fresh water; it is omitted in the ranges reported below, Figure 4.1, and further discussion. The δ^{18}O and δ^2H activity values for the Guelph samples range from –7.4 to –0.04‰ and –57 to –18‰, respectively. On the concentration scale, the range is from –6.9 to +2.4‰ and –63 to –33‰ for δ^{18}O and δ^2H, respectively.

Clinton and Cataract Groups

Nine samples were collected from the Clinton and Cataract groups, mostly from the Thorold and Grimsby formations, but two also from the Irondequoit Formation. All were from wells in Norfolk County, in the large sandstone-hosted gas pools of that region. Three samples are from the Norfolk pool, though relatively separated from each other; two other samples are from the South Walshingham 5-6-VI pool, and the remainder are all from different pools. There are no strong geographical trends in the data, although the easternmost two samples have the most ^{18}O-rich compositions. All samples are brines, and salt effect corrections range from 0.6-1.4‰ δ^{18}O and 7-15‰ δ^2H. The δ^{18}O and δ^2H activity values for these samples range from –4.8 to –2.3‰ and –46 to –25‰, respectively. The range in δ^{18}O and δ^2H concentration values is from –4.1 to –0.9‰ and –54 to –36‰, respectively.

Trenton and Black River Groups

Samples were collected from thirteen different wells completed in the Trenton and Black River groups; the producing intervals include the Cobourg, Sherman Fall, and Coboconk formations, but given the similarity between the lithologies of these units and the geochemistries of their waters, they have all been grouped together for the purposes of this study. The samples are from nine different pools, all from fault-controlled hydrothermal dolomite reservoirs in Essex and Kent Counties; beyond these reservoirs, these units are very tight and do not contain extractable groundwater. With the exception of one sample from the Dover 7-5-V E pool – suspected to be contaminated with fresh water, based on unusually low TDS and somewhat anomalous isotope compositions – these brines have salt effect corrections in the range of 0.6-1.6‰ δ^{18}O and 8-18‰ δ^2H.

Isotopic activity values for these samples have a relatively narrow range, from –2.7 to – 1.9‰ for $\delta^{18}O$, and –17 to –11‰ for δ^2H. Isotopic concentration values vary from –1.7 to –0.9‰ for $\delta^{18}O$, and –31 to –19‰ for δ^2H. There are no significant isotopic differences among reservoirs. Intrapool variation seems to be less than about 0.3‰ $\delta^{18}O$. One well was resampled at a later date, and its isotopic compositions were almost identical.

Cambrian units

Nine wells were sampled from Cambrian reservoirs, representing four different pools in Kent, Elgin, and Oxford Counties, all on the Appalachian side of the Algonquin Arch, as there is no production on the Michigan side. There is possibly a weak trend of isotopically more negative compositions going from southwest to northeast; Dollar et al. (1991) noticed a similar trend. These brines have salt effect corrections in the range of 0.8-1.8‰ $\delta^{18}O$ and 9-22‰ δ^2H. On the isotopic activity scale, these samples plot conspicuously above and to the left of the GLMWL, opposite the trend observed for the other brines, with $\delta^{18}O$ and δ^2H values ranging from –5.8 to –2.9‰ and –26 to –10‰, respectively. However, conversion to the concentration scale shifts them below and to the right of the GMWL, with $\delta^{18}O$ and δ^2H values ranging from –4.3 to –1.5‰ and –44 to –20‰, respectively. Intrapool variation in the Clearville pool is about 1‰ $\delta^{18}O$, while samples in the Willey West pool varied by about 2.5‰ $\delta^{18}O$. Two wells were resampled at a later date, and both had very similar isotopic compositions.

4.1.2   Sulphur and oxygen isotopes of sulphate

This section presents the sulphur and oxygen isotope compositions ($\delta^{34}S_{SO4}$ and $\delta^{18}O_{SO4}$) of the dissolved sulphate ions (Figure 4.2). Sulphide concentrations are also discussed in relation to isotope compositions, as there is often a connection between the two, as discussed in later sections.
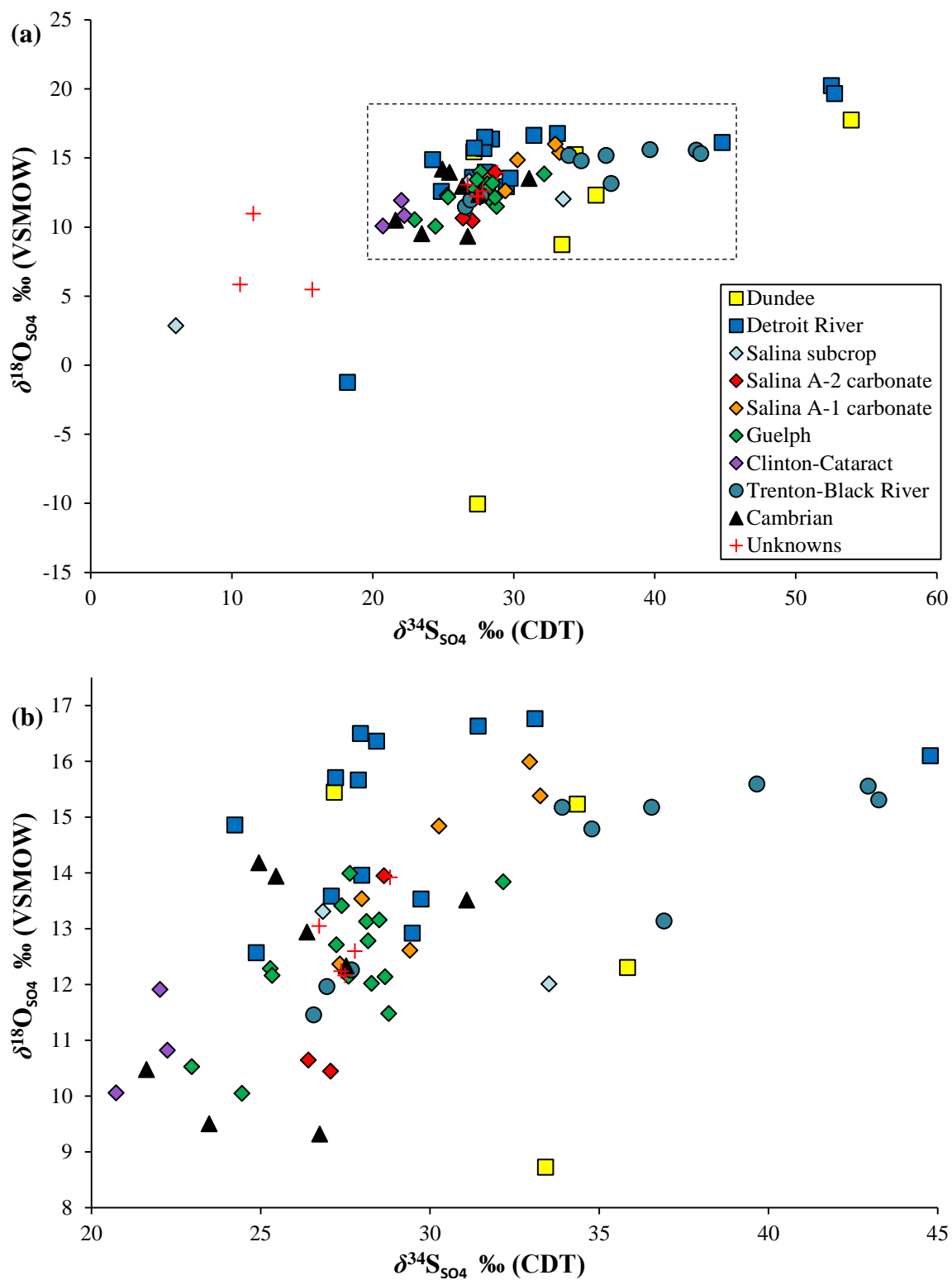
Figure 4.2: Sulphate oxygen and sulphur isotopic compositions for all groundwaters collected in this study. The full range of data is shown in **(a)**, while **(b)** shows an expanded view of the boxed area in **(a)** that contains most of the data.

Dundee Formation

BaSO$_4$ precipitates were generated from seven Dundee Formation samples. The δ^{34}S$_{SO4}$ values ranged from +27.2 to +53.9‰. There is a fairly clear isotopic separation between samples with low and high dissolved sulphide concentrations. Two samples with low (<0.2 ppm) sulphide concentrations have δ^{34}S$_{SO4}$ values near +27‰, while three samples with much higher sulphide levels have higher δ^{34}S$_{SO4}$ values (+34.4 to +53.9‰). The two samples with low sulphide concentrations are located near the Dundee Formation outcrop belt, while the samples with high sulphide concentrations are from deeper in the basin. The δ^{18}O$_{SO4}$ values range from +8.7 to +17.7‰; with the exception of one sample with a value of −10.1‰.

Detroit River Group

Precipitates were collected from seventeen of the Detroit River Group samples – fifteen from the Lucas Formation and one each from the Columbus and Amherstburg Formations. The Lucas Formation samples have a wide range in δ^{34}S$_{SO4}$ values, from +12.2 to +52.8‰. The Columbus and Amherstburg samples have δ^{34}S$_{SO4}$ values of +18.2 and +24.3‰, respectively; the former may not be truly representative since it came from a field undergoing water flooding, although the flood water had relatively low sulphate concentrations so its effect is probably minimal (a sample of the flood water did not yield sufficient BaSO$_4$ for isotopic analysis). There is a tightly clustered group of samples in the ~+27-30‰ δ^{34}S$_{SO4}$ range, and a more diffuse group above +30‰; there are also a few samples below +27‰. However, unlike the Dundee Formation samples, these samples show no clear relationship between δ^{34}S$_{SO4}$ values and sulphide concentrations. The δ^{18}O$_{SO4}$ values range from +12.9 to +20.2‰, with the exception of the Columbus Member sample, which is −1.6‰.

Salina Group

Precipitates were collected from twelve of the Salina Group samples – three from the subcrop region, three from the A-2 and six from the A-1 at depth. The subcrop samples have compositions of +6.0 to +33.5‰ δ^{34}S$_{SO4}$ and +12.0 to +13.3‰ δ^{18}O$_{SO4}$. Isotopic

values for A-2 samples range from +26.4 to +28.6‰ $\delta^{34}S_{SO4}$ and +10.6 to +13.9‰ $\delta^{18}O_{SO4}$. Values for the A-1 samples range from +27.4 to +33.3‰ $\delta^{34}S_{SO4}$ and +12.4 to +16.0‰ $\delta^{18}O_{SO4}$. All samples have relatively low (<~1 ppm) sulphide concentrations and there is no correlation with isotopic composition. There are no significant geographic trends in the data. While the overall spread in isotope compositions is much narrower than in the Devonian formations, local variation can still be quite high, as demonstrated by two samples from the Becher West pool with a 5.6‰ difference in $\delta^{34}S_{SO4}$ and a 3.6‰ difference in $\delta^{18}O_{SO4}$ values.

Guelph Formation

Sixteen precipitates were collected from the Guelph Formation samples. Their $\delta^{34}S_{SO4}$ values range from +23.0 to +32.2‰, although the majority of samples are in the ~+27-28‰ range; $\delta^{18}O_{SO4}$ values range from +10.0 to +14.0‰. Again, sulphide concentrations were low (≤2.3 ppm) and not correlated with isotopic composition. No significant geographic trends were observed in the isotopic data. Local variation in the Guelph Formation was lower than in the Salina Group, with same-pool samples varying by <1-2‰, for both $\delta^{34}S_{SO4}$ and $\delta^{18}O_{SO4}$. A noteworthy observation from well T008657, which was sampled both from a brine tank and from the wellhead, is that $\delta^{34}S_{SO4}$ values for the two samples were within 0.2‰ and the $\delta^{18}O_{SO4}$ values were within ~1‰. This suggests that sulphate isotope compositions preserve well in brine tanks over extended periods of time, and that the local groundwater compositions are fairly constant over time.

Clinton and Cataract Groups

Two precipitates were collected from the Grimsby Formation, with $\delta^{34}S_{SO4}$ values of +22.0 and +22.3‰, and $\delta^{18}O_{SO4}$ values of +10.8 and +11.9‰. Both were from the Norfolk pool, suggesting low intrapool variability. One sample from the Irondequoit Formation had $\delta^{34}S_{SO4}$ and $\delta^{18}O_{SO4}$ values of 10.0 and 20.7‰, respectively. Sulphide concentrations are low (0.6 ppm) and unrelated to isotopic compositions.

Trenton and Black River Groups

Eleven precipitates were collected from the Trenton and Black River samples. The $\delta^{34}S_{SO4}$ values range from +26.6 to +43.3‰, and $\delta^{18}O_{SO4}$ values range from +11.5 to +15.6‰. While sulphide concentrations are not particularly high (≤1.3 ppm) or strongly correlated with isotopic compositions, the two samples with the highest $\delta^{34}S_{SO4}$ values do have the highest sulphide concentrations. Intrapool variability of $\delta^{34}SSO4$ is quite variable, from a difference of <0.5‰ between samples in the Dover 7-5-V E pool, to an almost 10‰ difference between samples in the Mersea 6-23-VII pool. Intrapool variability was universally low (<0.5‰) for $\delta^{18}O_{SO4}$.

Cambrian units

Seven precipitates were collected from the Cambrian samples. The range in $\delta^{34}S_{SO4}$ values was +21.6 to +31.1‰, and for $\delta^{18}O_{SO4}$, +9.3 to +14.2‰. Sulphide concentrations were generally low (≤1.5 ppm), and not correlated with isotope compositions. Intrapool $\delta^{34}S_{SO4}$ variation in the Clearville Pool was high, almost 10‰; variation was lower (~ 3‰) for $\delta^{18}O_{SO4}$. No significant geographic trends were observed in the isotopic data. Well T008532 was sampled twice; the isotopic compositions varied between samples by ~0.5‰ for $\delta^{34}S_{SO4}$ and ~0.1‰ for $\delta^{18}OSO4$; well T007369 was also resampled and its values were consistent within ~3‰ for $\delta^{34}S_{SO4}$ and ~0.2‰ for $\delta^{18}O_{SO4}$.

4.1.3 Carbon isotopes of DIC

This section presents stable carbon isotope compositions ($\delta^{13}C$) for dissolved inorganic carbon (DIC) in the water samples (Figure 4.3). Data are relatively limited for the deeper formations, given the analytical difficulties associated with the very low DIC concentrations in these samples.

Dundee Formation

The $\delta^{13}C$ values of nine Dundee Formation samples range from −15.2 to +20.0‰. No significant geographic trends were observed in the isotopic results. Local variability was

site-dependant; samples from two different seeps within the Port Dover Quarry varied in $\delta^{13}C$ by only 0.3‰; samples in the Bothwell-Thamesville pool varied by 2‰, yet were about 10‰ higher than a sample from a nearby pool that was supposedly hydraulically connected, according to the operator.
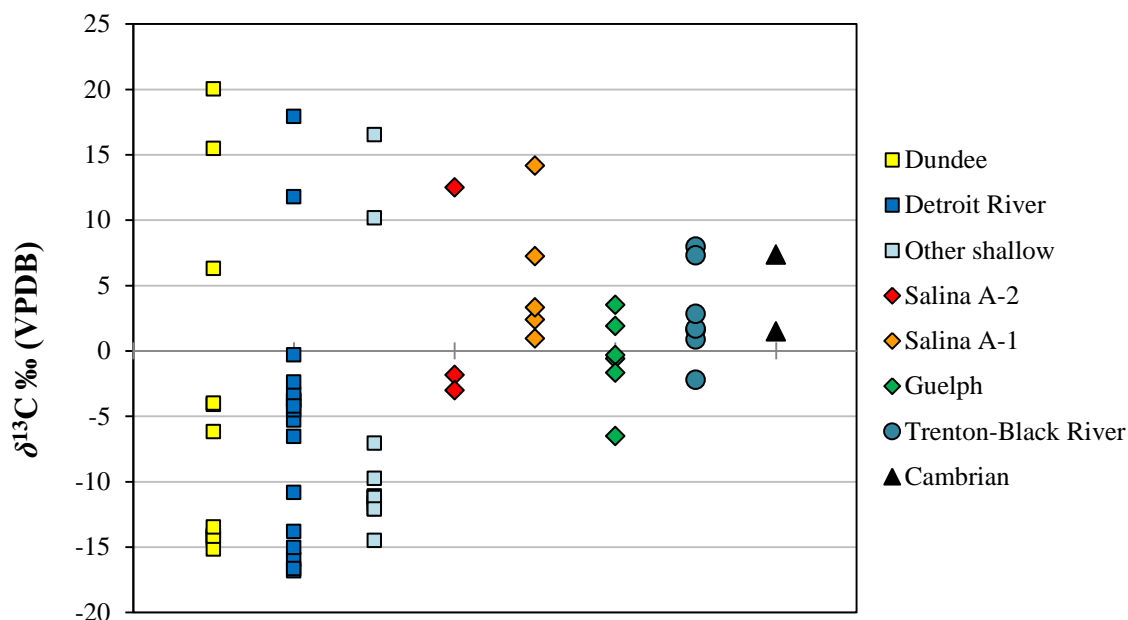
Figure 4.3: DIC carbon isotopic compositions of groundwaters collected in this study.

Detroit River Group

Seventeen Detroit River Group samples were analyzed, including three from the Columbus Member, one from the Amherstburg Formation, and thirteen from the Lucas Formation. Lucas Formation $\delta^{13}C$ values range from −16.8 to −0.3‰. The three Columbus Member samples were likely contaminated by flooding with fresh water from the drift aquifer ($\delta^{13}C$ = +17.2‰). Of these samples, the well closest to the injection site has a $\delta^{13}C$ value of +17.9‰, while the well furthest away has a composition of −5.3‰; a production battery of commingled waters has an intermediate composition of +17.2‰. The Amherstburg Formation sample has a $\delta^{13}C$ value of −4.2‰. While there were no strong geographical trends in the isotopic data, samples from the Petrolia field have the lowest $\delta^{13}C$ values, between −16.8 and −10.8‰, while other sites (with the exception of the Columbus Member) tend to have values near −3 ± 2‰.

Salina Group

In the Salina Group, four samples from the A-2 carbonate, five from the A-1 carbonate, and two from the E unit subcrop were analysed for δ^{13}C. In the A-2 unit, the two samples from the Goderich salt mine have much higher δ^{13}C values (+12.5 to +14.8‰) than the others (−3.0 to −1.9‰). The A-1 samples, all from Lambton County, have δ^{13}C values ranging from +0.9 to +14.2‰, with three samples from the same pool exhibiting this entire range. The sample with the highest value was from a brine tank, and so may not be representative due to atmospheric exchange or other surficial alteration; the next highest sample had a δ^{13}C value of +7.2‰.

Guelph Formation

Seven samples from the Guelph Formation have δ^{13}C values ranging from −6.5 to +3.5‰. No geographic trends were apparent in the isotopic data. For well T008657, samples were collected both from a brine tank and directly from the wellhead; their δ^{13}C values are −5.9‰ and −0.6‰, respectively, illustrating that atmospheric exposure within a brine tank may have an impact on carbon isotopic signatures.

Clinton and Cataract Groups

Only one sample, from the Irondequoit Formation, was successfully analyzed; it has a δ^{13}C value of −3.0‰.

Trenton and Black River Groups

Seven samples from the Trenton and Black River groups were successfully analysed, all from a relatively small area in Essex County. Their δ^{13}C values range from −2.2 to +8.0‰. Samples from the Gosfield North 2-21-VI pool differ in δ^{13}C by almost 4‰, yet variation was <1‰ within the Mersea 6-23-VII pool.

Cambrian units

Only two Cambrian samples were successfully analysed. They were from different pools, and had δ^{13}C values of +1.5‰ and +7.4‰.

4.1.4 Strontium isotopes ($^{87}Sr/^{86}Sr$)

This section presents the isotopic compositions ($^{87}Sr/^{86}Sr$) of dissolved strontium ions in the groundwater samples. The $^{87}Sr/^{86}Sr$ results for all formations are plotted against total strontium concentrations in Figure 4.4.
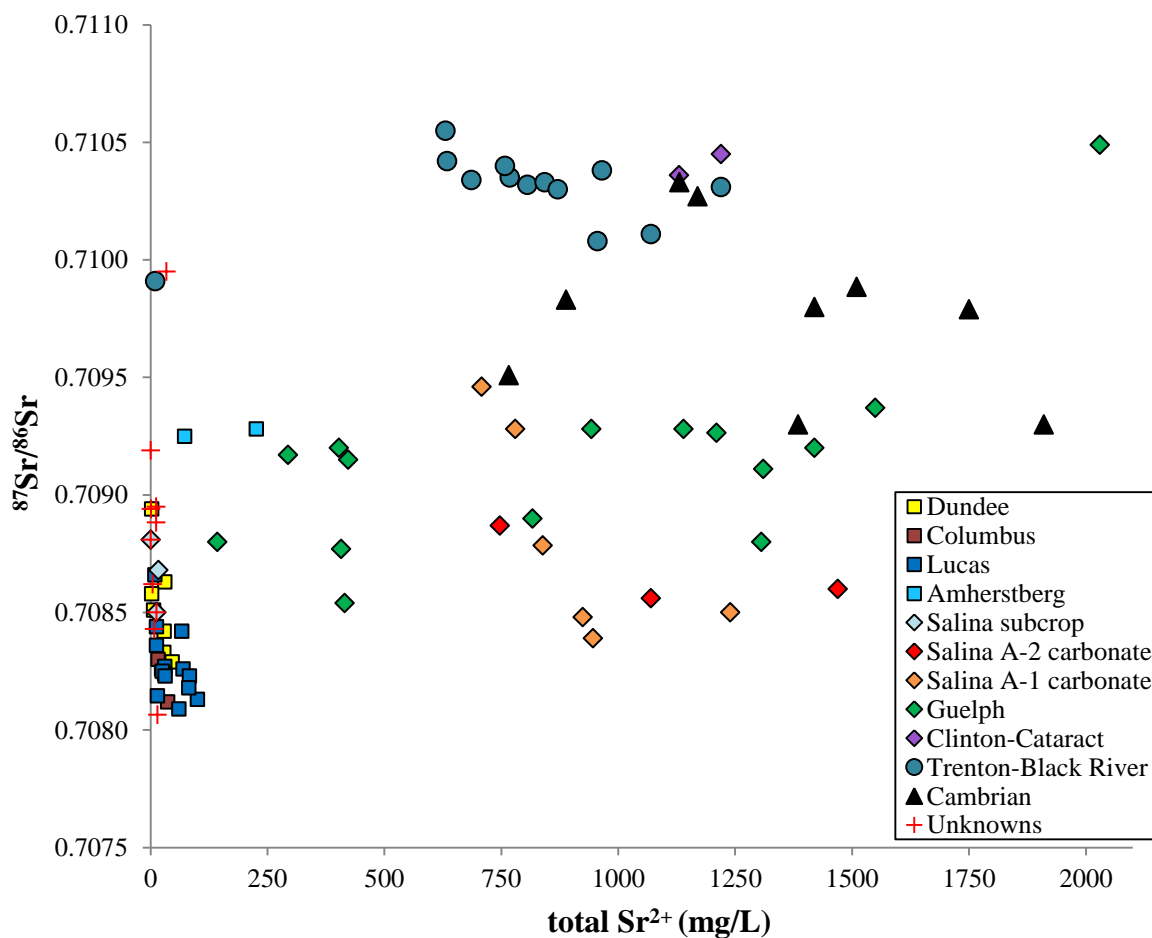
Figure 4.4: Strontium isotopic ratios plotted against total Sr^{2+} concentrations for all groundwaters collected in this study.

Dundee Formation

Nine Dundee Formation waters have $^{87}Sr/^{86}Sr$ ratios that vary from 0.70829 to 0.70894. No significant geographical trends were observed in $^{87}Sr/^{86}Sr$ ratios. Two samples taken from the Bothwell-Thamesville pool differ in $^{87}Sr/^{86}Sr$ ratio by 0.00013.

Detroit River Group

Twenty samples of the Detroit River Group waters – three from the Columbus Member, fifteen from the Lucas Formation, and two from the Amherstburg Formation have an overall variation in $^{87}Sr/^{86}Sr$ variation of 0.70812 to 0.70928; the range for the Columbus Member is 0.70812 to 0.70830, the Lucas Formation, 0.70813 to 0.70921; and the Amherstburg Formation, 0.70925 to 0.70928. The Columbus Member samples are likely contaminated by fresh water from a drift aquifer ($^{87}Sr/^{86}Sr$ = 0.70876); however there is no apparent effect of this on the strontium isotopes. Regionally, no clear geographic trends in $^{87}Sr/^{86}Sr$ were observed. Intrapool $^{87}Sr/^{86}Sr$ variation in the Lucas Formation is quite small – 0.00003 across the Petrolia pool, and 0.00008 in the Oil Springs pool. However, waters produced from the Dundee Formation within Oil Springs have $^{87}Sr/^{86}Sr$ ratios >0.00030 higher than coproduced Lucas Formation waters.

Salina Group

Strontium isotopic compositions were measured for ten samples of the Salina Group waters – three from the subcrop area, three from the A-2, and six from the A-1. $^{87}Sr/^{86}Sr$ of subcrop waters range from 0.70850 to 0.70881; for the A-2 samples, from 0.70856 to 0.70887, and for the A-1, from 0.70839 to 0.70946. Within the A-1, there is a geographic trend of increasing $^{87}Sr/^{86}Sr$ from west to east. Despite its distance from the other sample sites, and it uniquely being constrained by salt layers, the Goderich salt mine waters have $^{87}Sr/^{86}Sr$ ratios similar to the other Salina samples. Intrapool variability in the Brigden pool was 0.00029.

Guelph Formation

With the exception of one extreme outlier ($^{87}Sr/^{86}Sr$ = 0.71049), 13 samples of Guelph Formation waters have $^{87}Sr/^{86}Sr$ ratios ranging from 0.70854 to 0.70937. No strong geographic trends in $^{87}Sr/^{86}Sr$ are evident, although the three wells in Huron County have very similar ratios, varying by only 0.00003, despite being relatively far apart. Several wells in northwestern Lambton County also have $^{87}Sr/^{86}Sr$ ratios similar to one another (within 0.00026).

Clinton and Cataract Groups

Two Grimsby Formation waters from the Norfolk pool have ^{87}Sr/^{86}Sr ratios of 0.71036 and 0.71045.

Trenton and Black River Groups

The ^{87}Sr/^{86}Sr ratios of thirteen samples from the Trenton and Black River groups range from 0.71008 to 0.71055, except for one sample (^{87}Sr/^{86}Sr = 0.70991) that was likely contaminated by fresh water. Intrapool variation in ^{87}Sr/^{86}Sr is quite low: 0.00003 for the Dover 7-5-V E pool, 0.00005 for the Gosfield North 2-21-VI pool, and 0.00013 for the Mersea 6-23-VII pool.

Cambrian units

The ^{87}Sr/^{86}Sr ratios of nine Cambrian samples range from 0.70930 to 0.71033. Intrapool variation in the Willey West Pool is 0.00037, and in the Clearville Pool, 0.00004. Two wells were resampled; to the southwest, samples from well T007369 had ^{87}Sr/^{86}Sr ratios of 0.71033 and 0.71027 (in February and June 2012, respectively); to the northeast, samples from well T008532, collected over a year apart, had identical ratios, 0.70930, despite different total strontium concentrations.

4.2   Ion geochemistry

This section reports the major cation and anion compositions of the water samples. Minor and trace ions were also analysed for many samples; all ion chemistry data are listed in Appendices E and F. The main chemical characteristics of each stratigraphic unit are summarized in Table 4.1.

Formation/Group	Water chemistry type	Salinity category	TDS range (g/L)
Dundee	Na-Ca-Cl	Fresh to brackish	0.9 – 31.3
Detroit River	Na-Ca-Cl-(SO_4)	Mostly brackish	2.6 – 138
Salina A-2	Na-Ca-Cl	Brine	375 – 392
Salina A-1	Na-Ca-Cl	Brine	286 – 519
Guelph	Na-Ca-Cl / Ca-Na-Cl	Brine	153 – 441
Clinton-Cataract	Na-Ca-Cl	Brine	199 – 408
Trenton-Black River	Na-Ca-Cl	Brine	261 – 403
Cambrian	Na-Ca-Cl / Ca-Na-Cl	Brine	270 – 423

Table 4.1: Summary of principal ion chemistry, water classification, and TDS range for the main water-bearing formations in southwestern Ontario.

Table 4.1 highlights the salinity differences between the two major fluid regimes, as discussed in Section 2.1.3 – the deep Cambrian through Silurian brines, and the shallower Devonian waters, which range from fresh through saline but are mostly brackish. Most groundwaters exhibit a wide range in TDS, and these ranges largely overlap between formations. The major ion compositions are dominated by Na^+, Ca^{2+}, and Cl^-, although the relative importance of Na^+ and Ca^{2+} varies considerably between samples, even within formations. The major ion compositions of groundwaters in each stratigraphic unit are illustrated by Piper plot in Figure 4.5.
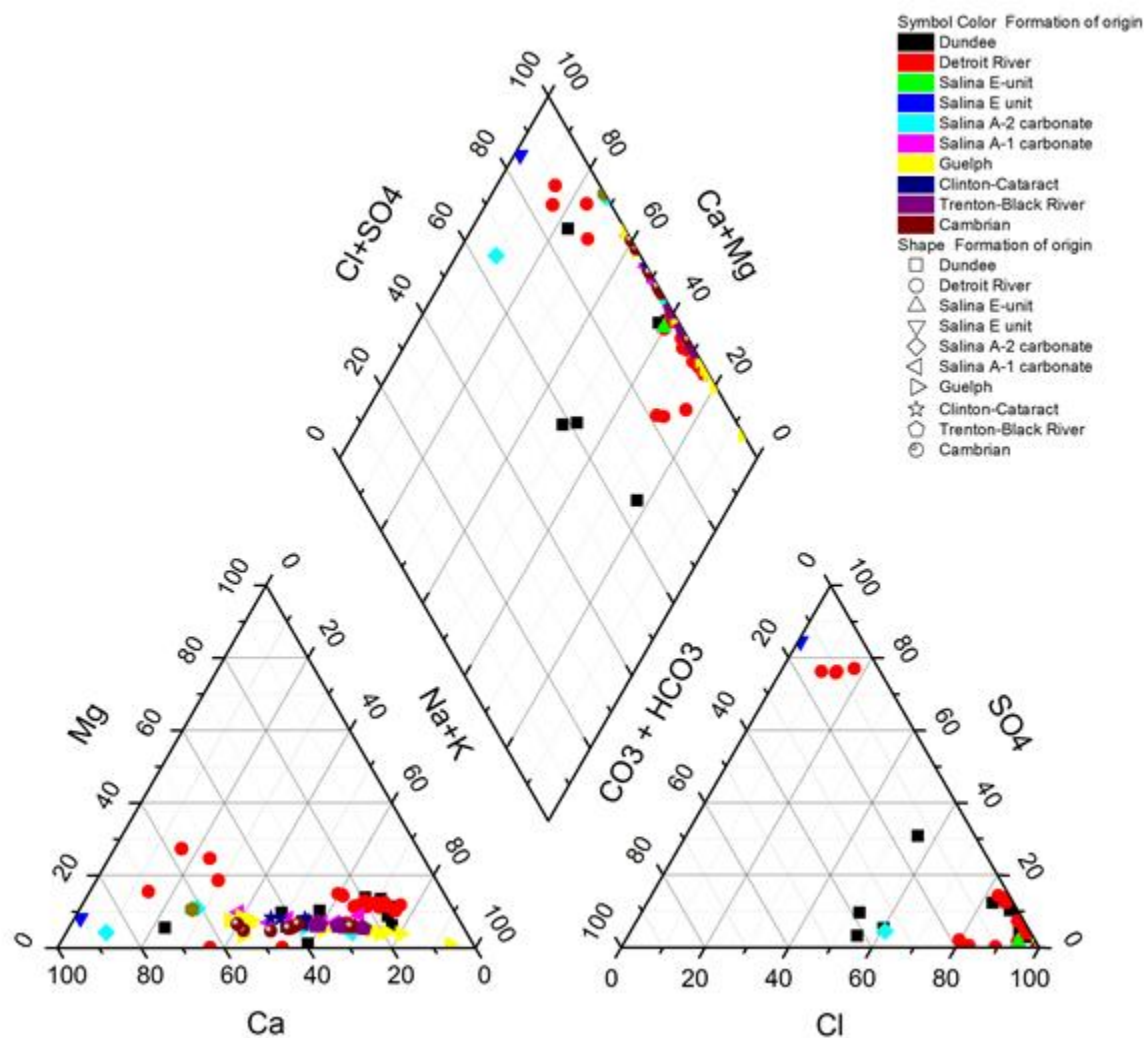
Figure 4.5: Piper (1944) trilinear plots for all groundwater samples collected in this study, separated into the main geological units considered in this study.

Figure 4.5 illustrates several hydrogeochemical matters of note. With the exception of a few of the Devonian waters, Mg^{2+} typically comprises <20% of the total cation content. Na^+ and Ca^{2+} are the dominant cations, although the Na^+:Ca^{2+} ratio varies considerably. While there is extensive interformation overlap in compositions, in general, the Cambrian samples tend to be more Ca^{2+}-dominated, while the Trenton-Black River samples tend towards a more Na^+-rich composition. The Clinton-Cataract groundwaters are somewhat intermediate between the two, and the Guelph Formation and Salina Group samples span

a much broader range of Na^+:Ca^{2+} ratios. The Piper plot does not illustrate the anion abundances particularly clearly, simply because Cl^- is of such overwhelming importance in almost all waters, especially in deeper formations. However, several Devonian samples have significant proportions of sulphate and bicarbonate.

Summary statistical information (minimum, maximum and mean values, quartiles 1 and 3, and standard deviation) for each major ion, as well as isotopic data for each formation, are provided in Tables 4.2a-g below. Extremely anomalous samples (>3σ above or below the mean) and/or samples showing obvious signs of contamination were omitted when generating these statistics. In cases where multiple samples were taken from within a very small area (e.g., quarries, the Goderich salt mine, well duplicates), average compositions for those locations were used, to avoid their over-representation in these statistics. Samples from the subcrop area are not included in the statistics for the Salina Group, as they are very different from the brines at depth. The stable isotopic data are given in ‰ ($\delta^{18}O$ and δ^2H are given on the concentration scale) and the ion data and TDS in mg/L.

Dundee Formation

Table 4.2a	Mean	Stdev	Min	Max	Q1	Q3
$\delta^{18}O_{H2O}$	−11.0	2.6	−15.7	−7.5	−12.2	−9.0
δ^2H_{H2O}	−75	18	−111	−53	−82	−64
$\delta^{13}C_{DIC}$	−3.9	12.3	−15.2	+20.0	−14.2	+5.7
$\delta^{34}S_{SO4}$	+36.4	9.3	+27.4	+53.9	+30.4	+39.1
$\delta^{18}O_{SO4}$	+13.6	3.2	+8.7	+17.7	+12.3	+15.4
$^{87}Sr/^{86}Sr$	0.70855	0.00020	0.70829	0.70894	0.70842	0.70863
Ca^{2+}	684	711	140	2050	154	903
Mg^{2+}	377	565	23	1460	50	352
Na^+	1992	2586	202	6850	513	2078
K^+	71	77	8	216	18	108
Sr^{2+}	20	17	2	46	6	30
Cl^-	5606	7548	230	18000	828	7425
Br^-	38	50	3	130	3	50
SO_4^{2-}	505	763	16	2100	38	413
HCO_3^-	234	154	3	522	142	349
TDS	9554	12186	899	31260	1972	11277

Detroit River Group

Table 4.2b	Mean	Stdev	Min	Max	Q1	Q3
$\delta^{18}O_{H2O}$	−10.0	3.8	−16.7	−6.5	−13.8	−6.7
δ^2H_{H2O}	−69	29	−122	−39	−91	−44
$\delta^{13}C_{DIC}$	−6.0	10.1	−16.8	+17.9	−14.4	−3.8
$\delta^{18}O_{SO4}$	+15.5	+1.9	+12.9	+19.9	+14.0	+16.5
$\delta^{34}S_{SO4}$	+29.3	+9.5	+12.2	+52.7	+27.2	+30.5
$^{87}Sr/^{86}Sr$	0.70822	0.00009	0.70807	0.70921	0.70816	0.70827
Ca^{2+}	1402	1025	183	3473	547	1991
Mg^{2+}	785	628	114	2071	190	927
Na^+	3616	2787	102	8316	832	5511
K^+	144	105	10	334	70	225
Sr^{2+}	40	26	13	84	21	65
Cl^-	9381	7558	230	23556	1800	13000
Br^-	65	75	2	321	12	69
SO_4^{2-}	1056	786	13	2000	72	1900
HCO_3^-	271	119	101	646	204	331
TDS	16892	12489	2474	40156	4143	23498

Salina Group

Table 4.2c	Mean	Stdev	Min	Max	Q1	Q3
$\delta^{18}O_{H2O}$	−1.5	3.0	−6.3	4.1	−3.4	−0.6
δ^2H_{H2O}	−45	9	−62	−32	−50	−37
$\delta^{13}C_{DIC}$	+4.6	6.5	−3.0	+14.8	−1.2	+12.0
$\delta^{18}O_{SO4}$	+29.3	2.5	+26.4	+33.3	+27.2	+31.6
$\delta^{34}S_{SO4}$	+13.3	1.9	+10.6	+16.0	+11.5	+15.1
$^{87}Sr/^{86}Sr$	0.70877	0.00037	0.70839	0.70946	0.70849	0.70908
Ca^{2+}	49354	16538	35600	84085	38900	57700
Mg^{2+}	9984	2923	6050	15177	8269	13500
Na^+	68098	21403	31007	99600	48300	79300
K^+	5277	1519	2660	7431	4130	6910
Sr^{2+}	965	225	708	1470	780	1070
Cl^-	221332	53768	180000	370000	190000	240000
Br^-	1994	703	1300	3502	1300	2700
SO_4^{2-}	237	96	89	360	150	360
HCO_3^-	13	12	2	38	2	18
TDS	357512	63086	286440	518533	325930	383732

Guelph Formation

Table 4.2d	Mean	Stdev	Min	Max	Q1	Q3
$\delta^{18}O_{H2O}$	−2.1	2.7	−6.9	2.4	−3.2	−0.3
δ^2H_{H2O}	−44	8	−63	−33	−49	−38
$\delta^{13}C_{DIC}$	−0.6	3.5	−6.5	+3.5	−2.9	+2.3
$\delta^{18}O_{SO4}$	+27.3	2.2	+23	+32.2	+25.3	+28.5
$\delta^{34}S_{SO4}$	+12.3	1.1	+10	+14	+12	+13.2
$^{87}Sr/^{86}Sr$	0.70906	0.00025	0.70854	0.70937	0.7088	0.70928
Ca^{2+}	49265	31425	13800	102000	20425	78194
Mg^{2+}	7708	3969	3120	16800	4875	10018
Na^+	64939	21006	31308	106000	52000	81700
K^+	3247	1579	1190	6020	1730	4633
Sr^{2+}	939	534	294	2030	415	1310
Cl^-	177342	48089	95000	240000	130000	221653
Br^-	1837	941	710	3853	933	2750
SO_4^{2-}	304	269	95	1000	130	355
HCO_3^-	18	28	2	93	2	26
TDS	308383	86231	153210	441259	234622	364171

Clinton and Cataract Groups

Table 4.2e	Mean	Stdev	Min	Max	Q1	Q3
$\delta^{18}O_{H2O}$	−3.0	1.0	−4.1	−0.9	−3.5	−2.9
δ^2H_{H2O}	−42	6	−54	−36	−47	−38
$\delta^{13}C_{DIC}$	−3.0	−	−3.0	−3.0	−	−
$\delta^{18}O_{SO4}$	+10.9	0.9	+10.0	+11.9	+10.4	+11.4
$\delta^{34}S_{SO4}$	+21.7	0.8	+20.7	+22.3	+21.4	+22.2
$^{87}Sr/^{86}Sr$	0.71041	0.00006	0.71036	0.71045	−	−
Ca^{2+}	38349	11150	27307	58000	30348	49201
Mg^{2+}	7189	2000	5631	10800	5794	9090
Na^+	50288	6563	40097	59500	46203	57171
K^+	1239	285	978	1700	1036	1554
Sr^{2+}	1175	64	1130	1220	−	−
Cl^-	173793	57778	122542	280000	138213	225890
Br^-	1600	391	1133	2400	1345	1816
SO_4^{2-}	369	118	180	519	269	471
HCO_3^-	2	0	2	2	−	−
TDS	273165	77692	198714	407661	224796	350535

Trenton and Black River Groups

Table 4.2f	Mean	Stdev	Min	Max	Q1	Q3
$\delta^{18}O_{H2O}$	−1.4	0.2	−1.7	−0.9	−1.6	−1.3
$\delta^{2}H_{H2O}$	−23	3	−31	−19	−24	−21
$\delta^{13}C_{DIC}$	+2.9	4	−2.2	+8.0	0.1	7.5
$\delta^{18}O_{SO4}$	+34.6	6.3	+26.6	+43.3	+27.5	+40.5
$\delta^{34}S_{SO4}$	+14.0	1.7	+11.5	+15.6	+12.1	+15.4
$^{87}Sr/^{86}Sr$	0.71032	0.00013	0.71008	0.71055	0.7103	0.71038
Ca^{2+}	32328	6215	27300	42700	27700	39509
Mg^{2+}	6791	1103	5610	9180	5814	7555
Na^{+}	68975	11225	57400	89400	58850	78175
K^{+}	3250	342	2800	3940	3075	3535
Sr^{2+}	851	178	631	1220	704	963
Cl^{-}	178523	26933	150000	230000	160000	188069
Br^{-}	1395	311	1100	2000	1200	1600
SO_4^{2-}	303	73	197	400	220	360
HCO_3^{-}	4	5	2	20	2	3
TDS	295542	43576	260593	403179	266973	305506

Cambrian units

Table 4.2g	Mean	Stdev	Min	Max	Q1	Q3
$\delta^{18}O_{H2O}$	−2.9	0.9	−4.2	−1.4	−3.6	−2.0
$\delta^{2}H_{H2O}$	−33	8	−46	−21	−39	−27
$\delta^{13}C_{DIC}$	+4.4	4.2	+1.5	+7.4	–	–
$\delta^{18}O_{SO4}$	+26.2	3.1	+21.6	+31.1	+24.2	+28.4
$\delta^{34}S_{SO4}$	+12.1	1.8	+9.4	+14.1	+10.2	+13.6
$^{87}Sr/^{86}Sr$	0.70977	0.00031	0.70930	0.71030	0.70951	0.70988
Ca^{2+}	62804	23053	37300	94200	39979	85000
Mg^{2+}	7602	1075	6009	8540	6370	8440
Na^{+}	69189	16982	48545	90100	52116	86500
K^{+}	2426	750	1496	4000	1963	2708
Sr^{2+}	1330	358	766	1750	954	1613
Cl^{-}	208193	20016	170000	240000	200000	218886
Br^{-}	2112	209	1800	2395	1925	2300
SO_4^{2-}	211	112	120	470	140	220
HCO_3^{-}	3	2	2	8	2	3
TDS	359335	44971	269504	402027	333208	399130

Tables 4.2a-g: Summary statistical information for the major ion and isotope geochemistry of groundwaters for each geological formation or group sampled in this study (Q1 and Q3 = first and third quartiles). Some parameters for some units have insufficient data to calculate all information.

Chapter 5

5 Discussion

5.1 SIAR modelling

This section discusses the development of the datasets to be used in the SIAR model (see Section 3.3) and the ability of the model to correctly predict the 'true' source proportions in several hypothetical mixing scenarios.

In the SIAR program, data are inputted as spreadsheets that are stored internally as matrices. The inputted data for the source formations are formatted in terms of a mean and standard deviation for all isotopic measurements being considered. Data for the unknown samples/potential mixtures are entered in a second spreadsheet as individual observations. Multiple samples can be modelled simultaneously by assigning them different group numbers, and more than one observation can be entered per sample (for instance, if it was analyzed more than once). A third spreadsheet can be created for isotopes for which the element concentrations vary between sources (such as strontium); the concentration data for each source are also reported in the same way as the sources.

5.1.1 Data processing and end-member selection

Two of the main challenges faced by all mixing models are (1) coping with large numbers of sources, and (2) similarity between sources or unfavourable source geometry, such that sources may substitute for one another to produce the same mixture composition. Thus, it is important to carefully select the data to be used in the model, to reduce complexity while preserving meaningfulness as much as possible. Phillips et al. (2005) advocated source aggregation as one method for addressing both of these difficulties. However, they stipulated that this should only be used in cases where the isotopic signatures of aggregated sources are relatively similar, and that the sources should be related in such a way that the combined source group has some functional significance.

Both *a priori* and *a posteriori* source aggregation are possible. In the former case, sources are combined before running the model; this is useful when source compositions are similar. With *a posteriori* source aggregation, the posterior distributions for two or more sources generated by the model are combined, ideally yielding a new posterior probability distribution that is narrower than those of the contributing sources. This method is more appropriate when sources are functionally related yet have significantly different source compositions and thus combining them *a priori* would produce a high standard deviation for the combined end-member. These source aggregation methods are useful for optimizing model performance in this study.

Adding isotopes is another method for constraining mixing models. While many researchers use only two or three isotopic systems in mixing-model simulations, our dataset includes six isotopic systems that can potentially be utilized. This extensive dataset will help the model better constrain the source proportions. In this study, the water data on the isotopic concentration scale have been used, as oxygen and hydrogen isotopes of water behave conservatively during mixing of different waters (Horita et al., 1993b). Incorrect use of the activity and concentration scales may lead to erroneous conclusions; for instance, in mixing problems if the activity scale were used, predicted proportions may be somewhat incorrectly estimated.

Water samples from a large number of geological units were collected in this study; these are: the Dundee, Lucas (including the Columbus Member), Amherstberg, Bass Islands, Salina E, A-2 and A-1 units, Guelph, Rochester/Irondequoit, Thorold, Grimsby, Cobourg, Coboconk, and Sherman Fall formations, as well as the undivided Cambrian strata. While some grouping of units has already been used to describe the data in previous sections, the formal *a priori* aggregation of formations for use in the SIAR modelling is described below. For each aggregate source, or "end-member", a mean and standard deviation are generated for use in the model, as presented in Table 5.1. All data are used, with the exception of a few extreme outliers and/or samples which show contamination with significant amounts of water from other units. When more than one sample was collected from a given site, average values are used.

Waters from the shallow Devonian units are isotopically indistinguishable from each other, spanning a wide and overlapping range in compositions for all isotopes (see Section 4.1.1). The Dundee Formation and Detroit River Group are also stratigraphically adjacent and lithologically similar, and considered as one vertically-continuous aquifer (T. Carter, personal communication, 2013). For these reasons, it is appropriate to aggregate these waters within SIAR. An issue in representing these samples in SIAR, however, is that the range of water $\delta^{18}O$ and δ^2H values is quite large and has a diagonal distribution, along the meteoric water line. Hence, rather than averaging all δ-values, which would result in a large standard deviation and not be fully representative of the true distribution, the range can be represented in SIAR as a mixing line between two end-members. The end-member representing the lower extreme of these waters (termed "Dev-low") is defined here as all samples with $\delta^{18}O < -15‰$, while the end-member at the higher extreme ("Dev-high") is generated from the cluster of samples with $\delta^{18}O > -9‰$. These cut-off points are somewhat arbitrary, but were selected to maintain a standard deviation similar to the other end-members while including a reasonable number of samples. One issue with using this two end-member system is that the samples with very high or low $\delta^{18}O$ and δ^2H values do not correspond with similar compositional extremes for the other isotopes (i.e., $\delta^{34}S_{SO4}$, $\delta^{18}O_{SO4}$, $\delta^{13}C_{DIC}$, $^{87}Sr/^{86}Sr$). Thus, different Dev-low and Dev-high compositions for the latter isotopes cannot be defined. However, SIAR requires that each end-member has data for all isotopes being used, so while Dev-low and Dev-high will have different values for $\delta^{18}O$ and δ^2H, for the other isotopes, an overall average of all samples is used for both end-members. This simply means that the model will only be able to differentiate between these end-members on the basis of $\delta^{18}O$ and δ^2H. It should also be noted that these end-members, while predominantly representing Devonian waters as suggested by their names, actually include all shallow (<350-450 m), relatively dilute groundwaters, regardless of their host formation, since the formations that contain brines at depth all contain fresh or brackish water at shallower levels that is isotopically and geochemically indistinguishable from waters in the Devonian formations. These two end-members can be aggregated *a posteriori* if desired, although this has not been done in this discussion.

Waters from the Salina A-2 carbonate, A-1 carbonate and Guelph Formations also have compositions that appear comparable to one another, for all isotopes considered in this study. This geochemical similarity, combined with the fact that these units are stratigraphically adjacent, suggests that there may be fluid communication between them. Accordingly, these units are combined as the "Guelph-Salina" end-member in the SIAR model. All data are considered, except for δ^{18}O and δ^2H results for the Goderich salt mine (excluded because of its unique geological environment and anomalously high ^{18}O enrichment) and δ^{18}O and δ^2H data from samples that were likely contaminated by meteoric water during production-related activities, such as water flooding. This SIAR end-member only applies to Salina and Guelph brines at depth (~>350-450 m), as these units can contain fresh or brackish waters with significantly different compositions at shallower depths. Geological knowledge of the area is thus important for appropriate end-member selection. The same caveat applies to the other end-members described below.

Samples from the Thorold, Grimsby and Rochester/Irondequoit formations are also isotopically comparable to each other. These samples were combined in SIAR as the "Clinton-Cataract" end-member. This end-member is less well-represented in the dataset; available data include δ^{18}O and δ^2H for nine samples, δ^{18}O$_{SO4}$ and δ^{34}S$_{SO4}$ for three samples, ^{87}Sr/^{86}Sr for two samples, and δ^{13}C$_{DIC}$ data are available for only one sample.

The compositions of brine samples from the Trenton and Black River groups (Cobourg, Coboconk, and Sherman Fall formations) are also isotopically comparable. These brines are from geologically similar, fault-controlled hydrothermal dolomite reservoirs (e.g., Middleton, 1991) and are thus combined as the "Trenton-Black River" end-member. All data collected in the present study are used in the SIAR model, excepting sample T007793, which has anomalous δ^{18}O, δ^2H, and ^{87}Sr/^{86}Sr values and very low TDS, consistent with fresh water contamination. Note that these waters are likely isotopically different from porewaters in regional, undolomitized Trenton-Black River rocks, as suggested by porewater data from the Nuclear Waste Management Organization's Deep Geological Repository site (Clark et al., 2010a,b; Clark et al., 2011), as well as boreholes OHD-1 and UN-2, slightly east of the study area (Sherwood-Lollar and Frape, 1989), and so this end-member only applies to brines in the hydrothermal dolomite reservoirs.

Cambrian brine samples are compositionally distinct from the other formations and will thus form the final end-member. The Cambrian brines do however share some isotopic similarities with the overlying Trenton-Black River brines, and so it may be desirable to aggregate these sources *a posteriori*.

In addition to the means and standard deviations of the source isotopic compositions, SIAR can also take into account differences in concentrations among sources for any given element. In the model's traditional ecological applications, this commonly adjusts for differences in carbon and nitrogen contents between food sources. In this study, four of the six isotopic systems ($\delta^{34}S_{SO4}$, $\delta^{18}O_{SO4}$, $\delta^{13}C_{DIC}$, $^{87}Sr/^{86}Sr$) have concentration differences among sources. Accounting for such differences is necessary for accurate model function, and can also be useful for constraining source proportions, particularly in the case of strontium, where the deeper formations typically have much higher total Sr^{2+} contents (as well as higher $^{87}Sr/^{86}Sr$ ratios) than the Devonian units. Thus, even a small addition of brine to a shallow water sample will significantly skew the mixture's $^{87}Sr/^{86}Sr$ ratio towards that of the brine. Conservative estimates of the means and standard deviations of these concentration dependencies for each end-member, based on the major ion data from this study, are presented in Table 5.2. This table uses the format required by SIAR: (i) inclusion of ^{18}O and ^2H is necessary despite the lack of concentration dependencies with these isotopes; and (ii) the sulphate columns need to be repeated to correspond to both $\delta^{34}S_{SO4}$ and $\delta^{18}O_{SO4}$; it is critical to maintain column order between SIAR datasheets. Note that the current version of SIAR does not in fact account for the variabilities in the concentrations, so the standard deviation columns in this table are merely placeholders necessary to maintain the column ordering that the program requires; future versions may however include the ability to incorporate these variabilities in the model.

The data from this study form one of various possible datasets upon which the model can be based, and will be referred to hereafter as Dataset 1. Another possible dataset is outlined in the following section.

End-member	$\delta^{18}O$ mean	$\delta^{18}O$ stdev	$\delta^{2}H$ mean	$\delta^{2}H$ stdev	$\delta^{13}C_{DIC}$ mean	$\delta^{13}C_{DIC}$ stdev	$\delta^{34}S_{SO4}$ mean	$\delta^{34}S_{SO4}$ stdev	$\delta^{18}O_{SO4}$ mean	$\delta^{18}O_{SO4}$ stdev	$^{87}Sr/^{86}Sr$ mean	$^{87}Sr/^{86}Sr$ stdev
Dev-low	−16.1	0.4	−117.2	4.0	−4.5	10.9	+30.8	8.7	+14.4	2.0	0.70836	0.00020
Dev-high	−7.3	0.8	−49.6	7.8	−4.5	10.9	+30.8	8.7	+14.4	2.0	0.70836	0.00020
Salina-Guelph	−0.8	1.7	−41.7	6.5	2.3	6.1	+28.1	2.4	+12.7	1.5	0.70895	0.00033
Clinton-Cataract	−2.8	0.9	−43.3	6.5	-	-	+21.7	0.8	+10.9	0.9	0.71041	0.00006
Trenton-Black River	−1.4	0.3	−23.7	3.7	2.9	3.6	+34.6	6.0	+14.0	1.6	0.71032	0.00013
Cambrian	−2.7	0.9	−34.5	8.4	4.4	4.2	+26.2	3.1	+12.1	1.8	0.70977	0.00031

Table 5.1: Means and standard deviations of the isotopic compositions for each end-member that can be incorporated into the SIAR model, based on data collected in this study (Dataset 1). All isotopic compositions are in units of ‰ relative to their respective international standard, except for $^{87}Sr/^{86}Sr$ ratios.

End-member	^{18}O mean	^{18}O stdev	^{2}H mean	^{2}H stdev	HCO_3^- mean	HCO_3^- stdev	SO_4^{2-} mean	SO_4^{2-} stdev	SO_4^{2-} mean	SO_4^{2-} stdev	Sr^{2+} mean	Sr^{2+} stdev
Dev-low	1.0	0.0	1.0	0.0	266.6	121.7	642.7	795.9	642.7	795.9	28.2	24.4
Dev-high	1.0	0.0	1.0	0.0	266.6	121.7	642.7	795.9	642.7	795.9	28.2	24.4
Salina-Guelph	1.0	0.0	1.0	0.0	10.0	10.5	227.1	126.1	227.1	126.1	1117.1	330.6
Clinton-Cataract	1.0	0.0	1.0	0.0	2.0	1.0	368.9	118.4	368.9	118.4	1175.0	63.6
Trenton-Black River	1.0	0.0	1.0	0.0	4.1	5.3	303.1	72.6	303.1	72.6	850.6	178.1
Cambrian	1.0	0.0	1.0	0.0	2.9	2.0	205.6	106.4	205.6	106.4	1377.0	362.5

Table 5.2: Means and standard deviations for the concentration dependencies of each end-member, in the format required by SIAR, based on Dataset 1. Ion concentrations are in mg/L.

5.1.2   Incorporation of data from other sources

The intention of this project was to build on the existing knowledge base regarding the chemistry of groundwater in the region to achieve a more complete characterization of the units. To that effect, users of this geochemical tool have the option to use a dataset for defining the source compositions that includes data previously published in the literature as well as the data from this study (this combined dataset will hereafter be referred to as Dataset 2). The additional data were drawn from McNutt et al. (1987), Dollar et al. (1991), Wilson and Long (1993a,b), Weaver et al. (1995), Lowry et al. (1988), Husain et al. (1996) and Freckelton (2013). Data were selected in a similar manner to Dataset 1. The end-member compositions and concentration dependencies for Dataset 2 are presented in Tables 5.3 and 5.4, respectively.

While the end-members in Dataset 2 tend to have broader compositional ranges compared to Dataset 1, the corresponding increases in standard deviations are partially balanced by the larger sample size. Unfortunately, SIAR does not have the capability to explicitly take into account the increased statistical power conferred by the larger dataset, since it is unaware of how many samples are used to generate the source compositions. Nonetheless, the large sample population in Dataset 2 is an implicit advantage that perhaps outweighs the slight worsening generally observed in model performance resulting from the increased variability in the end-member compositions.

5.1.3   Model testing

In the following sections, four hypothetical mixtures are generated and tested as unknowns, (i) to assess the performance of the SIAR model and (ii) to serve as examples for interpreting model results. Mixture 'samples', representing possible waters from AWP sites, are simulated using the mean values of various sources, mixed in various proportions. Different versions of these mixtures are simulated based on the different datasets and their relative performance is compared.

End-member	$\delta^{18}O$ mean	$\delta^{18}O$ stdev	δ^2H mean	δ^2H stdev	$\delta^{13}C_{DIC}$ mean	$\delta^{13}C_{DIC}$ stdev	$\delta^{34}S_{SO4}$ mean	$\delta^{34}S_{SO4}$ stdev	$\delta^{18}O_{SO4}$ mean	$\delta^{18}O_{SO4}$ stdev	$^{87}Sr/^{86}Sr$ mean	$^{87}Sr/^{86}Sr$ stdev
Dev-low	−16.2	0.5	−118.2	3.8	−4.5	10.9	+29.7	6.2	+15.5	1.9	0.70834	0.00021
Dev-high	−7.3	0.8	−49.4	7.5	−4.5	10.9	+29.7	6.2	+15.5	1.9	0.70834	0.00021
Salina-Guelph	−0.6	1.9	−43.0	6.2	2.3	6.1	+28.1	2.4	+12.7	1.5	0.70897	0.00034
Clinton-Cataract	−2.8	1.1	−42.2	3.8	-	-	+22.1	0.2	+11.4	0.8	0.71040	0.00068
Trenton-Black River	−2.0	0.5	−26.3	5.1	2.9	3.6	+34.6	6.0	+14.0	1.6	0.71005	0.00036
Cambrian	−3.1	1.0	−30.8	6.7	4.4	4.2	+26.2	3.1	+12.1	1.8	0.70990	0.00028

Table 5.3: Means and standard deviations of the isotopic compositions for each end-member that can be incorporated into the SIAR model, based on Dataset 2. All isotopic compositions are in units of ‰ relative to their respective international standard except for $^{87}Sr/^{86}Sr$ ratios.

End-member	^{18}O mean	^{18}O stdev	^2H mean	^2H stdev	HCO_3^- mean	HCO_3^- stdev	SO_4^{2-} mean	SO_4^{2-} stdev	SO_4^{2-} mean	SO_4^{2-} stdev	Sr^{2+} mean	Sr^{2+} stdev
Dev-low	1.0	0.0	1.0	0.0	294.8	148.2	1122.5	752.5	1122.5	752.5	36.6	22.2
Dev-high	1.0	0.0	1.0	0.0	294.8	148.2	1122.5	752.5	1122.5	752.5	36.6	22.2
Salina-Guelph	1.0	0.0	1.0	0.0	12.9	18.0	154.3	133.3	154.3	133.3	1637.8	1034.9
Clinton-Cataract	1.0	0.0	1.0	0.0	2.0	1.0	326.4	117.7	326.4	117.7	850.2	223.5
Trenton-Black River	1.0	0.0	1.0	0.0	4.1	5.3	382.0	127.3	382.0	127.3	648.4	181.9
Cambrian	1.0	0.0	1.0	0.0	2.9	2.0	264.8	223.0	264.8	223.0	1263.6	281.8

Table 5.4: Means and standard deviations for the concentration dependencies of each end-member, in the format required by SIAR, based on Dataset 2. Ion concentrations are in mg/L.

5.1.3.1   Dataset 1

This section tests model performance using four test mixtures created using mean values from Dataset 1 (Tables 5.1 and 5.2). The compositions of the mixtures and their 'true' source proportions are listed in Table 5.5. The Clinton-Cataract end-member is omitted here, given lack of $\delta^{13}C_{DIC}$ data and because this unit is not a major brine producer and production is only within a limited geographic area (Armstrong and Carter, 2010).

Mixture	Proportions	$\delta^{18}O$	$\delta^{2}H$	$\delta^{13}C_{DIC}$	$\delta^{34}S_{SO4}$	$\delta^{18}O_{SO4}$	$^{87}Sr/^{86}Sr$
1	50% Dev-low	−11.66	−83.40	−4.52	+30.82	+14.44	0.70836
	50% Dev-high						
2	25% Dev-low	−6.21	−62.57	−4.28	+30.10	+13.99	0.70893
	25% Dev-high						
	50% Salina-Guelph						
3	45% Dev-low	−10.92	−78.73	−4.52	+30.91	+14.43	0.70957
	50% Dev-high						
	5% Trenton-Black River						
4	33% Salina-Guelph	−1.62	−33.30	+2.78	+30.23	+13.09	0.70964
	33% Trenton-Black River						
	33% Cambrian						

Table 5.5: Isotopic compositions of four different hypothetical mixtures and their source proportions, based on mean source values from Dataset 1.

Mixture 1 is a 50/50 mix of the Dev-low and Dev-high end-members, representing a typical Devonian water sample, as expected to be commonly encountered for leaking fluids. Mixture 2 contains equal parts Dev-low and Dev-high as 50% the sample, with the other 50% composed of Salina-Guelph, a mixture that may also be encountered by the AWP. Mixture 3 is similar to 1, but also contains 5% Trenton-Black River water, and is aimed at testing the ability of the model to detect small amounts of brine in a predominantly shallow water sample. Mixture 4 contains equal portions of the deep end-members (33% each Salina-Guelph, Trenton-Black River, and Cambrian).

Figures 5.1a-c show isotope biplots generated by SIAR for the 6 isotopes. They illustrate the mixture and source compositions; error bars on the latter represent twice the standard deviation. These graphs are useful for visual understanding of how the model generates its results, although mixture visualization may be difficult with large-dimensional datasets.
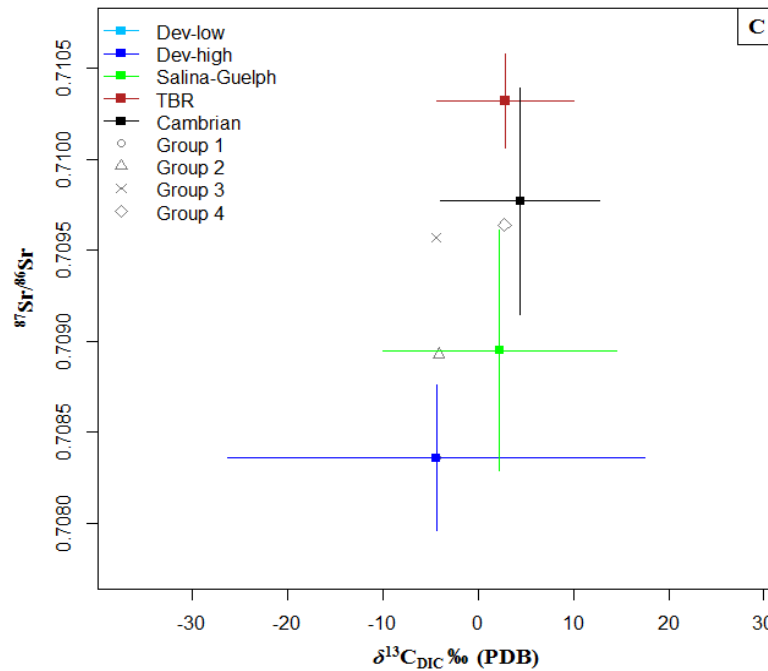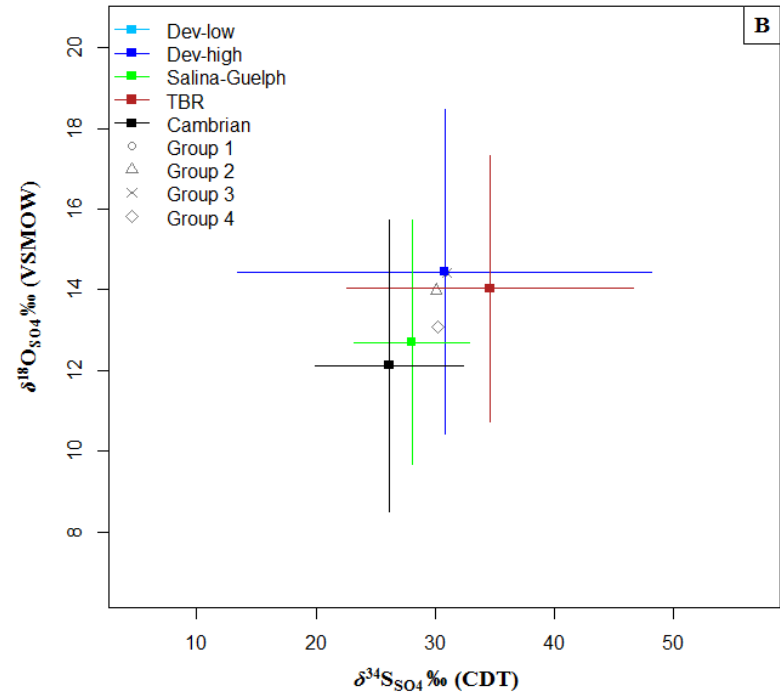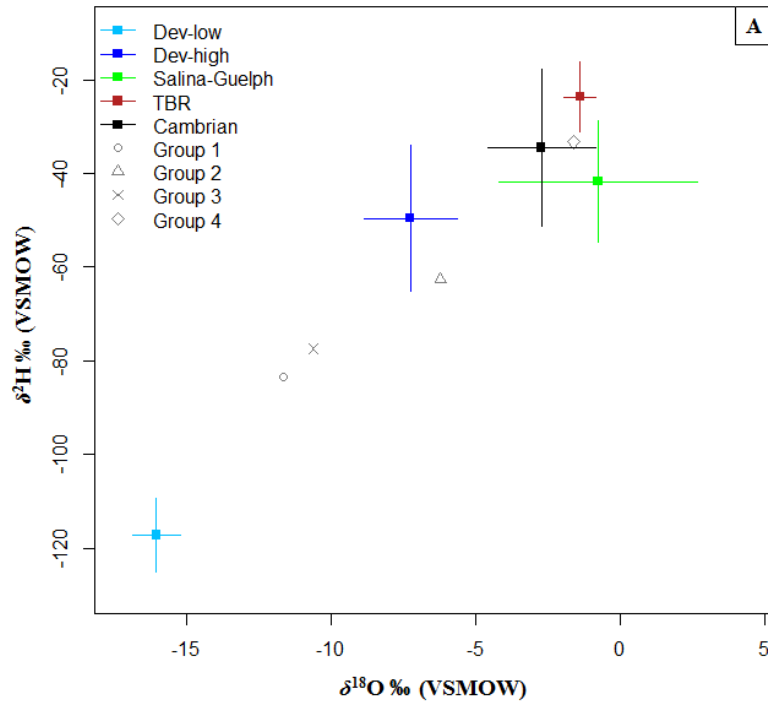
Figure 5.1: Isotope biplots for **(a)** oxygen and hydrogen, **(b)** sulphate sulphur and oxygen, and **(c)** carbon and strontium, constructed by SIAR. Compositions of the four different test mixtures are compared with the means and variability (error bars = 2x standard deviation) of the sources, based on Dataset 1 (TBR = Trenton-Black River end-member).

SIAR has several different options for presenting the posterior distribution data. The most commonly-used output presents the distribution as a histogram, with source proportions on the x-axis and probability density on the y-axis. Here all sources are presented on the same graph for a given sample, although they can be displayed separately.

A second option displays the distributions in boxplot format. Each boxplot contains several nested boxes representing different credibility intervals (CIs), which indicate the probability that the true value lies within the given interval. The default CIs are 50, 75, and 95%, although other intervals can be specified.

A different type of output is the matrix plot. For a given group, this plot shows the posterior distributions of each source as histograms in boxes along the diagonal. Boxes in the upper right-hand side display the correlations between sources graphically, and boxes in the lower left-hand side give the correlations numerically, presented as r^2 values that are scaled in size corresponding to their magnitude. A large negative correlation between sources indicates that the model can readily substitute one source for the other to achieve the mixture composition; in other words, when the proportion of one source is increased in the model, the other must decrease. Sources can also be positively correlated, a less common scenario, indicating that by increasing the proportion of one source, the other source must also increase in order to satisfy the model.

Finally, the SIAR high density regions (siarhdrs) function numerically displays the 95% CI upper and lower limits, modes and means of the estimated proportions for each source in each mixture. If multiple observations are provided for a given mixture, it also includes a measure of the residual error associated with intragroup variability. This summary also gives a list of the worst parameters for convergence; the MCMC algorithm that SIAR uses iteratively generates and evaluates source compositions and proportions; the posterior distribution thusly generated 'converges' towards the 'true' distribution as the number of iterations increases, and this convergence statistic reflects the degree to which it has done so. If many parameters have very low values (<0.01), a longer MCMC run is recommended (Parnell et al., 2010).

5.1.3.1.1   Mixture 1

The simulated proportions for Mixture 1 are presented below in Figures 5.2a-b as histograms and box-plots, respectively. A summary of the 95% credibility intervals, modes and means for each source mixture is presented in Table 5.6. The 'true' proportions for this sample are 50% Dev-low and 50% Dev-high. The model predicts the presence of considerable contributions from both sources, although it slightly overestimates the Dev-high component and underestimates the Dev-high component. It also allows for the inclusion of moderate amounts of Salina-Guelph water, but correctly predicts little or no Trenton-Black River or Cambrian contributions. As shown by the probability distribution (Figure 5.2a), the model's predicted range for Dev-low is fairly well-constrained, while the model is much less certain about the proper amounts of Dev-high and Salina-Guelph. The model is extremely certain about the fact that there is very little or no Trenton-Black River or Cambrian contributions.

Source	Lower 95% CI	Upper 95% CI	Mode	Mean
Dev-low	0.49	0.65	0.58	0.57
Dev-high	0.02	0.42	0.26	0.23
Salina-Guelph	0.04	0.33	0.14	0.17
Trenton-Black River	0.00	0.04	0.00	0.01
Cambrian	0.00	0.03	0.00	0.01

Table 5.6: Summary statistical information about the predicted proportions (in decimal format) of the different sources contributing to Mixture 1.

Examination of the matrix plot for this mixture (Figure 5.2c) and the isotope biplots (Figure 5.1) helps to understand these model behaviours. The matrix plot reveals a high negative correlation between the Dev-high and Salina-Guelph end-members, indicating that one may easily substitute for the other in the model. Figure 5.1a shows the reason for this behaviour: the low-δ^{18}O end of the Salina-Guelph range is close to being in line with the Dev-low, Dev-high, and Mixture 1 compositions, and so Salina-Guelph could act as the high-δ^{18}O end-member instead of (or more likely, in addition to) Dev-high. The compositional ranges for ^{87}Sr/^{86}Sr and the other solute isotopes for Salina-Guelph also overlap considerably with the Devonian range, and therefore a contribution of Salina-Guelph cannot be ruled out. In contrast, the Trenton-Black River and Cambrian ^{87}Sr/^{86}Sr

compositions are considerably higher and do not overlap the Devonian range, and hence these end-members can largely be eliminated. The interchangeability of Dev-high and Salina-Guelph also explains why these two sources have relatively low and broad posterior distributions, compared to the tighter range for Dev-low, for which there is no similarly substitutable end-member.

The positive correlation between Dev-low and Salina-Guelph reveals how incorporating some of the latter in the model (instead of Dev-high) requires the addition of more Dev-low to balance the mixture, since Salina-Guelph has considerably higher $\delta^{18}O$ values than Dev-high. This also explains why the model overestimates the Dev-low contribution, as any incorporation of Salina-Guelph would also require more than 50% Dev-low. Closer inspection reveals that the Salina-Guelph distribution has a positive skew while Dev-high has a slight negative skew. This reflects the fact that 'outlier' Salina-Guelph compositions, especially in terms of $\delta^{18}O/\delta^2H$ and $^{87}Sr/^{86}Sr$, would be required to replace Dev-high in the mixture, and thus Dev-high is the more likely high-$\delta^{18}O$ end-member.

If the Salina-Guelph end-member is excluded from the simulation, the model correctly predicts the proportions of all sources, with the means of both Dev-high and Dev-low at 0.5. However, their 95% CIs range from 0.42-0.57, and this is due the slight substitution possible between the two end-members, given their compositional variability. This effect can also be observed by their negative correlation in Figure 5.2c and is responsible for some of the spread in their proportions in Figure 5.2a-b.

When interpreting such results, other information can be used to determine whether or not a Salina-Guelph component is actually present. For instance, if the sample did contain a considerable amount of such brine, it would have fairly elevated TDS. Other isotopes, as described in later sections, may also help in discerning the presence of Salina-Guelph brine. Finally, any model-predicted small contribution of Salina-Guelph brines should be viewed with some skepticism, given their substitutability with the shallow waters in the model. That said, the putative presence of any predicted component with a non-zero mode should never be rejected outright, without further evaluation.
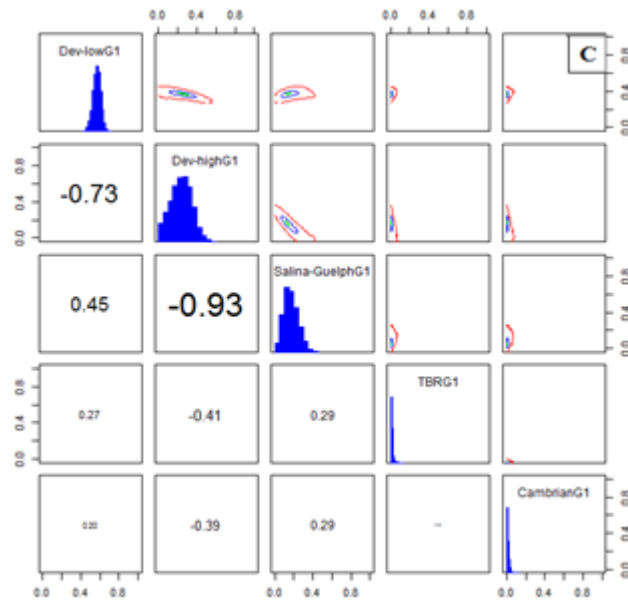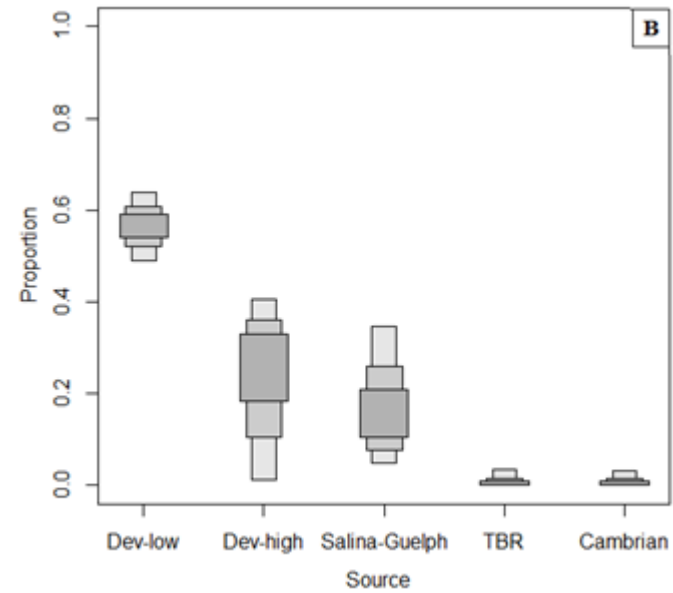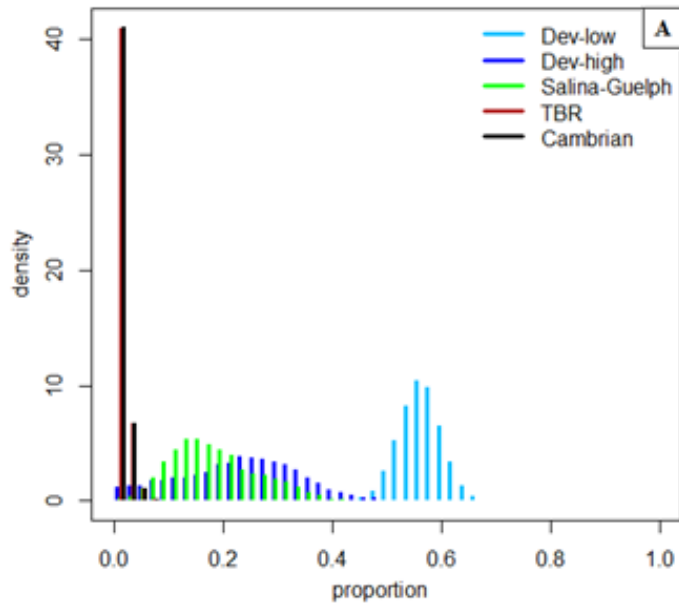
Figure 5.2: SIAR posterior probability distributions for Mixture 1 sources in **(a)** histogram format and **(b)** as boxplots (boxes represent 50, 75, and 95% CIs). The matrix plot is shown in **(c)**; the diagonal shows the posterior distributions for each source, while the upper right-hand boxes show correlations between sources graphically, and lower left-hand boxes give r^2 values.

5.1.3.1.2   Mixture 2

Mixture 2 represents a more complex case, with three source formations (25% Dev-low, 25% Dev-high, 50% Salina-Guelph). The posterior distribution histograms, boxplots and the matrix plot are shown in Figure 5.3a-c, respectively, and a statistical summary is given in Table 5.7. For this mixture, the model predicts the correct proportions more accurately than Mixture 1. The Dev-low proportion is estimated almost perfectly, with a mean and mode of 0.26 and a fairly tight range, while the Dev-low proportion is slightly underestimated, with a mode of 0.19, and has a considerably wider range. The Salina-Guelph contribution is also underestimated, with a mode of 0.35 and a range slightly smaller than that of Dev-high. The model also allows for a considerable amount of Trenton-Black River and Cambrian water (up to ~35% in the case of the 99% CI for the latter), although their modes (the highest probability proportion) are both near zero. The correct proportions for all sources lie within their 95% CIs; this was not the case for Mixture 1, where the CIs for Dev-high and Salina-Guelph had to be extended to 100% to encompass their true values.

Source	Lower 95% CI	Upper 95% CI	Mode	Mean
Dev-low	0.18	0.35	0.26	0.26
Dev-high	0.01	0.38	0.19	0.20
Salina-Guelph	0.21	0.53	0.35	0.36
Trenton-Black River	0.00	0.17	0.02	0.07
Cambrian	0.00	0.27	0.03	0.10

Table 5.7: Summary statistical information about the proportions of the different sources contributing to Mixture 2.

Some of the interpretations of model performance regarding Mixture 2 are similar to those for Mixture 1. The high predictive power for Dev-low is again because there are no nearby end-members that could substitute for it. Dev-high can again be substituted to a degree with Salina-Guelph, which is likely the reason for the former's underestimation and wider putative range of contribution. The underestimation and wide spread of Salina-Guelph contributions may be explained by the negative correlation between it and Cambrian, indicating a degree of substitutability between the two. The oxygen-hydrogen isoplot (Figure 5.1a) illustrates how the mixture composition can be achieved by mixing

some Cambrian brines with some Salina-Guelph brines with a higher-than-average $\delta^{18}O$ (and/or lower-than-average δ^2H) compositions, balanced by Dev-low. The considerable overlap between Cambrian and Salina-Guelph $^{87}Sr/^{86}Sr$ compositions facilitates this substitution.

The higher $^{87}Sr/^{86}Sr$ value of Mixture 2 compared to 1 accounts for the former's larger range in Trenton-Black River and Cambrian contributions. Further understanding of how SIAR is constraining the Salina-Guelph, Trenton-Black River and Cambrian contributions requires a more in-depth discussion of $^{87}Sr/^{86}Sr$. Due to the concentration dependency of $^{87}Sr/^{86}Sr$ (i.e., the deep formations having much higher Sr^{2+} concentrations than the shallow ones), any brine addition to a shallow water will quickly increase the $^{87}Sr/^{86}Sr$ of the mixture. If brine contribution exceeds ~10-20%, the mixture's composition will be approximately equal to that of the brine. The fact that the water isotopic composition of Mixture 2 lies well below the meteoric water line (i.e. the line between Dev-low and Dev-high) suggests that there is a considerable brine component. Thus, the $^{87}Sr/^{86}Sr$ must be similar to that of the brine, or possibly a mixture of multiple brines. Since Mixture 2's $^{87}Sr/^{86}Sr$ is close to that of the Salina-Guelph average, it is the most likely Sr^{2+} contributor; any inclusion of the higher-$^{87}Sr/^{86}Sr$ Trenton-Black River or Cambrian end-members would also require a Salina-Guelph component with below-average $^{87}Sr/^{86}Sr$. Given the much higher $^{87}Sr/^{86}Sr$ range for Trenton-Black River, only a very small amount of it could be included without being balanced by an improbably low-$^{87}Sr/^{86}Sr$ Salina-Guelph component. The Cambrian end-member can be more comfortably substituted for Salina-Guelph, given their overlapping $^{87}Sr/^{86}Sr$ ranges and the negative correlation observed between the two in the matrix plot. Thus the range of possible Cambrian proportions is wider than that of the Trenton-Black River. Finally, while the Trenton-Black River and Cambrian do have larger ranges than in Mixture 1, their highest probability proportions both fall close to the correct value of zero. This outcome reflects the fact that to achieve increasingly greater-than-zero proportions, not only are increasingly below-average Salina-Guelph $^{87}Sr/^{86}Sr$ compositions required, but also higher-(/lower-) than-average $\delta^{18}O(/\delta^2H)$ compositions are needed.

Figure 5.3: SIAR posterior probability distributions for Mixture 2 sources in **(a)** histogram format and **(b)** as boxplots. The matrix plot is shown in **(c)**.

5.1.3.1.3   Mixture 3

Mixture 3 (45% Dev-low, 50% Dev-high, 5% Trenton-Black River) was intended to test the model's ability to identify small contributions of brine in a mostly shallow water sample. The posterior distribution histograms, boxplots and the matrix plot are shown in Figure 5.4a-c, respectively, and the statistics for each source are summarized in Table 5.8. The model again estimates the proportion of Dev-low almost exactly and with a high degree of confidence, and again the Dev-high contribution is underestimated (by about 25%). The model correctly identifies the most probable Trenton-Black River proportion as ~5%, although it also allows for small amounts of Cambrian and Salina-Guelph.

Source	Lower 95% CI	Upper 95% CI	Mode	Mean
Dev-low	0.43	0.60	0.53	0.52
Dev-high	0.03	0.45	0.24	0.25
Salina-Guelph	0.00	0.15	0.04	0.06
Trenton-Black River	0.00	0.15	0.06	0.07
Cambrian	0.00	0.23	0.03	0.10

Table 5.8: Summary statistical information about the proportions of the different sources contributing to Mixture 3.

The fact that the most probable Dev-low contribution is slightly higher than the true proportion is unsurprising and reflects the possible inclusion of more than the true proportions for the deeper formations. Since the model constrains the likely contributions of these sources to relatively small ranges, the range in possible Dev-low proportions still remains fairly narrow. This is illustrated by the matrix plot, which shows small positive correlations between Dev-low and the deep formation waters; increasing the latter requires increasing the contribution of Dev-low to balance the model. It is not clear why the negative correlation between Dev-low and Dev-high is so large for this mixture. Perhaps increasing proportions of Dev-low, along with the deep formations, requires decreasing contribution of Dev-high so that the mixture composition does not get pulled too far to the higher side of the $\delta^{18}O/\delta^2H$ isoplot. This is reinforced by the negative correlations between the proportions of Dev-high and the deep end-members.

Again, the $^{87}Sr/^{86}Sr$ ratio helps to constrain the proportions of the deep end-members, in conjunction with $\delta^{18}O$ and δ^2H. While not evident on the basis of only $\delta^{18}O/\delta^2H$, the mixture's high $^{87}Sr/^{86}Sr$ requires some brine contribution. The fact that the mixture's water isotope composition plots on the meteoric water line suggests that not much Salina-Guelph brine is included; the same goes for Cambrian and Trenton-Black River but to a lesser extent, as they are closer to being in line with the Devonian end-members in $\delta^{18}O/\delta^2H$ space. This constraint on the deep end-member contribution thus limits the amount of brine strontium that can be added to the mixture. Since the amount of brine added must be low, there is likely insufficient Sr^{2+} added to overwhelm the mixture's $^{87}Sr/^{86}Sr$ to the point where it is indistinguishable from pure brine.

Mixture 3's $^{87}Sr/^{86}Sr$ is slightly below the mean Cambrian composition, so Cambrian brine with higher-than-average $^{87}Sr/^{86}Sr$ would be needed to satisfy the requirement for only a small brine contribution. Any inclusion of Salina-Guelph brines would likely need to be accompanied by one of the higher end-members, most likely Trenton-Black River, to drive the average $^{87}Sr/^{86}Sr$ of the brine mixture to ratios higher than that of Mixture 3. All Trenton-Black River compositions lie above the mixture's signature, making it the most probable option for the deep end-member. However, the model is unsure whether Trenton-Black River is the sole deep end-member or if it is mixed with a small amount of Salina-Guelph or Cambrian. Additional testing reveals that if the Trenton-Black River proportion is increased to 10%, thus increasing the $^{87}Sr/^{86}Sr$ ratio, the model is better able to resolve the Trenton-Black River contribution; the Cambrian contribution remains about the same since the $^{87}Sr/^{86}Sr$ ratio still lies comfortably within the Cambrian range, but the Salina-Guelph contribution contracts considerably with a mean around zero.

To summarize, this mixture demonstrates the ability for the model to detect the presence of small amounts of brine in an otherwise shallow water sample, which may be overlooked in a simple examination of $\delta^{18}O/\delta^2H$ isotopes and salinity. Further information, for instance regarding the geology and production history of the area, may help narrow down the precise identity of the brine component, which the model may be unsure of given such low brine amounts.
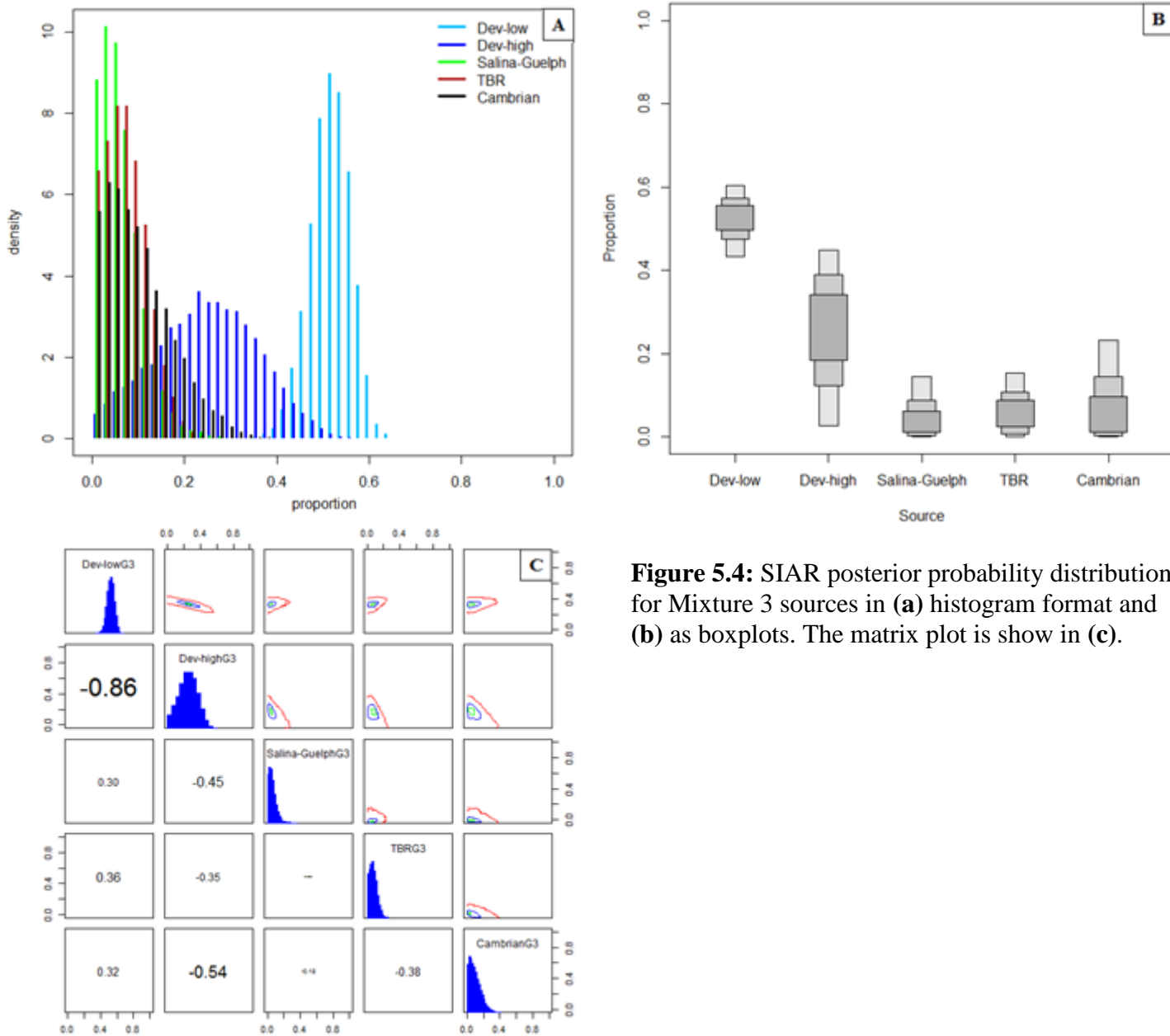
Figure 5.4: SIAR posterior probability distributions for Mixture 3 sources in **(a)** histogram format and **(b)** as boxplots. The matrix plot is show in **(c)**.

5.1.3.1.4   Mixture 4

Mixture 4 (33% Salina-Guelph, 33% Trenton-Black River, 33% Cambrian) was intended to test the model's ability to discriminate between the three deep end-members. The posterior distribution histograms, boxplots and the matrix plot are shown in Figure 5.5a-c, respectively, and a statistical summary is given in Table 5.9. The model correctly estimates the proportion of Dev-low as effectively zero. The mode of Dev-high is also near zero, although the range is somewhat higher. The Salina-Guelph and Trenton-Black River contributions are almost perfectly estimated, while the mode for the Cambrian is underestimated by less than 10%. However, the compositional ranges for all deep end-members are quite broad, indicating considerable uncertainty in the model.

Source	Lower 95% CI	Upper 95% CI	Mode	Mean
Dev-low	0.00	0.05	0.01	0.02
Dev-high	0.00	0.14	0.01	0.05
Salina-Guelph	0.14	0.53	0.32	0.33
Trenton-Black River	0.10	0.57	0.34	0.34
Cambrian	0.00	0.49	0.25	0.25

Table 5.9: Summary statistical information about the proportions of the different sources contributing to Mixture 4.

The low mode for the Dev-low contribution is likely because of it being very far from the mixture composition in $\delta^{18}O/\delta^2H$ space; addition of any significant amount of Dev-low water would considerably lower the mixture composition. The situation is similar for Dev-high water. However, since it is closer in $\delta^{18}O/\delta^2H$ space to the mixture composition, its addition would have a less extreme effect, permitting Dev-high to have a larger range of potential contributions.

The broad ranges of the deep end-members in their posterior distributions are largely a consequence of the fact that the three are all fairly close together in $\delta^{18}O/\delta^2H$ space with considerable overlap between their ranges; there is also considerable overlap in terms of the other isotopic compositions. $^{87}Sr/^{86}Sr$ also becomes a less powerful tool when the formations in question have similar strontium concentrations; the mixture composition

essentially lies on a mixing line between Salina-Guelph and Trenton-Black River, but could also be solved with only Cambrian due to the latter's intermediate composition. A similar mixing line is seen in sulphate $\delta^{18}O/\delta^{34}S$ space, although the positions of Salina-Guelph and Cambrian are reversed, which may help constrain the model. The matrix plot shows that the Cambrian can be substituted by both Salina-Guelph and Trenton-Black River, likely since the former overlaps with the ranges of both of the latter end-members across all isotopes. This is likely the reason why the Cambrian brine contribution is slightly underestimated, with lower mean, mode and CI limits than the other formations.

Although not readily apparent from the matrix plot, any inclusion of Devonian waters would decrease the required contribution of Cambrian brine, judging by the positions of the end-members in $\delta^{18}O/\delta^2H$ space and sulphate $\delta^{18}O/\delta^{34}S$ space. Any inclusion of Devonian waters could require raising the contribution of Trenton-Black River brine, which may explain why the latter has the highest modal proportion among the deep end-members. The negative correlation between Salina-Guelph and Trenton-Black River is much lower than the Cambrian correlations, since the ranges in isotope space for the former two do not overlap as much or at all.

Despite the relatively lower confidence in the model's predictions, SIAR does assign the highest probabilities to proportions reasonably close to the correct amounts. Also, aside from the Cambrian, the model does give non-zero lower 95% CIs to the deep end-members, correctly indicating that they are present. The upper 95% CIs are also not unreasonably high – within 0.25 of the correct proportions. Thus, the model performs quite well despite some difficulties resulting from the similarities in the compositions of various deep formations brines and the nature of their geometries in isotope space.
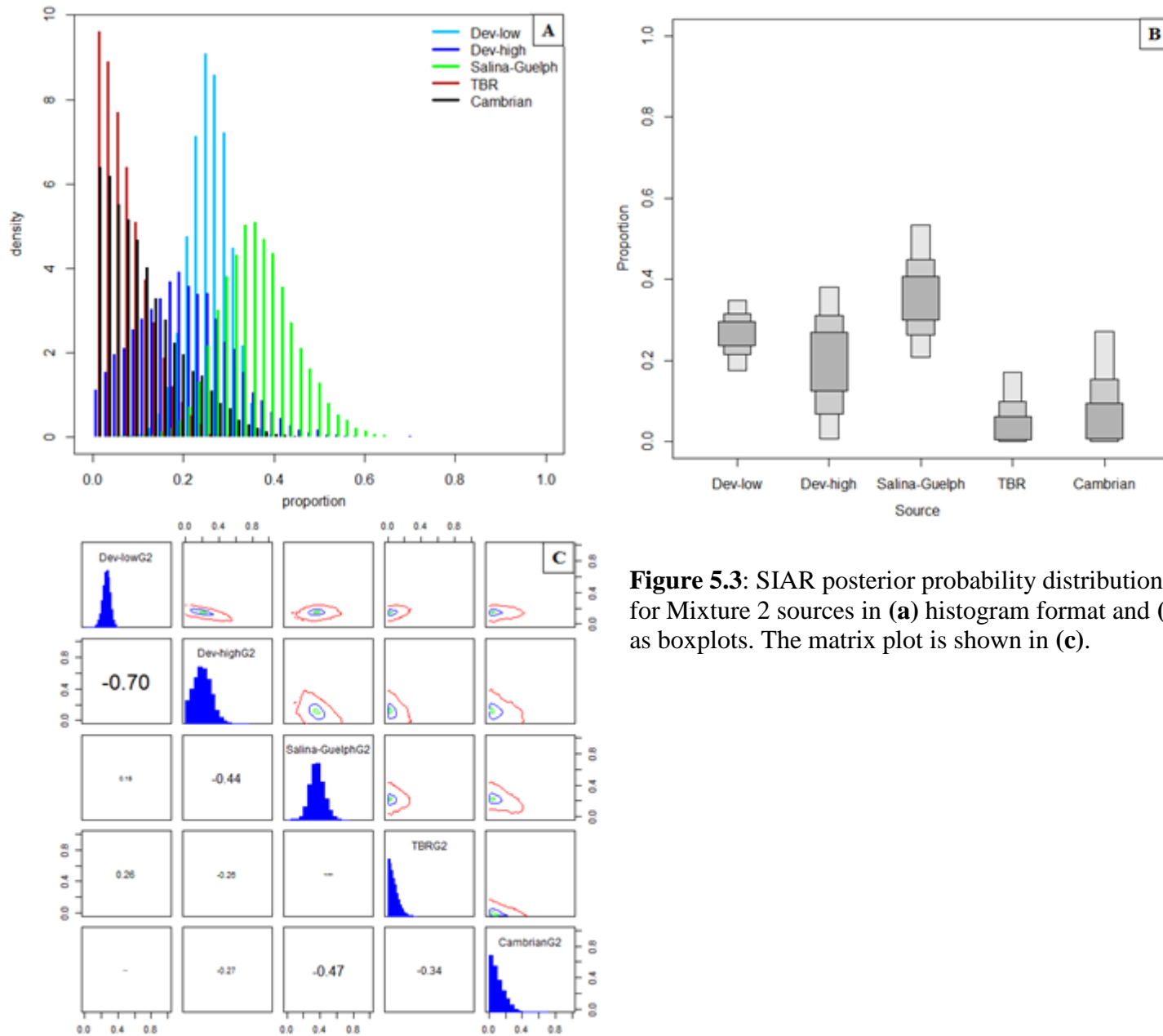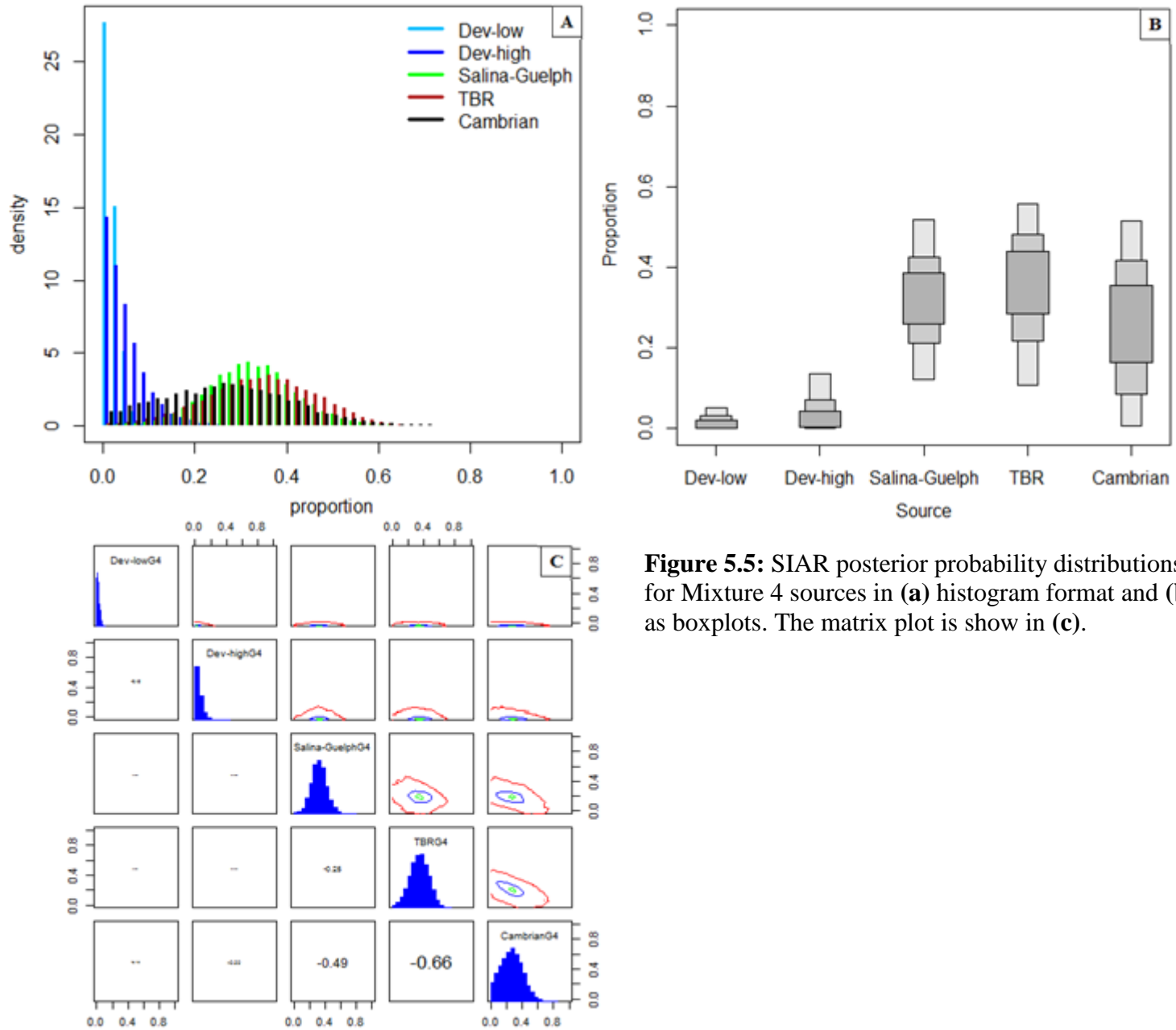
Figure 5.5: SIAR posterior probability distributions for Mixture 4 sources in **(a)** histogram format and **(b)** as boxplots. The matrix plot is show in **(c)**.

5.1.3.2   *Dataset 2*

The model testing can be extended to Dataset 2; the new isotopic compositions for the
four test mixtures are summarized in Table 5.10. Isoplots are presented in Figures 5.6a-c
and the posterior distributions of the mixtures are presented in Figures 5.7a-d; summary
statistics and matrix plots for the mixtures are available in Appendix F. The mixture
compositions and accordingly the posterior distributions are largely similar to those for
Dataset 1. The main differences between the two datasets are discussed in the following
sections.

Mixture	Proportions	$\delta^{18}O$	δ^2H	$\delta^{13}C_{DIC}$	$\delta^{34}S_{SO4}$	$\delta^{18}O_{SO4}$	$^{87}Sr/^{86}Sr$
1	50% Dev-low	−11.74	−83.83	−4.52	+29.67	+15.48	0.70834
	50% Dev-high						
2	25% Dev-low	−6.15	−63.44	−4.24	+29.48	+15.15	0.70895
	25% Dev-high						
	50% Salina-Guelph						
3	45% Dev-low	−11.03	−79.24	−4.52	+29.76	+15.46	0.70917
	50% Dev-high						
	5% Trenton-Black River						
4	33% Salina-Guelph	−1.89	−33.39	+2.70	+30.56	+13.14	0.70950
	33% Trenton-Black River						
	33% Cambrian						

Table 5.10: Compositions of four different hypothetical mixtures and their source
proportions, based on mean source values from Dataset 2.
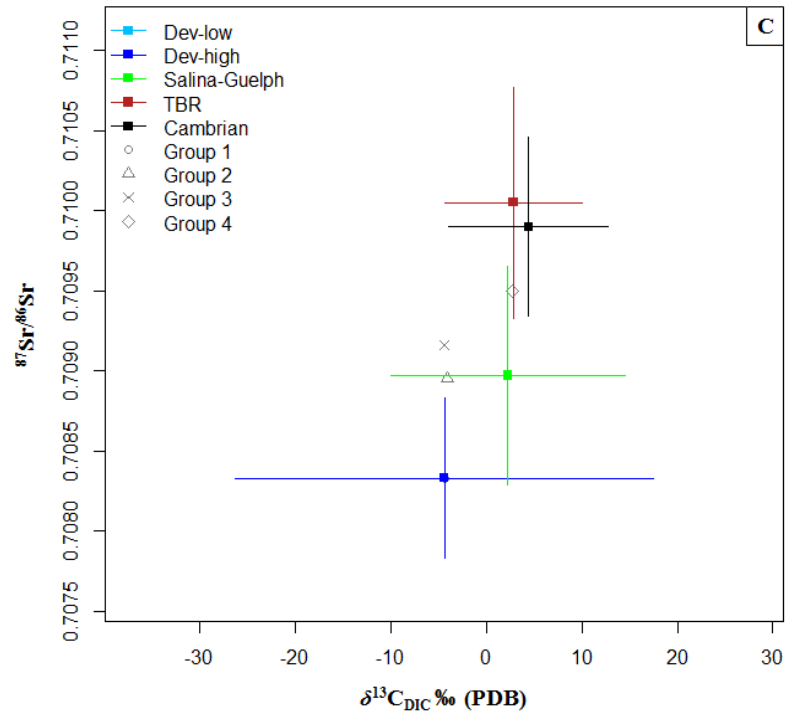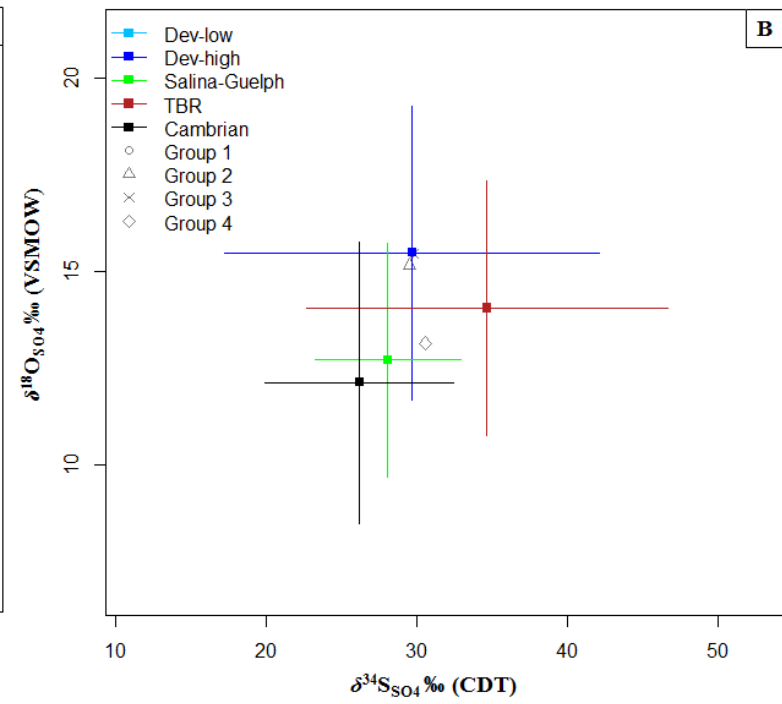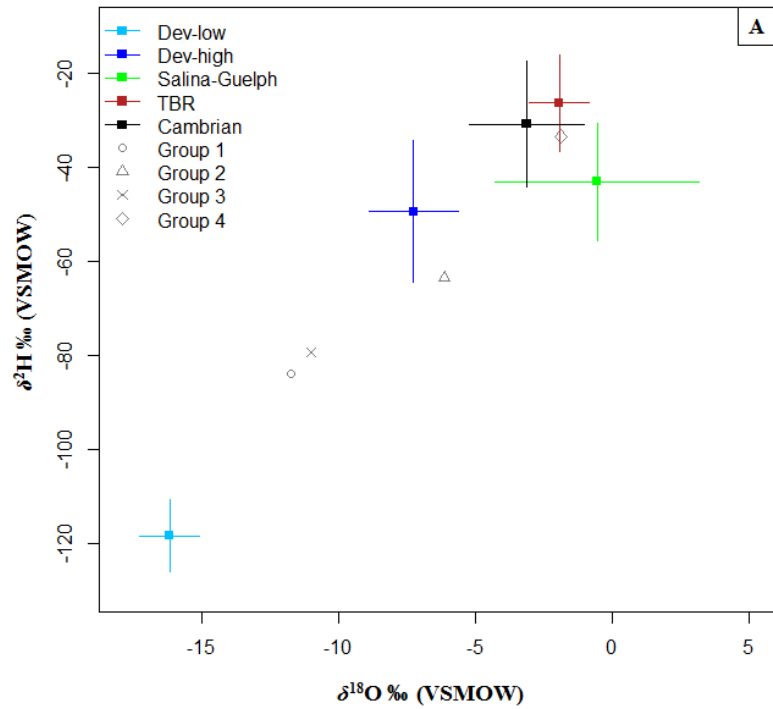
Figure 5.6: Isotope biplots for **(a)** oxygen and hydrogen, **(b)** sulphate sulphur and oxygen, and **(c)** carbon and strontium, constructed by SIAR. Compositions of the four test mixtures are plotted against the means and standard deviations of the sources, based on Dataset 2.
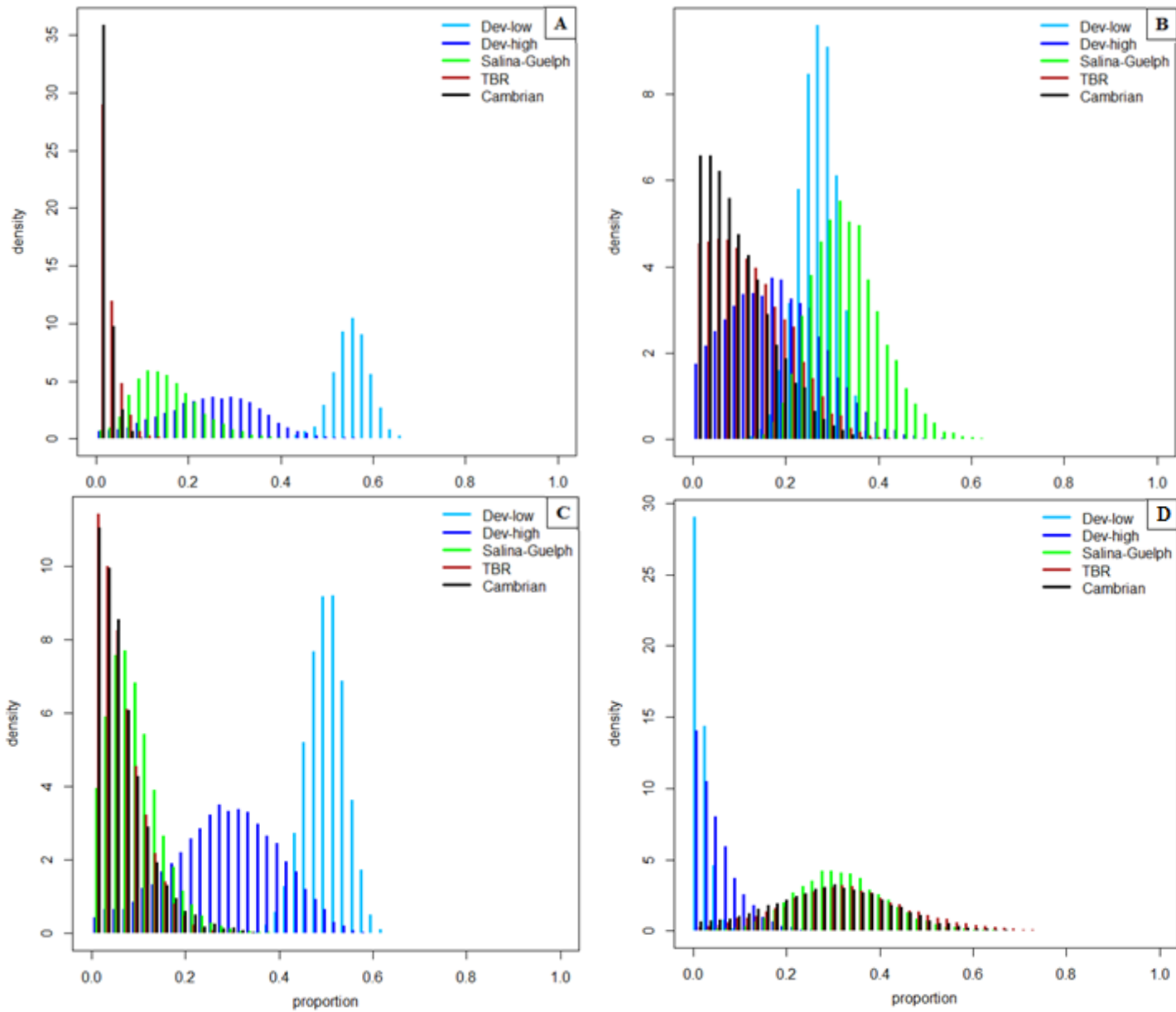
Figure 5.7: SIAR posterior distributions for Mixtures 1-4 (a-d, respectively) based on Dataset 2.

5.1.3.2.1   Mixture 1

For Mixture 1, the Devonian end-members' distributions (Figure 5.7a) are essentially unchanged relative to Dataset 1, while the Salina-Guelph distribution is slightly shifted towards lower values. The latter is likely due to the higher Sr^{2+} concentration in Dataset 2, making it more difficult to incorporate Salina-Guelph brine without significantly raising the mixture's $^{87}Sr/^{86}Sr$ ratio. The largest difference from the Dataset 1 results is that the Trenton-Black River and Cambrian distributions are slightly broader, although their modes still lie near zero. Several factors could cause these changes. The $\delta^{18}O$ values for Trenton-Black River and Cambrian end-members are lower in Dataset 2, bringing them closer to the meteoric water line and thus making them easier to substitute for Dev-high; this is reflected in increased correlation coefficients between them and Dev-high. Trenton-Black River and Cambrian are also closer to each other in $\delta^2H/\delta^{18}O$ and $^{87}Sr/^{86}Sr$ space and have greater variability than in Dataset 1. The lower mean $^{87}Sr/^{86}Sr$ ratio of Trenton-Black River and its and the Cambrian's lower mean Sr^{2+} concentrations, also enables increased contributions from these deep formations. That said, their potential contributions remain very constrained by their high $^{87}Sr/^{86}Sr$ ratios. These brines could only be contributors if the shallow component had a below-average $^{87}Sr/^{86}Sr$ composition, the probability of which decreases rapidly as the brine contribution increases.

5.1.3.2.2   Mixture 2

The distributions for the Mixture 2 end-members (Figure 5.7b) are also very similar to those for Dataset 1. However, the Salina-Guelph distribution has shifted slightly to lower proportions (mode of 0.30 rather than 0.35), the Trenton-Black River range is broader (upper 95% CI of 0.27 rather than 0.17) and that of the Cambrian is somewhat narrower (upper 95% CI of 0.23 rather than 0.27). The model is also less confident about the latter two end-members having near-zero proportions. These differences in the Trenton-Black River and Cambrian distributions are for similar reasons to those discussed for Mixture 1. The likely explanation for the lowered Salina-Guelph distribution is that the increased flexibility for incorporation of Trenton-Black River and Cambrian in the model allows for

these end-members to substitute for one another more readily. However, while Salina-Guelph and Trenton-Black River do show a correlation of -0.39 while they had essentially no correlation in the Dataset 1 simulation, the correlation between Salina-Guelph and Cambrian is lower (-0.19 vs. -0.44), possibly because of their increased $\delta^{18}O$ difference, which – along with its higher $^{87}Sr/^{86}Sr$ – may help explain the tighter Cambrian range.

5.1.3.2.3   Mixture 3

For Mixture 3, the Devonian distributions are again essentially unchanged from Dataset 1, although they are both shifted slightly towards their true proportions (Figure 5.7c). The distributions for Salina-Guelph and Trenton-Black River are broader, and the mode is higher for Salina-Guelph and lower for the other deep formations. These effects may in part be explained by the decrease in the mean Trenton-Black River $^{87}Sr/^{86}Sr$ mean, making it less distinguishable from the Cambrian. Also, since the Salina-Guelph's mean Sr^{2+} concentration is considerably higher, and the mixture's $^{87}Sr/^{86}Sr$ ratio is lower than for Dataset 1, it is easier for the model to use a small amount of Salina-Guelph brine with a slightly above average $^{87}Sr/^{86}Sr$ composition, possibly mixed with some Cambrian or Trenton-Black River, to explain the mixture composition. The negative correlation between Salina-Guelph and Dev-high is also larger (–0.60 vs. –0.45), possibly due to the former being slightly closer to the meteoric water line than in Dataset 1. The increased substitutability of Dev-high for Salina-Guelph may help to explain the higher estimated proportion of Salina-Guelph brine relative to Dataset 1.

5.1.3.2.4   Mixture 4

The Devonian distributions for Mixture 4 (Figure 5.7d) are also relatively unchanged from their Dataset 1 versions. The deep end-members' distributions are somewhat different; the Salina-Guelph range has shifted slightly lower (mode of 0.29 rather than 0.32), and the Trenton-Black River and Cambrian ranges are almost identical to one another and have modes nearer to the true proportions (0.33 and 0.30 respectively). In general, all of the deep end-members' distributions have become more similar to each other. It is unclear exactly why the Salina-Guelph distribution is shifted, but the increased

similarity between the Trenton-Black River and Cambrian ranges is likely a consequence of their closer proximity in $\delta^2H/\delta^{18}O$ and $^{87}Sr/^{86}Sr$ space.

5.1.3.3   Inclusion of $\delta^{37}Cl$ and $\delta^{81}Br$ data

One way to improve the performance of mixing models is to increase the number of isotopes used, particularly isotopes with good end-member separation. This is demonstrated in the following section by the addition of chlorine and bromine isotopic data ($\delta^{37}Cl$ and $\delta^{81}Br$). A few studies (Kaufman et al., 1993; Shouakar-Stash, 2008) have previously investigated the $\delta^{37}Cl$ and $\delta^{81}Br$ values of groundwaters in Ontario and the Michigan basin and found significant compositional differences between formations, which should help constrain the model performance. In the following sections, these data are added to Dataset 2 and compared with the earlier results for Mixtures 1-4.

 The $\delta^{37}Cl$ and $\delta^{81}Br$ values of the end-members, based on the data from the above studies, and Cl/Br concentration data from the studies in Dataset 2, are presented in Table 5.11, and the $\delta^{37}Cl$ ‰and $\delta^{81}Br$ values of Mixtures 1-4 are given in Table 5.12. The end-member and mixture compositions are shown in a $\delta^{81}Br/\delta^{37}Cl$ biplot (Figure 5.8).

End-member	$\delta^{37}Cl$ mean	$\delta^{37}Cl$ stdev	$\delta^{81}Br$ mean	$\delta^{81}Br$ stdev	Cl mean	Cl stdev	Br mean	Br stdev
Dev-low / Dev-high	+0.63	0.45	+0.58	0.14	9481	8486	52	49
Salina-Guelph	−0.38	0.21	-0.76	0.12	211195	32993	2258	687
Clinton-Cataract	+0.37	0.21	+1.52	0.20	151657	32857	1389	377
Trenton-Black River	−0.61	0.28	+0.70	0.28	140983	37706	1005	398
Cambrian	−0.23	0.13	+0.97	0.17	188835	31962	1763	410

Table 5.11: The $\delta^{37}Cl$ and $\delta^{81}Br$ values of the SIAR end-members, based on data from Kaufman et al. (1993) and Shouakar-Stash (2008). Cl and Br ion concentrations have been generated from the sources listed previously for Dataset 2. All isotopic compositions are in units of ‰ and solutes are in units of mg/L.

Mixture	$\delta^{37}Cl$ (‰)	$\delta^{81}Br$ (‰)
1	0.63	0.58
2	-0.33	-0.73
3	0.08	0.64
4	-0.39	0.14

Table 5.12: The $\delta^{37}Cl$ and $\delta^{81}Br$ values of the four test mixtures.
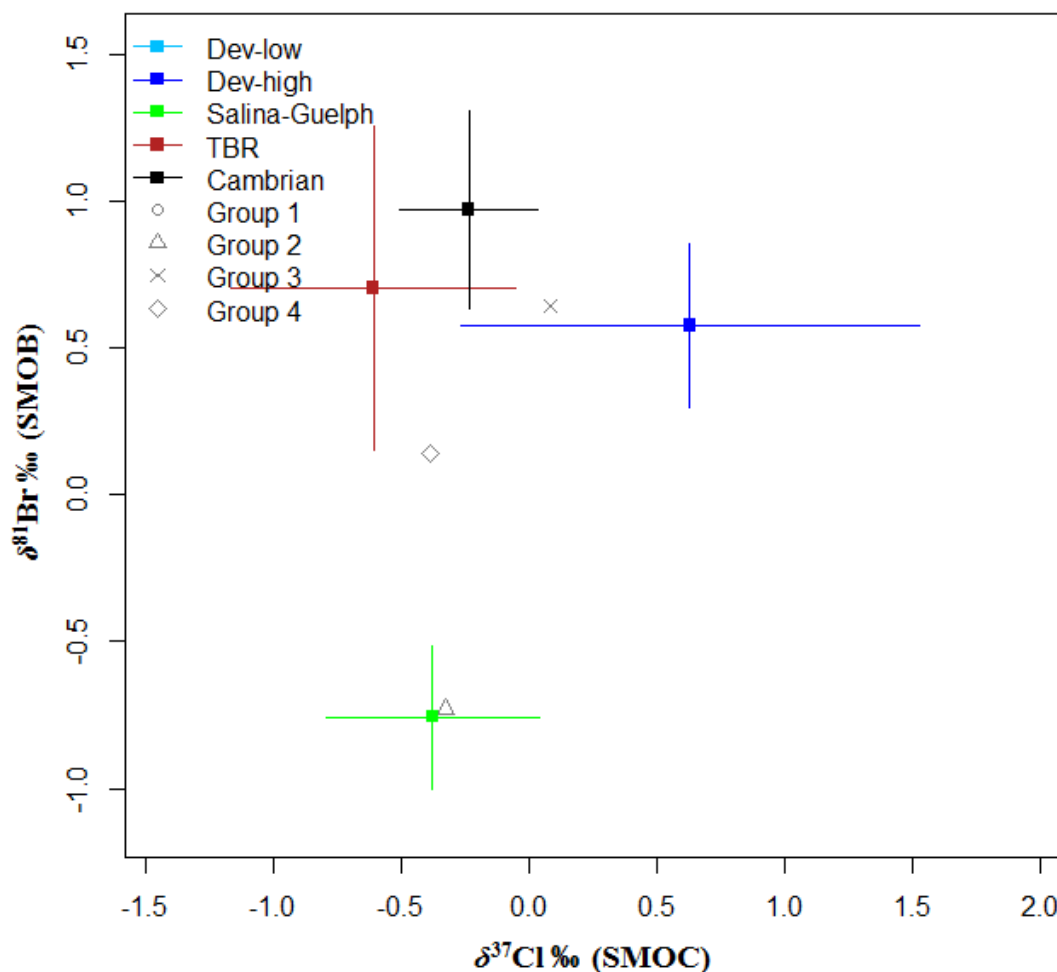
Figure 5.8: SIAR isotope biplot for δ^{37}Cl and δ^{81}Br showing the source and mixture compositions. Based on data from Kaufman et al. (1993) and Shouakar-Stash (2008).

The posterior probability histograms for the four mixtures are presented in Figure 5.9a-d. Summary statistics and matrix plots are available in Appendix F. In general, model predictions are significantly improved by the incorporation of the δ^{37}Cl and δ^{81}Br data. This improvement arises both from the favourable geometry of the source compositions and the fact that both isotopic systems act similarly to ^{87}Sr/^{86}Sr in that there are strong concentration differences between the shallow and deep waters. Specific model results are described in the following sections.
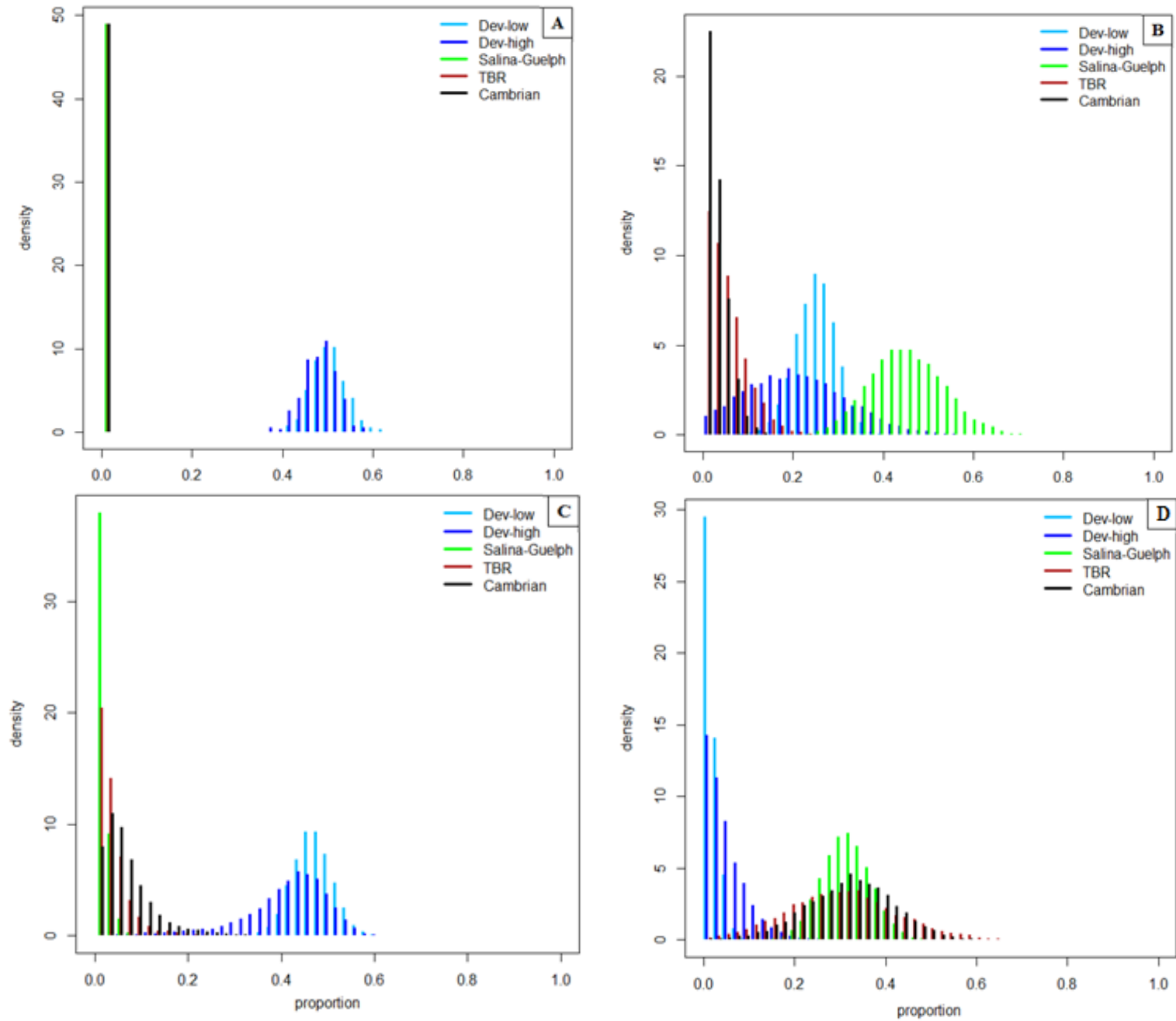
Figure 5.9: SIAR posterior distributions for Mixtures 1-4 based on Dataset 2 plus the $\delta^{37}Cl$ and $\delta^{81}Br$ data.

5.1.3.3.1   Mixture 1

For Mixture 1, both Dev-low and Dev-high are extremely well-predicted, with relatively tight, near-normal distributions with means and modes within 2% of the true proportions. The model is extremely confident that there are no Salina-Guelph, Trenton-Black River, or Cambrian contributions, with means, modes and 95% CI's well below 1%. This is a significant improvement over the previous simulations, where the model had considerable difficulty predicting the correct proportion of Salina-Guelph, due to the overlap of its $^{87}Sr/^{86}Sr$ ratios with those of Devonian end-members, and possible substitutability with Dev-low based on $\delta^2H/\delta^{18}O$. The Salina-Guelph position in $\delta^{81}Br/\delta^{37}Cl$ space is far removed from that of the Devonian end-members, making addition of Salina-Guelph impossible without significantly altering the mixture's $\delta^{37}Cl$ and $\delta^{81}Br$ values. Also, while the $\delta^{81}Br$ range for the Devonian end-members overlaps somewhat with those of the Trenton-Black River and Cambrian, they are quite well separated in terms of $\delta^{37}Cl$, which supplements $^{87}Sr/^{86}Sr$ in constraining their proportions. With such an exclusion of all brine components, the model can still accurately predict the proportions of Dev-low and Dev-high even if their proportions were different from the arbitrary 50/50 split chosen for this mixture. Although their relative proportions are of no real significance for the purposes of the AWP goals, such variations might significantly impact the model results of any dataset that did not include $\delta^{37}Cl$ and $\delta^{81}Br$.

5.1.3.3.2   Mixture 2

The proportions for Mixture 2 are also much better estimated than without the $\delta^{37}Cl$ and $\delta^{81}Br$ data. Dev-low and Dev-high have modes of 0.27 and 0.22, respectively, although the latter's distribution is still quite broad. The Salina-Guelph contribution is quite well-estimated, with a mode of 0.44, yet it also has a relatively wide distribution. The Trenton-Black River and Cambrian both have modes of 0.01, with significantly narrower distributions, although the distribution of the latter is approximately twice as wide as the former (upper 95% CI of 0.13 vs. 0.07). The improved Dev-high and Salina-Guelph estimations are again reflective of the large separation between their compositions in

δ^{81}Br/δ^{37}Cl space. Their wide distributions reflect the fact that once enough brine added to raise the mixture's δ^{37}Cl and δ^{81}Br compositions to near those of the brine, further brine addition will not significantly change the mixture composition.

The model is also able to significantly limit the Trenton-Black River and Cambrian proportions due to the unique geometry of the sources in δ^{81}Br/δ^{37}Cl space. Since the Trenton-Black River and Cambrian are well-separated from Salina-Guelph on the δ^{81}Br scale, while all having similar δ^{37}Cl values, any significant contribution of Trenton-Black River or Cambrian to a mixture containing Salina-Guelph would increase the δ^{81}Br in such a way that the mixture composition would fall off from the Devonian/Salina-Guelph mixing curve, and thus could not simply be a product of those sources alone. Nonetheless, because of the variability of Salina-Guelph compositions, there remains some possibility for a small Trenton-Black River or Cambrian contribution, given a below-average δ^{81}Br value for Salina-Guelph; this potential is higher for Trenton-Black River because it is closer to the Salina-Guelph composition.

As a final note, while Salina-Guelph proportions <0.5 are fairly well-estimated by the model (predicted modes within ~0.05 of the true proportion), they tend to become increasingly underestimated if the proportion is increased significantly beyond 0.5. The reason for this is unclear but one trend is that a negative correlation exists between Salina-Guelph and Trenton-Black River in underestimated samples, which increases as the Salina-Guelph proportion increases. This seems to indicate that Trenton-Black River can substitute for Salina-Guelph (thus reducing the proportion of the latter) but only when the Salina-Guelph proportion large enough such that the amount of Cl and Br added to the mixture by the Trenton-Black River brine is relatively small compared to their total concentrations, and the mixture's isotopic composition is very close to that of Salina-Guelph. Any increase of the mixture's δ^{81}Br value resulting from addition of Trenton-Black River can be balanced by lower-than-average Salina-Guelph δ^{81}Br values. However, this cannot be accomplished when the Salina-Guelph proportion is lower and the mixture composition differs more significantly from that of the Salina-Guelph average; that would require an improbably high Salina-Guelph δ^{37}Cl to balance the Trenton-Black River contribution.

5.1.3.3.3   Mixture 3

Mixture 3 proportions are also fairly well-estimated. The modal proportions for Dev-low and Dev-high are 0.46 and 0.45, respectively, although Dev-high does have a long (albeit low-probability) negative tail. The distributions of the Salina-Guelph, Trenton-Black River and Cambrian are well-constrained, with upper 95% CI's of 0.03, 0.10, and 0.15, respectively. The model is extremely confident that the Salina-Guelph proportion is near zero, again largely because of source geometry, with the Devonian δ^{81}Br value being intermediate between the Salina-Guelph and the other two deep formations; while the mixture composition lies above that of the Devonian end-members in terms of δ^{81}Br, any significant Salina-Guelph addition could easily bring it below the Devonian composition.

The Cambrian has the broadest distribution of the deep formations largely because its δ^{37}Cl and δ^{81}Br values are most similar to those of the Devonian waters – substitutability which is reflected in a large negative correlation between the two (r^2 = -0.71). However, while it is possible for the Cambrian to be the sole brine contributor, such would require an improbably low-δ^{37}Cl (and/or low-δ^{81}Br) Devonian counterpart. Thus if any Cambrian brine is to be included, it must likely be balanced by a very small amount of Salina-Guelph in order for the mixture to remain on the line between the Devonian and Trenton-Black River end-members. This arrangement is supported by a positive correlation (r^2 = 0.69) between Cambrian and Salina-Guelph, and would also result in a decrease in the Trenton-Black River fraction, as reflected by the small negative correlation between Cambrian and Trenton-Black River (r^2 = -0.31). The possibility for this mixing scenario is likely the cause of the underestimated proportions for the Trenton-Black River. Greater proportions of Trenton-Black River do result in non-zero modes for it, although its proportion is always somewhat underestimated due to the possibility of substitution by a combination of Cambrian and a small amount of Salina-Guelph.

The large negative skew in the Dev-high proportions is likely related to the facts that the Devonian waters are largely differentiated from the Trenton-Black River on the basis of δ^{37}Cl, and yet both end-members have a very wide range of δ^{37}Cl values and the Cl concentrations of both are also quite variable.

5.1.3.3.4   Mixture 4

The Mixture 4 distributions are largely unchanged from those produced without $\delta^{37}Cl$ and $\delta^{81}Br$ data, although those for the deep formations are somewhat narrower, particularly that of Salina-Guelph. That the Devonian end-members' distributions are unchanged is understandable considering that solute-based tracers such as $^{87}Sr/^{86}Sr$, $\delta^{37}Cl$ and $\delta^{81}Br$ are less useful for determining potential freshwater contributions to a largely brine mixture, since addition of freshwater would not contribute enough of the solute to affect its isotopic composition. Thus the Devonian contributions remain largely constrained by the $\delta^{18}O$ and δ^2H values. The tightening of the deep formations' distributions reflects the fact that their compositions in $\delta^{81}Br/\delta^{37}Cl$ space are more well-separated than for the other isotopes; however since the Salina-Guelph is much more separated from the Cambrian and Trenton-Black River than the latter two are from each other, its range is constrained the most. The fact that the Salina-Guelph, Trenton-Black River and Cambrian distributions are slightly underestimated (all have modes of ~0.31) reflects the possibility of a freshwater component, mostly likely Dev-high, judging from its broader distribution/proximity in $\delta^2H/\delta^{18}O$ space.

As this mixture represents an equitable mixture of the three deep formations, further tests were performed to assess the model's performance regarding variations of this mixture with different proportions of these sources. In general, predictions were not as good as for the even distribution of proportions, yet were still quite acceptable, with the modes of the predicted proportions generally within 20% of the true proportions.

5.1.3.4 Inclusion of Clinton-Cataract

The previous discussions excluded the Clinton-Cataract end-member in favour of reducing model complexity and inclusion of the $\delta^{13}C_{DIC}$ data (since this end-member only has one $\delta^{13}C_{DIC}$ datapoint). This exclusion is not unreasonable from an AWP perspective given that the Clinton-Cataract is a relatively minor brine producer and its production is confined to a limited area that does not overlap with some of the other end-members. Nonetheless, the consequences of its inclusion on the model's ability to predict the proportions of Mixtures 1-4 are evaluated in the following sections. Isoplots showing the position of Clinton-Cataract alongside the other end-members and mixtures are presented in Figures 5.10a-d. Model results are evaluated based on Dataset 2, both with and without $\delta^{37}Cl$ and $\delta^{81}Br$ data. The $\delta^{13}C_{DIC}$ data are omitted from these scenarios.

5.1.3.4.1 Without $\delta^{37}Cl$ and $\delta^{81}Br$ data

The posterior distributions for Mixtures 1-4 including Clinton-Cataract as a potential end-member but not using $\delta^{37}Cl$ and $\delta^{81}Br$ data are presented in Figures 5.11a-d.

For Mixture 1, the distributions of the other end-members are relatively unchanged by the addition of Clinton-Cataract. The model allows some Clinton-Cataract contribution, but its distribution is tightly confined near zero, similar to Trenton-Black River and Cambrian. The Clinton-Cataract distribution is likely controlled largely by its mean $^{87}Sr/^{86}Sr$, which is higher than any other end-member. However, it is also the most variable end-member in terms of $^{87}Sr/^{86}Sr$, with the lower end of the range overlapping considerably with Salina-Guelph brines, thus producing a long tail on the former's distribution. Finally, the Dev-high distribution is shifted slightly towards lower proportions, likely reflecting possible inclusion of small amounts of Clinton-Cataract.

Mixture 2 distributions are also largely unchanged. The model is in fact more confident that the correct proportions of Trenton-Black River and Cambrian lie towards the lower end of their ranges; this is likely due to the possibility of Clinton-Cataract substituting for them. Clinton-Cataract has a distribution that is largely similar to that of Trenton-Black River. The breadth of the Clinton-Cataract distribution is made possible by several factors
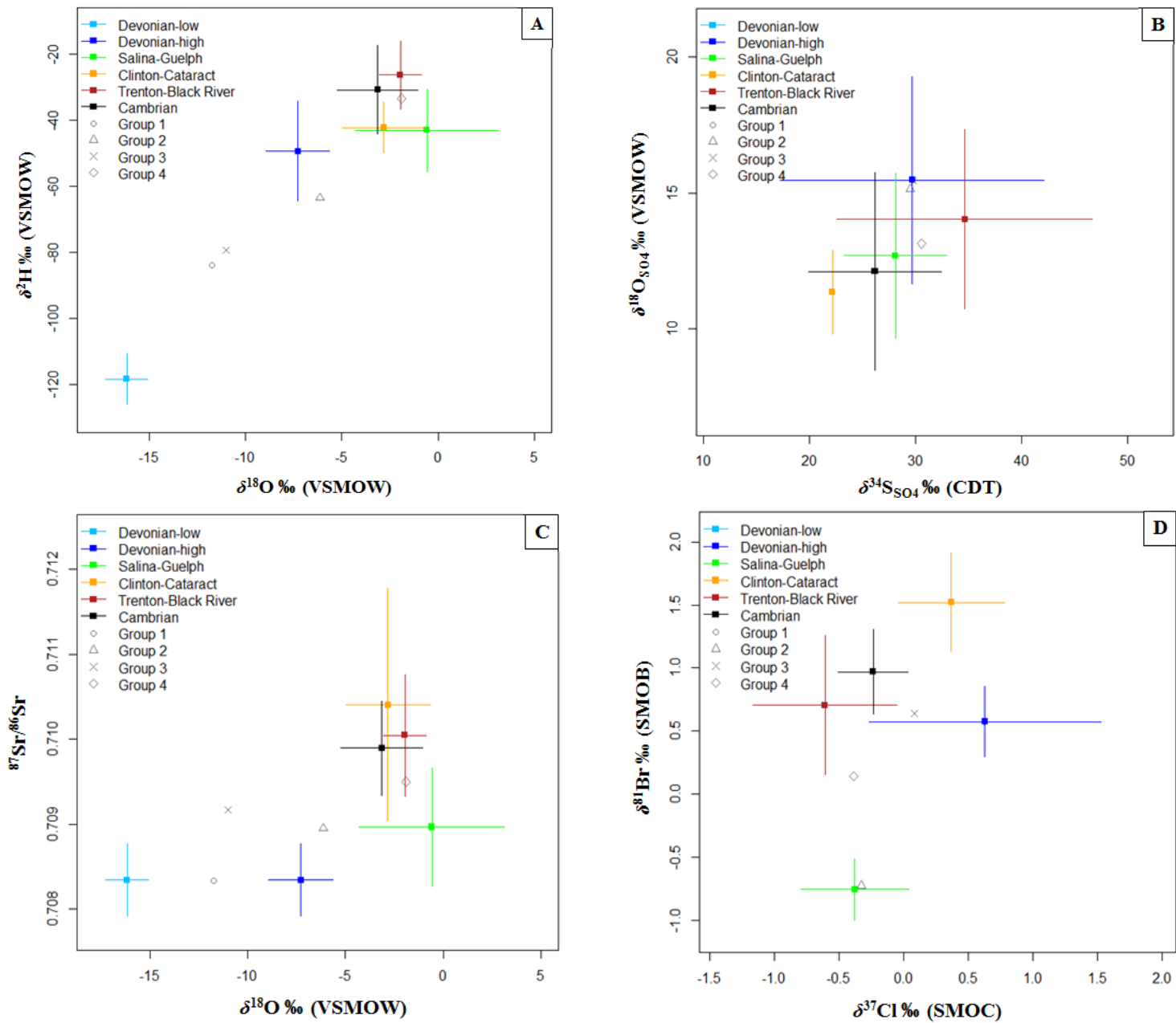
Figures 5.10: Isotope biplots for **(a)** oxygen and hydrogen, **(b)** sulphate sulphur and oxygen, **(c)** oxygen and strontium, and **(d)** bromine and chorine, constructed by SIAR.

such as its position in δ^2H/δ^{18}O space near Salina-Guelph and its wide range in ^{87}Sr/^{86}Sr; its composition in these isotope systems is overlapping with Salina-Guelph, which is reflected in a negative correlation (r^2 = -0.40) between the two end-members. Similar to Mixture 1, the lower end of the Dev-high distribution has higher probabilities, resulting from possible substitution with Clinton-Cataract.

Mixture 3 distributions are relatively similar to those without Clinton-Cataract. The probabilities towards the lower end of Trenton-Black River and Cambrian distributions are slightly increased. The Clinton-Cataract again has a tight distribution, and the model is confident in its proportion being near-zero, likely because of its high mean ^{87}Sr/^{86}Sr, and its position well below the meteoric water line. The Salina-Guelph proportion is more over-predicted, likely due to the possibility of mixing between it and Clinton-Cataract, resulting in a brine ^{87}Sr/^{86}Sr composition similar to that of Trenton-Black River.

In Mixture 4, inclusion of Clinton-Cataract as an end-member results in some worsening of the prediction of Salina-Guelph, Trenton-Black River, and Cambrian proportions, whose modes are now 0.27, 0.30, and 0.23. This underestimation reflects possible addition of a Clinton-Cataract component. The Salina-Guelph and Trenton-Black River proportions are better estimated than that of Cambrian because they are needed to maintain the mixture's position in δ^2H/δ^{18}O space, given some addition of Clinton-Cataract. Addition of Clinton-Cataract would decrease the δ^{18}O of the mixture, while Salina-Guelph has the opposite effect; similarly, Trenton-Black River is needed to counter the associated decrease in δ^2H resulting from addition of Clinton-Cataract. Addition of Clinton-Cataract would also raise the mixture's ^{87}Sr/^{86}Sr, which can only be balanced by increasing the contribution of Salina-Guelph. Increasing the contribution of Clinton-Cataract and/or Salina-Guelph would also decrease the sulphate δ^{18}O and δ^{34}S, thus requiring increasing the proportion of Trenton-Black River. By comparison, the Cambrian end-member is not in a position to have such a balancing influence, and so its proportion is underestimated. Finally, while the model does allow for a considerable (upper 95% CI = 0.29) range of possible Clinton-Cataract proportions, its mode is nonetheless quite low (0.06).
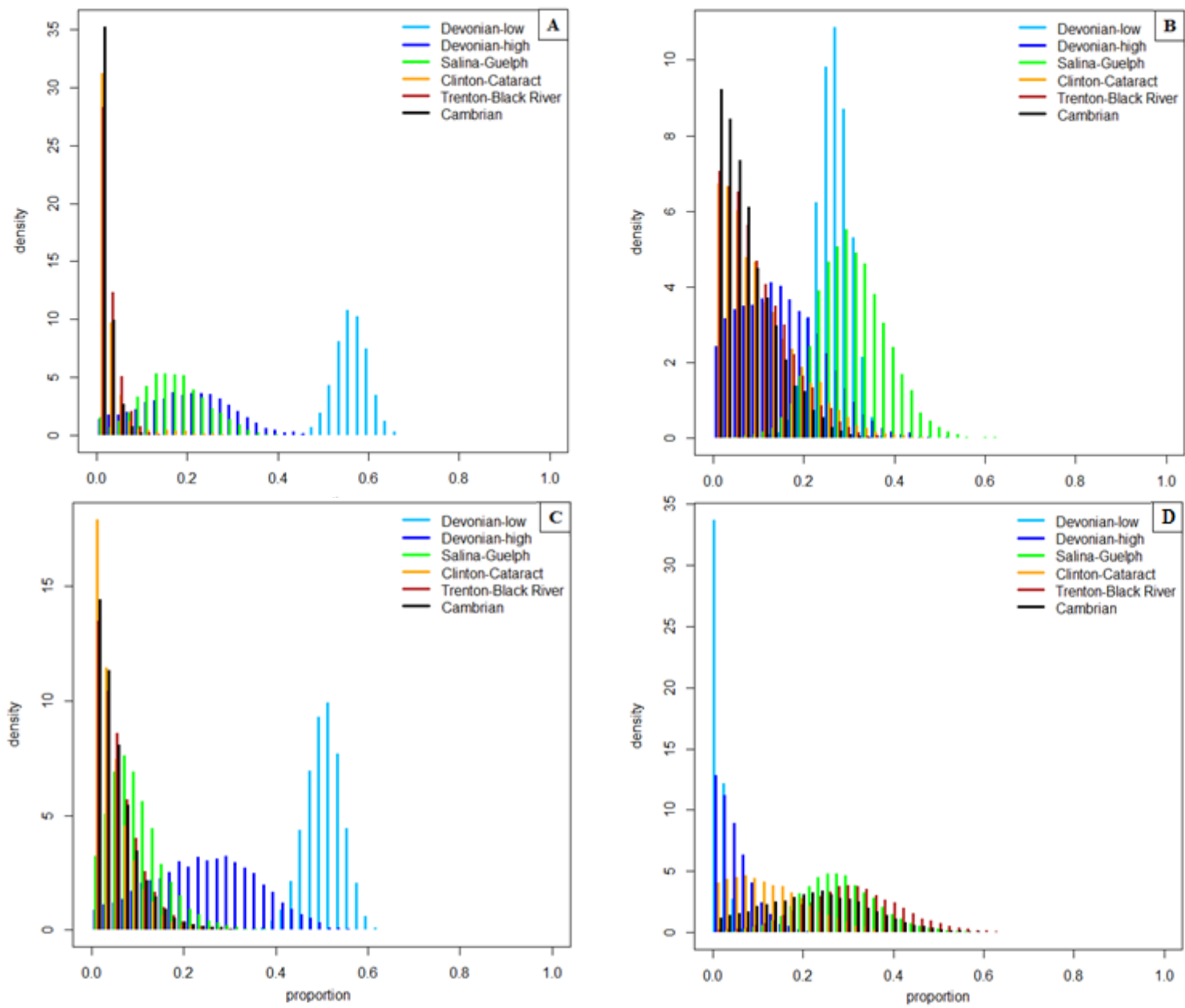
Figure 5.11: SIAR posterior distributions for Mixtures 1-4 based on Dataset 2, including all end-members but excluding $\delta^{13}C$, $\delta^{37}Cl$ and $\delta^{81}Br$.

5.1.3.4.2   With δ^{37}Cl and δ^{81}Br data

Simulation results for Mixtures 1-4 including Clinton-Cataract as a potential end-member and including δ^{37}Cl and δ^{81}Br data are presented in Figures 5.12a-d. Summary statistics and matrix plots for this and the previous section are given in Appendix F.

The Mixture 1 distributions are similar to those for the simulation excluding Clinton-Cataract but including δ^{37}Cl and δ^{81}Br. The only differences are a slightly broader Salina-Guelph distribution, and a long, negative but low-probability tail on Dev-high. The Clinton-Cataract proportion is strongly predicted to be near-zero, but also has a tail mirroring that of Dev-high. These tails reflect a small potential for substitution between Dev-high and Clinton-Cataract. This, as well as the slight increase in the Salina-Guelph distribution, can be explained by the fact that a brine component consisting of ~70% Clinton-Cataract and ~30% Salina-Guelph would have a δ^{81}Br composition similar to Devonian waters. Although such a brine would have a lower δ^{37}Cl, it could be balanced by a large Devonian proportion with slightly above-average δ^{37}Cl, which is not too improbable given its high variability in δ^{37}Cl. While the Clinton-Cataract and Salina-Guelph proportions could be thusly quite high based on δ^{37}Cl and δ^{81}Br data alone, the other isotopic systems place significant constraints on their distributions; for instance, both of these brines plot well below the meteoric water line. The above mixing scenario is reflected the high positive correlation ($r^2 = 0.93$) between Clinton-Cataract and Salina-Guelph, and negative correlations of similar magnitudes between them and Dev-high. Positive correlations between them and Dev-low demonstrate how such a mixture composition must also be balanced by increasing Dev-low proportions to maintain the mixture's position in δ^2H/δ^{18}O space.

Mixture 2 results also show very little change upon addition of Clinton-Cataract. Aside from small differences in the shape of the Dev-high distribution, all other distributions are essentially unaffected. Clinton-Cataract has a very tight range, with an upper 95% CI of just 0.06. It is constrained by the large distance between it and the Salina-Guelph end-member in δ^{37}Cl/δ^{81}Br space. The mixture's composition is near that of Salina-Guelph;

any significant addition of Clinton-Cataract could not be easily balanced by outlier values of Salina-Guelph.

Interestingly, addition of the δ^{37}Cl and δ^{81}Br data worsens the predicted Mixture 3 proportions for Clinton-Cataract. Rather than having a Clinton-Cataract distribution where probability increases rapidly as the proportion nears zero, a near-normal distribution is predicted with a mode of 0.10. The other end-members, however, are better predicted, particularly Salina-Guelph, although it still has a mode near 0.04. The explanation for this outcome is that the mixture's δ^{37}Cl and δ^{81}Br values lie on a line between Clinton-Cataract and Salina-Guelph and hence can be generated simply by mixing these two sources; such a mixture could also feasibly generate the mixture's ^{87}Sr/^{86}Sr value, allowing these sources to substitute for Trenton-Black River. While in such a situation the model is not able to well-predict the proper proportions, other information could be used to help guide a proper interpretation. For instance, if the modelled mode proportions for Salina-Guelph and Clinton-Cataract were true, the mixture would have a considerably higher TDS than if the only brine component was a 5% contribution of Trenton-Black River. Furthermore, the main Clinton-Cataract and Trenton-Black River reservoirs are located in significantly different parts of the study area, and so in real situations, one of the two could be eliminated *a priori*.

The δ^{37}Cl and δ^{81}Br data somewhat improve the predicted proportions determined for Mixture 4. The modes for the Salina-Guelph, Trenton-Black River, and Cambrian distributions are raised slightly to 0.32, 0.28 and 0.23, respectively, and their ranges are tighter. The Clinton-Cataract distribution is also significantly better constrained (upper 95% CI = 0.21, vs. 0.30), likely because its position in δ^{81}Br/δ^{37}Cl space is distant from that of the mixture. The Cambrian proportion is again underestimated due to its relative isotopic similarities to Clinton-Cataract; in δ^{81}Br/δ^{37}Cl space, the Cambrian lies on a line between Clinton-Cataract and Trenton-Black River, allowing some substitution by a combination of the latter two, constrained only by slight differences in the geometry of these source compositions observed for the other isotopic systems considered.
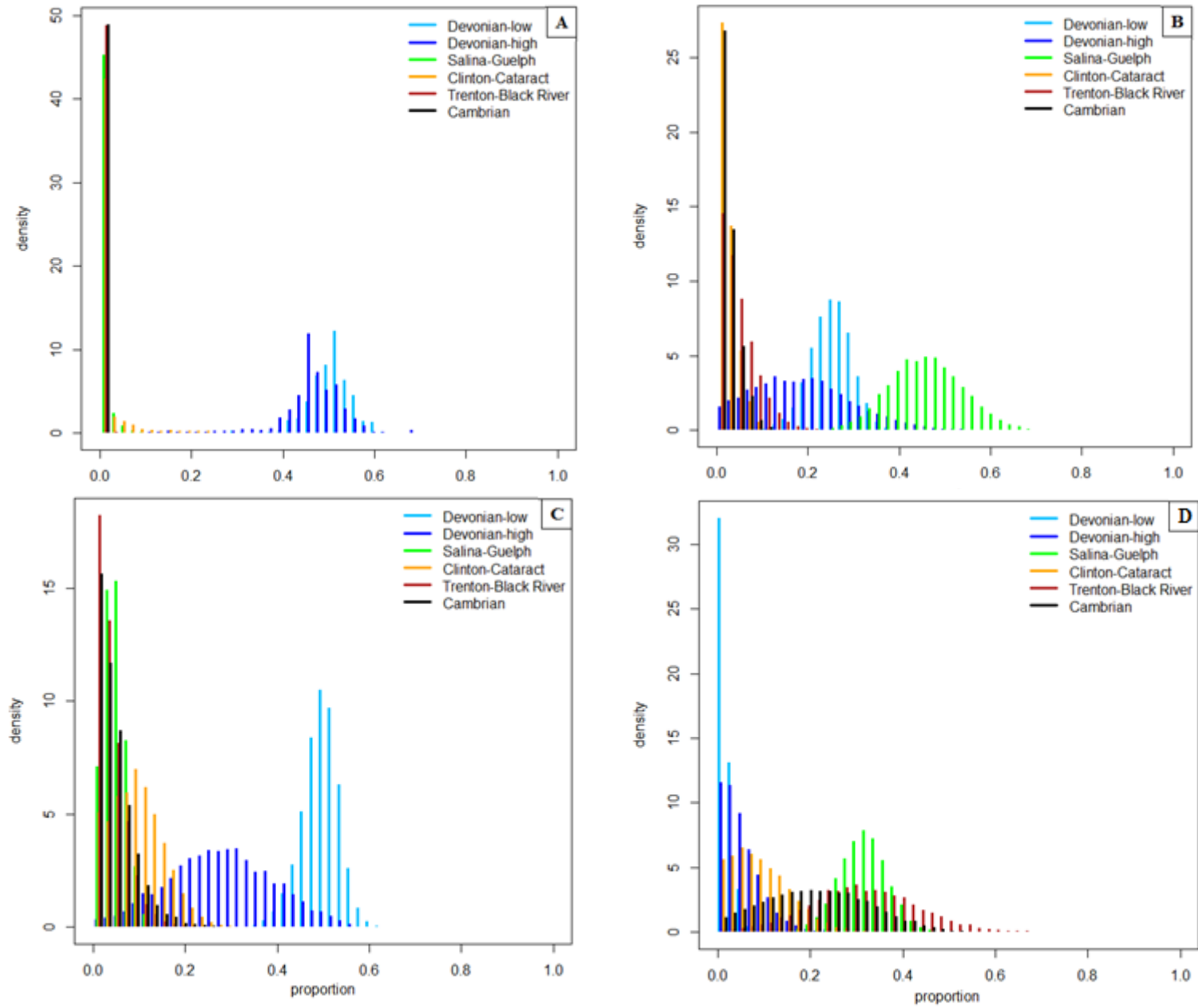
Figure 5.12: SIAR posterior distributions for Mixtures 1-4 based on Dataset 2, including all end-members and all isotopic systems except for $\delta^{13}C$.

5.1.4 Final notes and considerations

While mixing models are very useful tools for determining source proportions, no model can perfectly predict the 'true' proportions in systems with variability in source compositions, especially when the number of sources is large and their geometries in isotope space are not ideal. Therein lies the advantage of Bayesian mixing models like SIAR, which can not only account for such complexity but also produce a range of possible source proportions with relative probabilities for each source. However, given the complexity of the model, a thorough understanding of its performance under different situations is required for optimal interpretation of the results. The previous sections have attempted to impart such an understanding using several example mixtures. While these test mixtures simulate various possible natural mixing scenarios, there are an infinite number of other mixtures that may be encountered. Thus, some key points regarding the mixing model are outlined below, to ensure that the reader has the best possible understanding of the model's behaviour.

Two important decisions for any user of this tool are: (1) which isotopic systems to use, and (2) which end-members to include in the model. In the study outlined here, there are six potential isotopic systems to incorporate, eight if δ^{37}Cl and δ^{81}Br are available, and six different end-members. Addition of isotopic systems will improve model performance, some more so than others, as discussed later. As illustrated earlier for Clinton-Cataract, the exclusion of end-members can also enhance model performance, but must be done carefully lest a contributing end-member be wrongly excluded. Proper selection of end-members requires geological knowledge of the area from which the unknown sample was collected. For instance, many of the deep formations in southwestern Ontario exist or are significant brine producers only in certain areas. The Cambrian sandstones pinch out against the Algonquin Arch, so if a well is located near the crest of the Arch, the Cambrian can be excluded from the list of possible end-members. The Trenton and Black River groups generally only contain producible quantities of brine where dolomitized along faults and fractures; the locations of such reservoirs are fairly well-known and tend to be concentrated in the southwesternmost part of the region; therefore this end-member

can likely be safely excluded when a well is not located near one of these reservoirs. The Clinton and Cataract groups are quite shaley and typically do not produce significant quantities of brine unless void space is opened during oil and gas production; such production only occurs near the northeastern shore of Lake Erie and offshore Lake Erie, predominantly in Norfolk, Haldimand and Welland counties, since these units pinch out against the Algonquin Arch. Other information, such as the producing intervals of known oil and gas pools nearby, in addition to well logs of nearby wells, can also help inform the end-member selection. Another consideration that should help with selection is to closely examine the data before running the model, visually comparing the mixture's composition to that of the end-members across all isotopic systems. The end-members with the most extreme compositions define an area known as the 'convex hull', a polygon in isotope space within which all mixture compositions must lie. It is important to not omit any end-members that, in doing so, would place the mixture outside the convex hull. The model would still try to generate proportions for such mixtures, but results would be unreliable.

An important caveat regarding end-member selection is that water chemistry changes with depth within a given formation. In this study, the end-members for waters from the Cambrian through Silurian formations were defined based on brines present at depths greater than ~350-450 m, and these formations contain less saline waters at shallower depths that are more similar to those in the Devonian formations (see Section 2.1.3.1). Thus if any AWP sites are in locations where one or more of these units are present at depths of ~<350 m, their end-members should be tentatively excluded from the model since any water in those formations may not have an isotopic signature similar to that defined for the corresponding end-member. Users are also reminded that any "Devonian" water contribution predicted by the model may be from any formation above that transition depth; other information will be needed to interpret the unit(s) from which it likely originated (e.g., TDS, porosity, permeability; see Section 2.1.3.4).

In terms of selection of isotopic systems, the more that are used the better the model will generally perform, but ultimately it is likely that not all will be analyzed for a given sample because of cost and time reasons. However, not all isotopes are equally powerful in terms of constraining the model, and so analysis of certain ones can be prioritized.

The water isotopes, $\delta^{18}O$ and δ^2H, are useful parameters and are relatively easy and inexpensive to analyze. The shallow meteoric waters have significantly different signatures from the deep brines. However, there are certain aspects of the geometry of the different end-members that can inhibit the model's performance if based solely on these two isotopic systems. First, the Cambrian and Trenton-Black River compositions are both relatively close to the meteoric water line, and thus nearly in line with the Dev-low and Dev-high end-members. This facilitates substitution between Cambrian, Trenton-Black and Dev-high, making it difficult for the model to constrain their proportions. On one hand, a mixture composition between Dev-low and Dev-high *could* contain a Cambrian and Trenton-Black River component if the Dev-low:Dev-high ratio was higher than if there were no such component. On the other hand, if the sample's $\delta^{18}O$ and δ^2H values are higher than Dev-high, the model will know that some Cambrian and/or Trenton-Black River brine is present, although that amount can vary considerably, again depending on the relative amounts of Dev-low and Dev-high.

The positions of the Clinton-Cataract and Salina-Guelph end-members in $\delta^2H/\delta^{18}O$ space make them more easily identifiable than the other brines, being relatively ^{18}O-enriched and ^2H-depleted; any mixture between them and a shallow water will lie along a mixing line that falls below the meteoric water line. However, the model's ability to identify them still depends on both the composition of the shallow water (i.e. the relative amounts of Dev-low and Dev-high) and the amount of brine. The closer the shallow water is to the Dev-low composition, and the lower the brine proportion, the closer the mixture will lie to the meteoric water line, and so the more difficult it will be for the model to constrain the proportions.

In addition, given a sample that is purely or largely brine, considerable model uncertainty can still occur if using only $\delta^{18}O$ and δ^2H, because the brine end-member compositions are relatively close and somewhat overlapping in $\delta^{18}O/\delta^2H$ space. A pure Trenton-Black River or Salina-Guelph sample (or a mixture thereof) will be relatively well-constrained by the fact that these end-members represent extremes in the convex hull of possible water compositions. However, the Cambrian, Clinton-Cataract and Dev-high end-members are within this hull, and are less easily defined since their compositions can be

generated by mixtures of other end-members. Any mixture containing these end-members will be alternatively attainable by several different mixing scenarios, and thus the model will be too underdetermined to give good results based solely on $\delta^{18}O$ and δ^2H. Nonetheless, if the model is able to recognize a significant brine component, for instance by the mixture composition plotting below the meteoric water line or above the Dev-high composition, that information can help inform the other, solute-based isotopes.

The $^{87}Sr/^{86}Sr$ ratio is generally a very useful parameter because the large Sr^{2+} concentration gradient between shallow and deep waters facilitates the detection of the presence of brine in a sample that may, on the basis of $\delta^{18}O/\delta^2H$, appear to be purely of shallow origin. Additions of small amounts of brine will distinctively increase the mixture's $^{87}Sr/^{86}Sr$ ratio. However, there are some challenges. The Cambrian, Trenton-Black River and Clinton-Cataract end-members have relatively similar $^{87}Sr/^{86}Sr$ ratios, and have large standard deviations, particularly in Dataset 2. Salina-Guelph brine has a more unique mean composition, although its range overlaps with both the shallow waters and the other deep end-members. A mixture with $^{87}Sr/^{86}Sr$ near or below that of the Salina-Guelph could either indicate a significant proportion of Salina-Guelph, or a lesser proportion of one or more of the other formations; $\delta^{18}O$ and δ^2H may help constrain which is the case. A mixture with $^{87}Sr/^{86}Sr$ intermediate between the Salina-Guelph and Cambrian mean compositions could be the result of a substantial amount of brine from a mixture between Salina-Guelph and one or more of the other deep formations, or it could be generated by a lesser amount of brine from Cambrian, Trenton-Black River and/or Clinton-Cataract. Prediction can be significantly improved if one or more of the Cambrian, Trenton-Black River or Clinton-Cataract end-members can be excluded. The Cambrian and Trenton-Black River are particularly difficult for the model to separate due to their similar compositions in Dataset 2. Finally, in cases involving significant amounts of brine (>10-20%), $^{87}Sr/^{86}Sr$ is not very useful for predicting the relative amounts of brine and shallow water, since most of the strontium in the mixture would be brine-derived and so variations in the brine amount would not significantly affect the $^{87}Sr/^{86}Sr$ ratio of the mixture.

δ^{37}Cl and δ^{81}Br data appear to be very useful for constraining source proportions in a range of situations. They both act like ^{87}Sr/^{86}Sr in that they are based on solutes that have significantly higher concentrations in the deep formations than in the shallow meteoric water. The geometry of the different end-members in δ^{37}Cl/δ^{81}Br space is also quite favourable for source discrimination. The Salina-Guelph and Clinton-Cataract end-members are particularly well-separated from the other end-members, although more so by δ^{81}Br than by δ^{37}Cl. Cambrian and Trenton-Black River have comparable δ^{81}Br ranges to the shallow waters but are well separated by δ^{37}Cl; while they are also relatively close to each other in δ^{37}Cl/δ^{81}Br space, the proximity is less than for other isotopic systems. Any addition of Salina-Guelph or Clinton-Cataract to shallow water is easily distinguishable given their positions on opposite sides of the shallow water δ^{37}Cl and δ^{81}Br compositions, and that geometry also prevents significant substitution by Cambrian or Trenton-Black River. However, the end-member geometry is such that mixtures of the latter two end-members and shallow water can be mimicked by a mixture of Salina-Guelph and Clinton-Cataract. Also, like ^{87}Sr/^{86}Sr, given a large brine component, δ^{37}Cl and δ^{81}Br values are not good at quantifying the relative amounts of brine and freshwater.

The δ^{13}C$_{DIC}$ values are generally not very useful for constraining the mixing model, for several reasons. First, the deep formation brines have relatively similar means and large standard deviations, and so cannot be easily distinguished from each other, and the shallow waters have a very large range of δ^{13}C$_{DIC}$ values that fully encompasses those of the deep formations. Second, the shallow waters tend to have considerably higher DIC concentrations. It is expected that most AWP samples will have a significant shallow component, so that even if the deep formations had more distinctive values, their contributions would not be evident on the basis of δ^{13}C$_{DIC}$ alone.

The δ^{18}O$_{SO4}$ and δ^{34}S$_{SO4}$ values also have generally little power for discriminating among fluid sources. The separations between end-member mean compositions are relatively small compared to their compositional variability. The shallow waters also typically have higher sulphate concentrations than the deeper systems, rendering any brine addition to shallow water very difficult to identify using this system alone. In some situations, the sulphate isotopes may be useful for identifying a small amount of shallow water in a

largely brine mixture. They may also be useful in determining the proportions of certain components in a mixture consisting of various brines. All the deep end-members lie on a line in $\delta^{18}O_{SO4}/\delta^{34}S_{SO4}$ space, with Clinton-Cataract and Trenton-Black River at the extremes. Cambrian and Trenton-Black River also have relatively good separation in $\delta^{18}O_{SO4}/\delta^{34}S_{SO4}$ space. However, as for DIC, the amount of sulphate isotope data available for the deep formations is limited, resulting in end-member compositions that remain relatively poorly characterized, and so their use may be questionable.

When interpreting the model results to ascertain whether or not a particular formation is likely actually contributing water to a mixture, one should consider both the range of the possible proportions of that end-member and the distribution of probabilities therein. The mode represents the most probable proportion, but if the distribution is very wide, the model is not very well-constrained and the true proportion could easily lie elsewhere. Also one should consider the data itself; for instance if the model fits a small range of possible proportions, with modes near zero, for the deep formations, this could simply be the model reflecting the flexibility afforded by the variability in the end-members, or it might indicate a small amount of brine in the mixture, but not enough for the model to be very confident about its origin. Examination of the data to check whether or not the TDS, $^{87}Sr/^{86}Sr$ ratio, $\delta^{37}Cl$ and/or $\delta^{81}Br$ values are particularly abnormal for a pure shallow water could help discriminate between those two scenarios.

When making interpretations about the validity of the results, one should also consult the isoplots and the matrix plots to obtain a better understanding of how the model is achieving its results. Misleading results may be generated if the configuration exists for one or more end-members to substitute for another end-member to produce the same mixture composition; this is for instance illustrated in the Clinton-Cataract/Salina-Guelph pair being able to substitute for a Trenton-Black River/Devonian mixture in Figure 5.12c. One should be mindful of such possibilities and consider the likelihood of such mixtures occurring in reality. In the latter case, for example, it is perhaps unlikely for the brine contribution to be split among multiple formations when that contribution is known or suspected to be small. Also, given the fact that the Salina-Guelph units are much more

prolific brine producers than the Clinton-Cataract, it seems implausible that the latter would provide a significantly larger contribution to the mixture.

Due to the possibility of substitution between end-members, SIAR also has a general tendency to better predict 'generalist' solutions (to borrow from ecology terminology), that is, where many or all end-members contribute to the mixture, over 'specialist' solutions, with only a small number of contributing end-members. This substitutability will typically lead to underestimation of some sources that are present in greater proportions, and overestimation of others that are not present or are only present in small amounts. However, in almost all situations, the true proportions should still lie within the 99% if not the 95% credibility intervals.

These points underline the reality that while the model generally performs quite well, with modes of the predicted proportions relatively near their true values, it will not (at least generally) give a definitive answer as to the true proportions, and thus some interpretive skill and experience is required on the part of the user to extract the most valuable information. The model can constrain the ranges of possible source proportions, but in some situations the ranges can be large and the mode may not be representative of the actual proportions. Ultimately, the model is intended to be used to supplement, and be supplemented by, other information and lines of reasoning.

5.2   Hydrogeochemical discussion

This section discusses the nature of the different bedrock hydrogeological systems in southwestern Ontario, in light of the new and existing geochemical data, focusing on the origins of the groundwaters and their solutes.

5.2.1   Shallow flow system

A relatively shallow flow system exists in southwestern Ontario at depths of less than approximately 350 – 450 m. Within this shallow flow zone, a gradation from fresh to sulphurous, brackish and occasionally saline water with depth is observed, although waters from these zones are all isotopically relatively similar. These shallow waters are found in the more permeable Devonian units, as well as the shallower portions of some Silurian units. The Devonian aquifers appear to be separated from the deeper brine regime by impermeable evaporite and carbonate units of the Salina Group, as well as the strong density gradient between these systems. See Section 2.1.3 for more details.

5.2.1.1   Oxygen and hydrogen isotopes of water

Apart from their lower salinities, the shallow waters can be distinguished from the deeper brines by their relatively low water isotope signatures, below ~ –6‰ δ^{18}O and ~ –40‰ δ^2H. The waters also distinctively span a large isotopic range, to as low as ~ –17‰ δ^{18}O and ~ –120‰ δ^2H. Most of the shallow water samples collected in this study are from Devonian formations (Dundee, Lucas, Columbus, Amherstberg and Bass Islands), although several samples from the subcrop region of the Salina Group have similar isotopic compositions. Several samples were also collected whose origins are not well-constrained but are strongly suspected of being from relatively shallow units based on their water chemistry and information regarding the geology of their locations.

The shallow water isotopic data from this study are presented in Figure 5.13, categorized by formation. All data are presented on the concentration scale, although for most samples the salt effect correction is negligible, given their low TDS. The Great Lakes

Meteoric Water Line (GLMWL) (δ^2H = 7.1[δ^{18}O] + 1.0; Longstaffe et al., 2011) is shown for comparison. The regression line for all data in this study (δ^2H = 7.43[δ^{18}O] + 5.9) is very close to the GLWML, and waters from all units have similar isotopic compositions, suggesting that they share a common origin, namely meteoric water. The three Columbus Member samples with the lowest δ-values are from an oilfield that has been flooded with water from the overlying drift aquifer, the composition of which is indicated on Figure 5.13. These samples appear to lie on a mixing line between the drift composition and a higher δ^{18}O end-member, possibly similar to the other Columbus Member sample; the samples closest to the injection well have compositions closest to the drift sample.
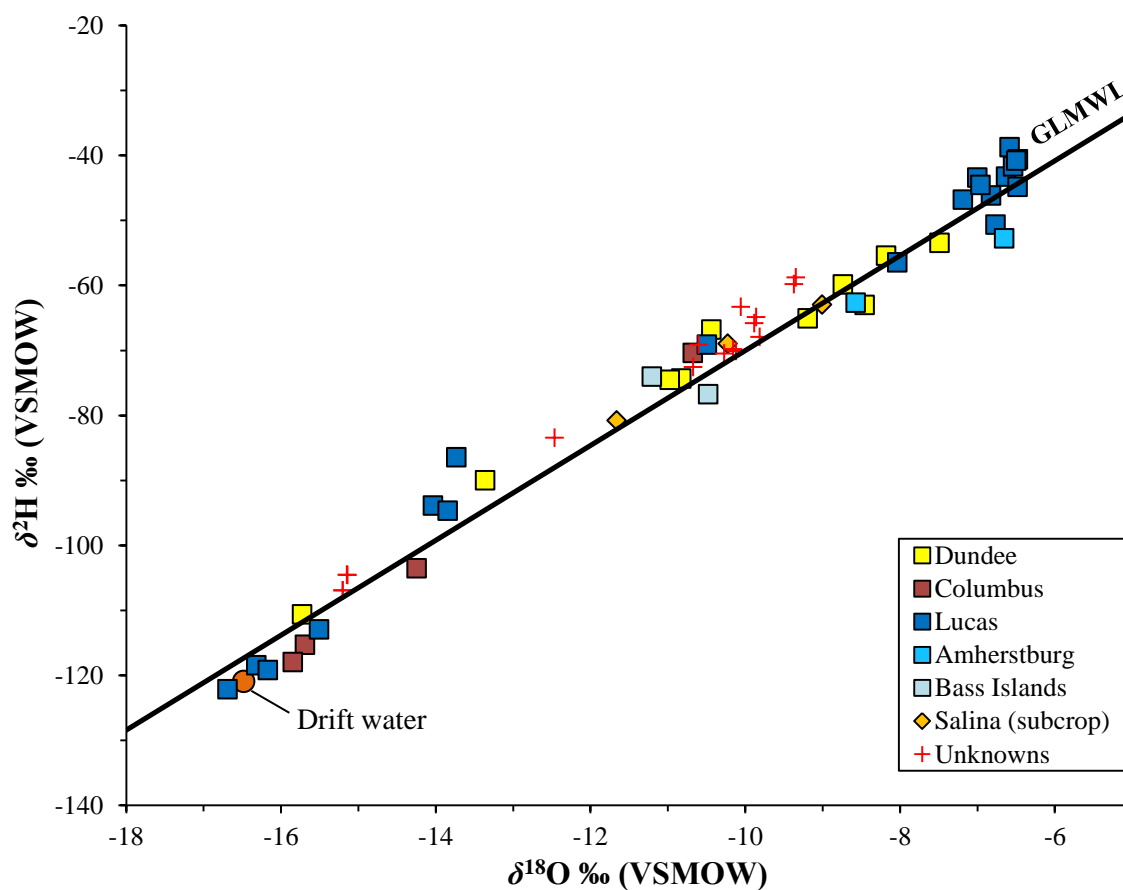
Figure 5.13: Plot of δ^2H vs. δ^{18}O for the shallow groundwaters sampled in this study, by formation.

The data from this project are compared in Figure 5.14 to other studies in southwestern Ontario (and slightly beyond, in the case of McIntosh and Walter, 2006). The distribution of the shallow groundwater isotopic compositions spans the full range of modern

precipitation δ-values; the average $\delta^{18}O$ of winter (Dec-Mar) precipitation is $-14.6‰$, and the summer (June-Sept) average is $-6.5‰$ (based on GNIP data from the Simcoe area; IAEA/WMO, 2014). The majority of the groundwaters fit comfortably within this modern seasonal range. The scatter in δ-values can be explained by local variations in the proportions of precipitation recharged at different times of year, latitudinal variations, and possibly other processes, as discussed later. When the data from other studies are considered, it is clear that most waters appear to lie slightly above the GLMWL. The slightly higher deuterium excess (Dansgaard, 1964; $d = \delta^2H - 8[\delta^{18}O]$) of these samples may indicate a low-humidity moisture source and/or inland moisture recycling. This suggests that recharge to these shallow aquifers is derived disproportionately from winter precipitation/snowmelt and/or precipitation recycled from the Great Lakes.
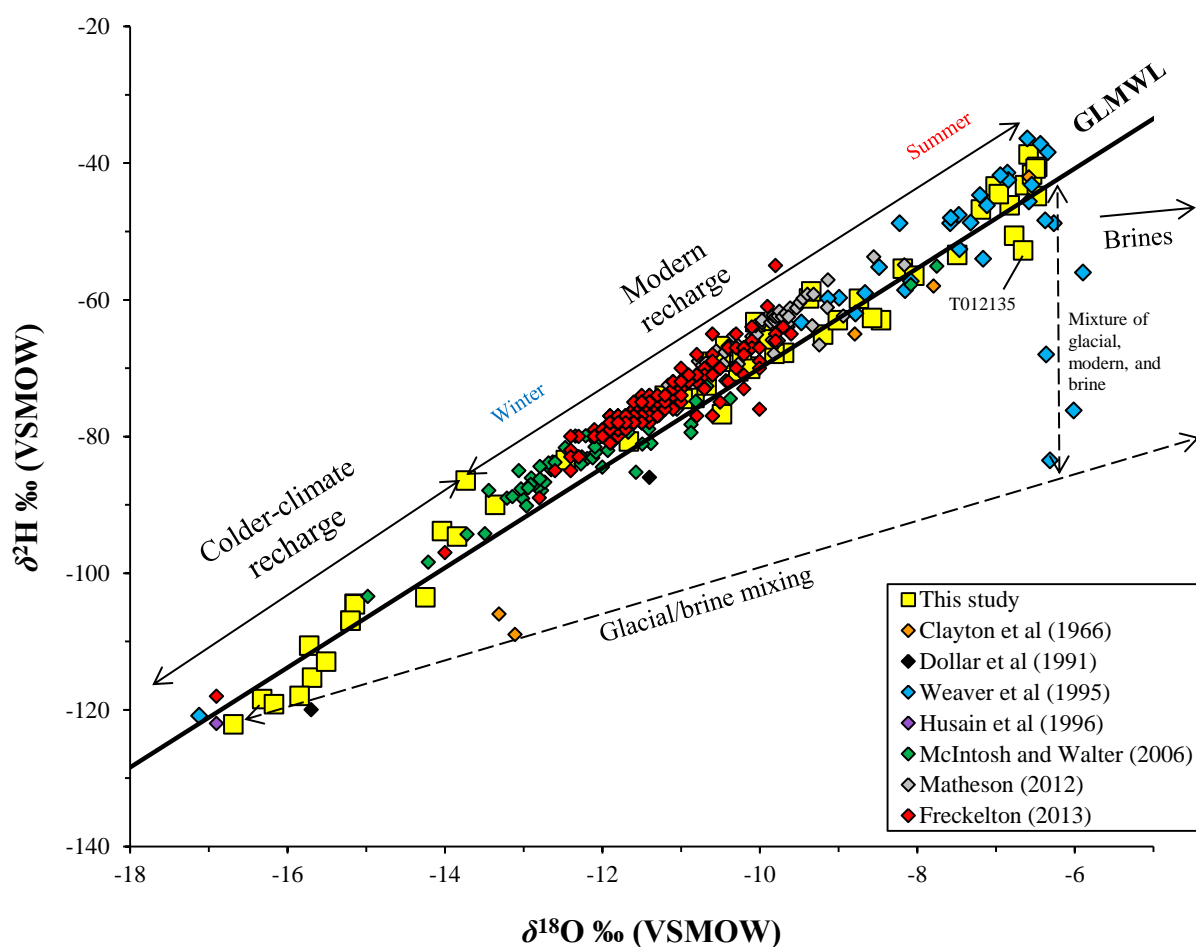
Figure 5.14: Shallow water δ^2H vs. $\delta^{18}O$ data from this study compared to other studies.

While the majority of the data fit within the range of modern precipitation, there are some samples with significantly lower values ($\delta^{18}O \approx < -13‰$). While these isotopic compositions could be explained by recharge from extreme winter storms, it is unlikely that all of the recharge contributing to those samples would be so derived. These particularly low δ-values can be explained by a component of older water, recharged under cooler climate conditions. While their isotopic compositions too high for them to be pure glacial meltwaters from the Laurentide Ice Sheet ($\delta^{18}O \approx -31‰$; Sima et al., 2006), they may either represent meltwaters mixed with modern meteoric water, or meteoric recharge during cooler climate conditions, such as during the late Pleistocene or early Holocene. Several other authors (e.g., Clayton et al., 1966; Desaulniers et al., 1981; McIntosh and Walter, 2006) have also identified such waters in the area and suggested a Pleistocene origin, with Desaulniers et al. (1981) calculating an age of at least 8,000 (cal.) years B.P. While these older waters are present in both drift and bedrock aquifers, their lateral and vertical distributions are regionally not very well understood. Several researchers (e.g., Desaulniers et al., 1981, 1986; Weaver, 1994; Husain et al., 2004) demonstrated a gradual change from modern values (–11 to –9‰ $\delta^{18}O$) at shallow depth to a Pleistocene signature (–17 to –16‰ $\delta^{18}O$) at the bottom part of a drift aquitard and in the underlying aquifer. Although in this and other recent studies there does not seem to be a strong relationship between depth and $\delta^{18}O$ regionally, the most negative values are generally found at relatively shallow depths (Figure 5.15).
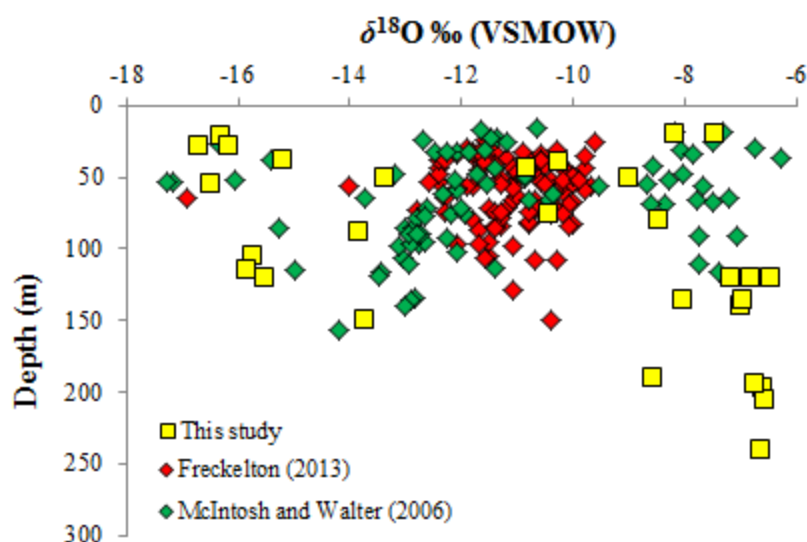
Figure 5.15: Plot of depth vs. $\delta^{18}O$ for the shallow groundwaters.

5.2.1.2 *Salinity and brine mixing*

Several authors have suggested that some shallow meteoric groundwaters in the region have mixed with brines, to explain the elevated salinities that are commonly reported for these waters (e.g., Long et al., 1988; Ging et al., 1996, Kolak et al., 1999, Ma et al. 2005). Some of the proposed mixing scenarios are illustrated in Figure 5.14. Dollar et al. (1991) hypothesized that the oxygen and hydrogen isotopic compositions of Ontario Dundee Formation waters were the product of mixing between cooler-climate waters and brines originally present in the formation, such as were found in Devonian strata deeper in the Michigan Basin. Weaver et al. (1995) proposed a scenario wherein several Upper Detroit River Group samples from southern Oil Springs with unusually low δ^2H values and high chloride contents were a mixture of glacial waters and a brine similar to that from the Salina A-2 salt, which then mixed with modern meteoric waters. Such mixing was attributed to upward hydraulic gradients following glaciation, with flow localized along fractures. While unusual samples such as those reported by Weaver et al. (1995) were not found in this study, there is some evidence for a brine component within the shallow waters. As shown in Figure 5.16, several samples, mostly associated with oil-fields, have TDS > 10,000 mg/L. These samples also have some of the highest $\delta^{18}O$ values for shallow waters, and their high δ values may in part be due to addition of brines, which are typically enriched in ^{18}O.
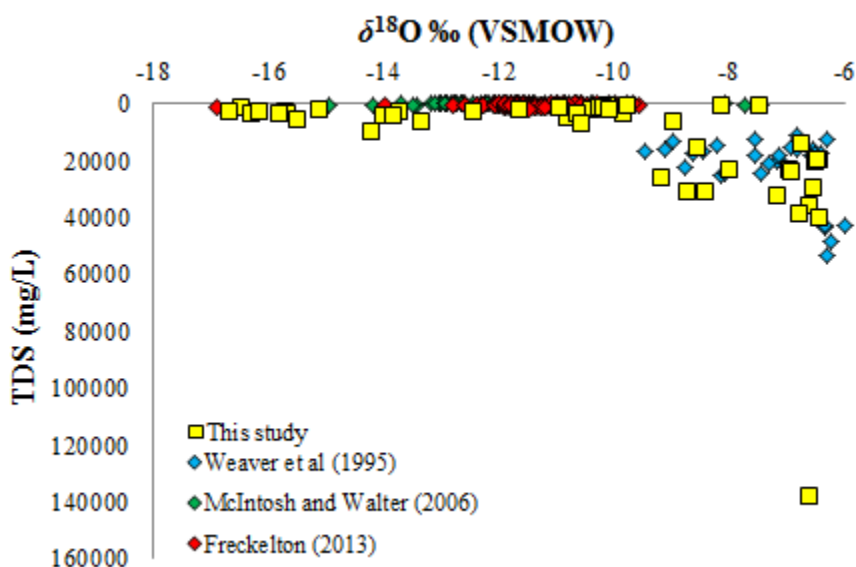
Figure 5.16: Plot of TDS vs. $\delta^{18}O$ for shallow groundwaters.

However, the large TDS differences between the shallow waters and the deep brines, coupled with the position of the latter significantly below the GLMWL, limit the amount of brine that can possibly be mixed with fresh waters given their observed chemical and isotopic compositions. The more saline shallow waters have TDS in the range of roughly 20-40,000 mg/L. Assuming mixture of a low-TDS meteoric water with a Salina A-2 unit brine (TDS ≈ 380,000 mg/L), only about 10% brine can be added without exceeding the observed TDS range. For a typical meteoric composition of −10‰ $\delta^{18}O$, a 10% brine addition only raises the $\delta^{18}O$ by about 1.4‰, with a relatively small (~2%) increase in δ^2H; other, less-^{18}O-enriched brine end-members would yield even smaller isotopic shifts. Thus while these samples' elevated salinities can be explained by small brine additions, their isotopic signatures appear to be largely controlled by other factors. For instance, their ^{18}O-enrichment may reflect predominantly summer recharge and/or evaporation effects. Any decrease in d-excess associated with evaporation or brine mixing might be countered by exchange of water ^2H with hydrocarbons or H_2S (Horita, 2005).

Nonetheless, there are some anomalous samples with particularly low d-excess (~<10‰; see samples plotting significantly below the GLMWL in Figure 5.14). For these samples, their isotopic compositions may be readily explained by mixing of brines with meteoric water. As one extreme example, sample T012135 has very high TDS (~138,000 mg/L – the highest yet observed for Devonian waters in Ontario), and lies considerably below the GLWML (Figure 5.14). Both its isotopic composition and salinity can be explained by a ~50% Silurian brine component (TDS = 300,000 mg/L; $\delta^{18}O = -2.5$‰) mixed with meteoric water. Several of the very low $\delta^{18}O$ (<−13‰) samples from this study as well as Dollar et al. (1991) and Clayton et al. (1966) that plot considerably below the GLWML, may also be mixtures of cooler-climate waters and brines. For all these mixed samples, the brines could either have migrated upwards from deeper units, or be remnant Devonian brines, such as those still present in Michigan (Dollar et al., 1991).

The salinities of some samples can be explained by other processes. One similar mechanism is that solutes migrated upward from deeper brines via diffusion rather than advection. Diffusion is expected given the extreme concentration gradient between the shallow brackish waters and underlying brines (Hobbs et al., 2011). This scenario is

supported by the fact that the more saline waters appear to be located near the Chatham Sag (Figure 5.17), at relatively deep levels for their respective formations. The Devonian carbonates in this area are also capped by the low permeability Kettle Point and Hamilton shales. This position would likely inhibit meteoric water circulation, facilitating the build-up of upward-diffusing salts over long periods of time.
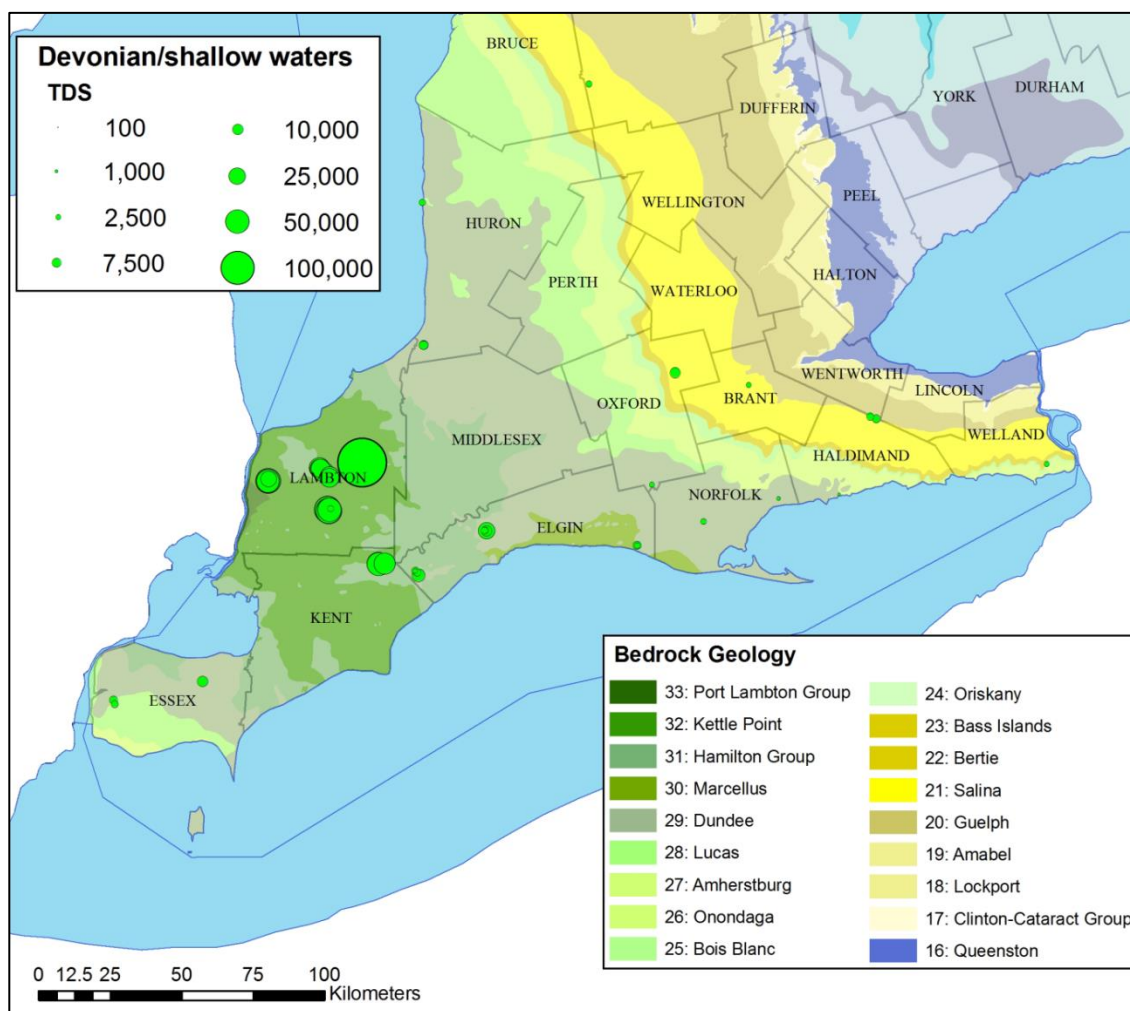
Figure 5.17: Geographical variations in TDS for shallow groundwaters in the study area.

The Devonian carbonates in southwestern Ontario also locally contain evaporite minerals such as halite and anhydrite (Armstrong and Carter, 2010). Relatively impermeable lacustrine clays and tills deposited during the Pleistocene likely helped to preserve these highly soluble evaporite minerals at shallow depths along the basin margins (McIntosh et

al., 2006). Dissolution of these evaporites by modern recharge may contribute to the salinity of some shallow waters. This possibility is supported by δ^{81}Br and δ^{37}Cl data of Shouakar-Stash (2008) (Figure 5.18). Not only do the isotopic compositions of Devonian samples from southwestern Ontario differ significantly from Devonian waters in central Michigan, they also differ from the Silurian brines in Ontario and Michigan. This appears to rule out a brine origin for the solute contents of these shallow groundwater samples. However, given the limited data there is a possibility that brine-mixed waters exist but simply were not sampled. Due to the relatively large spread in δ^{37}Cl values compared to δ^{81}Br and a lack of a systemic relationship between δ^{37}Cl and TDS, Shouakar-Stash (2008) concluded that these solutes were likely derived mainly from halite dissolution.
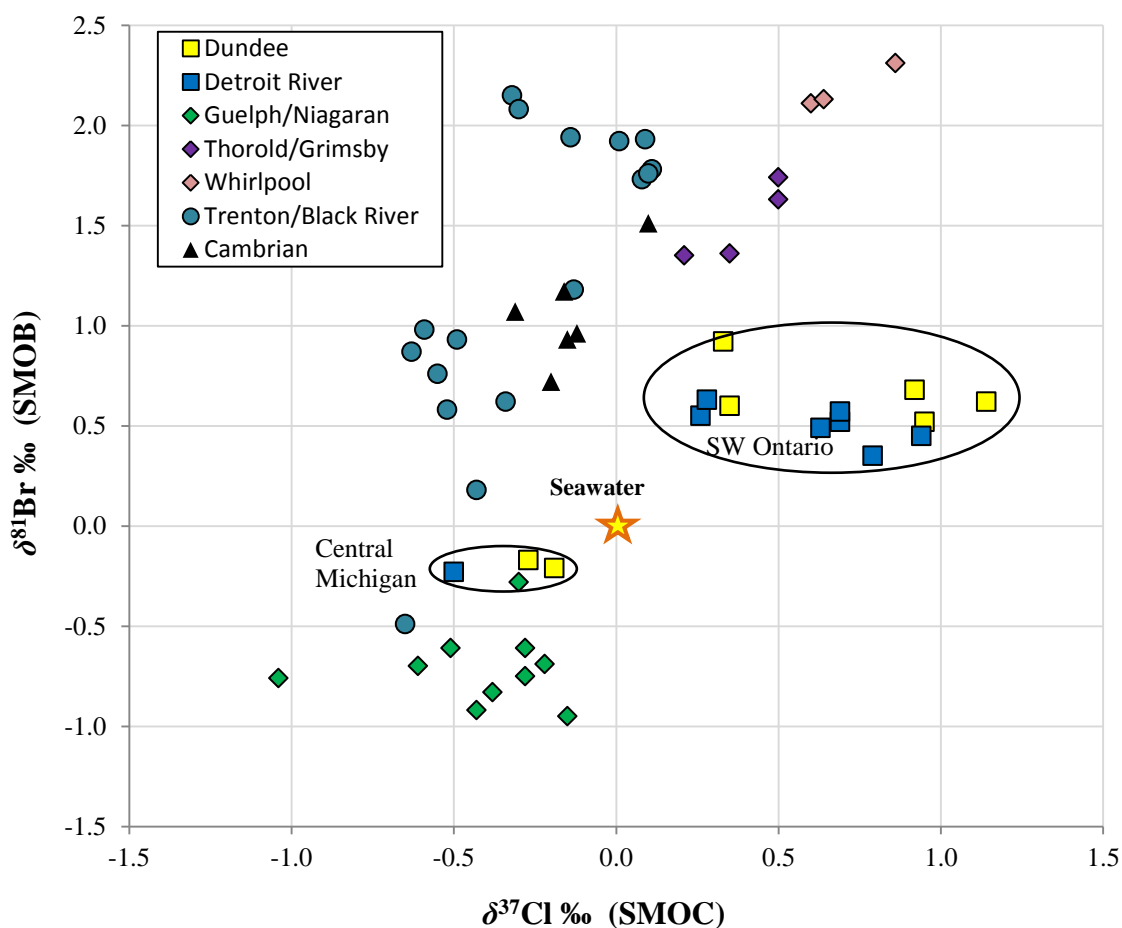
Figure 5.18: Plot of δ^{81}Br vs. δ^{37}Cl for groundwaters from various formations in southwestern Ontario and Michigan (modified from Shouakar-Stash, 2008).

5.2.1.3 *Sulphur and oxygen isotopes of sulphate*

The sources of other solutes can also be investigated through isotopic means. For instance, the δ^{34}S and δ^{18}O compositions of dissolved sulphate reflect its origin and geochemical evolution (e.g., Krouse and Mayer, 2000). Several processes affecting the composition of sulphate may be operating in the shallow groundwater system in southwestern Ontario. These include sulphate dissolution, sulphide oxidation, dissimilatory bacterial sulphate reduction, and mixing.

The isotopic compositions of sulphate for the shallow water samples from this study are shown in Figure 5.19. Results for the Lucas Formation, Columbus Member and Amherstberg Formation are combined as the Detroit River Group, as only one water sample from each of the latter two units was analysed for sulphate isotopes. The δ^{34}S$_{SO4}$ and δ^{18}O$_{SO4}$ values vary considerably (from +10.6 to +52.8‰ and −1.6 to +18.2‰, respectively) but there are no clear differences among units.
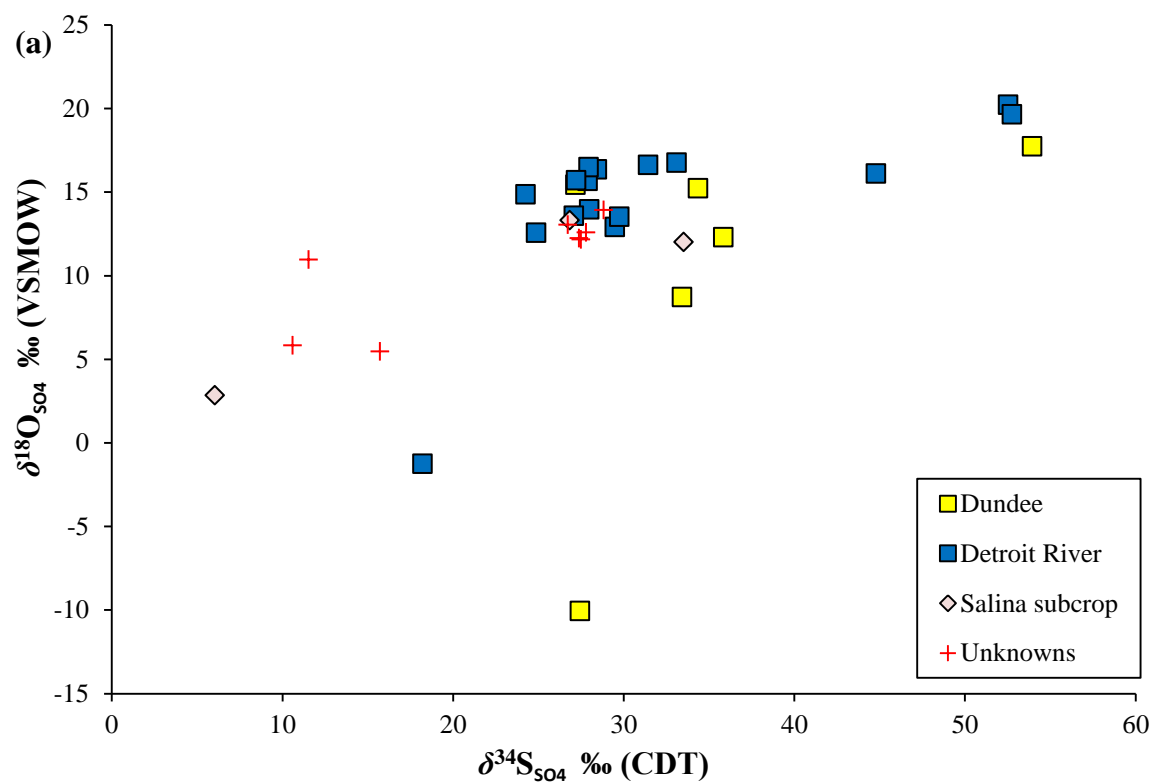
Figure 5.19: Plot of δ^{18}O$_{SO4}$ vs. δ^{34}S$_{SO4}$ from this study for shallow groundwaters.

The δ^{34}S and δ^{18}O results from this study are compared to previous studies of shallow Ontario waters (Weaver et al., 1995; McIntosh and Walter, 2006; Matheson, 2012; and Freckelton, 2013) in Figure 5.20. Possible processes controlling their origin and evolution are also illustrated.
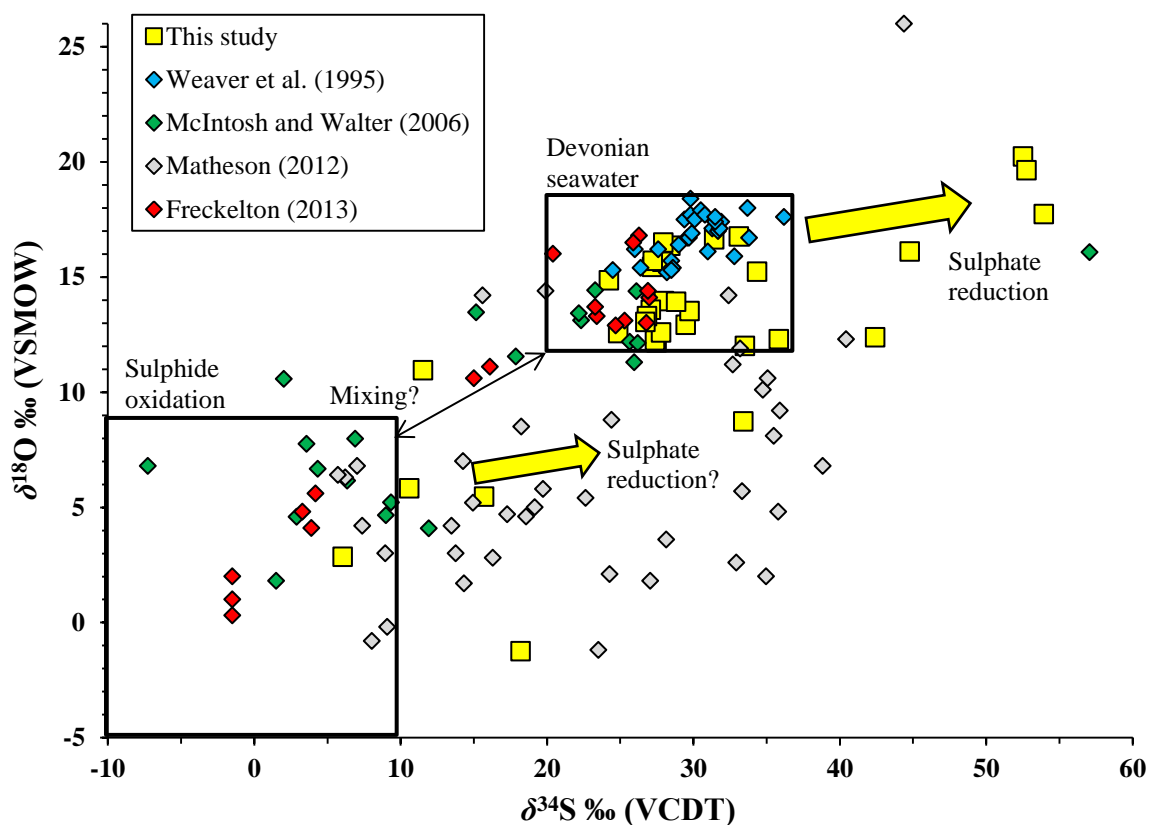
Figure 5.20: Plot of shallow groundwater $\delta^{18}O_{SO4}$ vs. $\delta^{34}S_{SO4}$ data from this study compared to other studies, and processes controlling their compositions.

One possible source of groundwater sulphate is dissolution of marine evaporites such as gypsum and anhydrite, which are common in the Devonian formations (Frizzell et al., 2011). Reported $\delta^{34}S_{SO4}$ values for anhydrite in Silurian-Devonian carbonates from the Michigan Basin range from +24.9 to +28.7‰ (Das et al., 1990; Eberts and George, 2000), although Devonian seawater $\delta^{34}S_{SO4}$ had considerably greater, with a low of ~ +17‰ in the Lower Devonian, later increasing to ~ +25‰, with some samples having values > +30‰ (Claypool et al., 1980). Devonian seawater $\delta^{18}O_{SO4}$ values are less variable, averaging +15.3 ± 0.3‰, but values as low as +12.5‰ and as high as +17.8‰ have been reported (Claypool et al., 1980). The seawater $\delta^{34}S_{SO4}$ and $\delta^{18}O_{SO4}$ compositions are

illustrated by a box in Figure 5.20. While small enrichments in ^{34}S and ^{18}O (~+1.65 and +3.6‰, respectively; Thode and Monster, 1965) accompany gypsum precipitation, dissolution thereof is largely non-fractionating, and oxygen isotopic exchange between sulphate and water is very slow (Clark and Fritz, 1997). Thus, both the $\delta^{34}S_{SO4}$ and $\delta^{18}O_{SO4}$ values of sulphate dissolved from evaporite minerals should be within a few permil of the original seawater sulphate compositions. Many samples plot within or near the range of seawater sulphate (Figure 5.20), indicating that marine evaporites are an important source of sulphate in the shallow groundwater system.

A second source of groundwater sulphate is oxidation of sulphide minerals such as pyrite. The δ^{34}S values of sedimentary sulphides typically range from −50 to +10‰ (Karim and Veizer, 2000). The δ^{34}S values for sulphides in the Findlay Arch District of northwestern Ohio range from −24.2 to +7.0 ‰ for pyrite/marcasite, −0.9 to +4.8 ‰ for sphalerite, and −3.4 to +0.6 ‰ for galena (Carlson, 1994). Several different reactions, both inorganic and bacterially-mediated, can be involved in sulphide oxidation. The overall stoichiometry of pyrite oxidation is described in Equation 5.1 although intermediate steps (Equations 5.2-5.4) are also involved (Taylor et al., 1984):

$$FeS_2 + \frac{15}{2}O_2 + \frac{7}{2}H_2O \rightarrow Fe(OH)_3 + 2H_2SO_4 \qquad (5.1)$$

$$FeS_2 + 14Fe^{3+} + 8H_2O \rightarrow 15Fe^{2+} + SO_4^{2-} + 16H^+ \qquad (5.2)$$

$$Fe^{2+} + \frac{1}{4}O_2 + H^+ \rightarrow Fe^{3+} + \frac{1}{2}H_2O \qquad (5.3)$$

$$FeS_2 + \frac{7}{2}O_2 + H_2O \rightarrow Fe^{2+} + 2SO_4^{2-} + 2H^+ \qquad (5.4)$$
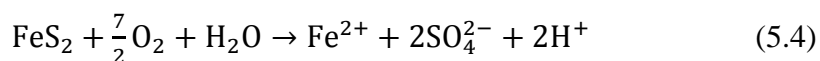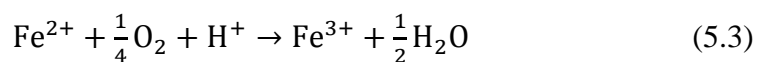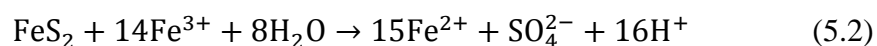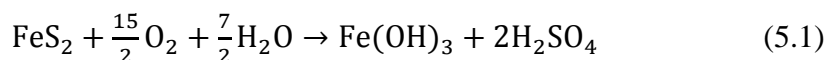
Sulphur isotopes are generally considered to not fractionate significantly during pyrite oxidation (Taylor et al., 1984), although some studies (e.g., Kaplan and Rafter, 1958; Fry et al., 1983, 1988) have found ^{34}S enrichments of a few permil. Depending on the oxidation pathway, oxygen from either the atmosphere ($\delta^{18}O \approx +23.5$‰; Kroopnick and Craig, 1972) and/or water ($\delta^{18}O \approx -17$ to −6‰ in this study) can be incorporated into the resulting sulphate, thus leading to a wide range in $\delta^{18}O_{SO4}$ values, which can be used to trace the principal oxidation mechanisms (Sidle, 2002; Taylor et al., 1984). In reaction 5.2, the oxygen is derived purely from water, while in reaction 5.4 it is derived both from

water (12.5%) and dissolved atmospheric oxygen (87.5%) (Taylor et al., 1984). Kinetic fractionations are observed between atmospheric oxygen and sulphate oxygen of –4.6‰ during inorganic oxidation, and –11.12‰ for oxidation mediated by *Thiobacillus ferrooxidans*. In fully submerged environments, fractionations between water oxygen and sulphate oxygen have been observed, with enrichments of +4.1 to +6.2‰ under sterile conditions, and +8.9 to +10.9‰ with *T. ferrooxidans* (Taylor et al., 1984).

Although the boundaries for the sulphide oxidation box in Figure 5.20 are somewhat arbitrarily defined, it is clear that several samples of groundwater in the study area contain a sulphate component derived from sulphide oxidation. The variation in $\delta^{34}S$ for these samples is on the order of about 10‰, and values are in the upper range for pyrite reported by Carlson (1994); this variation may reflect different $\delta^{34}S$ compositions for the sulphide minerals. The variation in $\delta^{18}O$ is similar, and likely reflects differences in the oxidation pathways. Some variation is also likely the product of other processes, such as mixing of water bodies with different sulphate compositions, and bacterial reactions.

The $\delta^{18}O_{SO4}$ values can be used to assess the relative importance of the different sulphide oxidation pathways. Figures 5.21a-b illustrate the importance of reaction (5.2), which derives all oxygen from water, compared to reaction (5.4), which derives 87.5% from atmospheric oxygen and the remainder from water; the diagonal lines indicate the sulphate percentage derived from reaction (5.2), with the remainder from reaction (5.4). Figure 5.21a represents a sterile system and uses oxygen isotope fractionation factors of +5.1‰ for $\Delta_{H2O\text{-}SO4}$ and –4.6‰ for $\Delta_{O2\text{-}SO4}$. Figure 5.21b includes *T. ferrooxidans,* with fractionation factors of +9.9‰ for $\Delta_{H2O\text{-}SO4}$ and –11.1‰ for $\Delta_{O2\text{-}SO4}$ (Taylor et al., 1984).

The $\delta^{18}O_{SO4}$ values of samples from the study area are between ~6-20‰ higher than their respective $\delta^{18}O_{H2O}$ values. Most samples fall within the 25-75% contribution range of reaction (5.2), indicating that reaction pathways are quite variable within the study area. One sample lies close to the 100% line in Figure 5.21a, representing mostly water-derived oxygen; it lies beyond that line in Figure 5.21b, indicating that either *T. ferrooxidans* is not present at that location, or that the fractionation induced by it is less than suggested by Taylor et al. (1984). Two samples lie above the 0% line (100% reaction (9)) in Figure

5.21b, with similar implications. Apart from these three samples, however, the influence of sulphide-oxidizing bacteria cannot be confirmed nor denied.
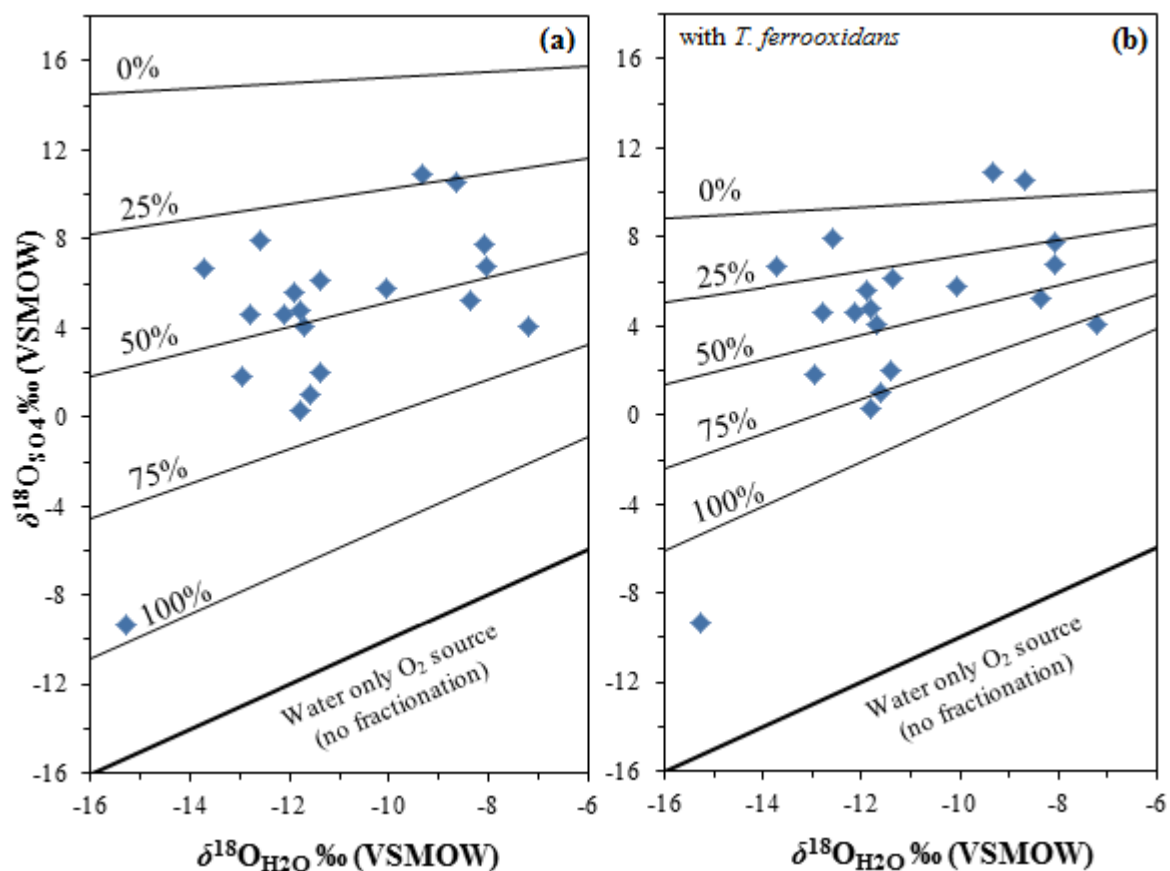
Figure 5.21: Plot of $\delta^{18}O_{SO4}$ vs. $\delta^{18}O_{H2O}$ for groundwater samples from the study area (data from this study, Freckelton (2013) and McIntosh and Walter (2006)). Lines indicate the percentage of sulphate generated by equation (5.2) with the remainder by equation (5.4). **(a)** represents a system without *T. ferrooxidans*, while **(b)** includes it. Fractionation factors from Taylor et al. (1984) are applied, as described in text. The thicker 1:1 lines indicate a purely water-oxygen source without any fractionation. These diagrams assume pyrite oxidation with no other modifying processes involved, and that the sulphate was oxidized in water of composition similar to that from which it was sampled.

Bacterially-mediated dissimilatory sulphate reduction (DSR) is another important process in many shallow groundwater systems, and appears to be active in the study region. DSR occurs when bacteria (e.g,. *desulphovibrio, desulphotomaculum* and *desulphomotas*) oxidize organic matter, generally under anaerobic conditions, releasing H_2S and causing large isotopic fractionations (Thode, 1991). This process preferentially consumes the light

isotopes, raising the $\delta^{18}O_{SO4}$ and $\delta^{34}S_{SO4}$ values of the remaining sulphate, following a Rayleigh-type reaction (Harrison and Thode, 1958; Mizutani and Rafter, 1969). The enrichment factors are not equal for the two isotopes; reported enrichment factors are typically ~2.5 to 4.5 times higher for sulphur than oxygen (Fritz et al., 1989), although exceptions are known (e.g., Mizutani and Rafter, 1969; Qureshi, 1986) where oxygen enrichments are even smaller.

Sulphur isotopic fractionation between sulphate and sulphide during DSR can be quite large; reported fractionations vary widely, up to approximately –46‰ (Thode, 1991), although some evidence suggests fractionation can be much larger, on the order of −70‰ (Brunner and Bernasconi, 2005). This fractionation is related to a sequence of enzyme-catalyzed kinetic fractionation steps (Rees, 1973). Its magnitude is dependent on a number of external and bacterial strain-specific factors. In terms of oxygen, the residual sulphate may be enriched in ^{18}O by up to ~17‰ (Brunner et al., 2005), although the exact mechanisms of fractionation are still debated, with kinetic effects (e.g., Aharon and Fu, 2000) and exchange with surrounding water molecules during intermediate steps (e.g., Fritz et al., 1989) often proposed. For more detailed discussions of these complex isotopic systems, see Chambers and Trudinger (1979) and Brunner et al. (2005).

The observation of H_2S in many shallow groundwaters in southwestern Ontario strongly suggests that DSR is active in the subsurface. The presence of (unidentified) yellowish-white, filamentous bacteria along sulphur water seeps in quarries and springs further confirms the existence of a highly active microbial community associated with groundwaters in the region. Lesage et al. (1991) also inferred the presence of DSR in the Lucas Formation aquifer on the basis of low E_H values (~100 ± 50 mV).

The sulphate isotopic data seem to confirm the existence of DSR. Several samples from this study, as well as McIntosh and Walter (2006) and Matheson (2012), have unusually high (>35‰) $\delta^{34}S_{SO4}$ values that are not easily explained by Devonian seawater sulphates. These samples most likely represent residual sulphate that has been enriched in ^{34}S by DSR relative to the original sulphate reservoir, which appears to have been derived from marine sulphate based on $\delta^{18}O_{SO4}$ values. A number of samples from this study and Matheson (2012) also have moderate $\delta^{34}S_{SO4}$ values, between +10 and +35‰, and

$\delta^{18}O_{SO4}$ values below the range for marine sulphate ($\sim<12‰$). These sulphates were likely originally produced through sulphide oxidation, judging from their low $\delta^{18}O_{SO4}$ and moderate $\delta^{34}S_{SO4}$ values, and subsequently affected by DSR. The fact that these oxidative and reductive processes both exist indicates a large degree of spatial and/or temporal heterogeneity in the redox conditions in the shallow flow system; these complex redox conditions are also apparent from the presence of secondary gypsum with $\delta^{34}S_{SO4}$ values matching reduced sulphides (Eberts and George, 2000). DSR is less evident in the study area on the basis of oxygen isotopes, since fractionations are variable and tend to be low. Nonetheless, several samples that are enriched in ^{34}S by DSR are also slightly ^{18}O-enriched relative to the average compositions of their probable pre-DSR reservoirs.

Figures 5.22a-b plot total sulphate and sulphide concentrations, respectively (sulphide data is only available for this study), versus $\delta^{34}S_{SO4}$. Contrary to expectations, Figure 5.22b does not show a strong relationship between $\delta^{34}S$ and sulphide concentrations. While this may in part be attributable to difficulties with sample preservation and analysis of the volatile H_2S phase, it may also reflect the complexities of this system. While two samples with high $\delta^{34}S_{SO4}$ values (+42.2‰ and +53.9‰) have elevated sulphide levels as expected for sulphate reduction, three others do not (although two are from the same well). It is possible that the latter waters experienced H_2S loss either post-sampling, or within the aquifer by gas migration, precipitation of metal sulphides, or re-oxidation to sulphate. All samples with $\delta^{34}S_{SO4}$ values >40‰ also have lower sulphate levels than most samples derived from marine evaporite dissolution, consistent with DSR. On that note, several of the marine sulphate samples also show elevated sulphide levels; this might represent H_2S that has migrated in from elsewhere, or it may be that these samples are also undergoing DSR but because of their very high concentrations, the effects of DSR on the sulphate reservoir are not detectable. The samples in the sulphide oxidation range show low sulphide levels, although one sample enriched in ^{34}S relative to the sulphide oxidation range shows elevated H_2S, indicating that some sulphate so derived may also undergoing DSR.
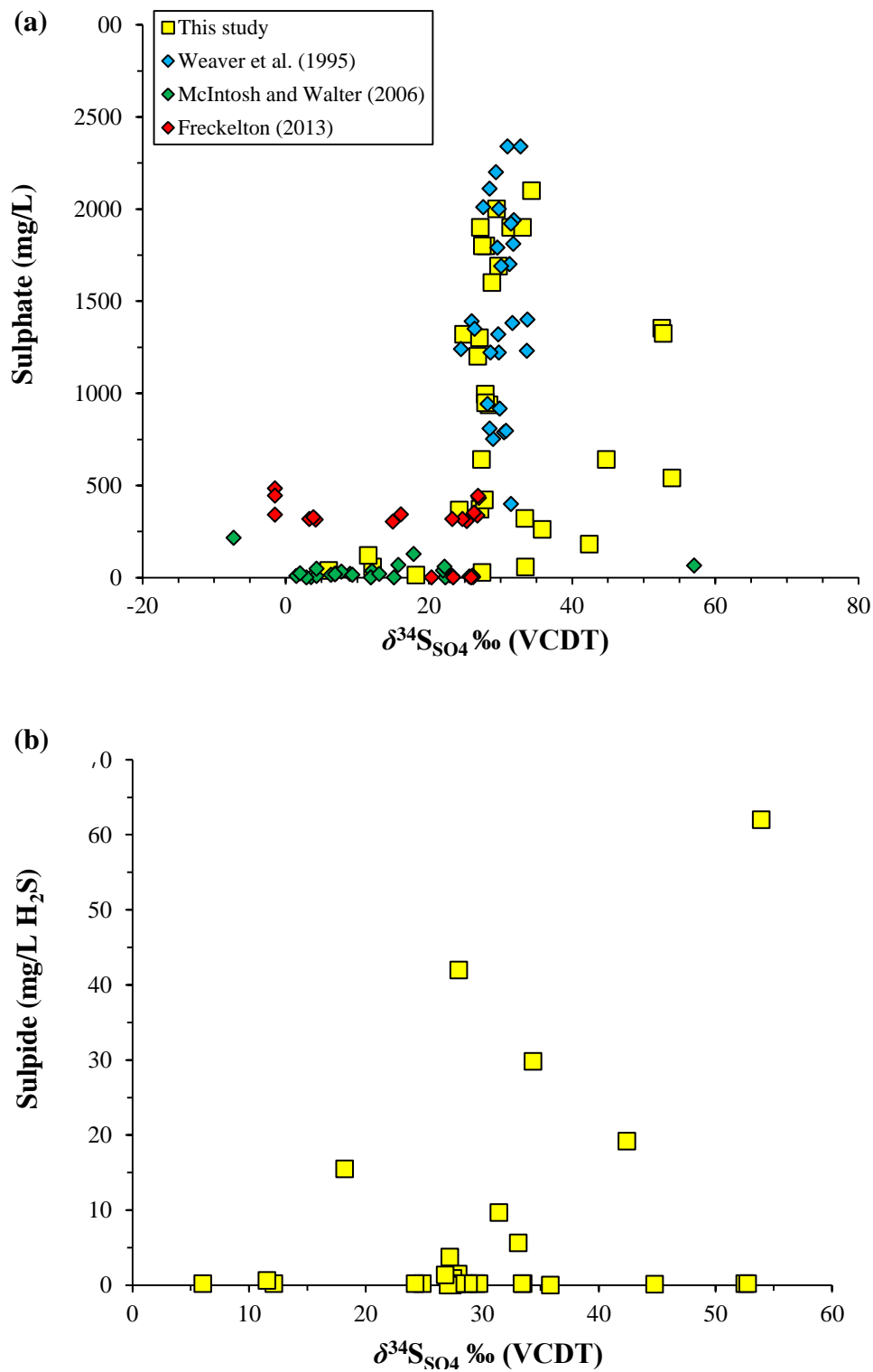
Figure 5.22: Total sulphate **(a)** and sulphide **(b)** concentrations vs. $\delta^{34}S_{SO4}$ for shallow groundwaters in the study area (sulphate data from this study, Freckelton, 2013, Weaver et al., 1995 and McIntosh and Walter, 2006; sulphide data from this study).

Finally, mixing of waters with different $\delta^{34}S_{SO4}$ and $\delta^{18}O_{SO4}$ values is another factor possible affecting sample compositions. Mixing is perhaps most evident in several samples which have $\delta^{34}S_{SO4}$ and $\delta^{18}O_{SO4}$ values intermediate between marine sulphate and sulphate derived from sulphide oxidation (Figure 5.20). While it is possible that these samples may simply have undergone reduction of sulphate originally produced by sulphide oxidation, the ^{18}O enrichments relative to those of ^{34}S under such a scenario are higher than would be expected from DSR.

Several samples from Matheson (2012), apparently originally derived from sulphide oxidation based on their lower $\delta^{18}O_{SO4}$ values, are enriched in $^{34}S_{SO4}$ relative to the sulphide oxidation range by ~30‰. Given the high (750-2000 mg/L) sulphate concentrations reported for these samples, extensive DSR is not a likely explanation for these large enrichments. Instead, the high $\delta^{34}S_{SO4}$ values of these samples may be due to mixing between a sulphide oxidation end-member (which may have undergone some DSR) and a seawater sulphate end-member affected by DSR. The $\delta^{18}O_{SO4}$ values for these samples are also consistent with such a mixing scenario.

5.2.1.4   Strontium isotopes

The $^{87}Sr/^{86}Sr$ ratio of dissolved strontium is useful for tracing the origins of strontium and water-rock interactions. Wickman (1948) predicted that the decay of ^{87}Rb to ^{87}Sr would increase the $^{87}Sr/^{86}Sr$ ratio of seawater over time. Peterman et al. (1970) determined that the $^{87}Sr/^{86}Sr$ of Phanerozoic marine fossils both increased and decreased with time. Veizer and Compston (1974) provide a summary of early work, and reasoned that seawater $^{87}Sr/^{86}Sr$ being uniform at any given time, marine precipitates will incorporate the seawater ratio, and that diagenesis either increases the ratio or leaves it unaffected. A comprehensive summary of the seawater $^{87}Sr/^{86}Sr$ literature is given by Veizer et al. (1999), and their $^{87}Sr/^{86}Sr$ age curve, generated from 2128 calcitic and phosphatic shells, mainly brachiopods with some conodonts and belemnites, is presented in Figure 5.23. The $^{87}Sr/^{86}Sr$ composition of seawater varied from approximately 0.7095 to 0.7075 from the Cambrian to the Mississippian, with several large oscillations during that span.

Devonian seawater had $^{87}Sr/^{86}Sr$ ratios between ~ 0.7077–0.7089 (Veizer et al., 1999). Most shallow carbonates in southwestern Ontario are Middle Devonian in age, during which time seawater $^{87}Sr/^{86}Sr$ tended towards the lower end of the above range. Haeri-Ardakani et al. (2013) measured $^{87}Sr/^{86}Sr$ ratios for the Lucas Formation, and reported values between 0.70797–0.70838 (mean 0.70814 ± 0.00015) for fine-crystalline dolomite, and similar values of 0.70798–0.70815 (mean 0.70807 ± 0.00012) for late-stage calcite. These values are perhaps slightly higher than coeval seawater, and the authors attributed this increase to interaction with more radiogenic waters from Upper Devonian siliciclastic rocks (i.e. the Berea sandstone and Kettle Point shales).
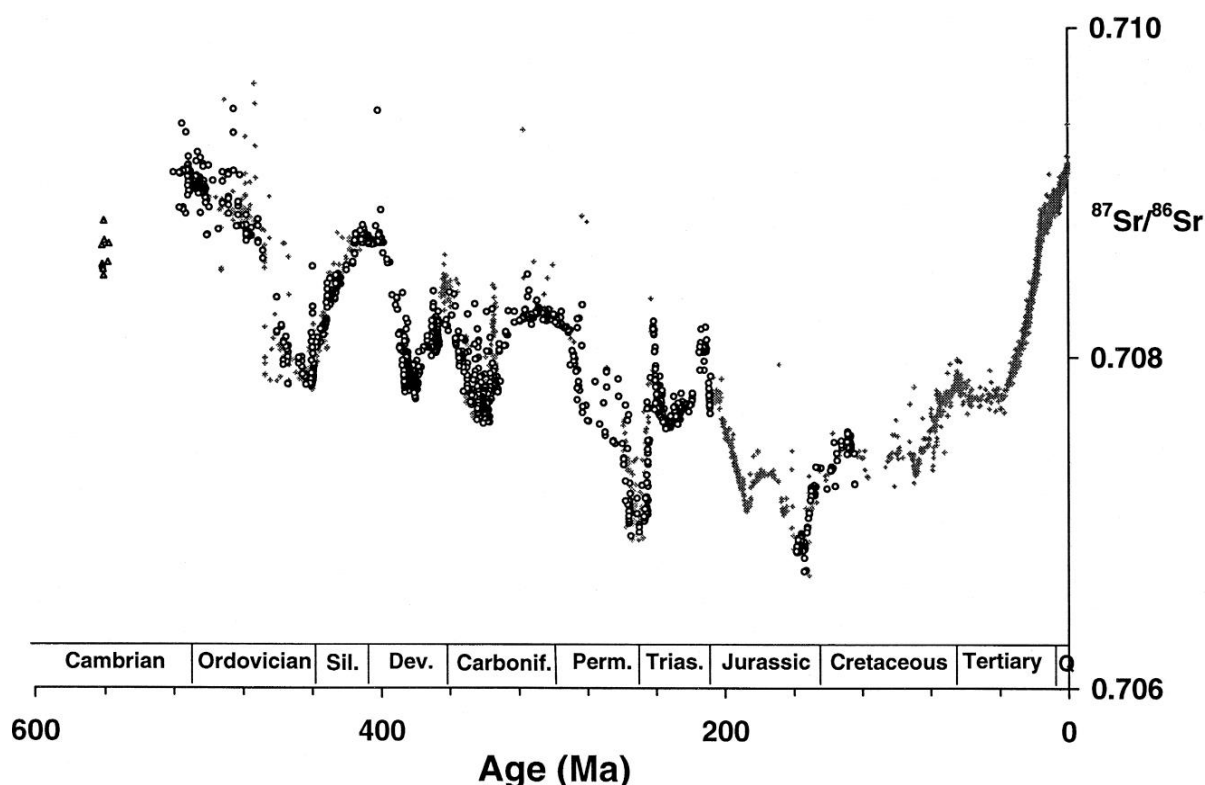
Figure 5.23: Seawater $^{87}Sr/^{86}Sr$ variations throughout Phanerozoic time (from Veizer et al., 1999; dots were from previous studies, circles are samples from the Bochum/Ottawa area, and triangles are micritic matrix samples).

The Devonian groundwaters sampled in this study have $^{87}Sr/^{86}Sr$ ratios between 0.70812 – 0.70928 (mean 0.70843 ± 0.00032). The Salina Group subcrop water samples have $^{87}Sr/^{86}Sr$ ratios of 0.70850 – 0.70881, well within the Devonian range, although somewhat higher than average. When they and the shallow samples of unknown origin are included,

the full $^{87}Sr/^{86}Sr$ range for the shallow waters becomes $0.70812 - 0.70995$ (mean 0.70854 ± 0.00041). This range is comparable to that observed by McIntosh and Walter (2006) for shallow groundwaters in the U.S. Great Lakes region. It also overlaps with, although overall is somewhat higher than, the $^{87}Sr/^{86}Sr$ ratios reported for local Devonian carbonates by Haeri-Ardakani et al. (2013), and some of the more radiogenic samples have considerably higher ratios than any Devonian seawater samples reported by Burke et al. (1982). A plot of $^{87}Sr/^{86}Sr$ ratio against total Sr^{2+} concentration for the shallow groundwaters in this study, as well as McIntosh and Walter (2006) for comparison, is shown in Figure 5.24.
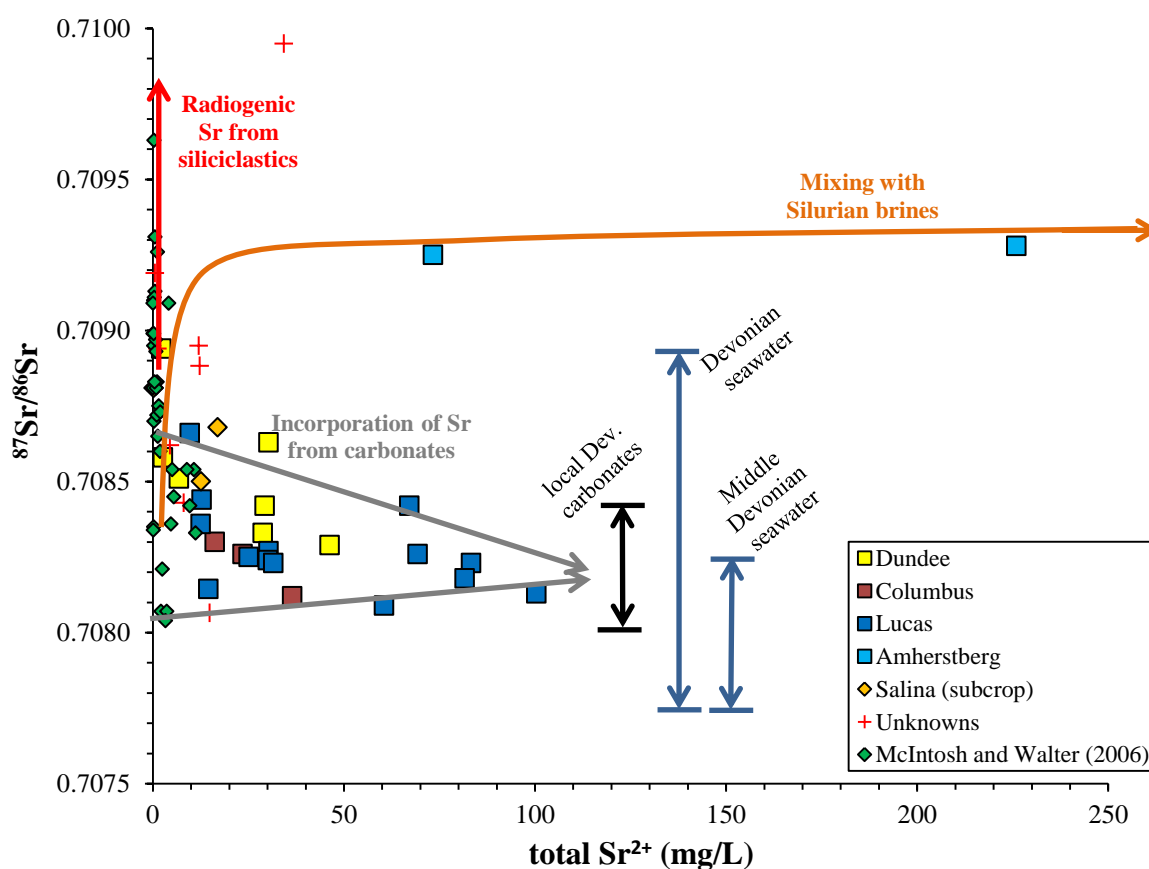
Figure 5.24: Plot of $^{87}Sr/^{86}Sr$ ratios vs. total Sr^{2+} concentrations for shallow groundwater samples from this study and McIntosh and Walter (2006). The compositions of Devonian seawater and local carbonates are also plotted for comparison, as are various geochemical processes possibly responsible for the observed ratios, as discussed in the text.

A large number of the shallow groundwater samples have $^{87}Sr/^{86}Sr$ ratios near that of the Devonian carbonates. Several samples show a trend of increasing Sr^{2+} concentrations that

converges to the carbonate $^{87}Sr/^{86}Sr$ composition. This trend suggests that rock-water interaction with the carbonates is an important factor controlling the $^{87}Sr/^{86}Sr$ ratios and Sr^{2+} concentrations of the shallow groundwaters. This rock-water interaction may either take the form of cation exchange reactions (McIntosh et al., 2004) or dissolution of the carbonates. These water samples are also typically located deeper in the basin, where longer residence times and thus increased rock-water interaction would be expected. They also have compositions similar to two Dundee samples ($^{87}Sr/^{86}Sr = 0.70812$ and 0.70823) from central Michigan reported by McNutt at al. (1987), suggesting that the same processes control their compositions despite greatly different locations in the basin. The samples showing this rock-water interaction trend are among the more saline Devonian waters. If their strontium was derived largely from brines in the deeper formations, as discussed in Section 5.2.1.2, they should show a different trend, with increasing $^{87}Sr/^{86}Sr$ ratios and Sr^{2+} concentrations. However, the observed trend could be alternatively be interpreted as converging towards the Devonian seawater compositions, implying mixing with the brines originally present in these units, although if such were the case, it might be expected that the $\delta^{18}O$ and δ^2H values of these waters would plot below the meteoric water line; it is also expected that in this active, shallow system, the original brines would have been long since flushed out by glacial and/or meteoric waters.

At least two samples, both from the deeper Amherstberg Formation, do show such a brine-mixing trend (Figure 5.24). Both have relatively elevated $^{87}Sr/^{86}Sr$ ratios (0.70925 and 0.70928) and Sr^{2+} concentrations (73.3 and 226 mg/L). Their $^{87}Sr/^{86}Sr$ ratios are similar to many brine samples from the Guelph Formation. Combined with their high TDS and $\delta^{18}O/\delta^2H$ signatures plotting below the GLMWL, this strongly suggests a Silurian brine component. It seems reasonable that these two samples would have the greatest brine contribution, given that they are among the deepest and from the stratigraphically lowest Devonian units sampled.

Several samples from this study, as well as McIntosh and Walter (2006), have very high $^{87}Sr/^{86}Sr$ ratios that cannot be explained easily by mixing with Silurian brines. While they may have a component of high $^{87}Sr/^{86}Sr$ brine from a unit deeper than the Guelph Formation, if a conduit between these formations was available, they also typically have

low Sr^{2+} concentrations, suggesting another process is more likely responsible. The most likely explanation is addition of Sr^{2+} from siliciclastic sediments, which contain minerals such as feldspars and micas with higher Rb contents and thus have more radiogenic $^{87}Sr/^{86}Sr$ signatures (Stueber et al., 1972). Such sources may include the Hamilton or Kettle Point shales, as well as glacial overburden. This process likely affected most if not all shallow samples, and variations in the extent of this radiogenic input may be in part responsible for the relatively wide range of $^{87}Sr/^{86}Sr$ ratios in this system. Haeri-Ardakani et al. (2013) also invoked radiogenic Sr^{2+} from Rb-rich sources to explain the $^{87}Sr/^{86}Sr$ ratios higher than Middle Devonian seawater in the Lucas Formation dolomite; thus, it could also be seen to have an indirect influence on groundwaters that dissolve or exchange Sr^{2+} with those dolomites.

To summarize, the strontium characteristics of the shallow groundwaters can be attributed to several processes that produce apparent relationships among depth, $^{87}Sr/^{86}Sr$ and Sr^{2+} concentration, as illustrated in Figure 5.25. The evolution of Sr^{2+} in the shallow bedrock system can be explained by the following scenario. Meteoric water, containing little or no Sr^{2+}, infiltrates the drift and incorporates small amounts of relatively radiogenic Sr^{2+} from Rb-rich siliciclastic minerals therein. The $^{87}Sr/^{86}Sr$ ratios of groundwaters as they enter the bedrock aquifers are thus typically high but can vary considerably depending on factors such as the flow path, residence time in the drift, and spatial variations in drift mineralogy. Once in the bedrock, the groundwaters begin to interact with the reservoir carbonates through exchange and dissolution, lowering the $^{87}Sr/^{86}Sr$ ratio of the waters and increasing their Sr^{2+} concentrations. During dolomitization, similarly radiogenic waters were likely responsible for raising the $^{87}Sr/^{86}Sr$ ratio of the carbonates above that of the seawater from which they were deposited. The longer the residence time of the waters in the bedrock, the more their $^{87}Sr/^{86}Sr$ ratios will approach that of the surrounding carbonates, and hence deeper waters tend to have lower ratios as well as higher Sr^{2+} concentrations. Locally in the deepest parts of the Devonian sequence, upward advection or diffusion of Sr^{2+} from Silurian brines has mixed with the Devonian waters, raising both their $^{87}Sr/^{86}Sr$ ratios and Sr^{2+} concentrations. Likewise, it is also possible that some of the deeper waters may have been influenced by radiogenic Sr^{2+} diffusing or leaking

downwards from the Hamilton or Kettle Point shales, and/or cross-formational flow from the drift, through these formations along fractures.
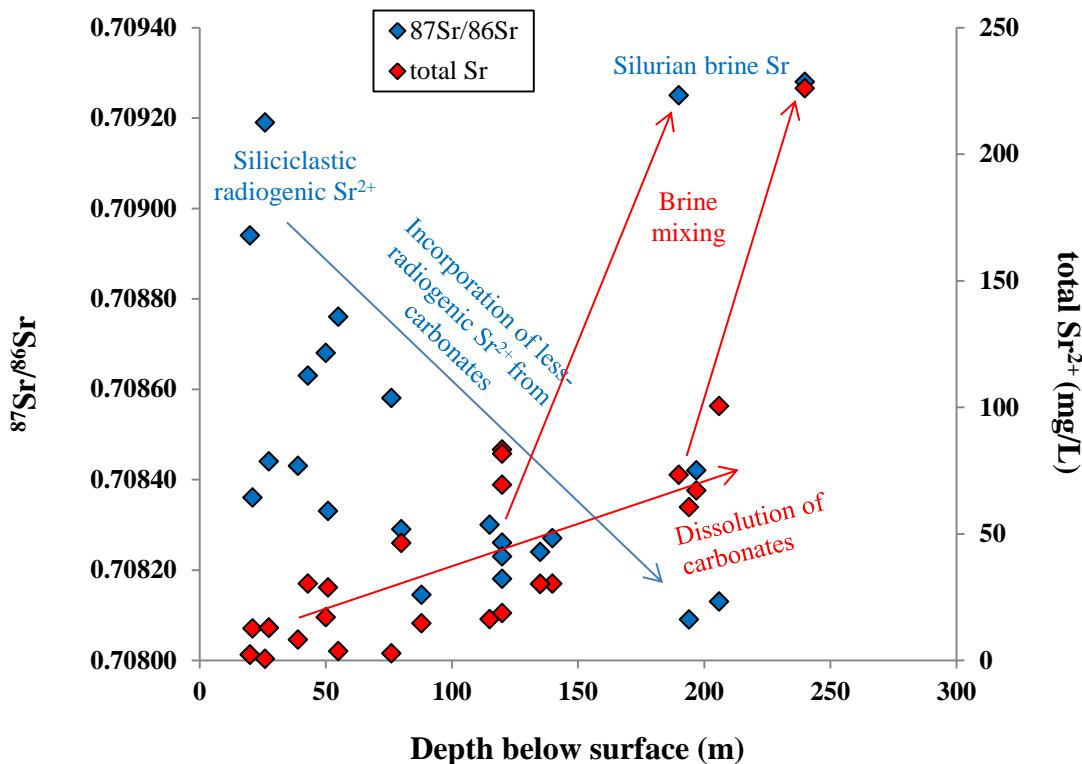
Figure 5.25: Plot of ^{87}Sr/^{86}Sr ratios and Sr^{2+} concentrations with depth for shallow groundwaters sampled in this study. Several processes are illustrated to explain the observed trends (see text).

5.2.1.5 *Carbon isotopes of DIC*

The shallow groundwater samples collected in this study have a wide range (−16.7 to +20‰) of dissolved inorganic carbon isotopic compositions (δ^{13}C$_{DIC}$) (Figure 5.26). To our knowledge this is the first major study to measure δ^{13}C$_{DIC}$ values of groundwaters in southwestern Ontario, apart from a few samples collected from the DGR boreholes, which were from a variety of shallow and deep formations (Jackson and Heagle, 2010; Heagle and Pinder, 2010). McIntosh and Walter (2006) studied the shallow drift and bedrock aquifers throughout the US Great Lakes region, and found δ^{13}C$_{DIC}$ values between −20.5 and +23.5‰. Long et al. (1988) reported δ^{13}C$_{DIC}$ values between −21.4 and −8.1‰ for groundwaters from east-central Michigan, near Saginaw Bay.
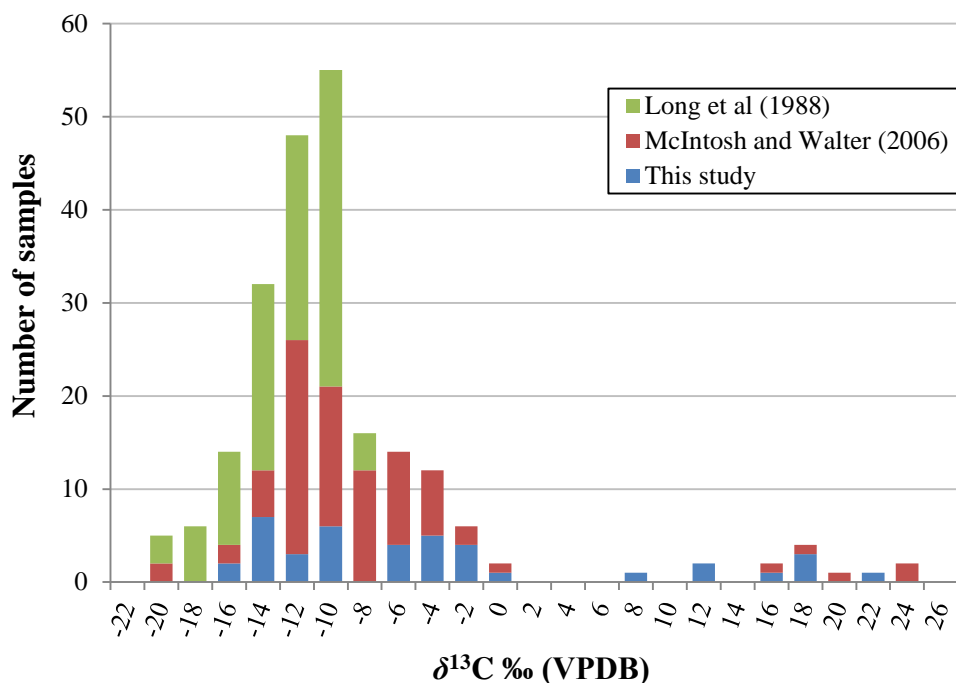
Figure 5.26: Histogram of $\delta^{13}C_{DIC}$ values for shallow groundwaters in Ontario (this study) and the US Great Lakes region (Long et al., 1988; McIntosh and Walter, 2006).

With the exception that Long et al. (1988) did not report any samples above −8‰, the $\delta^{13}C_{DIC}$ values found in these studies are largely comparable, suggesting similar carbon systematics exist in shallow aquifers throughout the Great Lakes region. Most samples have $\delta^{13}C_{DIC} < −10‰$, although a few are unusually ^{13}C-enriched, near +20‰.

Several mechanisms can add bicarbonate to the DIC pool, and thus affect its $\delta^{13}C_{DIC}$. The first is exchange with CO_2 in the soil air reservoir, which is derived from heterotrophic oxidation of soil organic matter and from respiration from plant roots, both of which involve negligible isotopic fractionation between the organic matter substrate and the CO_2 produced (Park and Epstein, 1961; Lin and Ehleringer, 1997). Most plants in the study region are largely C_3-type, which have average δ^{13}C values of ~ −27‰ (Kohn, 2010). However, agriculture is a major industry in southwestern Ontario, and corn represents a significant portion (~32% by land use; OMAF, 2011) of the cropland. Corn is a C_4 plant and thus has different metabolic pathways and carbon fractionation, with average δ^{13}C values of ~ −13‰ (shifted 2‰ from −11‰; Bender, 1968, Tieszen and Fagre, 1993, to account for the Suess effect). An overall average of −22.5‰ can thus be calculated for

soil CO_2 in the region. If soil CO_2 is in equilibrium with groundwater bicarbonate at 20°C, the latter would be enriched in ^{13}C by ~8.5‰ (Mook, 2001), and thus would have an average $\delta^{13}C_{DIC}$ value of ~ −14‰. This coincides well with many of the observed $\delta^{13}C_{DIC}$ values, suggesting that exchange with soil CO_2 is likely a dominant process affecting the lower-$\delta^{13}C$ samples. Variations in local C_3/C_4 plant abundances and other processes, such as crop burning (resulting in ^{13}C depletions of ~1‰; Turney et al., 2006), may also affect organic matter-derived $\delta^{13}C_{DIC}$ values and contribute to their variability.

Sulphate reduction, having been identified on the basis of sulphate isotopes (Section 5.2.1.3), is another process that could likely be influencing the lower $\delta^{13}C_{DIC}$ values of many samples, as also suggested by Long et al. (1988). In addition to H_2S, this process generates bicarbonate (Equation 5.5), the $\delta^{13}C$ composition of which is similar to that of the organic matter being oxidized (Raiswell, 1987):

$$SO_4^{2-} + 2(CH_2O) \rightarrow H_2S + 2HCO_3^- \tag{5.5}$$
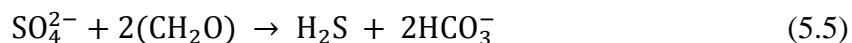
Another potentially important source of DIC is dissolution of carbonate minerals. Haeri-Ardakani et al. (2013) found an average $\delta^{13}C$ value of +2.3‰ for matrix dolomite (making up >95% of the rockmass) in the Lucas Formation in Ontario. If these carbonates are being dissolved by soil-CO_2-derived carbonic acid ($\delta^{13}C_{CO2(aq)} \approx -23.5‰$), dissolution of dolomite according to equation 5.6,

$$2H_2CO_3^{2-} + CaMg(CO_3)_2 \rightarrow 4HCO_3^- + Ca^{2+} + Mg^{2+} \tag{5.6}$$
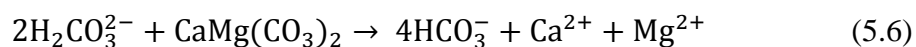
will yield bicarbonate with an average $\delta^{13}C_{DIC}$ value of −10.6‰ (as the carbon is supplied equally by the reactants). Thus, a combination of low-$\delta^{13}C_{DIC}$ from vegetation-derived soil CO_2 or sulphate reduction, with higher-$\delta^{13}C_{DIC}$ from carbonate dissolution, can explain much of the variation measured for the more negative samples.

However, there are several samples with somewhat higher $\delta^{13}C_{DIC}$ values (between −10.6 and +2‰). While these may be explained to some degree by dissolution of carbonates by carbonic acid generated predominantly from C_4-based carbon, it is likely that some other process is also contributing to their higher $\delta^{13}C_{DIC}$ values, probably as is responsible for the samples with values significantly above 0‰, as discussed below.

The large ^{13}C enrichment (up to ~ +25‰) observed in some of the samples in the study area is almost certainly due to bacterial methanogenesis. The fact that only a few samples appear to be thusly affected may be related to the high sulphate concentrations in many of the shallow waters; methane production is typically not significant until sulphate is nearly depleted, as sulphate-reducing bacteria will outcompete methanogens (Whiticar, 1999). This is consistent with the observation that all ^{13}C-enriched samples have relatively low sulphate concentrations. Below the zone of sulphate reduction, methanogenesis generally occurs by the CO_2 reduction pathway (Raiswell, 1987; Claypool and Caplan, 1974):

$$4H_2 + CO_2 \rightarrow CH_4 + 2H_2O \qquad (5.7)$$

This reaction preferentially consumes the light isotopes of existing dissolved CO_2, enriching the residual DIC pool in ^{13}C as methanogenesis progresses. Depending on substrate availability, methanogenesis may also occur via acetate fermentation (equation 5.8), which produces ^{13}C-enriched CO_2 (Whiticar, 1999):

$$CH_3COOH \rightarrow CH_4 + CO_2 \qquad (5.8)$$

Martini et al. (1998) and McIntosh et al. (2004) studied waters in the Antrim shale in Michigan, and identified unusually high δ^{13}C values for CO_2 coproduced with methane (~ +22‰), and corresponding DIC with δ^{13}C up to ~ +28‰. Similar enriched $\delta^{13}C_{DIC}$ values up to +29.4‰ have been reported in shallow Devonian-Mississippian aquifers in Illinois (McIntosh et al., 2002). Generation of ^{13}C-enriched CO_2 by methanogenic bacteria thus appears to be a widespread phenomenon in shallow aquifers throughout the Great Lakes region. All but two of the ^{13}C-enriched samples measured in this study were from carbonate aquifers overlain by shales. Since all the samples that Martini et al. (1998) and McIntosh et al. (2004) analyzed from the Antrim shale were ^{13}C-enriched, often more so than our samples, it is likely that organic-rich shales represent the main focus of methanogenesis in the region. DIC produced therein would migrate into the underlying carbonates, mixing with more negative DIC produced in the drift and/or by carbonate dissolution. This scenario is consistent with samples from Oil Springs where water from higher in the reservoir (closer to the shales) has significantly higher $\delta^{13}C_{DIC}$ (~ +20‰) than water deeper at greater depths (~ –4‰).

5.2.2   Deep water system

Below ~ 350-450 m, all groundwaters in the study region are highly saline brines (see Section 2.1.3). Deep brines are common in many sedimentary basins (Collins, 1975; Hanor, 1994; Land, 1997; Kharaka and Hanor, 2007). As discussed in Section 2.2, Dollar et al. (1991) were the first to study brines in detail in southwestern Ontario, and observed differing isotopic signatures among the deep formations. Dollar et al. (1991) hypothesized that the different formations represented relatively separate hydrological systems, although all brines originated as evaporated paleoseawaters that infiltrated sediments when the formations were deposited, and were since modified by other processes. These brines have extremely high, although quite variable, TDS contents (153,000-518,000 mg/L). Thus, their isotopic activities differ significantly from their isotopic concentrations, and salt effect corrections are applied (on average, +1.1‰ δ^{18}O and −12‰ δ^2H), as discussed in Section 2.3.2; concentration values are used in the following discussion unless stated otherwise.

Sections 5.2.2.1 – 5.2.2.5 provide a broad overview of the various isotopic systems and their general implications for brine origin and evolution. More detailed discussions of the individual units follow in Sections 5.2.2.6 – 5.2.2.10.

5.2.2.1   Oxygen and hydrogen isotopes of water

One major feature of the deep brines is that they have significantly different δ^{18}O and δ^2H values than the shallower waters, being considerably enriched in ^{18}O and slightly enriched in ^{2}H, plotting to the right of the GMWL – a common feature for sedimentary brines (Kharaka and Hanor, 2007). This study confirms the observation of Dollar et al. (1991) that the different formations waters have different isotopic compositions, as illustrated in Figure 5.27, which also shows data from the Guelph Formation in Michigan (Wilson and Long, 1993b) and the Clinton Group in eastern Ohio (Lowry et al., 1988). While there are some slight differences, and thus study reveals an overall greater variability in brine compositions, generally the data from these studies are remarkably similar.
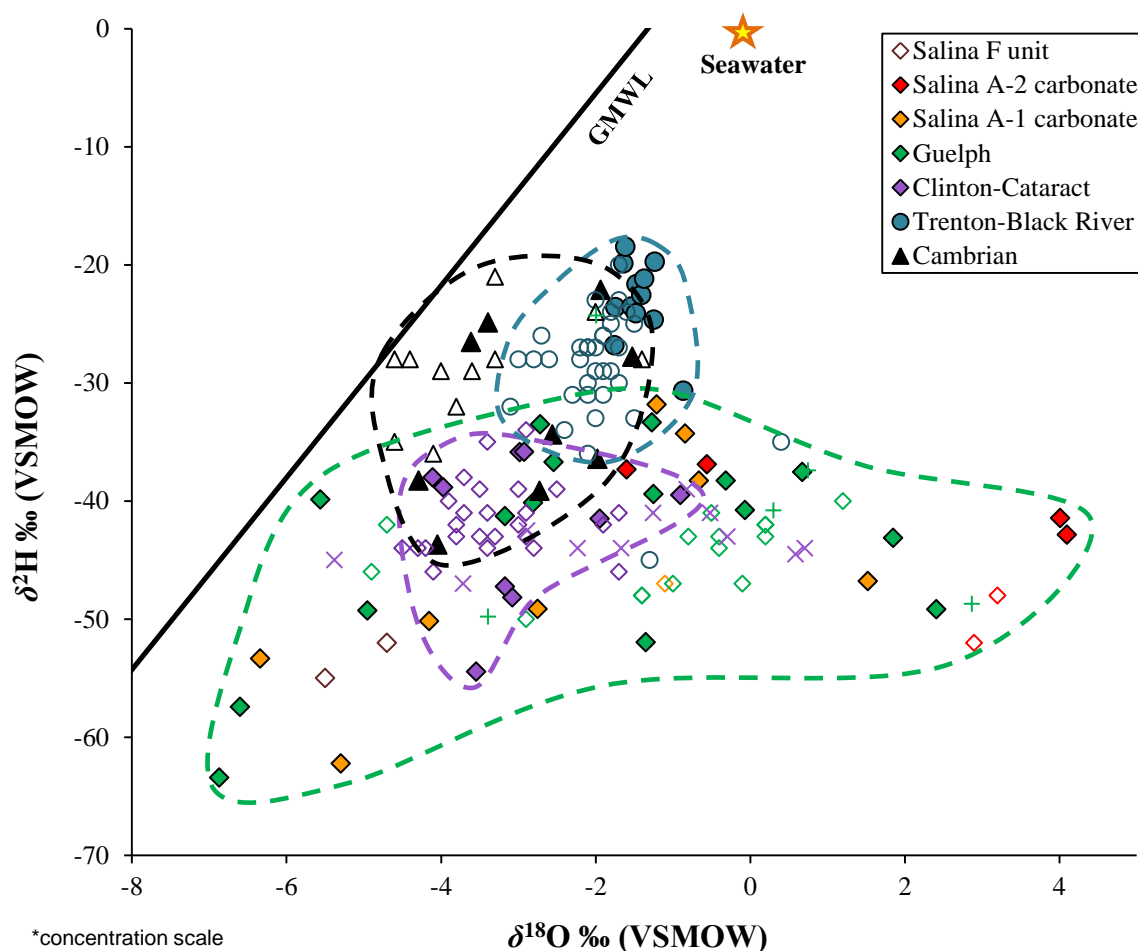
Figure 5.27: Plot of δ^2H vs. $\delta^{18}O$ of deep brines from southwestern Ontario and the surrounding area. Brines from the major bedrock units plot within relatively distinct ranges, as contoured (contour colours correspond to symbol colours). Solid symbols are from this study, hollow symbols of corresponding colour are from Dollar et al. (1991); crosses are from Wilson and Long (1993b) and X's are from Lowry et al (1988). All data are reported on the isotopic concentration scale.

Interpretation of the data in Figure 5.27 requires a mechanism to explain the enrichment in ^{18}O and ^2H beyond meteoric levels, and in the case of several samples, enrichment of ^{18}O beyond seawater values (~0‰). The origin of sedimentary brines is still a matter of some debate (see a review by Hanor, 1994), and several mechanisms to explain their unusual compositions have been proposed. Two leading hypotheses are described below.

Some researchers have proposed that brines formed from recent or old meteoric water (e.g., Clayton et al., 1966) and/or seawater (e.g., Hitchon and Friedman, 1969), which were subsequently modified by rock-water interaction and/or membrane filtration. Rock-water interaction exchanges water isotopes with the reservoir rock, generally resulting in ^{18}O enrichment of water, and little/no enrichment in ^{2}H due to the small amount of hydrogen in most rocks. Membrane filtration occurs as water is slowly forced through low permeability units such as shales, during which lighter isotopes pass through more readily, causing ^{18}O- and ^{2}H-enrichment of residual water (Graf et al., 1965).

Others (e.g., Holser, 1979; Knauth and Beeunas, 1986; Dollar et al., 1991) proposed that the unique δ^{18}O and δ^{2}H compositions of sedimentary brines were largely the result of extreme seawater evaporation, during which, the isotopic composition of seawater follows a hook-shaped trajectory, initially becomes enriched in both ^{18}O and ^{2}H, a trend that later reverses once gypsum starts to precipitate (see Section 2.3.1). Extended continuation of this trend can lead to brines more depleted of ^{18}O and ^{2}H than seawater, and hence such waters need not be interpreted as being related to meteoric water.

The 'evolved meteoric water' and 'evaporated seawater' theories were cited by Clayton et al. (1966) and Dollar et al. (1991), respectively, to explain the compositions of the deep brines in southwestern Ontario and Michigan. If the brines were the product of meteoric waters modified by rock-water interaction, their compositions should plot along a linear trend intersecting the composition of the meteoric water from which they originated, such as observed in several basin brines by Clayton et al. (1966). However, no such general trend is apparent in our data or those of Dollar et al. (1991) (Figure 5.27), and the trend observed by Clayton et al. (1966) may be due to the shallower nature of their samples.

The 'evaporated seawater' hypothesis can be investigated using Figure 5.28, which illustrates the available data relative to the seawater evaporation curve of Holser (1979), extrapolated by Knauth and Beeunas (1986) to 45x concentration; other processes and mixing scenarios are also illustrated. The majority of the data plot close to the 45x concentration point, indicating that the isotopic compositions of these brines could be explained by extensive seawater evaporation. Much of the scatter could be attributed to differences in degree of evaporation, and/or variations in the exact shape of the

evaporation curve, which is dependent on factors such as temperature and humidity. However, other processes were likely also involved, as discussed in further detail in later sections. Several samples appear to have mixed with recent meteoric waters, and some show ^{18}O enrichments likely associated with rock-water interaction. The fact that the data plot relatively close together suggests that the brines had a similar source, although, given the isotopic differences between the various units, there must either have been some differences in source composition, or these differences were diagenetic in nature, arising due to hydrological isolation of the different units by the aquitard units between them.
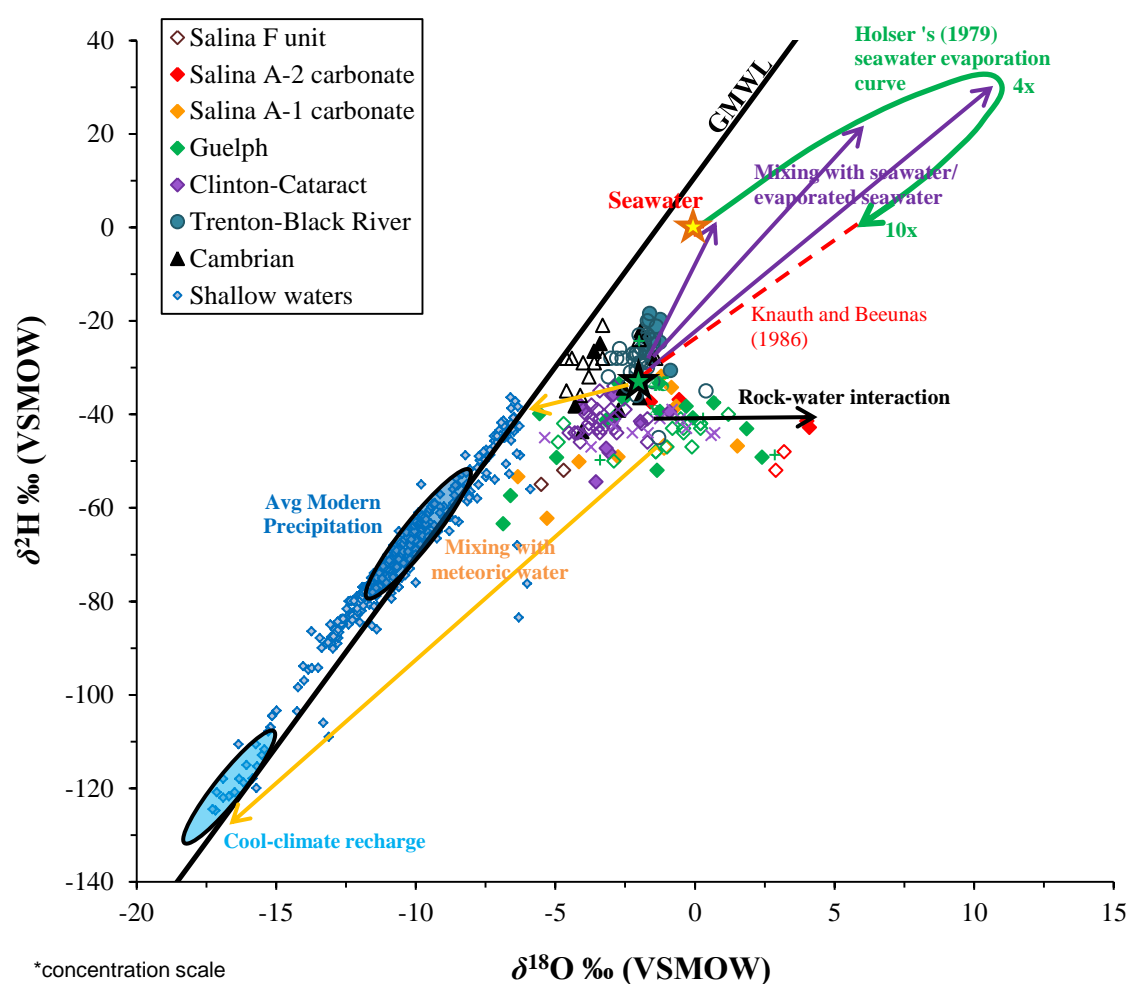
Figure 5.28: Plot of δ^2H vs. δ^{18}O of the deep brines from southwestern Ontario and nearby basins compared with various end-members and processes potentially affecting their evolution (Solid symbols: this study; hollow symbols: Dollar et al., 1991; crosses: Wilson and Long, 1993b; X's: Lowry et al., 1988; ★ : 45x seawater concentration).

5.2.2.2   *Sulphur and oxygen isotopes of sulphate*

This study represents the first comprehensive isotopic investigation of dissolved sulphate in the deep southwestern Ontario brines. Silurian anhydrite samples from the Michigan Basin have $\delta^{34}S$ values of +26.9 to +28.6‰ in the Salina F unit (Das et al., 1990), and +23.5 and +26.3‰ in the Salina A unit (Holser and Kaplan, 1966).

The brine $\delta^{34}S_{SO4}$ and $\delta^{18}O_{SO4}$ values are illustrated in Figure 5.29, alongside a subset of the shallow water data. The brines have less variable isotopic compositions than the overall range for the shallow waters, and tend to have lower $\delta^{18}O_{SO4}$ values than the evaporite-derived shallow waters. Most brine sulphates have isotopic compositions falling within the range of Cambrian-Silurian seawater sulphate, as discussed below. This marine sulphate could be from an original seawater component, or gypsum/anhydrite dissolution.
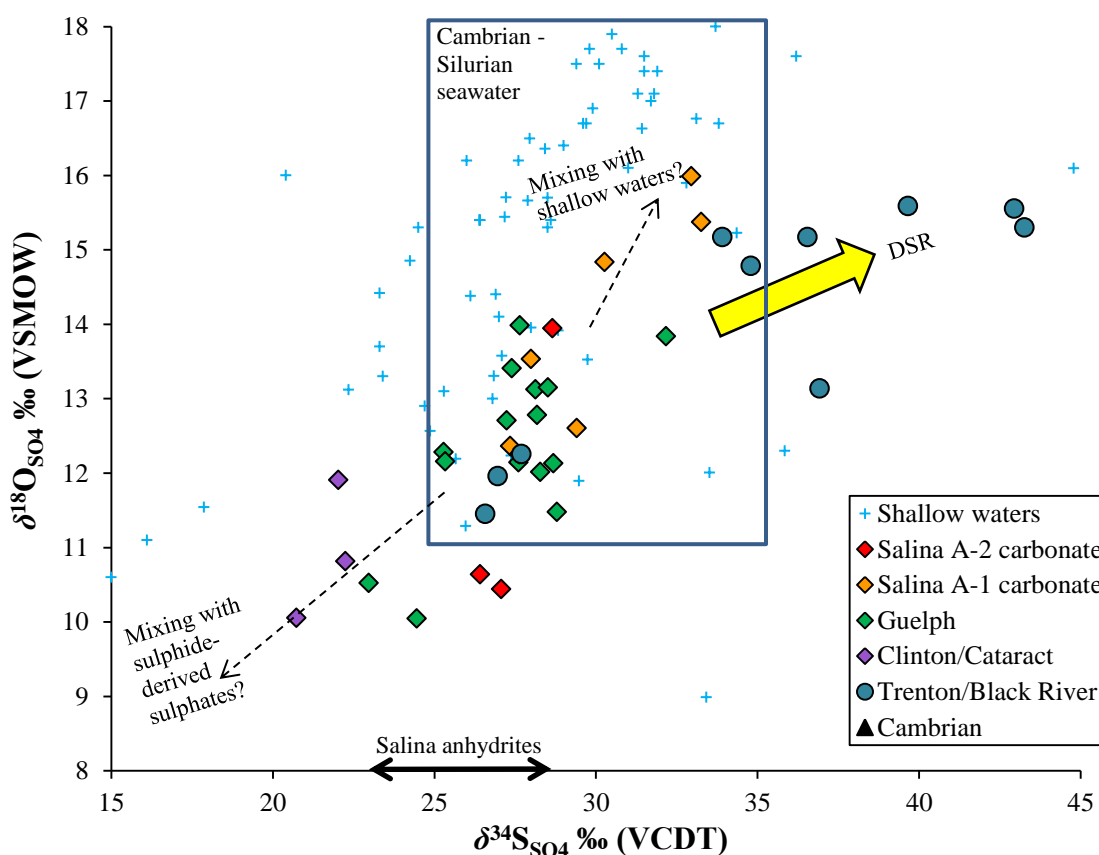
Figure 5.29: Plot of $\delta^{18}O_{SO4}$ vs. $\delta^{34}S_{SO4}$ for the deep formation brines, compared with data for shallow water in the study area. See Figure 5.20 for references for the shallow water data. Seawater composition box based on Claypool et al. (1980).

Seawater $\delta^{34}S_{SO4}$ and $\delta^{18}O_{SO4}$ values did not vary much during the Cambrian through Silurian (Figure 5.30). Precambrian $\delta^{34}S_{SO4}$ values were considerably lower (~ +17 ± 3‰), but rose sharply to +30 to +35‰ at the end of the Precambrian, and decreased slowly during the early Paleozoic, before decreasing sharply in the Late Silurian. $\delta^{18}O_{SO4}$ values were relatively constant (~ +14 to +17‰) throughout (Claypool et al., 1980).
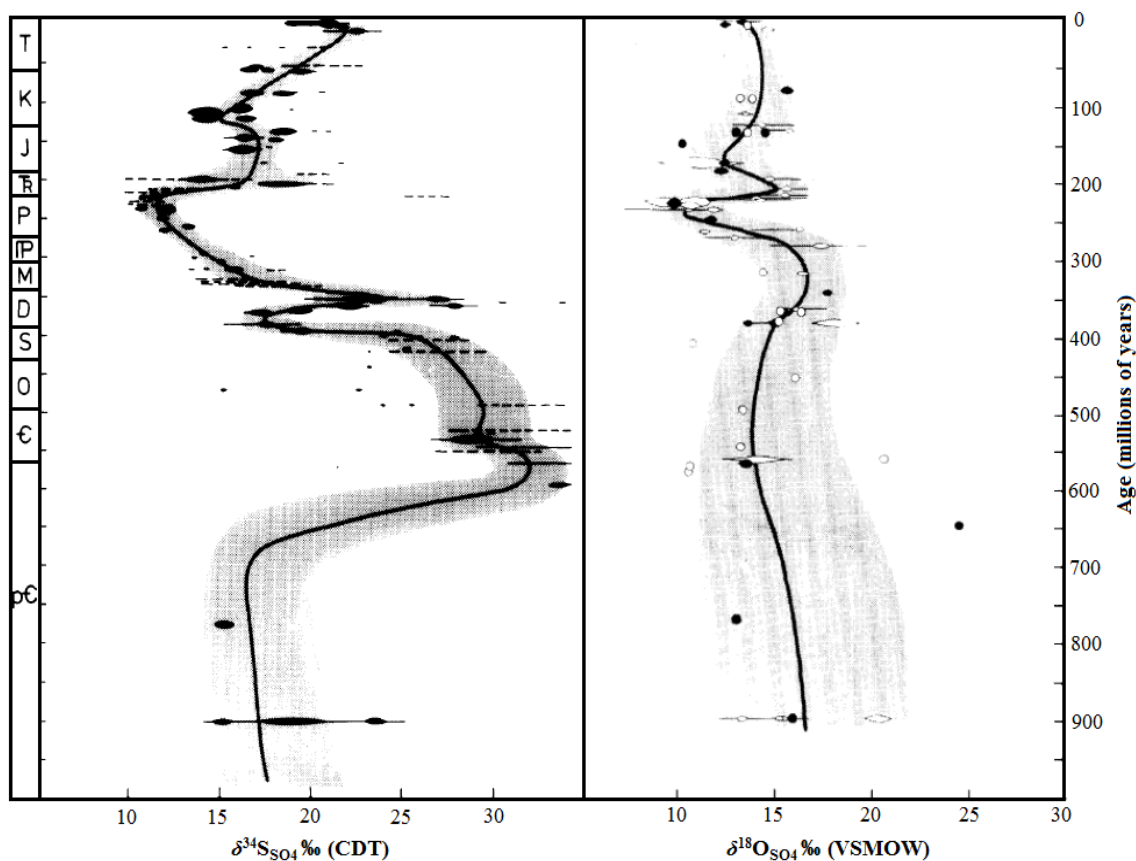
Figure 5.30: The seawater $\delta^{34}S_{SO4}$ and $\delta^{18}O_{SO4}$ age curves (from Claypool et al., 1980).

While most brine sulphates in the study area have $\delta^{34}S_{SO4}$ values easily attributable to seawater sulphate of the same age as their host units, some exceptions suggest that other processes are also involved. The high $\delta^{34}S_{SO4}$ values (~ +35 to +45‰) of several samples do not readily correspond to any seawater compositions. Also, some samples have $\delta^{18}O_{SO4}$ values (~ +9 to +11‰) lower than most Cambrian-Silurian seawater, and most samples have $\delta^{18}O_{SO4}$ values lower than the seawater average (+15 to +17‰). Several samples also have lower $\delta^{34}S_{SO4}$ values (~<25‰) than might be expected from seawater.

The low $\delta^{34}S_{SO4}$ and $\delta^{18}O_{SO4}$ values of some samples may be due to a small component of sulphate derived from sulphide oxidation, mixed with marine sulphate. The Silurian-aged units which these samples are from are known to contain sulphide minerals (Mostaghel, 1983; Tworo, 1985). Alternatively, these low values are close enough to the marine sulphate composition that they may simply be from seawater sulphate with a below-average $\delta^{34}S_{SO4}$ and $\delta^{18}O_{SO4}$ composition, or perhaps Precambrian or Late Silurian/Early Devonian seawater.

Sulphate reduction is the only likely explanation for several sulphate samples that are conspicuously enriched in ^{34}S, mostly from the Trenton and Black River groups. Besides these very ^{34}S-enriched samples, there is some indication that minor DSR may operate on a more widespread basis in the deep subsurface, judging from the overall positive relationship between $\delta^{34}S_{SO4}$ and $\delta^{18}O_{SO4}$ in Figure 5.29, and by the presence of low levels (0.7 ± 0.4 mg/L) of H_2S in all brine samples.

Some Silurian samples also have higher $\delta^{34}S_{SO4}$ and $\delta^{18}O_{SO4}$ values than the majority of samples, which may be influenced by mixing with shallow waters, which generally have more enriched compositions. This is supported by several of these samples having relatively high sulphate concentrations and low $\delta^{18}O_{H2O}$ values. Such mixing could either be natural, by cross-formational flow or intraformational mixing at the brine transition zone, or may be anthropogenic, by deliberate injection or through faulty well casings.

5.2.2.3   Strontium isotopes

The strontium isotopic compositions ($^{87}Sr/^{86}Sr$) and concentrations of the deep brines show considerable variability, with the various formations plotting within fairly unique albeit overlapping ranges (Figure 5.31). Variations in seawater $^{87}Sr/^{86}Sr$ can partially explain the differences in their compositions, although other processes are also likely involved. In general, the brines have higher $^{87}Sr/^{86}Sr$ ratios than the shallow waters. The $^{87}Sr/^{86}Sr$ results obtained in this study are largely comparable to those of Dollar et al. (1991), with the exception of samples from the Trenton and Black River groups.
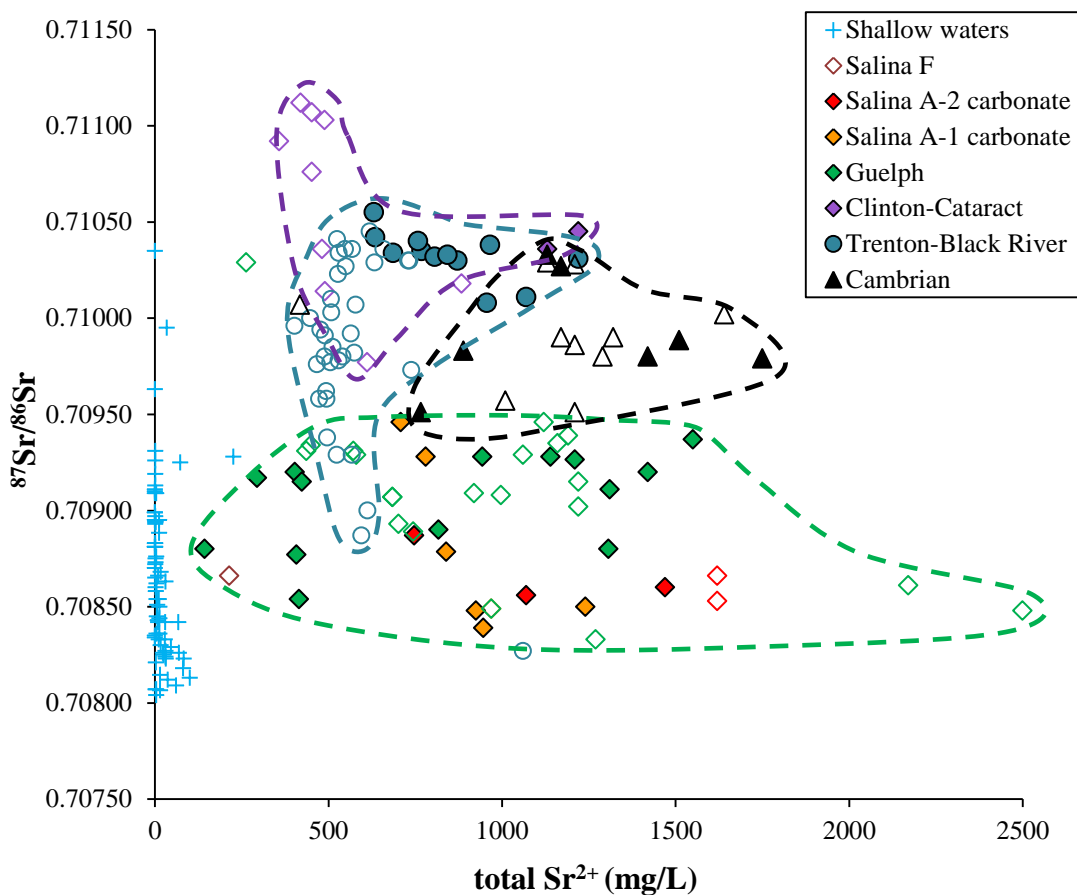
Figure 5.31: Plot of ^{87}Sr/^{86}Sr vs. Sr^{2+} concentrations for deep brines from this study (solid symbols) and Dollar et al. (1991) (open symbols), in comparison to the shallow waters (see Section 5.2.1.3). Different compositional ranges of the various formation waters are outlined; outline colours correspond to symbol colour.

Figure 5.32 compares the ^{87}Sr/^{86}Sr ratios of brines from the various deep formations with the seawater ^{87}Sr/^{86}Sr curve (Veizer et al., 1999) and local reservoir rock compositions. Seawater ^{87}Sr/^{86}Sr varied from about 0.7077 – 0.7097 from the Cambrian to Silurian, with several oscillations during that time. With a few exceptions, the majority of the brines have higher ^{87}Sr/^{86}Sr ratios than seawater of the same age as their reservoir rocks.

The brine ^{87}Sr/^{86}Sr ratios are also commonly higher than those of the rocks hosting the brines. For Guelph Formation dolomites, Coniglio et al. (2003) reported a ^{87}Sr/^{86}Sr range of 0.70854 – 0.70910. Haeri-Ardakani et al. (2013) measured ^{87}Sr/^{86}Sr between 0.70800 – 0.70877 for the most common dolomite fabric types and Zheng (1999) reported similar

ratios of 0.70845 – 0.70877; less abundant dolomite types had higher ratios, up to 0.70925. For the Trenton Group, Haeri-Ardakani et al. (2013) reported matrix dolomite $^{87}Sr/^{86}Sr$ ratios of 0.70830 – 0.70918, while McNutt et al. (1987) reported ratios 0.70838 – 0.70889, with the exception of two samples above 0.7100. For the Cambrian units, significantly higher $^{87}Sr/^{86}Sr$ ratios (0.73302) were noted for arkose rocks, although late-diagenetic calcite had a ratio of 0.70964, within the range of the brine compositions (McNutt et al., 1987).
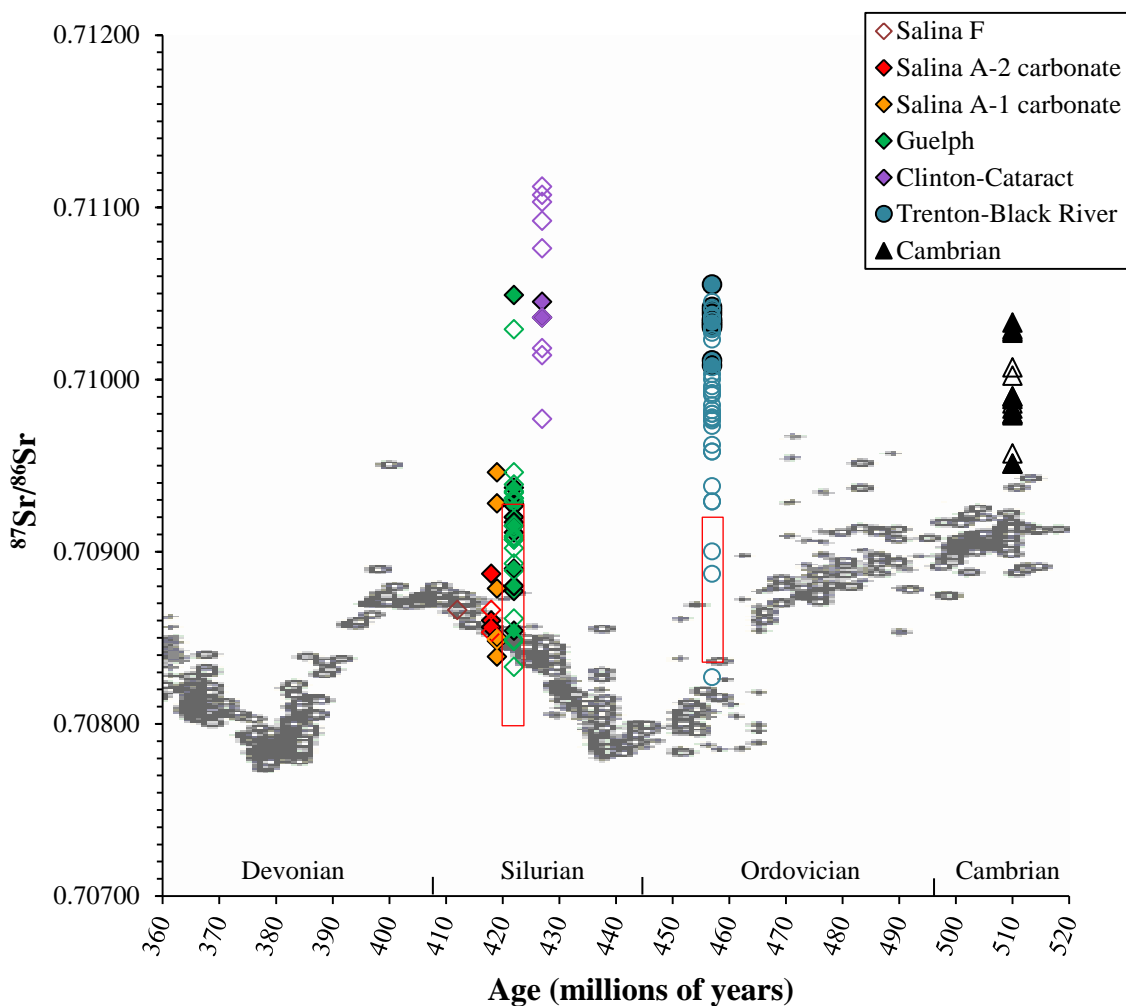
Figure 5.32: $^{87}Sr/^{86}Sr$ ratios of brines (solid symbols = this study; open symbols = Dollar et al., 1991), reservoir rocks (boxes; references in text), and Paleozoic seawater (Veizer et al., 1999).

If the deep formation brines are assumed to be of the same age as their reservoir rocks, almost all have $^{87}Sr/^{86}Sr$ ratios higher than that of seawater during the time the sediments were deposited. The brines also mostly have $^{87}Sr/^{86}Sr$ ratios higher than their reservoir rocks, indicating that either the rocks were formed/dolomitized in contact with different fluids, or that the $^{87}Sr/^{86}Sr$ compositions of the fluids have evolved since then. Thus, if the brines were formed from seawater coeval with their reservoir rocks, the brines' higher $^{87}Sr/^{86}Sr$ ratios require some radiogenic ^{87}Sr input from phases such as clays or feldspars. This radiogenic strontium could either have been produced *in situ*, or have migrated into the reservoirs via diffusion or advection.

Alternatively, if brines are not coeval with the formations, some samples could be explained by migration of seawater of a different age, when seawater $^{87}Sr/^{86}Sr$ was higher. However, this seems unlikely given the apparent isolation of the different units. It is also unlikely that no exchange of radiogenic Sr^{2+} has occurred between rock and water, and indeed many brines have considerably higher $^{87}Sr/^{86}Sr$ ratios than recorded seawater values at any point in geologic time (Veizer et al., 1999; Shields and Veizer, 2002).

While the masking effect of rock-water interaction prevents conclusive determination of whether or not the brines are the same age as their reservoirs, there is some evidence to suggest they are. First, the lowest $^{87}Sr/^{86}Sr$ ratios for brines of several units are near the average compositions of coeval seawater. Second, the extent of ^{87}Sr-enrichment relative to seawater appears to be proportional to the degree of rock-water interaction expected based on unit lithology. For instance, while all units contain some siliciclastic material, the Salina Group and Guelph Formation consist largely of evaporites and carbonates, and appear to have undergone less ^{87}Sr enrichment than the Clinton and Cataract groups, which contain thick shale sequences, representing a major source of radiogenic Sr.

Mixing between brines and shallow meteoric water would not significantly alter the brine's $^{87}Sr/^{86}Sr$ composition, although it would lower its Sr^{2+} concentration. In particular, the Salina Group and Guelph Formation show a wide range of Sr^{2+} concentrations that could be attributed to dilution, although this variation may also in part reflect differing degrees of dissolution of, and/or Sr^{2+} exchange with, the reservoir rocks.

5.2.2.4 Carbon isotopes of DIC

All deep brines have much lower concentrations of bicarbonate than the shallow waters
(11 ± 19 mg/L vs. 267 ± 122 mg/L), likely because of the lower pH of the deep waters
and their high concentrations of Ca^{2+}, the latter of which could drive carbonate
precipitation. The brine $\delta^{13}C_{DIC}$ values span a range of ~20‰ (less variable than the
shallow waters), and tend towards ^{13}C-enriched compositions (Figure 5.33).
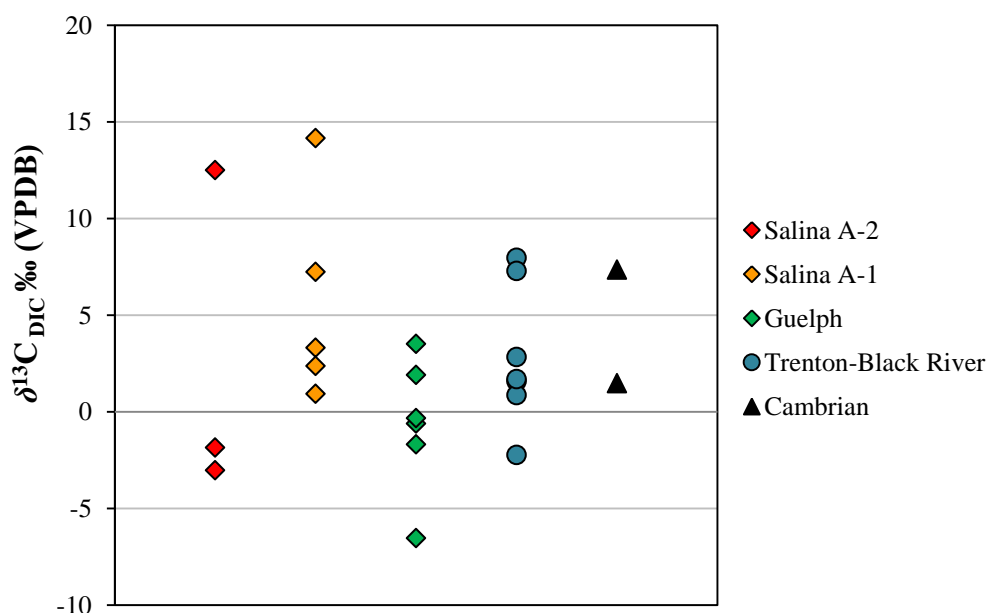
Figure 5.33: The $\delta^{13}C_{DIC}$ values of the deep brines collected in this study.

Haeri-Ardakani et al. (2013) reported rock δ^{13}C values between –0.2 and +5.9‰ for
dolomite from the Guelph Formation, and between –1.0 and +1.4‰ for the Trenton
Group. Several brine samples have similar $\delta^{13}C_{DIC}$ values, indicating that dissolution of
the host rocks, may be an important control on their DIC isotopic compositions.

A few samples have $\delta^{13}C_{DIC}$ values several permil lower than any host rock compositions
(–6.5 to –1.7‰). These negative values could indicate: (1) decomposition of organic
matter within the reservoir; (2) mixing with shallow waters carrying organic matter-
derived DIC; (3) microbial hydrocarbon oxidation; (4) sulphate reduction; and/or (5)
reaction with unusually low-δ^{13}C carbonates.

CO_2 generated by *in situ* aerobic decay of organic matter is likely to be of negligible importance relative to shallow depths, given the anoxic conditions typically present in such deep environments; oxygen may however be introduced via boreholes, permitting localized aerobic activity. Thermal decarboxylation of organic matter is likely of greater influence, and is known to produce CO_2 with $\delta^{13}C$ between -25 and -10‰ (Irwin et al., 1977). Mixing with shallow water is another possibility, and even a small shallow component could significantly affect the brine $\delta^{13}C_{DIC}$ values, given the higher DIC concentrations in the former. This scenario is supported by low $\delta^{18}O$, $\delta^{2}H$ and TDS and high DIC concentrations in the most ^{13}C-depleted sample. DIC may also have been produced by methane oxidation, which can use either oxygen or sulphate as an electron acceptor, and produces CO_2 that is considerably ^{13}C-depleted (by up to ~30‰; Barker and Fritz, 1981) relative to the residual methane. Methane $\delta^{13}C$ values in these reservoirs range between ~ -55 and -35‰ (Barker and Pollack, 1984; J. Potter, unpublished data), and thus CO_2 produced by methane oxidation would have very low $\delta^{13}C$ values. Similarly, ^{13}C-depleted DIC (~ -33 to -20‰) can be produced by bacterial degradation of petroleum (Bailey et al., 1973). Sulphate reduction also produces very negative $\delta^{13}C$ values, depending on the source of organic matter oxidized in the reaction (see Section 5.2.1.3). Coniglio and Williams-Jones (1992) and Zheng (1999) have also reported very low $\delta^{13}C$ values (≥ -31.8‰) in late-stage calcite cement throughout the Paleozoic succession of southwestern Ontario. Such calcites likely formed from processes such as described above, and their dissolution could also yield low $\delta^{13}C_{DIC}$ values. Since all of these processes produce more ^{13}C-depleted DIC than observed in the brines, they are likely of relatively small importance and must be coupled with a ^{13}C-enriching process.

Most brine samples contain DIC that is enriched in ^{13}C, with $\delta^{13}C_{DIC}$ commonly being higher than their host carbonate rocks. This enrichment may be a product of microbial methanogenesis, which, as discussed in Section 5.2.1.4, produces CO_2 that is significantly ^{13}C-enriched relative to the co-produced methane (Whiticar, 1999). However, most methane in these formations appears to be of thermogenic in origin (Barker and Pollack, 1984; J. Potter, unpublished data), and thermogenic methanogenesis does not produce much CO_2. Nonetheless, some microbial gas has been identified in some reservoirs (J. Potter, unpublished data), and may be more widespread than commonly believed,

although of lesser importance to thermogenic methane. If the most positive brine $\delta^{13}C_{DIC}$ value observed (~ +15‰) can be assumed to represent methanogenic CO_2 unmodified by mixing and other processes, maximum CO_2-CH_4 fractionations in the study area between 50-70‰ can be determined based on the aforementioned range for regional methane $\delta^{13}C$ (–55 to –35‰), relatively consistent with acetotrophic methanogenesis ($\Delta_{CO2\text{-}CH4} \approx$ 40-60‰, Whiticar, 1999). Alternatively, Stiller et al. (1985) found that extreme ^{13}C enrichments (up to +35‰) could be produced during seawater evaporation. If the brines were indeed thusly formed, and DIC was preserved in the system from the time of brine formation, the ^{13}C enrichment could also reflect such a process.

5.2.2.5 *Major ion geochemistry*

The high solute concentrations present in brines can be generated by several mechanisms. The main processes controlling the ion geochemistry of brines include: (1) evaporation of seawater, (2) mixing with meteoric water or other brines, (3) dissolution of halite and other evaporite minerals, (4) dolomitization, (5) carbonate precipitation or dissolution, (6) sulphate reduction, and/or (7) formation or alteration of aluminosilicate minerals (Carpenter, 1978). The relationships among various ions can help elucidate the relative importance of these different reactions.

The Paleozoic sedimentary rocks comprising the bedrock in southwestern Ontario were deposited predominantly in shallow inland seas, and thus the brines found in the deep formations could be of marine origin (paleoseawater), modified by evaporation and diagenetic reactions. While consistent with the isotopic data, this hypothesis can also be investigated through ion chemistry, as the behaviour of major ions in seawater is well understood (Carpenter, 1978; Kharaka et al., 1987; McCaffrey et al., 1987).

In order to evaluate the origins and evolution of brines, the concentrations of major ions (e.g., Na^+, Ca^{2+}, Mg^{2+}, K^+, Sr^{2+}, Cl^- and SO_4^{2-}) are commonly compared to bromine concentrations (Carpenter, 1978; Rittenhouse, 1967; Hanor, 1994; Kharaka et al., 1987; Shouakar-Stash, 2008). Br^- is an ideal conservative ion, as mineral phases generally do not contain appreciable amounts of Br^-; even at very high ionic strengths, it remains

partitioned predominantly into the solution (Zherebtsova and Volkova, 1966). Figure 5.34 illustrates the evolution of the major ions relative to Br⁻ during seawater evaporation.
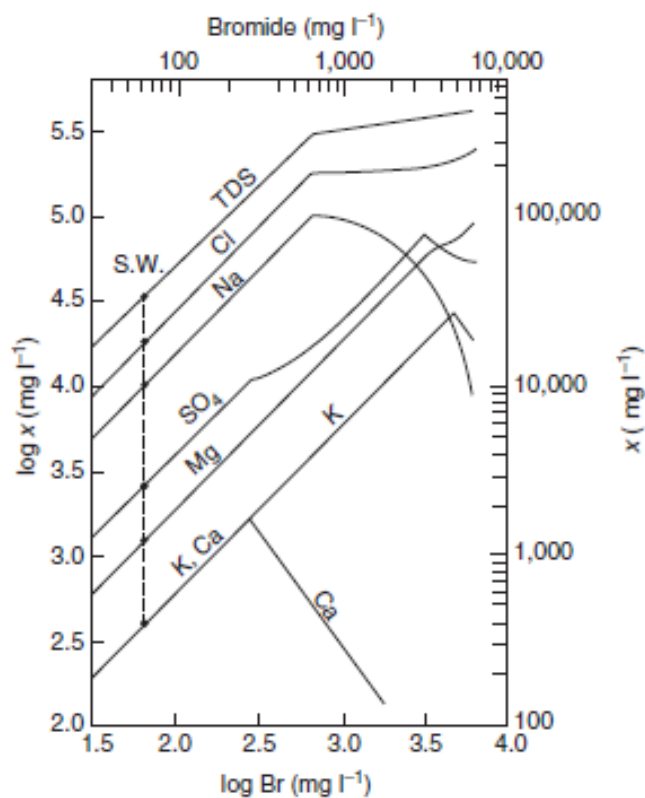
Figure 5.34: Concentration trends of major seawater constituents vs. Br⁻ during evaporation (Carpenter, 1978).

A plot of Cl⁻ vs. Br⁻ concentrations is a very useful tool for investigating the origin and evolution of brines, as chloride is also relatively conservative, being only involved in reactions with halite (Carpenter, 1978; Hobbs et al., 2011). Figure 3.35 illustrates the Cl⁻ vs. Br⁻ relationships for the deep formation waters examined here and by Dollar et al. (1991). Also shown are the initial precipitation points for evaporite minerals (Matray, 1988), various mixing scenarios between end-members, and halite dissolution, as examined by several previous researchers (e.g., Rittenhouse, 1967; Carpenter, 1978; Kharaka and Hanor, 2007; Shouakar-Stash, 2008).
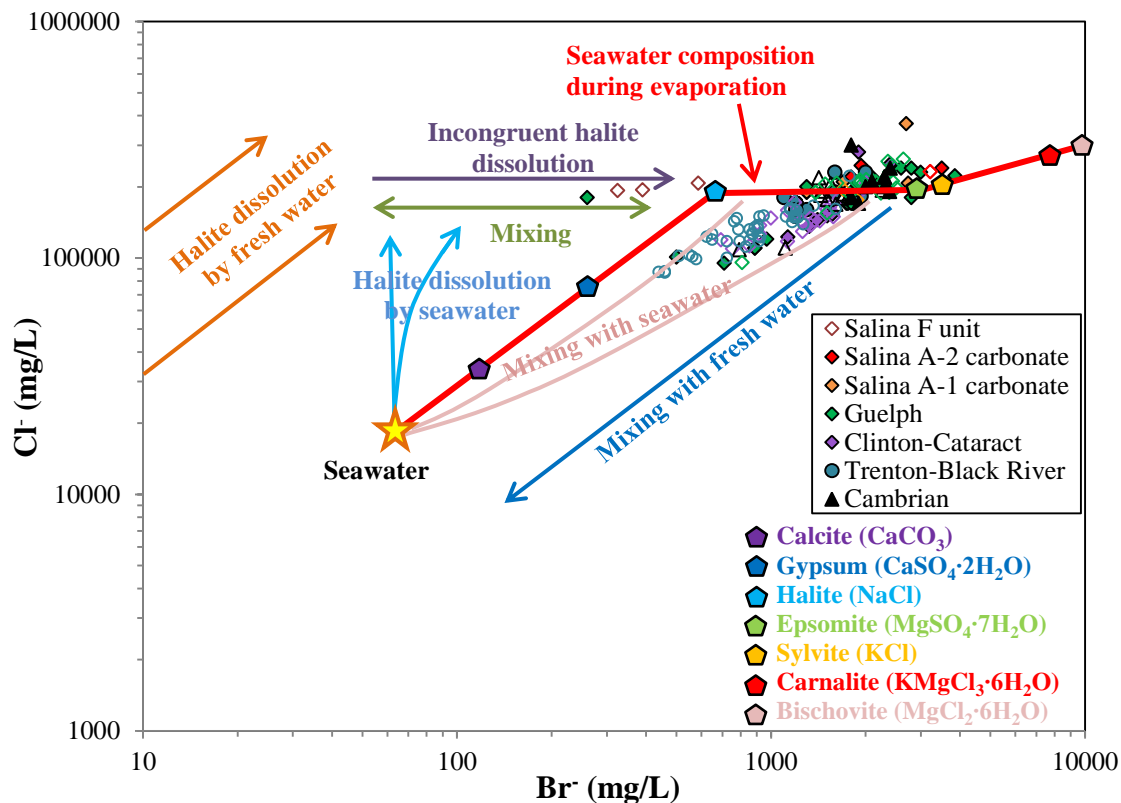
Figure 5.35: Logarithmic plot of Cl⁻ vs. Br⁻ concentrations for the brines in this study (solid symbols) and Dollar et al. (1991) (hollow symbols), compared with the seawater evaporation trend (McCaffrey et al., 1987) initial precipitation points for evaporite minerals (Matray, 1988), and some possible mixing scenarios (references in text). Modified from Shouakar-Stash (2008).

Most brine samples have relatively similar Cl⁻ and Br⁻ compositions, plotting near the seawater trend between halite and sylvite precipitation, strong evidence that they are related to extensively evaporated seawater. This is consistent with the presence of halite in many units, and sylvite towards the center of the Michigan basin (Cercone, 1988). As the halite facies corresponds to a seawater concentration of 11-65x (Knauth and Beeunas, 1986), this is consistent with the position of many samples near the 45x point along the δ^2H/δ^{18}O evolution curve in Figure 5.28. Many brine samples also plot below the seawater evaporation line in Figure 5.35, indicating some dilution by either meteoric water or less evaporated seawater. Their proximity to the seawater trend suggests that the brines are largely composed of the evaporated seawater end-member, although the exact mixture proportions for a given brine cannot be determined due to the different mixing scenarios and modifying processes possible (Carpenter, 1978).

Halite dissolution is likely responsible for some of the scatter in the data in Figure 5.35, although the extent of dissolution is similarly difficult to assess. A number of samples above the seawater evaporation trend, and a few to the left of it, were almost certainly influenced by halite dissolution. The latter samples formed either by mixing between brines and dilute waters that congruently dissolved halite, or by both congruent and incongruent halite dissolution by dilute waters; during incongruent halite dissolution, the fluid dissolves then reprecipitates halite, accumulating Br^- in the process (Land and Prezbindowski, 1981; Stoessell and Carpenter, 1986). No samples are consistent with congruent halite dissolution by dilute waters alone, as would yield very high Cl/Br ratios.

The other major ions differ considerably from their expected concentrations based solely on seawater evaporation and dilution, as illustrated in Figures 5.36-5.41. These variations are consistent with dissolution, precipitation, and diagenetic reactions expected based on reservoir lithologies. Generally speaking, the ion chemistry of the Ontario brines show features similar to brines in other basins, such as enrichment in Ca^{2+} and Sr^{2+} and depletion of Mg^{2+}, K^+, and sulphate relative to seawater (Kharaka and Hanor, 2007).

Calcium concentrations in these brines are much higher than in evaporated seawater, in which Ca^{2+} largely removed by gypsum precipitation (Figure 5.36). Based on the large volumes of carbonates in the Ontario strata, the Ca^{2+} enrichment is expected to be due primarily to dolomitization of limestone (Equation 5.9; Carpenter, 1978):

$$2CaCO_3 + Mg^{2+} \rightarrow CaMg(CO_3)_2 + Ca^{2+} \tag{5.9}$$
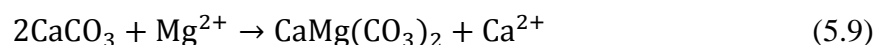
Calculations by Hobbs et al. (2011) indicate that while dolomitization was of principal importance, it could not fully explain the Ca^{2+} enrichments in the region, and thus other reactions must be involved. Albitization of plagioclase feldspar, particularly in the more siliciclastic units, is likely one such process (Equation 5.10; Kharaka and Hanor, 2007):

$$Na_{0.7}Ca_{0.3}Al_{1.3}Si_{2.7}O_8 + 0.6Na^+ + 1.2SiO_2 \rightarrow 1.3NaAlSi_3O_8 + 0.3Ca^{2+} \tag{5.10}$$
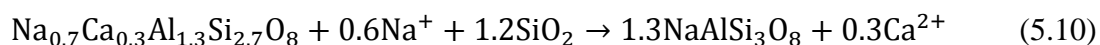
Dissolution of minerals such as calcite, dolomite, anhydrite, and calcium aluminosilicates is likely also responsible for some of the Ca^{2+} enrichment.

Samples with higher Ca^{2+} concentrations show little relation to Br^-, reflecting variations in the extent of the diagenetic reactions producing the Ca^{2+} enrichment. However, several brines with lower Ca^{2+} concentrations, such as those of the Clinton, Cataract, Trenton and Black River groups, show linear trends toward the origin which likely reflect mixing with more dilute waters; similar trends are also observed for these samples in the plots of other ions vs. Br^-. That these trends do not seem to be much obscured by subsequent diagenetic reactions suggests the dilution was likely relatively recent.

Although not shown here, Ca^{2+} and Sr^{2+} show very similar relationships to Br^-, reflecting the fact that Sr^{2+} readily substitutes for Ca^{2+} in many mineral structures, and thus is affected by the same geochemical processes.
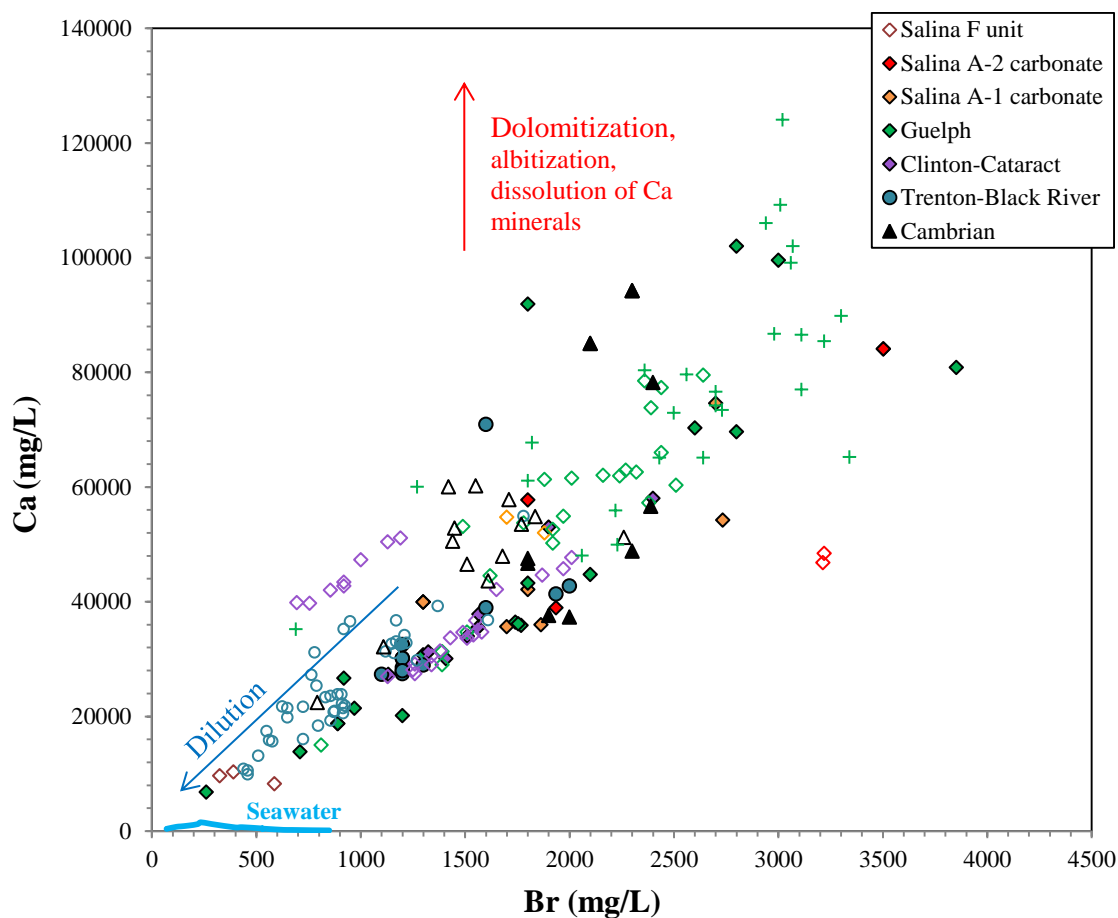
Figure 5.36: Plot of Ca^{2+} vs. Br^- concentrations for the brines in southwestern Ontario and Michigan (solid symbols: this study; hollow symbols: Dollar et al., 1991; crosses: Wilson and Long, 1993b). Evaporated seawater trend is from McCaffrey et al. (1987).

Like chloride, the concentration of sodium in brine is largely controlled by the extent of evaporation, and dissolution/precipitation of halite. As mentioned above, its concentration is also reduced by albitization of plagioclase. Albite can also be formed by alteration of clay minerals such as kaolinite (Equation 17; Carpenter, 1978); both albite and kaolinite have been reported in Silurian units in southwestern Ontario (Miles et al., 1986).

$$2Na^+ + Al_2Si_2O_5(OH)_4 + 4SiO_2 \rightarrow 2NaAlSi_3O_8 + H_2O + 2H^+ \qquad (17)$$
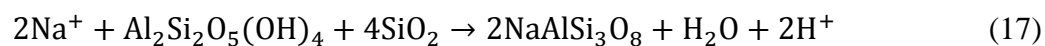
Most samples plot below the Na^+ seawater evaporation trend (Figure 5.37), which may be due to the formation of halite or albite. Linear trends within certain units suggest that dilution is likely also partially responsible for this depletion, although differences in their trajectories may indicate different diluting end-members are involved. Several samples plotting above the seawater trend are consistent with halite dissolution or alteration of albite into less Na^+-rich minerals, such as potassium feldspar (Carpenter, 1978).
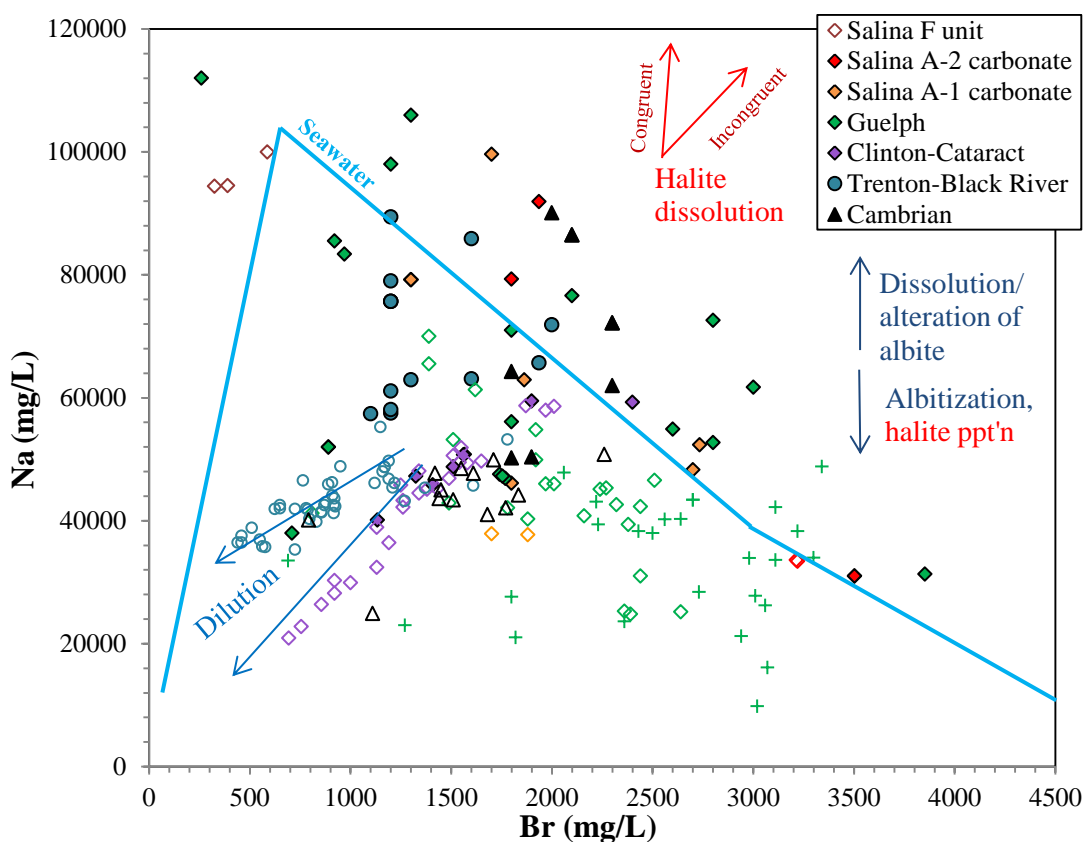
Figure 5.37: Plot of Na^+ vs. Br^- concentrations for the brines in southwestern Ontario and Michigan (solid symbols: this study; hollow symbols: Dollar et al., 1991; crosses: Wilson and Long, 1993b). Evaporated seawater trend is from McCaffrey et al. (1987).

Magnesium concentrations are considerably lower than the evaporated seawater trend (Figure 5.38). As discussed above, most of this depletion is likely due to dolomitization, although other reactions, such as formation of chlorite and ankerite may have also contributed. Ankeritization becomes particularly important at temperatures above 120°C (Hower et al., 1976; Boles, 1978); fluid inclusion data by Haeri-Ardakani et al. (2013) suggest that such temperatures existed in the region in the past. Ankerite and diagenetic chlorite have also been reported in some Ontario strata (Ziegler and Longstaffe, 2000; Sharma and Dix, 2004).
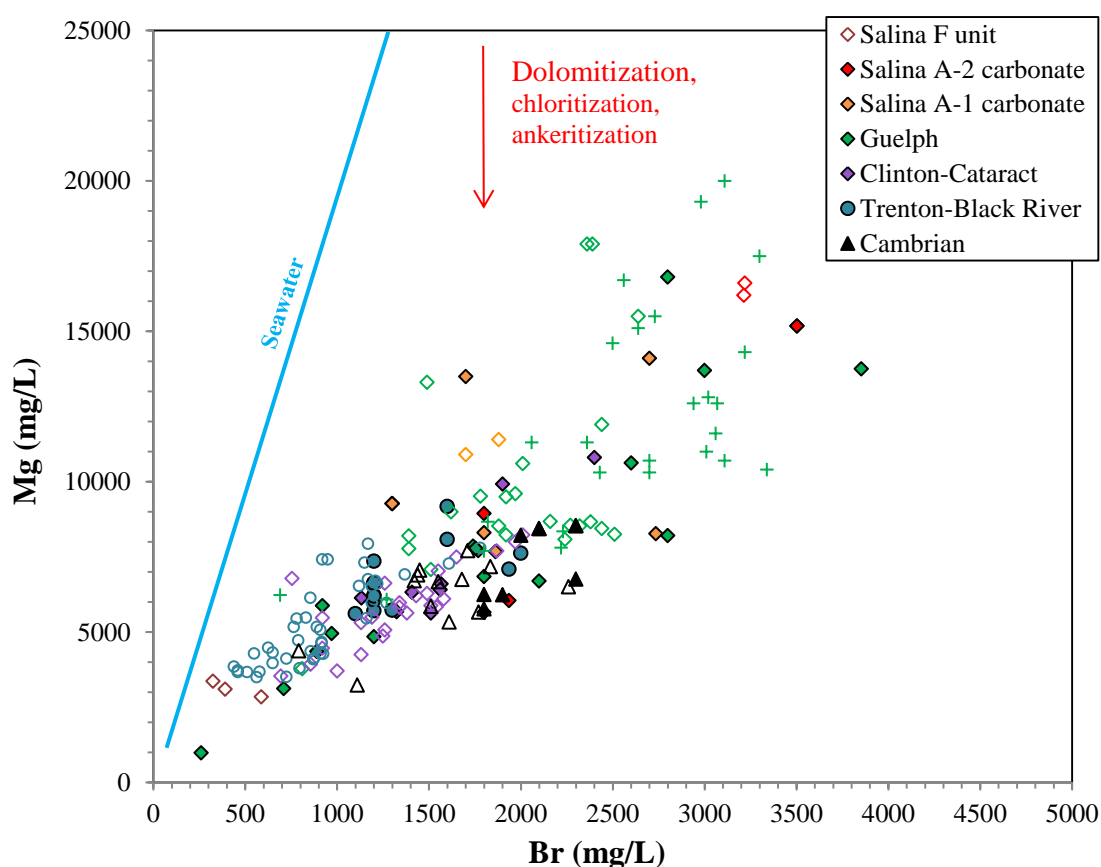
Figure 5.38: Plot of Mg^{2+} vs. Br^- concentrations for the brines in southwestern Ontario and Michigan (solid symbols: this study; hollow symbols: Dollar et al., 1991; crosses: Wilson and Long, 1993b). Evaporated seawater trend is from McCaffrey et al. (1987).

Potassium concentrations in the brines are also depleted relative to seawater, with the exception of several samples reported by Wilson and Long (1993), for which the

enrichment mechanism is not clear (Figure 5.39). Loss of K^+ from the brine likely reflects precipitation of authigenic illite, or transformation of low-K^+ clays such as kaolinite or smectite to illite (Carpenter et al., 1974; Kharaka et al., 1987); the sedimentary units in southwestern Ontario and the adjacent basins are rich in illite and illite-smectite (Elliott and Aronson, 1987). Formation of potassium feldspar, for instance by alteration of albite or clays, is also commonly cited as a K^+-depleting mechanism in brines (Carpenter, 1978; Egeberg and Aagaard, 1989), although feldspars are relatively sparse in the region, with the exception of the Cambrian units. Carpenter (1978) also notes that formation of K^+-rich clays and feldspars can release substantial amounts of H^+, and such diagenetic reactions may be in part responsible for the relatively low pH of the deep brines.
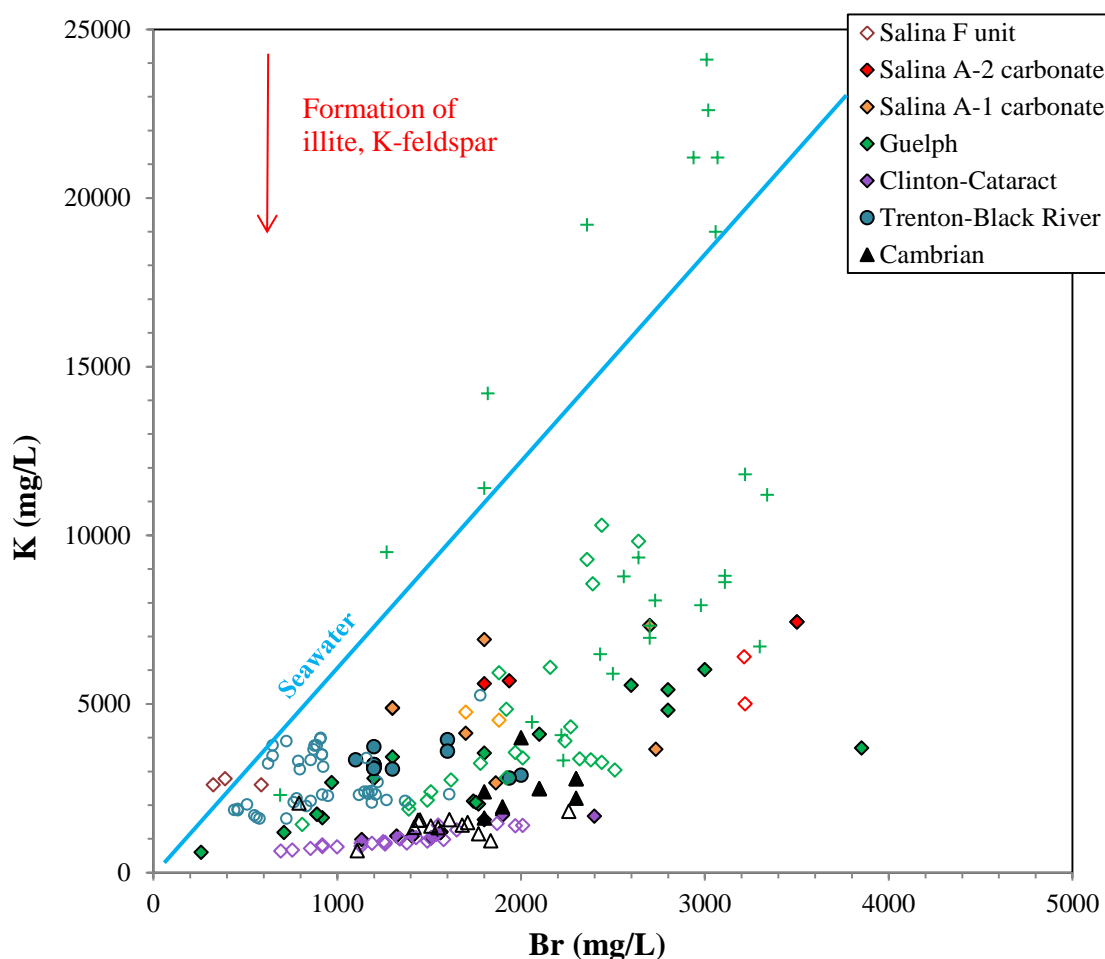
Figure 5.39: Plot of K^+ vs. Br^- concentrations for the brines in southwestern Ontario and Michigan (solid symbols: this study; hollow symbols: Dollar et al., 1991; crosses: Wilson and Long, 1993b). Evaporated seawater trend is from McCaffrey et al. (1987).

Sulphate is also at very low concentrations in the brines relative to seawater (Figure 5.40; seawater values [>2,700 mg/L] are off-scale). Wilson and Long (1993b) suggested that this depletion was partially due to bacterial sulphate reduction, but based on sulphate isotopes (see Section 5.2.2.2), this is likely only important for several samples from the Trenton and Black River groups. Alternatively, thermochemical sulphate reduction (TSR) may have operated in the past under high temperature regimes (<143°C, Haeri-Ardakani et al., 2013); unlike bacterial sulphate reduction, TSR typically produces sulphide of similar isotopic composition to the parent sulphate, and so would be less evident by isotopic means (Machel, 2001). Another major sink for sulphate is likely precipitation of gypsum or anhydrite, driven by the high calcium concentrations. The samples also show an inverse relationship between SO_4^{2-} and Br^-, which may either reflect a greater degree of sulphate precipitation as seawater evaporation increases, or more likely, mixing with relatively sulphate-rich meteoric water and/or dissolution of sulphate minerals thereby.
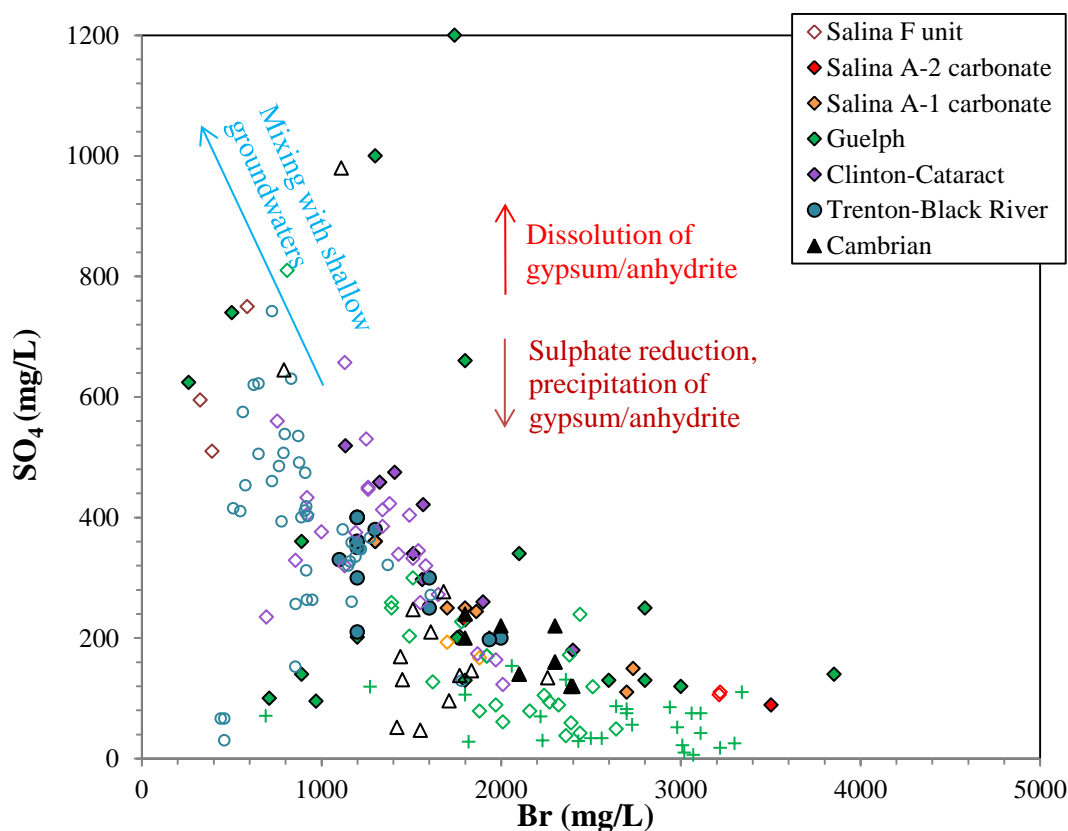
Figure 5.40: Plot of SO_4^{2-} vs. Br^- concentrations for the brines in southwestern Ontario and Michigan (solid symbols: this study; hollow symbols: Dollar et al., 1991; crosses: Wilson and Long, 1993b).

Carpenter (1978) defined a function, denoted as MCl_2, which represents the amount of divalent ions that are electrically balanced by chloride (Equation 18):

$$MCl_2 = Ca^{2+} + Mg^{2+} + Sr^{2+} - SO_4^{2-} - HCO_3^- \text{ meq/L} \qquad (18)$$

MCl_2 is a conservative value during seawater evaporation, being unaffected by precipitation or dissolution of calcite, dolomite, gypsum, anhydrite, halite, or sulphate reduction. During seawater evaporation, $logMCl_2$ has an essentially 1:1 relation to $logBr^-$ (Figure 5.41). All brine samples from the study area plot above this line, indicating enrichment in MCl_2 and/or depletion of Br relative to seawater. The former is the more likely case, and can be explained by diagenetic reactions such as formation of potassium aluminosilicates or albitization of plagioclase (Carpenter, 1978).
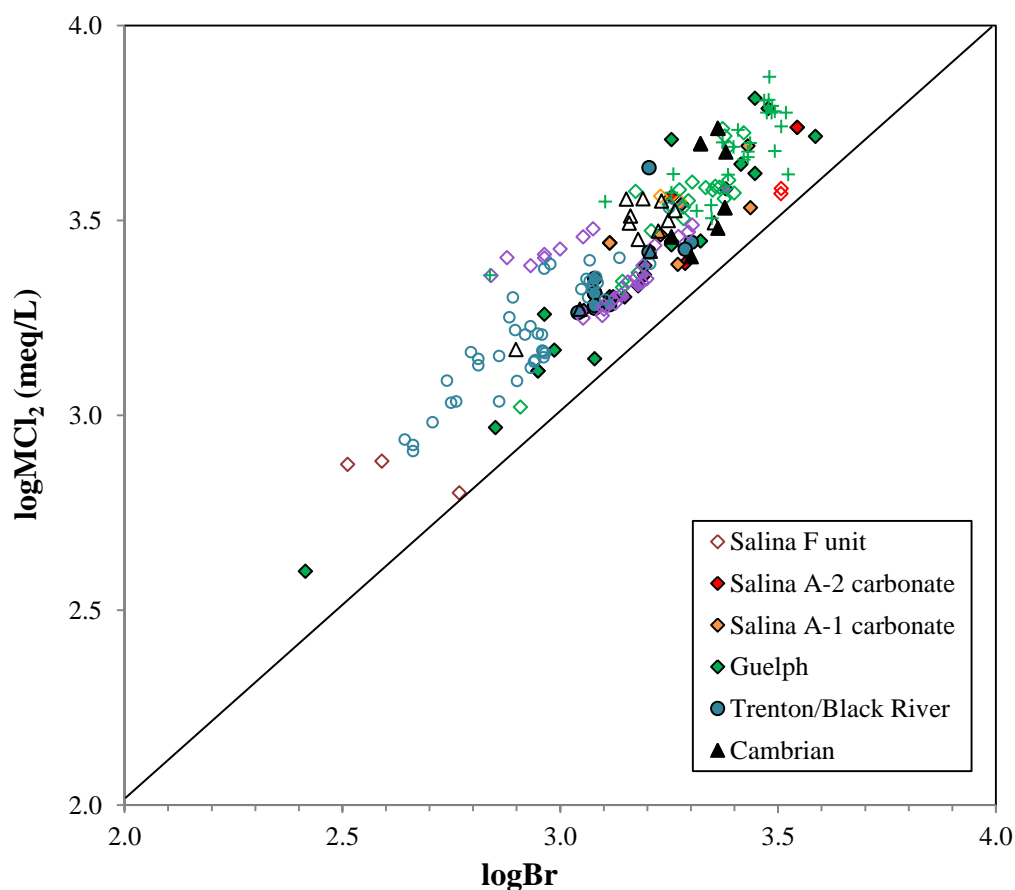
Figure 5.41: Plot of $logMCl_2$ (Carpenter, 1978) vs. logBr for the brines in southwestern Ontario and Michigan. The solid line represents expected values for seawater and evaporated seawater. Solid symbols are from this study, hollow symbols are from Dollar et al. (1991) and crosses are from Wilson and Long (1993b).

5.2.2.6　　　　　*Guelph Formation and Salina Group*

The Upper/Middle Silurian Guelph and Salina carbonates contain the main brine aquifer in the region. Figure 5.42 provides a detailed look at the $\delta^2H/\delta^{18}O$ systematics for these brines. Several samples plot near the 45x seawater concentration point of Knauth and Beeunas (1986), although the majority of samples have lower δ^2H values, which may indicate that evaporation had progressed even further. The samples have a relatively small range of δ^2H values compared to $\delta^{18}O$, which likely indicates that their $\delta^{18}O$ compositions have been significantly influenced by rock-water interaction, as described below.
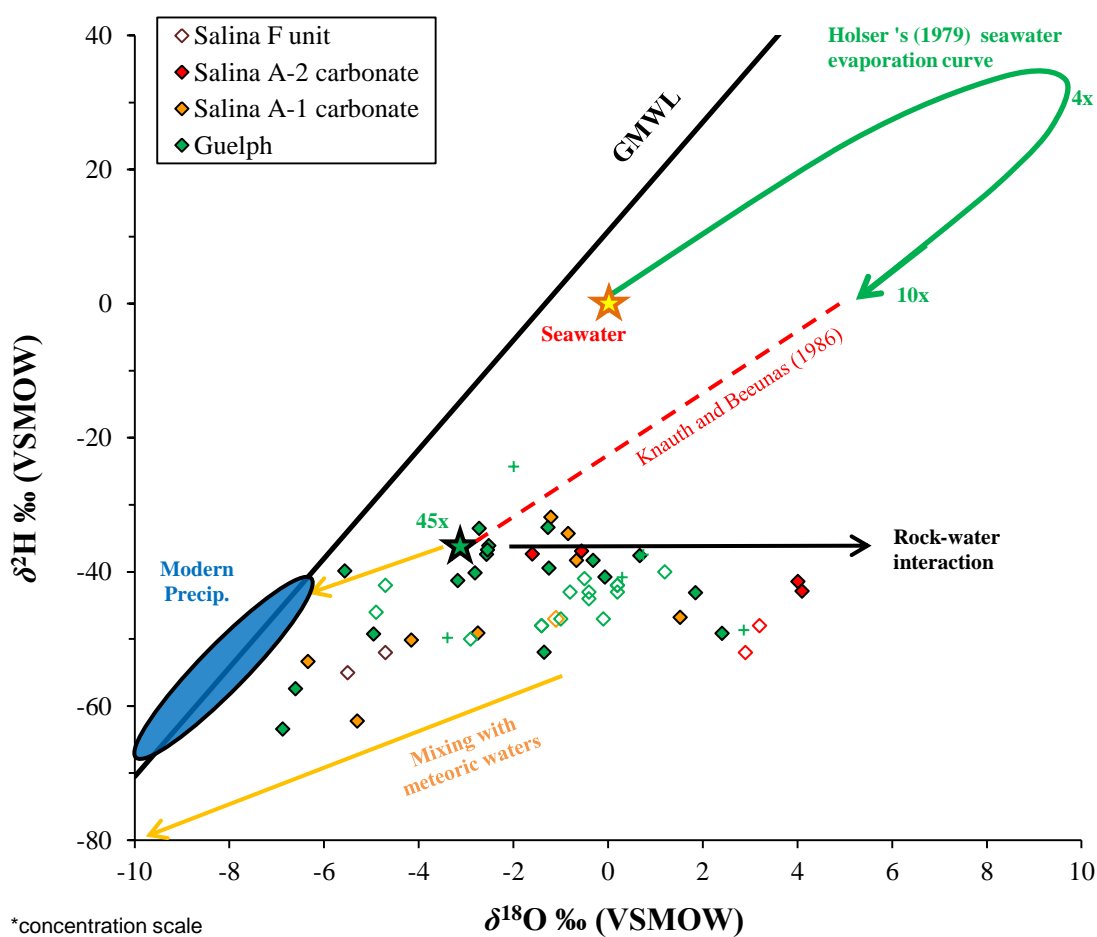
Figure 5.42: Plot of δ^2H vs. $\delta^{18}O$ for the Salina Group and Guelph Formation brines, compared with various end-members and processes likely affecting their evolution. The seawater evaporation curve is from Holser (1979) and its extension by Knauth and Beeunas (1986) to 45x concentration. Solid symbols are from this study, hollow symbols are from Dollar et al. (1991) and crosses are from Wilson and Long (1993b).

Haeri-Ardakani et al. (2013) reported δ^{18}O values for Ontario Guelph Formation matrix dolomite from –8.1 to –4.1‰ VPDB (+22.6 to +26.7‰ VSMOW). At current reservoir temperatures (~23-28°C; T. Carter, personal communication, 2014), fluids in equilibrium with these dolomites would have δ^{18}O values of –10.6 to –5.3‰ (calculated using the equation of Land, 1985: $1000\ln\alpha_{dolomite-water} = 3.2 \times 10^6 T^{-2} - 3.3$), significantly lower than the compositions of the present brines, indicating that they are out of equilibrium under current conditions. Fluid inclusion microthermometry data suggest that these rocks were dolomitized under much hotter conditions than present ($T_h = 104 \pm 19$°C; Haeri-Ardakani et al., 2013), corresponding to fluids with δ^{18}O values generally higher (+0.5 to +9.7‰) than the current brines. Such temperatures suggest that these brines were hydrothermal fluids that migrated from deeper in the Michigan Basin; Barnes et al. (2008) showed that temperatures were even higher (140-170°C) in the central part of the basin, and cooling of the brines as they moved towards the basin margins could explain the trend of gradual ^{18}O enrichment of dolomite in that direction observed by Coniglio et al. (2003). Brines may have also migrated in from the Appalachian Basin, given similarities in lead isotopes between Appalachian sediments and Guelph Formation galenas in the Niagara peninsula (Farquhar et al., 1987). If the current brines are related to these hot, dolomitizing fluids, as is suggested by their elevated Ca^{2+} and depleted Mg^{2+} concentrations (Section 5.2.2.5), they must have since been depleted in ^{18}O. This may have been achieved in part by mixing with meteoric waters with a similar δ^2H composition, similar to the least negative waters found today, although this appears to be of minor influence, as discussed later. More likely, the ^{18}O depletion reflects a trend towards re-equilibration with the reservoir rocks as the brines slowly cooled. Thus, while the original composition of the parent hydrothermal fluids would have likely evolved, deeper in the basin, along a trend such as indicated by the rock-water interaction arrow in Figure 5.42, the more recent trend, under a cooling temperature regime, is in the opposite direction. The equilibrium δ^{18}O values calculated above suggest the brines have not yet achieved equilibrium with the rock, and perhaps never will, due to unfavourable exchange kinetics at low temperatures.

Derivation of the Guelph Formation and Salina Group brines purely through diagenetic modification of recent meteoric waters, as suggested by Clayton et al. (1966), or significant dilution thereby, seems unlikely. While the least negative meteoric waters

observed in the study area have δ^2H values near –40‰, similar to these brines, rock-water interaction under recent conditions could not produce the ^{18}O enrichment that would be required to generate the observed compositions, as explained above. Lack of a meteoric origin for these ^{18}O-enriched brines is further supported by the absence of a significant relationship between TDS and δ^{18}O (Figure 5.43). Nonetheless, several brines show evidence of some dilution by meteoric waters, having lower δ^{18}O and δ^2H values than most other samples (Figure 5.42) and relatively low TDS (Figure 5.43). The dilution trend is less obvious in Figure 5.43 for the Salina Group brines than the Guelph Formation. The three low-δ^{18}O Salina A-1 samples were taken from one pool and unfortunately only one was analysed for ion compositions. The two Salina F unit samples have unusually high Cl/Br ratios, suggesting that addition of fresh water coincided with halite dissolution, raising their TDS values. The dilution trends in Figures 5.42-5.43 are also likely masked by differences in brine and fresh water end-member compositions.
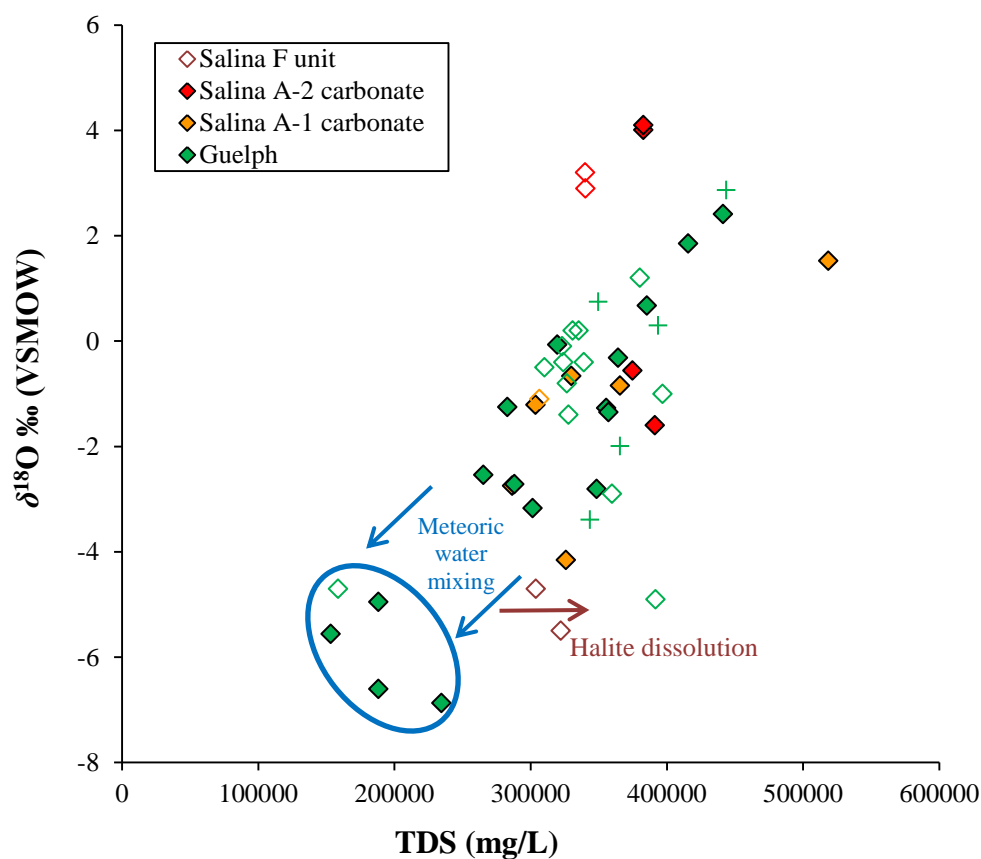
Figure 5.43: Plot of δ^{18}O vs. TDS for the Salina and Guelph brines. Solid symbols = this study, hollow symbols = Dollar et al. (1991), crosses = Wilson and Long (1993b).

Mixing of these samples with meteoric water is unsurprising given that many were taken from pools known to have undergone fresh water injection to enhance production; some of that water evidently still remains in the reservoirs. Thus, this dilution is likely an anthropogenic effect; natural meteoric water mixing would be inhibited by the overlying aquitard layers within the Salina Group, among other factors (see Section 2.1.3.2).

The strontium isotopic compositions of the Guelph Formation and Salina Group brines range from ~ 0.70850 to 0.70935, lower than most of the deep brines, and somewhat higher than most of the shallow waters (Figure 5.31). The brines have ^{87}Sr/^{86}Sr values comparable to or more radiogenic than Silurian seawater and the host carbonates (Figure 5.32). The enrichment in ^{87}Sr above seawater values in many samples is likely from ^{87}Rb decay. As the brines are hosted in carbonate-dominated reservoirs, possible sources of the ^{87}Sr include shale units within the Salina Group or the underlying Clinton Group. Strontium concentrations are also higher than evaporated seawater and are quite variable (143-2500 mg/L); they show no relationship with ^{87}Sr/^{86}Sr. Guelph Formation calcites contain significantly more Sr^{2+} (130-1052 ppm) than dolomites (27-85 ppm) (Coniglio et al., 2003), so most Sr^{2+} in these brines is likely derived from carbonate dissolution or dolomitization, and the variability in Sr^{2+} concentrations reflects different extents thereof.

Figure 5.44 presents a more detailed view of the Cl/Br systematics of the Guelph Formation and Salina Group brines. Also shown are fluid inclusion data from Salina Group halites from the margins of the Michigan basin (Das et al., 1990). Most samples have compositions indicative of seawater evaporated past the halite facies, some almost to the point of epsomite and sylvite precipitation (~4200-4700 mg/L Br⁻; McCaffrey et al., 1987). The brines typically have lower Br⁻ and Cl⁻ concentrations than the halite inclusion fluids. While this may indicate the latter were formed from more evaporated seawater, the fact that the Br⁻ concentrations are past the point of precipitation of minerals typically not found in the area suggests that their Cl⁻ and Br⁻ enrichments are likely due to a greater degree of congruent and incongruent halite dissolution, respectively. Halite dissolution is almost certainly responsible for the compositions of the many brine samples plotting above the seawater trend. Several samples plotting below the seawater curve also reflect dilution, likely by meteoric waters, as per the previous discussion. Congruent halite

dissolution by relatively fresh water can be identified in all three Salina F unit samples and one Guelph Formation sample. Their Br⁻ concentrations are also somewhat higher than might be expected from congruent halite dissolution alone, suggesting that they may have also incongruently dissolved some halite, and/or mixed with more Br⁻-rich brines.
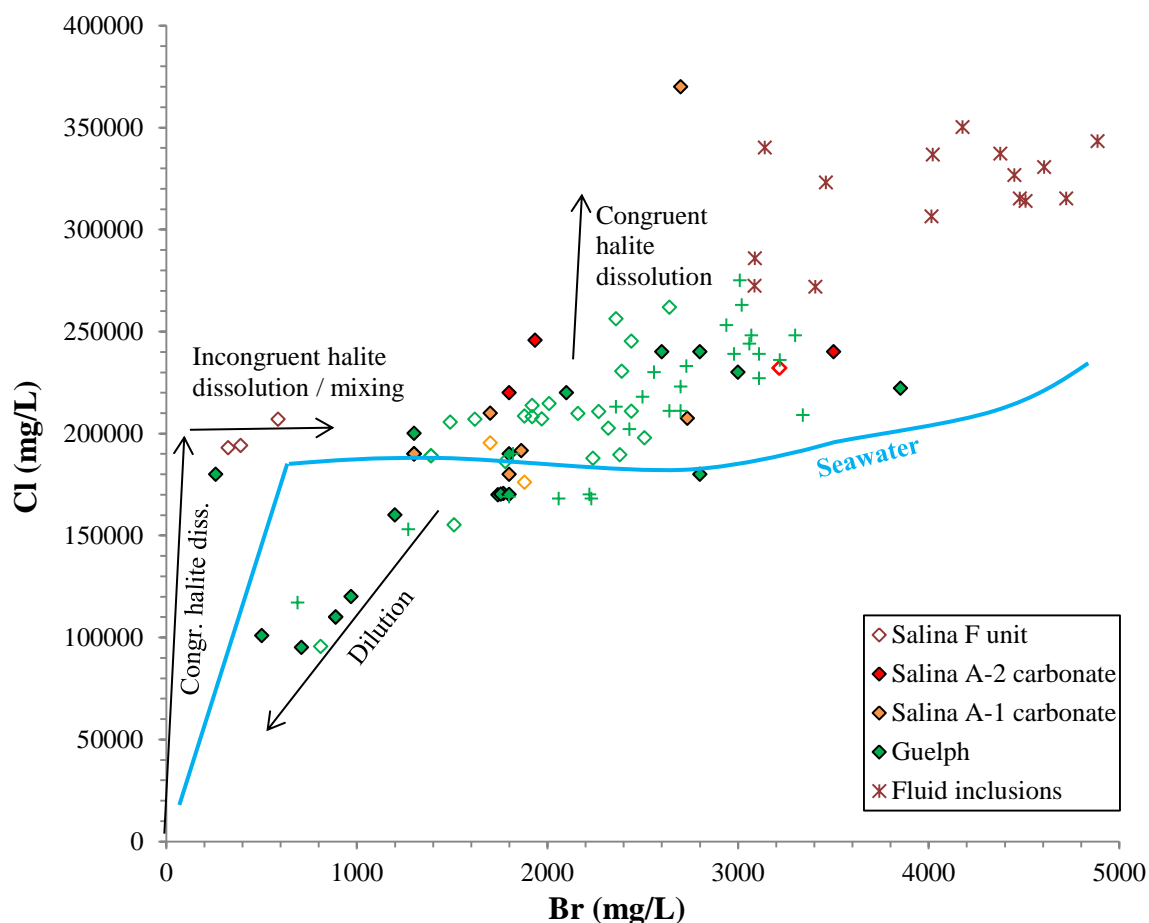
Figure 5.44: Plot of Cl⁻ vs. Br⁻ for the Salina and Guelph brines. The seawater evaporation path (McCaffrey et al., 1987), fluid inclusion data (Das et al., 1990) and likely modifying processes are shown. Solid symbols are from this study, hollow symbols are from Dollar et al. (1991) and crosses are from Wilson and Long (1993b).

The other major ions show considerable scatter when plotted against Br⁻, consistent with extensive and variable modification of evaporated seawater by diagenetic processes, most likely dolomitization, precipitation and dissolution of halite and anhydrite, and possibly some clay or feldspar alteration (see Section 5.2.2.5). Dilution is also expected to be responsible for some of the variability, although clear linear trends are not particularly apparent in these units.

5.2.2.7   *Clinton and Cataract Groups*

The groundwaters from the Lower Silurian Clinton and Cataract groups have δ^{18}O and δ^2H values relatively similar to the Salina Group and Guelph Formation brines (Figure 5.45). This may indicate that these brines share a similar origin, namely, evaporated Silurian seawater. However, they do not show as much variability in δ^{18}O as the Salina Group and Guelph Formation brines. This may reflect a lesser degree of rock-water interaction, as expected considering that these brines are mostly hosted in sandstones, which are less reactive than carbonates. Data from this study and Dollar et al. (1991) plot within similar regions, although our data show greater δ^2H variability (Figure 5.45). Data from the Clinton sandstones in eastern Ohio by Lowry et al. (1988) also plot in a relatively similar position, although they have greater δ^{18}O variability.
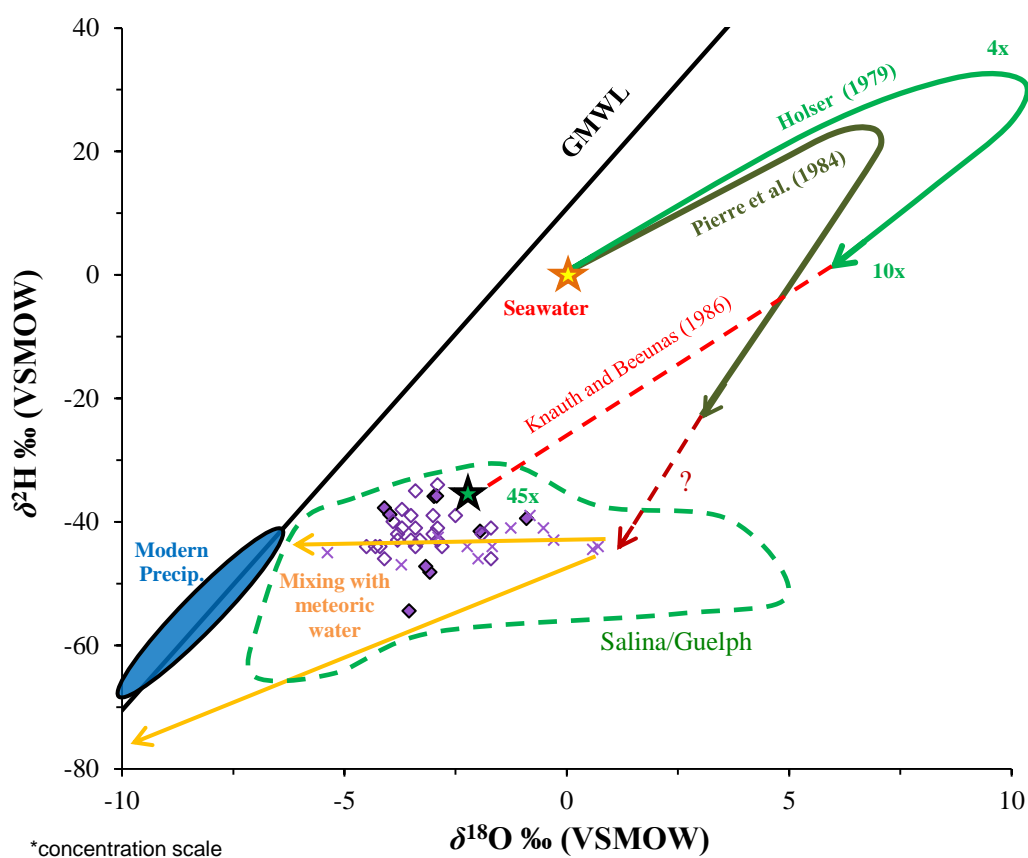
Figure 5.45: Plot of δ^2H vs. δ^{18}O for the Clinton and Cataract brines. Solid symbols are from this study, hollow symbols are from Dollar et al. (1991) and X's are from Lowry et al. (1988). For reference, the Salina-Guelph brines' compositions are outlined in green (see Figure 5.52).

In a plot of $\delta^{18}O$ versus TDS (Figure 5.46), Dollar et al. (1991) and Lowry et al. (1988) both noted linear trends in brine compositions that they attributed to dilution. The regression slopes for $\delta^{18}O$ versus TDS in these two studies are similar, perhaps suggesting a genetic link between the Clinton-Cataract brines in Ohio and Ontario. The intercepts on Figure 5.46 suggest that the diluting end-member is recent meteoric water ($\sim$ –8‰ $\delta^{18}O$). A similar dilution trend may be present in this study, although its slope is different; this trend is heavily influenced by two outliers having anomalously high TDS, likely resulting from halite dissolution. Apart from these outliers, the data from this study falls along the line for Dollar et al. (1991). The Ontario Clinton-Cataract reservoirs are relatively shallow, so they may be more susceptible to natural dilution than other brines in the region. Also, while there are no reports of fresh water injection in these units, dilution may nevertheless arise from anthropogenic influences; there are many abandoned, unplugged wells in the region (T. Carter, personal communication, 2013) which could facilitate infiltration of surface water or shallow groundwater.
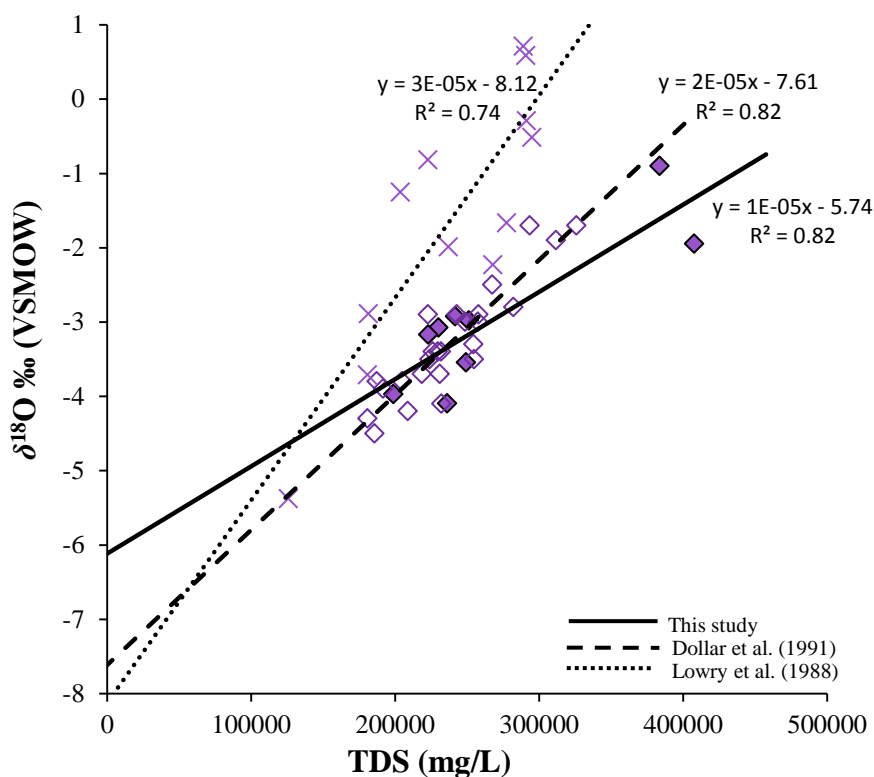
Figure 5.46: Plot of $\delta^{18}O$ vs. TDS for the Clinton and Cataract brines. Linear trends are indicated, suggesting dilution with meteoric waters (solid symbols = this study, hollow symbols = Dollar et al., 1991 and X's = Lowry et al., 1988).

If the limited $\delta^{18}O$ variation in these brines is predominantly due to dilution rather than rock-water interaction, then the 45x evaporative concentration point based on Holser (1979) and Knauth and Beeunas (1986) would result in a pre-dilution brine too ^{18}O-depleted to explain the data. However, Pierre et al. (1984) proposed a slightly different curve that, if extrapolated slightly in a similar fashion, could presumably yield brine with an isotopic composition similar to the highest TDS samples (Figure 5.45).

While the linear trends in Figure 5.46 are quite strong, similar correlations are not found between δ^2H and TDS, and the dilution trend is not particularly evident in Figure 5.45. This could be explained by the meteoric water having similar δ^2H values as the non-diluted brine end-member, consistent with the higher modern values. However, the relatively high variability in δ^2H may suggest that other processes are also modifying these brines. One possibility is exchange of hydrogen with clay minerals in the surrounding shales (O'Neil and Kharaka, 1976). Diagenetic reactions involving these clays, such as the conversion of smectite to illite, as perhaps suggested by the ion geochemistry, would facilitate such isotopic exchange (Whitney and Northrop, 1988). Given the gas-rich nature of these reservoirs, exchange of ^2H between brines and gases may also be an important process affecting δ^2H variability (Hitchon and Friedman, 1969).

Lowry et al. (1988) proposed that two different brine types were present in these units, which mixed with each other, and were subsequently diluted with meteoric water. This was based primarily on the observation that on a plot of Na^+ versus Ca^{2+}, the samples do not plot along a simple mixing line, but rather fall within a mixing triangle, as illustrated in Figure 5.47. They defined a Na^+-rich and a Ca^{2+}-rich end-member based on the apexes of this triangle. The Clinton-Cataract brines in Ontario sampled in this study and Dollar et al. (1991) also seem to fall into two groups, one with higher $Na^+:Ca^{2+}$ ratios (~1.3-1.6), and one with lower $Na^+:Ca^{2+}$ ratios (~0.5-0.7). However, they do not all plot within the mixing triangle of Lowry et al. (1988), and in general tend to have lower $Na^+:Ca^{2+}$ ratios than the Ohio brines. While the Ontario brines could also be fitted within a mixing triangle (Figure 5.47), it would larger and is less well defined than that of Lowry et al. (1988); rather, the two brine types in Ontario seem less intermixed, and fall along separate mixing lines.
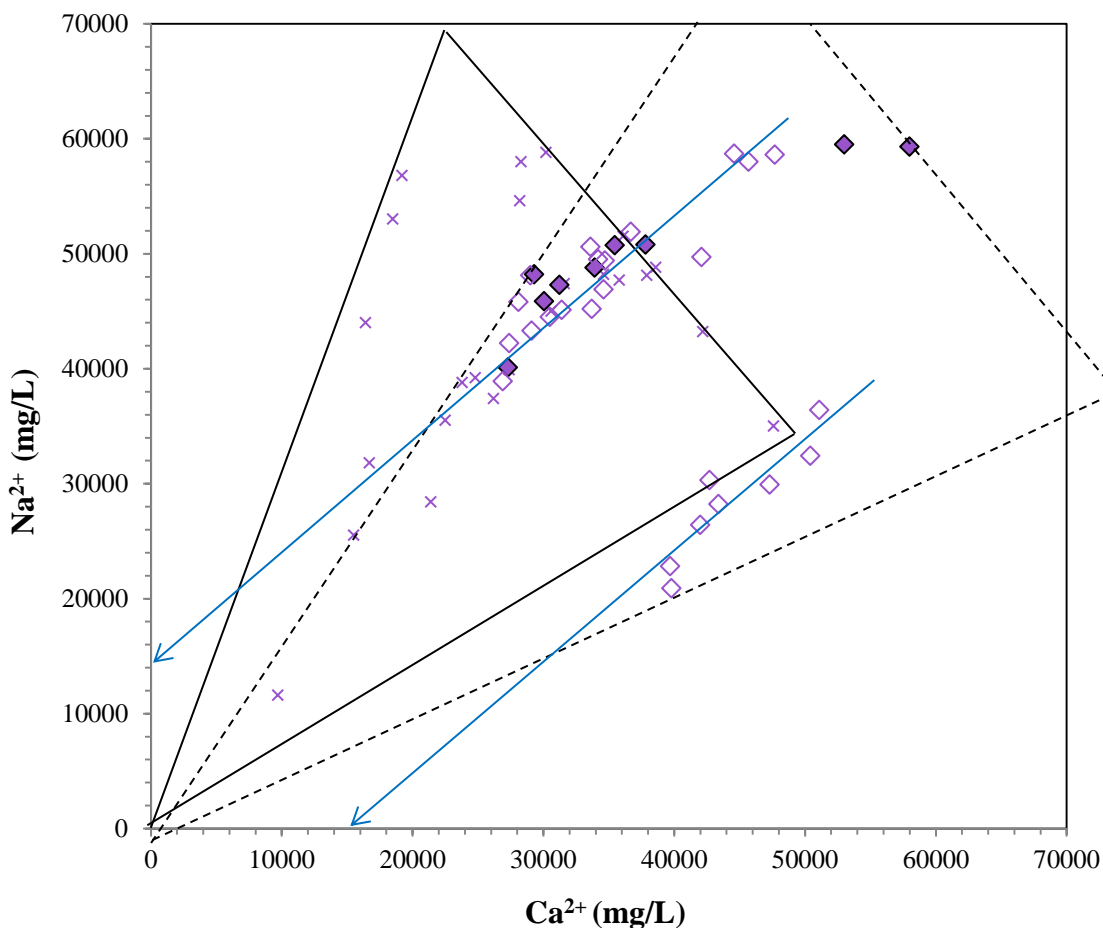
Figure 5.47: Plot of Na^+ vs. Ca^{2+} concentrations the Clinton and Cataract brines (solid symbols: this study, hollow symbols: Dollar et al., 1991 and X's: Lowry et al., 1988). Ohio samples from Lowry et al. (1988) form a mixing triangle (indicated by solid lines). A different triangle (dashed lines) would be required to contain the Ontario data, which seem to fall along two separate mixing lines.

Lowry et al. (1988) hypothesized that the Na-rich brine migrated down into the Clinton-Cataract groups from the Salina Group, while the Ca^{2+}-rich brine had a deep-seated origin in the Appalachian Basin. In a plot of Cl^- against Br^- (Figure 5.48), the two brine groups from Ontario also plot in different locations, with the Ca^{2+}-rich brines generally lower in Br^-. This supports differing origins for these brines, rather than their $Na^+:Ca^{2+}$ differences being purely a product of diagenetic modification. The Na^+-rich end-member appears to be a more highly evaporated seawater, similar to many of the Salina Group and Guelph Formation brines, consistent with Lowry et al. (1988)'s theory. Several of the Na^+-rich

brines plot above the seawater trend, indicating halite dissolution. Regression lines for the two brine groups share very similar intercepts on Figure 5.48, indicating that they were likely both diluted by the same fluid. However, the intercepts are not at the origin, suggesting that either the diluting waters or the brines dissolved similar amounts of halite.
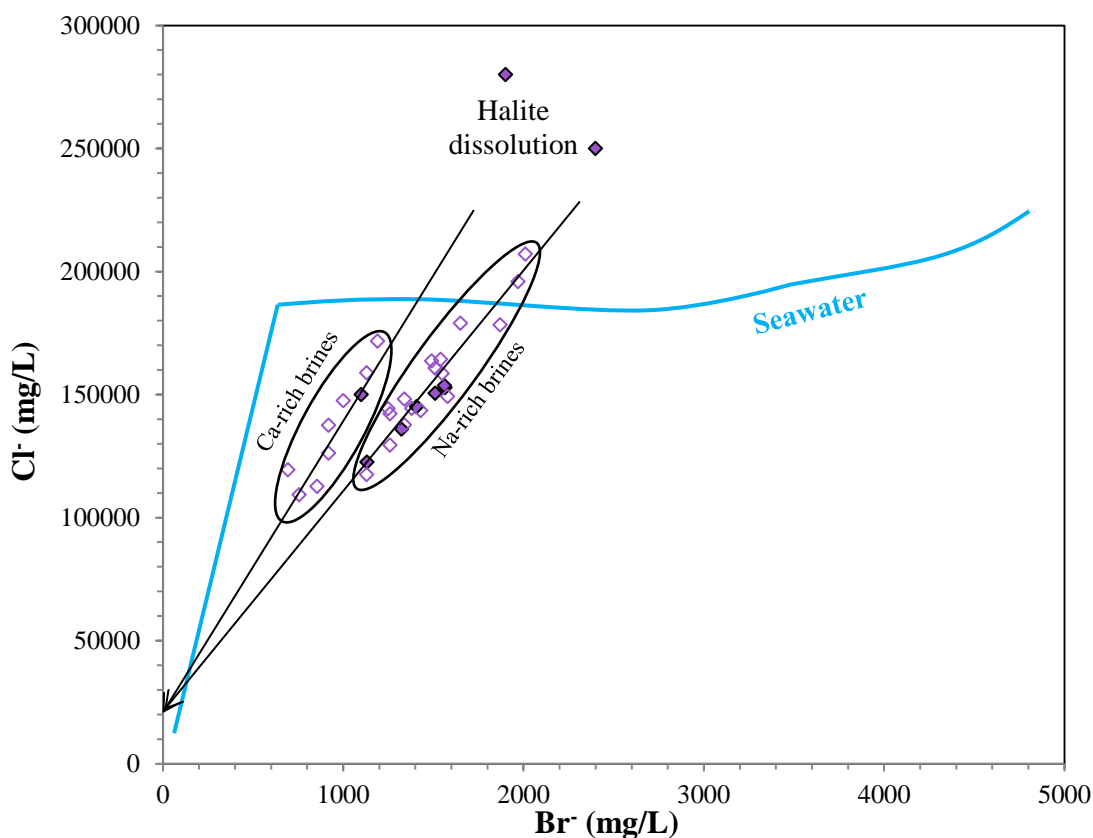
Figure 5.48: Plot of Cl⁻ vs. Br⁻ for the Clinton and Cataract brines (solid symbols: this study, hollow symbols: Dollar et al., 1991, seawater evaporation path from McCaffrey et al., 1989). The two brine types appear to be derived from differently-evaporated seawaters, and plot along different dilution trends.

The similarities in brine compositions between Ontario and Ohio suggest that both brine types have undergone long-distance migration, from deeper in the Appalachian Basin, and the existence of these two brine types indicates that flow occurred within separate formations. While the Na^+-rich brines share a similar degree of evaporation to the Salina Group and Guelph Formation brines, they are not necessarily genetically related. The higher $\delta^{18}O$ variability of the latter brines, and the fact that even the least-diluted Na-rich brine samples have lower concentrations of Ca^{2+} and several other ions, suggest they may

not be strongly associated, and Br/Cl similarities are coincidental. If the Na^+-rich brines did migrate updip from a deep-seated source, the permeable sandstones of the Thorold Formation would represent a likely conduit. Long-distance migration of the Ca^{2+}-rich brines is consistent with the fact that half the samples thereof are found within the basal Whirlpool Formation sandstone, which could have acted as the conduit for these brines. Brines of both types could then have dispersed outwards from these conduit formations, perhaps facilitated by fractures, into nearby units, predominantly the Grimsby Formation. While the geochemical evidence supports fluid migration along such conduits, future studies of the mineralogy of these units may be useful for confirming this hypothesis.

The strontium isotopic compositions of the brines from the Clinton and Cataract groups are significantly more radiogenic than seawater during the Silurian or at any point in geological time (Figures 5.31, 5.32). Their highly ^{87}Sr-enriched compositions can only be explained by leaching of radiogenic strontium from Rb-rich clays and feldspars in the surrounding shale layers, which suggests some fluid contact therewith, either dewatering of the shales into the sandstones, or migration of fluids between sandstone beds, through the shales, presumably along fractures. While the variability in $^{87}Sr/^{86}Sr$ ratios among samples likely reflects differing degrees of shale-derived Sr^{2+}, differences in Sr^{2+} concentrations seem to be controlled primarily by degree of dilution, since Sr^{2+} has a strong relationship with TDS ($r^2 = 0.87$); such dilution would have little effect on the $^{87}Sr/^{86}Sr$ ratios. Lowry et al. (1988) suggested the $^{87}Sr/^{86}Sr$ ratios of their samples were controlled by mixing between the two brine end-members, having different ratios and concentrations. However, a clear mixing trend is not evident in the Ontario data, consistent with the observation made earlier for other tracers that the two brine types in Ontario are relatively separate from each other.

The major ion compositions of the Clinton and Cataract group brines are distinctive in the sense that they are all strongly controlled by dilution, as discussed previously (Section 5.2.2.5). They also notably have the lowest K^+:Br^- ratios of all brines, except for some of the Cambrian samples. Given the siliciclastic nature of these reservoirs, this supports the theory that K^+-depletion is controlled largely by diagenetic reactions involving clays and feldspars.

5.2.2.8 *Trenton and Black River Groups*

Brines from the Upper Ordovician Trenton and Black River groups show relatively distinct signatures compared to the younger formation waters (Figure 5.49). Of all the groundwaters studied, their compositions constitute the tightest grouping, having very little variability in $\delta^{18}O$ and δ^2H, apart from a few outliers attributed to mixing with Silurian brines via casing leaks (Dollar et al., 1991). They are more ^2H-enriched than most Silurian brines, and have compositions similar to the Cambrian brines. Their proximity to the 45x evaporation point of Knauth and Beeunas (1986) suggests an evaporated seawater origin for these brines.
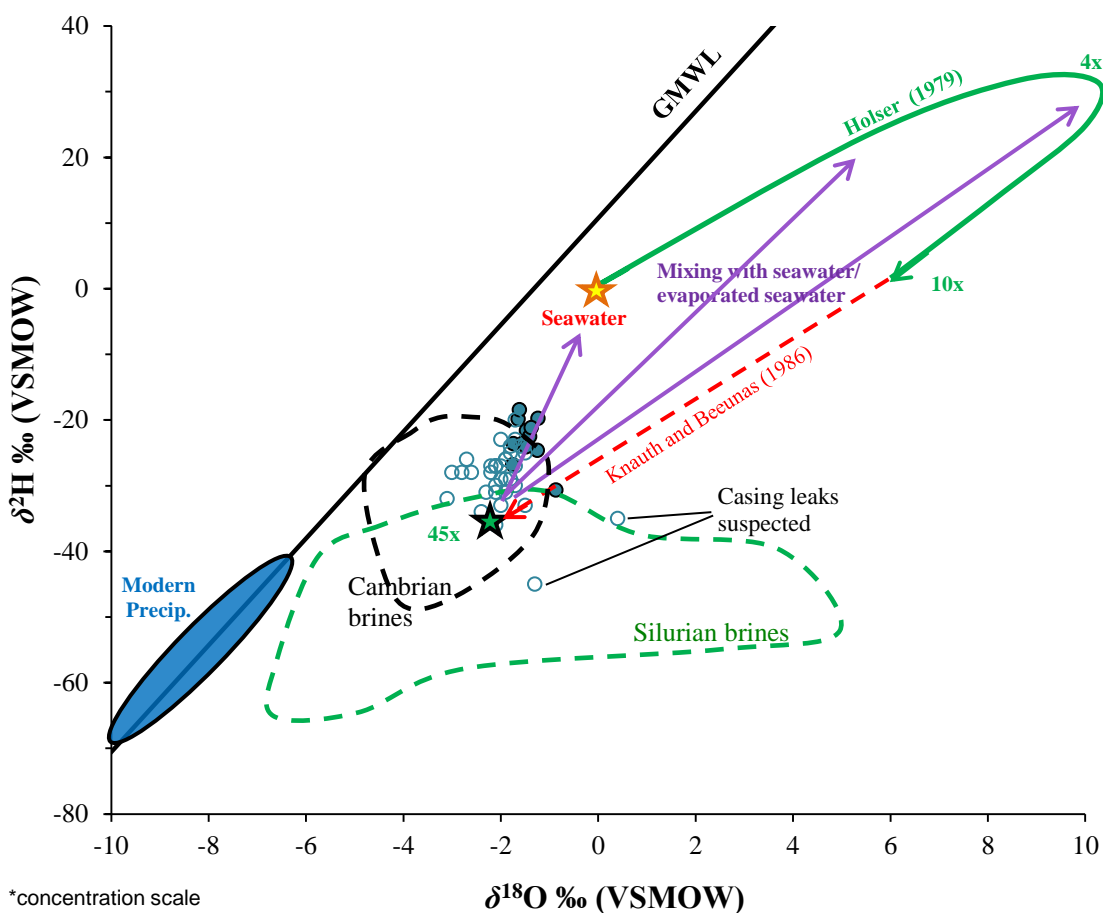
Figure 5.49: Plot of δ^2H vs. $\delta^{18}O$ for the Trenton and Black River brines; the compositions of the Cambrian and Silurian brines are outlined for comparison. Solid symbols are from this study, hollow symbols are from Dollar et al. (1991).

The Trenton-Black River $\delta^2H/\delta^{18}O$ data from this study are similar to those of Dollar et al. (1991). Several of their samples were from central Michigan, yet show no significant isotopic differences from the Ontario samples. This similarity suggests that all Trenton-Black River samples may have a common origin, which may be explained by long-distance fluid migration. Several diagenetic mineral phases in the Ordovician reservoirs have isotopic compositions that indicate several episodes of past fluid movement. High fluid inclusion homogenization temperatures (up to ~140°C) indicate these fluids were hydrothermal (Middleton, 1991; Haeri-Ardakani et al., 2013). However, there is very low porosity and permeability in the non-dolomitized portions of the Trenton and Black River groups (Armstrong and Carter, 2010), so migrating fluids must have travelled within adjacent, more permeable units prior to entering the Trenton-Black River via faults. The overlying shales have low permeabilities, so the underlying Cambrian sandstones almost certainly would have been the conduit for migrating fluid. This is supported by the similarity in the $\delta^2H/\delta^{18}O$ compositions for the Cambrian and Trenton-Black River brines. Similar minerals (e.g., secondary chlorite and illite; Ziegler and Longstaffe, 2000) in these two units also suggest common fluids have passed through them.

While the Trenton-Black River and Cambrian brines have relatively similar $\delta^{18}O$ and δ^2H values, there is a difference in their average compositions, which Dollar et al. (1991) attributed to rock-water interaction in the Ordovician reservoirs. However, several lines of evidence suggest that another process is likely responsible. First, while the Trenton-Black River and Cambrian brines of Dollar et al. (1991) had comparable δ^2H values, samples analyzed in this study indicate the Cambrian brines range to more negative δ^2H values, which cannot be easily explained by rock-water interaction. Second, rock-water interaction would be expected to cause a wider spread in $\delta^{18}O$ values than observed, due to local variations in reservoir conditions. Third, fluids in equilibrium with the reservoir rocks (matrix dolomite $\delta^{18}O = -11.5$ to -7.8‰ VPDB / $+19.01$ to $+22.9$‰ VSMOW; Haeri-Ardakani et al., 2013) at current reservoir temperatures (~30°C; T. Carter, personal communication, 2014) would have $\delta^{18}O$ values much lower (-12.5 to -8.7‰; calculated as in Section 5.2.2.7) than present brines. Temperatures in excess of 80-90°C would be required to induce any positive $\delta^{18}O$ shift given current water and rock compositions.

The slightly different compositions of the Trenton-Black River brines may be explained by mixing with a ^{2}H/^{18}O-enriched end-member. From their position in Figure 5.49, it appears that they may fall along a mixing line between the Cambrian brines and seawater or slightly evaporated seawater. Given petrological evidence that multiple generations of fluids have passed through these rocks over geological time (e.g., Ziegler and Longstaffe, 2000; Haeri-Ardakani et al., 2013; see Section 5.2.2.9 for details), the original porewaters in the Trenton-Black River limestones have likely been flushed from the system. This dilute seawater component in the brines was expelled during compactional dewatering of the overlying shales, which is evidenced by the existence of regional cap dolomite at the base of the shales (Middleton, 1991), and by rare earth element similarities between the Trenton-Black River dolomites and the shales (Haeri-Ardakani et al., 2013).

This mixing scenario is perhaps better illustrated by a plot of Cl$^-$ versus Br$^-$ (Figure 5.50). The Cambrian brines typically have higher Cl$^-$ and Br$^-$ concentrations than those from the Trenton-Black River groups, plotting near or above the seawater evaporation trend past halite saturation. Together with the Trenton-Black River brines, they form a clear mixing envelope together that converges to a point early in seawater evaporation.
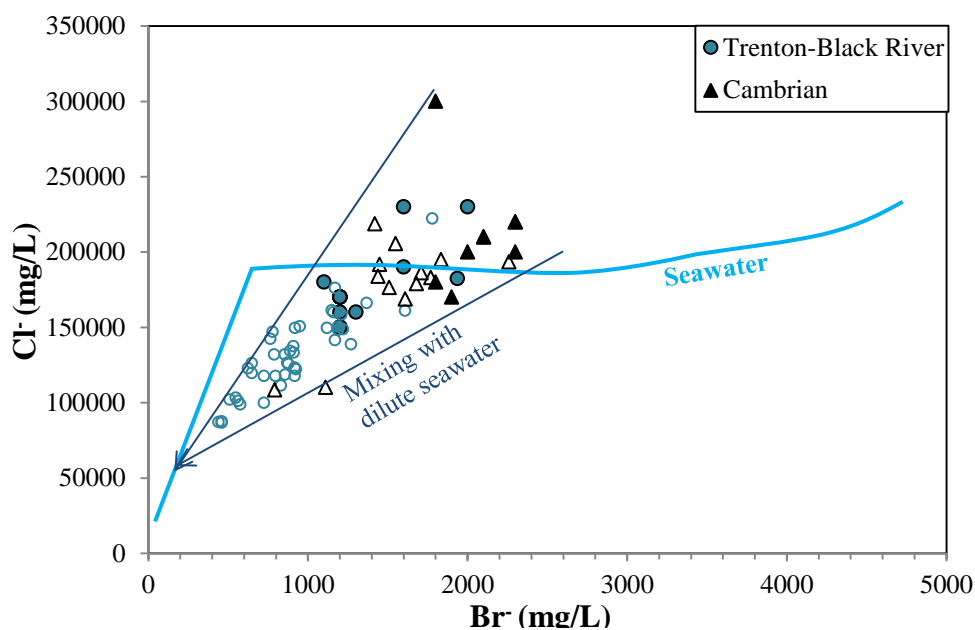
Figure 5.50: Plot of Cl vs. Br concentrations for the Cambro-Ordovician brines, compared to the seawater evaporation trend (McCaffrey et al., 1987). The brines appear to form a mixing envelope, converging on a point during early seawater evaporation. Solid symbols are from this study, hollow symbols are from Dollar et al. (1991).

The strontium isotope data show considerably different trends between this study and Dollar et al. (1991), with the former data having a linear trend with a very narrow range of $^{87}Sr/^{86}Sr$ ratios, and a large range in Sr^{2+} concentrations, while the opposite is observed in the latter data (Figure 5.51). A mixing curve between the compositional extremes does not fit the data very well, as shown. The most concentrated sample from this study has a Sr^{2+} concentration and $^{87}Sr/^{86}Sr$ ratio similar to several Cambrian brine samples. Thus, the trend observed in samples from this study is consistent with dilution of Cambrian brine by Ordovician porewater. Such a dilution trend would be roughly horizontal on a $^{87}Sr/^{86}Sr$ versus total Sr^{2+} plot over most of its extent, regardless of the $^{87}Sr/^{86}Sr$ ratio of the Ordovician porewater component, since Sr^{2+} concentrations thereof would presumably be low enough that the mixture would be dominated by the Cambrian brine Sr^{2+}; several dilution scenarios are illustrated in Figure 5.51 by the dashed lines.
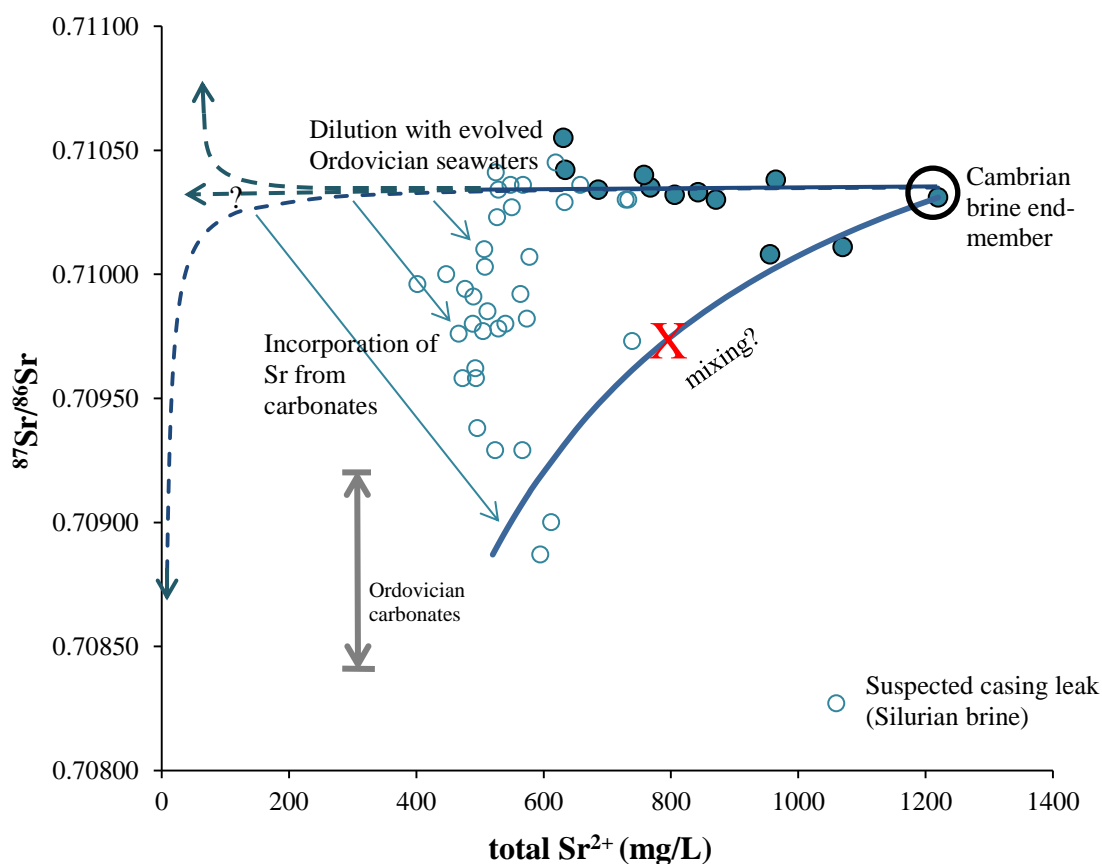
Figure 5.51: Plot of $^{87}Sr/^{86}Sr$ versus Sr^{2+} concentrations for the Trenton-Black River brines. Solid symbols are from this study and hollow symbols are from Dollar et al. (1991). Possible evolution scenarios are illustrated, as described in text.

The seawater dilution trend is not evident in Figure 5.51 for Dollar et al.'s (1991) samples, but their samples do show a correlation between Sr^{2+} and Br^- (Figure 5.52), indicating that Sr^{2+} concentrations are being affected by dilution. However, there is considerable scatter in this trend and the intercept is much higher than seawater Sr^{2+} concentrations (~8 mg/L; Angino et al., 1966), indicating that Sr^{2+} is also being added by other processes. Haeri-Ardakani et al. (2013) found $^{87}Sr/^{86}Sr$ ratios between 0.70830 – 0.70918 for the Trenton-Black River dolomites. Dissolution of these reservoir carbonates would result in both an increase in the Sr^{2+} concentration and a decrease in $^{87}Sr/^{86}Sr$; a negative correlation in Dollar et al. (1991)'s samples between $^{87}Sr/^{86}Sr$ and $Sr^{2+}:Br^-$ ratio ($r^2 = 0.68$) indicates that the extent of carbonate dissolution is proportional to the degree of dilution. As illustrated in Figure 5.51, this scenario could produce the vertical trend observed in these samples. Perhaps the more concentrated nature of the samples in this study explains why they do not show much evidence for incorporation of carbonate Sr.

At least one sample from Dollar et al. (1991) with very low $^{87}Sr/^{86}Sr$ and high Sr^{2+} was inferred to be mixed with Silurian brine due to a well casing leak. Two other samples (the 2nd and 3rd lowest $^{87}Sr/^{86}Sr$ values in Figure 5.51) were also suspected to have a Silurian leak component, on the basis of relatively low $Sr^{2+}:Br^-$ ratios for their $^{87}Sr/^{86}Sr$ values.
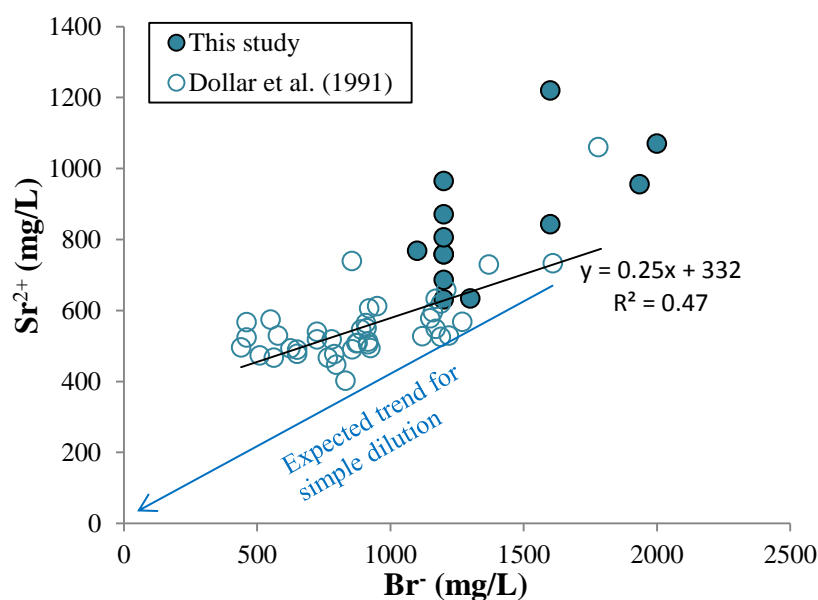
Figure 5.52: Plot of Sr^{2+} vs. Br^- concentrations for the Trenton-Black River brines.

5.2.2.9 Cambrian units

The Cambrian (and Precambrian) rocks in the region have undergone several episodes of alteration associated with large-scale fluid migrations and different fluid types, largely associated with tectonic activity along the east coast of North America. Harper et al. (1995) described a complex paragenetic sequence of alteration minerals near the Precambrian unconformity. They calculated ages of 453-412 Ma for secondary potassium feldspar, which they inferred to have formed from fluids with temperatures $\geq 100°C$, consistent with temperatures obtained for K-feldspar elsewhere in mid-continental North America (100-200°C; Hearn et al. 1987); they also noted that earlier alteration minerals (albite, chlorite) likely formed at higher temperatures. Formation of K-feldspar was followed by a later alteration episode that formed illitic clays, estimated at 355 ± 10 Ma (Tiller and Selleck, 1992). Still later (e.g., 322-284, 310-300, 280-255, and 230-215 Ma) phases of fluid migration have been associated with various alteration minerals in mid-continental North American Cambro-Ordovician rocks (Hearn and Sutter, 1985; Hearn et al., 1987; Hay et al., 1988; Lee and Aronson, 1991).

Ziegler and Longstaffe (2000) measured $\delta^{18}O$ and $\delta^2 H$ values of chlorites and illites in Ontario for the 453-412 Ma and 355 ± 10 Ma alteration events, respectively, and based on assumed temperatures of 150°C and 40°C, respectively, calculated isotopic ranges for their putative alteration fluids. Chlorites from the Appalachian side of the Algonquin Arch formed from fluids with compositions of +6 to +9‰ $\delta^{18}O$ and −15 to −40‰ $\delta^2 H$. These are considerably more ^{18}O-enriched than the current brines in Ontario, and were interpreted as hydrothermal brines derived from modified evaporated Paleozoic seawater, migrating from deeper in the Appalachian Basin. Minimum chlorite ages corresponding to the middle or late stages of the Taconic Orogeny (480-420 Ma) suggest that this episode of migration resulted from tectonic overpressuring associated with the orogeny. Putative brine compositions varied with distance from the Algonquin Arch, with more proximal fluids closer in composition to Michigan Basin brines, suggesting mixing between brines of the two basins. Illites from the second stage of alteration (365-321 Ma) had putative fluid compositions that plotted close to the GMWL; Appalachian-side fluids had values of ~ −5 to −2‰ $\delta^{18}O$ and −18 to 0‰ $\delta^2 H$, and Michigan-side fluids had values

of ~ −7.5 to −1.0‰ $\delta^{18}O$ and −30 to −15‰ δ^2H. Ziegler and Longstaffe (2000) interpreted these waters as meteoric waters that infiltrated locally during a period of uplift and erosion following the Acadian Orogeny.

As discussed in Section 5.2.2.8, fluids from the Cambrian rocks were likely responsible for dolomitization of the fault-related Ordovician reservoirs. Ordovician replacive matrix dolomite formed by the main alteration event has $\delta^{18}O$ values between −11.5 to −7.8‰ VPDB, and later saddle dolomite cement has comparable values ($\delta^{18}O$ = −11.8 to −8.1‰ VPDB) (Middleton, 1991; Haeri-Ardakani et al., 2013), leading Middleton (1991) to conclude that both dolomite types formed from the same fluid. However, Haeri-Ardakani et al. (2013) noted that the matrix dolomite had lower fluid inclusion homogenization temperatures (T_h: 67.6-98.9°C, mean 81.8°C) than the saddle dolomite (T_h: 96.7-143.5°C, mean 121.1°C), and were thus formed from different fluids; they calculated fluid $\delta^{18}O$ values for replacive and saddle dolomite of −6 to +2‰ and −2 to +6‰, respectively.

The isotopic activities (the correct scale for assessing mineral-fluid reactions) of the Cambrian brines measured in this study ($\delta^{18}O$ = −5.8 to −2.9‰) coincide very closely with the putative ranges of both the Ordovician matrix dolomite fluids of Haeri-Ardakani et al. (2013) and the illitizing fluids of Ziegler and Longstaffe (2000). However, despite their isotopic similarities, it seems unlikely that these were the same fluids. The illitizing fluids were supposedly much cooler than any of the dolomitizing fluids and of meteoric origin, unlike the Cambrian brines, which have Cl^-:Br^- ratios indicative of an evaporated seawater origin (Figure 5.50). Also, as mentioned above, the fluids that formed the matrix dolomite seem to later have been at least partially replaced by hotter, more ^{18}O-enriched fluids that differ from the current Ordovician and Cambrian brine compositions. This indicates they the current Cambrian brines are related to a more recent episode of fluid movement than any in the above discussion.

Despite the fact that all modern Cambrian brines seem to have evolved from evaporated seawaters, their exact origins, in a spatial sense, are difficult to determine. As mentioned earlier, brines are known to have migrated updip along the Paleozoic unconformity in the past from the Appalachian Basin, and the isotopic similarity of Ordovician reservoir fluids in Ontario and Michigan suggests migration of brines from the central Michigan

Basin as well. Thus, the Cambrian aquifer in Ontario may represent a zone of mixing between brines of the two basins. While fluid migration from the Appalachian Basin seems to be related to tectonic overpressuring resulting from orogenic events, migration from the Michigan Basin may be caused by convection of hydrothermal fluids generated by the buried midcontinent rift (MCR) at the basin's center, reactivation of which may also be related to orogenic forces (Haeri-Ardakani et al., 2013). Present Cambrian brines are still quite overpressured, to the extent that wells completed in Cambrian units will commonly exhibit artesian flow (Jackson and Heagle, 2010). This indicates that updip fluid migration from the adjacent basins may still be operating today.

The Cambrian brines currently found in Ontario differ isotopically from most of the basinal brines reported in the region. They are significantly ^{18}O-depleted relative to the ~ +6 to +9‰ $\delta^{18}O$ Appalachian Basin chloritizing brines proposed by Ziegler and Longstaffe (2000), and are also lower than the ~ +3.5‰ $\delta^{18}O$ brine inferred by Liu et al. (2003) to have formed authigenic K-feldspar in west-central Wisconsin. They are also more [2]H-enriched than the local Silurian brines. The Cambrian brines also fall too close to the GMWL and are too saline to be readily explained by a mixture of Paleozoic meteoric water and an ^{18}O-enriched basin brine. However, they could be generated by mixing of an ^{18}O-rich brine with an end-member that is more saline and ^{18}O-depleted than meteoric water. Canadian Shield brine may constitute such an end-member; many studies (e.g., Frape et al., 1984; Bottomley et al., 2003) have found brines in crystalline shield rocks from Canada and elsewhere that have isotopic compositions plotting to the left of the GMWL; these unusual compositions have been attributed to mineral hydration reactions in an environment with a high rock:water ratio (Fritz and Frape, 1982). Given the position of the Cambrian rocks directly overlying the Precambrian Shield, and the existence of fractures penetrating both, such mixing would be plausible. A hypothetical Canadian Shield brine composition can be estimated based on the apparent convergence of $\delta^{18}O$ and δ^2H trends from mine waters in Yellowknife, Thompson, and Sudbury from Frape and Fritz (1984). The composition of this Shield brine is illustrated in Figure 5.53 alongside the Cambrian brine data, the illite- and chlorite-forming fluids of Ziegler and Longstaffe (2000) (the latter representing a possible basinal brine end-member), the GMWL, and other possible relevant processes.
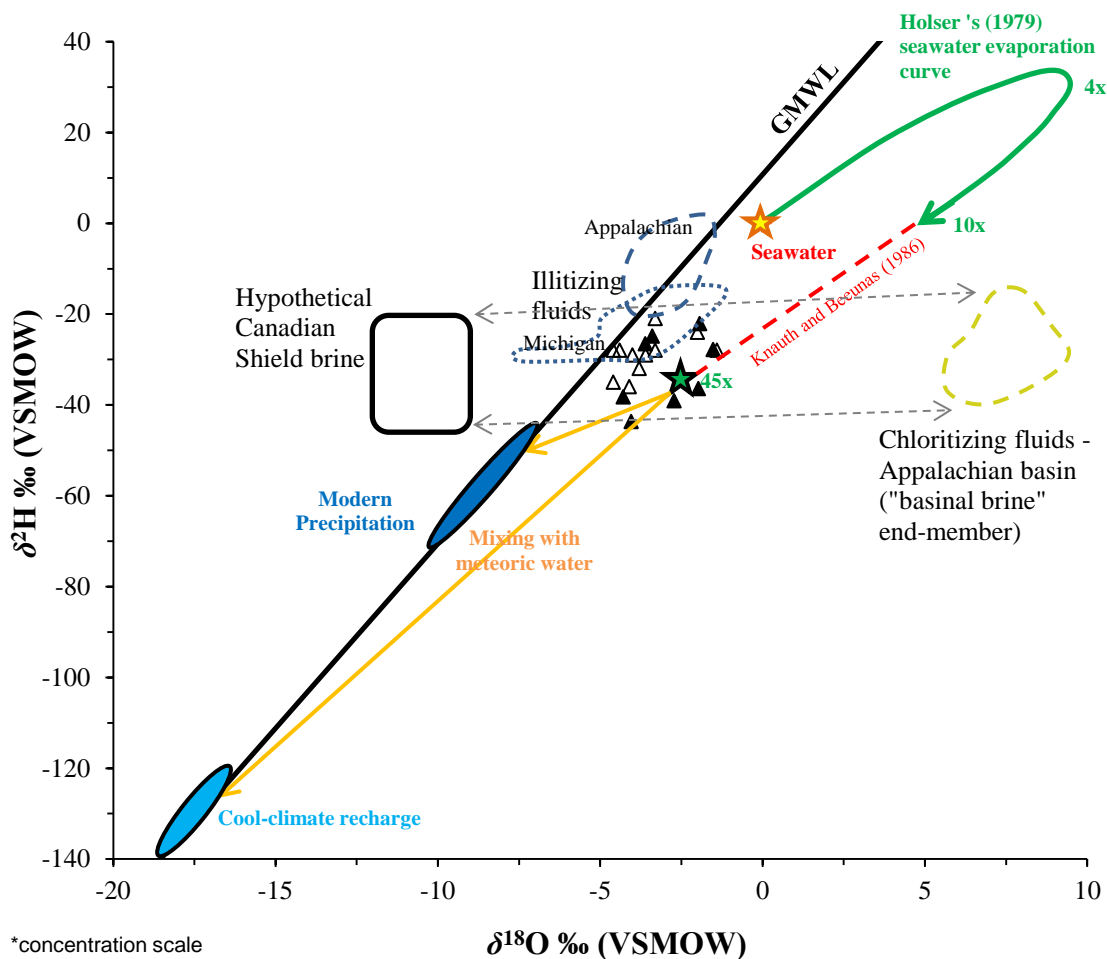
Figure 5.53: Plot of δ^2H vs. δ^{18}O for Cambrian brines from this study (solid triangles) and Dollar et al. (1991) (open triangles). Their position may be explained by mixing between a low-^{18}O end-member such as a Canadian Shield brine (based on Frape and Fritz, 1984) and a high-^{18}O brine end-member from deeper in one/both of the adjacent basins (perhaps similar to the chlorite-forming Appalachian brine proposed by Ziegler and Longstaffe, 2000). The illite-forming brines proposed by Ziegler and Longstaffe (2000) fall closer to the GMWL, likely meteoric waters, and are too ^{2}H-enriched and presumably too dilute to form a significant portion of the present brines. Alternatively, the brines could be formed without mixing, by extensive seawater evaporation as per Holser (1979) and Knauth and Beeunas (1986).

The Cambrian brine compositions in Figure 5.53 plot about halfway between the hypothetical Canadian Shield and basinal brines, suggesting such a mixing scenario could be possible. Thus, the δ^{18}O variability in the Cambrian samples could be attributed to varying proportions of these two end-members and/or variations in their compositions. In addition, the ^{18}O-rich basinal brine end-member may itself be a mixture of different brines - for instance, one from the Michigan Basin and one from the Appalachian Basin -

and so, variations in their proportions would also affect the compositions of the Cambrian brines. If the Ordovician matrix dolomite was formed from a brine mixture with a composition similar to that of the modern brines, then an increase in the basinal component(s) could have produced a more ^{18}O-rich brine similar to that calculated for the later saddle dolomite (Haeri-Ardakani et al., 2013). Such a shift would also presumably involve an increase in the temperature of the brine mixture, given the commonly-inferred hydrothermal nature of basinal brines, thus being consistent with the higher saddle dolomite T_h values reported by Haeri-Ardakani et al. (2013).

It should be noted that the Canadian Shield end-member may be more ^{2}H-rich than illustrated in Figure 5.53; for instance, Pearson (1987) suggested δ^2H values between –10‰ and +10‰. In such a case, the Cambrian brines would not fall along a simple mixing line as discussed above, unless the basinal brine end-member was more ^{2}H-depleted than shown in Figure 5.53. Nonetheless, their compositions could be arrived at by mixing Canadian Shield and basinal brines with a small amount of meteoric water. Based on Cl/Br systematics (Figure 5.50), some such dilution is apparent in some samples. Even if the suggested end-member compositions were correct, a meteoric water component could explain some of the variability in Cambrian brine compositions.

Two alternative scenarios exist, which do not require Canadian Shield brine component. In the first, the basinal brines themselves became depleted of ^{18}O during formation of secondary minerals within the Cambrian strata. Second, the brines could have formed through evaporation of seawater as shown in Figure 5.52; all samples plot close to the 45x evaporation point of Knauth and Beeunas (1986). The ^{18}O-enriched basinal brines discussed above presumably formed in a similar manner, and were later enriched in ^{18}O by rock-water interaction. These explanations seem less plausible; the first, because minerals thusly formed would have isotopic compositions with corresponding putative fluid compositions trending towards the modern brine values, which are not observed. The second explanation is unlikely because it would require a source of seawater that had somehow not been isotopically modified by rock-water interactions, and thus be a different source than that of the previous fluids that have migrated through these rocks.

Chapter 6

6   Conclusions

The Paleozoic bedrock formations in southwestern Ontario contain a range of geochemically diverse groundwaters, which can largely be differentiated from one another by their isotopic compositions. The relatively unique geochemical signatures of these different waters can be exploited using the Bayesian mixing model SIAR to help determine the probable source(s) of fluids leaking from abandoned wells in the region. While the model performance varies depending on a number of factors such as the composition of the unknown sample, which isotopic data are available, and which end-members are included in the model, testing of several hypothetical samples indicates that in most cases, source proportions are relatively well predicted. The addition of chlorine and bromine isotope data, not measured in this study, has the potential to significantly improve the model's predictive power. That said, knowledge of the geology of the sample location is important for guiding the model and optimal interpretation of the results. The model returns the full range of proportions possible for each potential end-member composition along with their probabilities. Thus, unless the geological setting is addressed at the outset, it is possible for the model to predict contributions of fluids from formations that are not actually present in the unknown sample. Possibilities for end-members to substitute for one another to generate the mixture composition can also lead to poorer estimations of the probable source proportions contributing to the leaking fluid. In short, a thorough understanding of how the model functions and a geology-based choice of end-members appropriate to the sample's location are essential to effective application of the SIAR modelling tool.

The success of the geochemical tool for accurately predicting fluid sources in the test mixtures examined in this study suggests it will be of considerable use for identifying the origins of leaking well fluids. This is validated by the fact that one abandoned well (T012111) has already been successfully plugged with the help of the geochemical tool, even though it was still in early development stages at the time, and plugging of a second well is underway. Fluids from both wells were predicted to originate solely from the

Dundee-Detroit River Group aquifer. It is thus expected that this research will be of great assistance to the Abandoned Works Program, and may have applications to other fluid source determination problems in the future.

The large number of new water samples collected in this study also represent an important addition to the existing geochemical database for southwestern Ontario groundwaters. The data reveal that the hydrology of the study area can be broadly divided into shallow and deep aquifer systems, each with significantly different geochemical properties.

The shallow groundwater system is defined in this study as a region of relatively dilute (<100,000 mg/L TDS) waters of predominantly meteoric origin, and are generally found a depths of less than ~350-450 m. These waters are mostly contained within Devonian carbonate aquifers, but are also found in the shallower portions of some Silurian units. The shallow groundwaters do not show clear isotopic differences between formations, suggesting they and their solutes are largely derived from similar sources. The waters have oxygen and hydrogen isotopic signatures that span a broad range, falling on or near the Great Lakes Meteoric Water Line, and are relatively depleted of both heavy isotopes compared to the waters in the deep bedrock aquifers. Most of these shallow waters have δ^2H and δ^{18}O signatures within the range of modern precipitation, although some are conspicuously more negative, indicating recharge under cooler climate conditions, possibly during the Late Pleistocene. On the other end of the spectrum, groundwaters from several Devonian oil-fields have isotopic signatures that appear to be influenced slightly by mixing with deep brines, suggesting that cross-formational flow is or was at least locally active, likely along fractures. Elevated TDS concentrations in some samples may also be derived from brines, although other sources may be responsible.

Sulphate oxygen and sulphur isotope compositions reflect diverse sources of sulphate in the shallow groundwaters. Most samples plot within the range of Devonian seawater, indicating *in situ* dissolution of marine sulphate minerals. However, some samples with more negative δ^{34}S$_{SO4}$ values appear to reflect oxidation of sulphide minerals; the δ^{18}O$_{SO4}$ values indicate that variable proportions of oxygen from water and atmospheric oxygen were used therein. Several very [34]S-enriched samples also point to bacterially-mediated

dissimilatory sulphate reduction, likely responsible for the H_2S-rich 'sulphur waters' commonly found in the shallow system. The shallow groundwater strontium isotopic compositions are quite variable, but generally tend to be lower than those of the deeper waters. The trends of $^{87}Sr/^{86}Sr$ versus total Sr^{2+} concentrations indicate that the shallow groundwaters assimilate varying degrees of radiogenic strontium from siliciclastic minerals as they pass through the drift, but equilibrate isotopically with the Devonian carbonates during residence in the bedrock aquifers. A few of the deeper waters also show evidence of mixing with more radiogenic Silurian brines. The carbon isotopic compositions of DIC in the shallow waters span a broad range, but most samples have negative values, suggestive of DIC derived from decay of organic matter or sulphate reduction. However, most of the ^{13}C-depleted compositions are higher than likely generated solely from such processes, which may indicate the involvement of additional processes that disproportionally contribute ^{13}C, such as dissolution of carbonates or methanogenesis. The very ^{13}C-enriched signatures of several samples almost certainly reflect methanogenesis, which seems to be predominantly associated with organic-rich shales, as has been reported in the area by other researchers. Such enriched DIC signatures may represent a possible exploration vector for biogenic shale gas plays.

Underlying the shallow, meteoric groundwater system is a series of deep brine aquifers. They have water oxygen and hydrogen isotopic compositions that plot distinctively to the right of the Global Meteoric Water Line. Their isotopic compositions and Cl/Br ratios strongly indicate that these brines formed from seawater evaporated beyond halite saturation. Dissolved sulphate isotopic compositions are mostly within the range of coeval seawater, although a few samples show evidence of sulphide oxidation and bacterial sulphate reduction. The brine $^{87}Sr/^{86}Sr$ ratios are variably higher than seawater, which is most likely a product of the leaching of radiogenic strontium from siliciclastic minerals. Major ion concentrations indicate that these brines have been significantly modified by diagenetic reactions, most notably dolomitization.

These brines appear to be related to hydrothermal fluids that migrated updip from deeper in the adjacent Appalachian and Michigan basins. Brines in the Salina Group and Guelph Formation may be modified from the hotter and more ^{18}O-enriched fluids that

dolomitized these formations, having later become more depleted of ^{18}O as they cooled and mixed with small amounts of meteoric water; the more extensive dilution apparent in a few samples is likely attributable to anthropogenic activities. The Clinton and Cataract groups contain two distinct brine types, one Na^+-rich and one Ca^{2+}-rich, which may have migrated into these units from depth using different conduits. These brines have been substantially diluted by meteoric water, although whether or not this dilution was natural or anthropogenic remains uncertain. Brines from the Trenton and Black River groups originated from long-distance migration focused within the underlying Cambrian strata. Inside the Ordovician hydrothermal dolomite reservoirs, these brines were then mixed with less-evaporated seawaters expelled from the overlying shales. Brines present today in the Cambrian reservoirs differ from several fluids that have migrated through those units in the past. The present brines may be mixtures between ^{18}O-enriched brines originating from deeper within the adjacent Appalachian and/or Michigan basins, and a more ^{18}O-depleted brine originating from the underlying Canadian Shield.

In future work, measurement of other isotopes could likely be used to improve the SIAR model and supplement our knowledge of these groundwater systems. $\delta^{37}Cl$ and $\delta^{81}Br$ are currently being analyzed for 75 of the samples collected in this study, and other isotope systems may also potentially be of use. For instance, lithium isotopes have proven useful for discriminating between *in situ* vs. marine origin for Canadian Shield brines, as well as assessing the influence of diagenetic mineral formation and mixing with meteoric waters (Bottomley et al., 2003). Further sampling, particularly of some of the less well-represented deep aquifers, such as the Clinton and Cataract groups and Cambrian units, would also be of value for improving the robustness of the geochemical characterization. Detailed petrological and isotopic investigations of the reservoir rocks may also aid in verifying the occurrence and timing of long-distance fluid migrations into southwestern Ontario from the Appalachian and Michigan basins. Studies using radiological dating techniques (e.g., ^{81}Kr, ^{4}He, ^{36}Cl, ^{40}Ar, ^{129}I; see a review by Kazemi et al., 2005), to determine the ages of the brines may also be useful for verifying a seawater-origin hypothesis, whereas a detailed study of $^{3}H(+ ^{3}He)$, ^{14}C, or ^{85}Kr in the shallow aquifers may help assess the residence times of water in those aquifers. Further isotopic regional studies of the shallow aquifers, perhaps involving multi-level wells and time-series

sampling, could investigate complexities in these systems that could not be studied in detail in this project, given the limits on time and sampling. Such studies might also investigate the exact nature and depth of the transitions between the water types (e.g., fresh, sulphurous, brackish/saline) in these aquifers, and the interface with the underlying brines. Finally, a next step in this project should be to integrate the water geochemical data obtained in this study with natural gas isotopic data from various reservoirs that is currently being collected in a separate portion of this project. Such data may help to further refine the source resolution capabilities of the SIAR mixing model, as well as providing complementary information about the origins and evolution of natural gases in southwestern Ontario.

References

Aharon P. and Fu B. (2000) Microbial sulfate reduction rates and sulfur and oxygen fractionations at oil and gas seeps in deepwater Gulf of Mexico. *Geochimica et Cosmochimica Acta* **64**, 233–246.

Angino E. E., Gale K. B. and Andersen N. (1966) Observed variations in the strontium concentration of sea water. *Chemical Geology* **1**, 145–15.

APHA (1998) Standard methods for the examination of water and wastewater, 20th ed. *American Public Health Association*, Washington, D.C.

Aravena R., Wassenaar L. I. and Plummer L. N. (1995) Estimating ^{14}C groundwater ages in a methanogenic aquifer. *Water Resources Research* **31**, 2307-2317.

Armstrong D. K. (2000) Paleozoic geology of the Lake Simcoe area, south-central Ontario. *Ontario Geological Survey,* Open File Report 6011, 51p.

Armstrong D. K. and Dodge J. E. P. (2007) Paleozoic geology of southern Ontario. *Ontario Geological Survey*, Miscellaneous Release – Data 219.

Armstrong D. K. and Carter T. R. (2010) The subsurface Paleozoic stratigraphy of southern Ontario. *Ontario Geological Survey*, Special Volume 7, 301p.

Bailey S. M. B. (1986) A new look at the development, configuration and trapping mechanisms of the Silurian Guelph reefs of southwestern Ontario. In *Proceedings of the Ontario Petroleum Institute, 25th Annual Meeting*, London, Ontario, Technical Paper 16, 28p.

Bailey Geological Services Ltd. and Cochrane, R. O. (1984a) Evaluation of the conventional and potential oil and gas reservoirs of the Ordovician of Ontario. *Ontario Geological Survey*, Open File Report 5498, 77p.

Bailey Geological Services Ltd. and Cochrane, R. O. (1984b) Evaluation of the conventional and potential oil and gas reservoirs of the Cambrian of Ontario. *Ontario Geological Survey*, Open File Report 5499, 72p.

Bailey Geological Services Ltd. and Cochrane, R. O. (1985) Evaluation of the conventional and potential oil and gas reservoirs of the Devonian of Ontario (Volume 1). *Ontario Geological Survey*, Open File Report 5555, 178p.

Barker J. F. and Fritz P. (1981) Carbon isotope fractionation during microbial methane oxidation. *Nature* **293**, 289-291.

Barker J. F. and Pollock S. J. (1984) The geochemistry and origin of natural gases in southern Ontario. *Bulletin of Canadian Petroleum Geology* **32**(3), 313-326.

Barnes D. A., Parris T. M. and Grammer G. M. (2008) Hydrothermal Dolomitization of Fluid Reservoirs in the Michigan Basin, USA. Search and Discovery Article #50087, Adapted from oral presentation at AAPG Annual Convention, San Antonio, Texas.

Barnett P. J., Cowan W. R. and Henry A. P. (1991) Quaternary geology of Ontario, southern sheet. *Ontario Geological Survey*, Map 2556, scale 1:1,000,000.

Barnett P. J. (1992) Quaternary geology of Ontario. In *Geology of Ontario*; Ontario Geological Survey, Special Volume 4, Part 2, p.1011-1090.

Bender M. M. (1968) Mass spectrometric studies of carbon 13 variations in corn and other grasses. *Radiocarbon* **10**(2), 468-472.

Bigeleisen J., Perlman M. L. and Presser H. C. (1952) Conversion of hydrogenic materials to hydrogen for isotopic analysis. *Analytical Chemistry* **24**, 1356-1357.

Birchard M. C., Rutka M. A. and Brunton F. R. (2004) Lithofacies and Geochemistry of the Lucas Formation in the Subsurface of Southwestern Ontario: A High-Purity Limestone and Potential High-Purity Dolostone Resource. *Ontario Geological Survey*, Open File Report 6137, 180p.

Bolton T. E. (1957) Silurian stratigraphy and paleontology of the Niagara Escarpment in Ontario. *Geological Survey of Canada*, Memoir 289, 145p.

Boles J. R. (1978) Active ankerite cementation in the subsurface Eocene of southwest Texas. *Contributions to Mineralogy and Petrology* **68**, 13–22.

Bottomley D. J., Chan L. H., Katz A., Starinski A. and Clark I. D. (2003) Lithium isotope geochemistry and origin of Canadian Shield brines. *Ground Water* **41**(6), 847-856.

Boyce J. J. and Morris W.A. (2002) Basement-controlled faulting of Paleozoic strata in southern Ontario, Canada: New evidence from geophysical lineament mapping. *Tectonophysics* **353**, 151-171.

Brett C. E., Tepper D. H., Goodman W. M., LoDuca S. T. and Eckert, B.-Y. (1995) Revised stratigraphy and correlations of the Niagaran Provincial Series (Medina, Clinton and Lockport groups) in the type area of western New York. *United States Geological Survey*, Bulletin 2086, 66p.

Brett C. E., Tetreault D. K., Goodman W. M. and LoDuca, S. T. (2004) Silurian-Early Devonian sequence stratigraphy, event, and paleoenvironments of the Niagara Peninsula area of New York and adjacent Ontario, Canada. In *Sedimentology and Depositional Environments of Silurian Strata of the Niagara Escarpment, Ontario and New York*. Geological Association of Canada – Mineralogical Association of Canada, Joint Annual Meeting, St. Catherines 2004, Field Trip B4 Guidebook, 56p.

Brigham R.J. (1971) Structural geology of southwestern Ontario and southeastern Michigan. Ph.D. thesis, The University of Western Ontario, London, Ontario, Canada.

Brintnell C. (2012) Architecture and stratigraphy of the Lower Silurian Guelph Formation, Lockport Group, Southern Ontario and Michigan. M. Sc. thesis, The University of Western Ontario, London, Ontario, Canada.

Brogly P. J., Martini I. P. and Middleton G. V. (1998) The Queenston Formation: Shale-dominated, mixed terrigenous-carbonate deposits of Upper Ordovician, semi-arid, muddy shores in Ontario, Canada. *Canadian Journal of Earth Sciences* **35**(6), 702-719.

Brunner B. and Bernasconi S. M. (2005) A revised isotope fractionation model for dissimilatory sulfate reduction in sulfate reducing bacteria. *Geochimica et Cosmochimica Acta* **69**(20), 4759-4771.

Brunner B., Bernasconi S. M., Kleikemper J. and Schroth M. H. (2005) A model for oxygen and sulfur isotope fractionation in sulfate during bacterial sulfate reduction processes. *Geochimica et Cosmochimica Acta* **69**(20), 4773-4785.

Byerley M. and Conigilio M. (1989) Stratigraphy and sedimentology of the Upper Ordovician Georgian Bay Formation, Manitoulin Island and Bruce Peninsula. In *Geoscience Research Grant Program, Summary of Research 1990-1991*, Ontario Geological Survey, Miscellaneous Paper 143, p.227-237.

Carlson E. H. (1994) Geologic, fluid inclusion, and isotopic studies of the Findlay Arch District, Northwestern Ohio. *Economic Geology* **89**(1), 67-90.

Carmody R. W., Plummer L. N., Busenberg E. and Coplen T. B. (1998) Methods for collection of dissolved sulfate and sulfide and analysis of their sulfur isotopic composition. *United States Geological Survey*, Open File Report 97-234.

Carpenter A. B., Trout M. L., and Pickett E. E. (1974) Preliminary report on the origin and chemical evolution of lead- and zinc-rich brines in central Mississippi. *Economic Geology* **52**, 1191–1206.

Carpenter A. B. (1978) Origin and chemical evolution of brines in sedimentary basins. *Oklahoma Geological Survey Circular* **79**, 60–77.

Carter T. R. and Fortner L. (2012) Regional bedrock aquifers and a geological groundwater model for southern Ontario. *International Association of Hydrogeologists, 39th International Congress*, Session TH1-G, Abstract 369, p.238.

Carter T. R., Trevail R. A. and Smith L. (1994) Core workshop: Niagaran reef and inter-reef relationships in the subsurface of southwestern Ontario. *Geological Association of Canada – Mineralogical Association of Canada, Annual Meeting*, Waterloo 1994, Field Trip A5 Guidebook, 38p.

Carter T. R. (1991) Dolomitization patterns in the Salina A-1 and A-2 Carbonate units, Sombra Township, Ontario. In *Proceedings of the Ontario Petroleum Institute, 30th Annual Conference*, London, Ontario, Technical Paper 4, 35p.

Carter T. R. (2012) All is Well: Regional groundwater systems in southern Ontario. *Ontario Petroleum Institute, 2012 Ontario Oil & Gas magazine.*

Cartwright K., Hunt C. S., Hughes G. M. and Brower R. D. (1979) Hydraulic potential in Lake Michigan bottom sediments. *Journal of Hydrology* **43**, 67-78.

Catacosinos P. A., Harrison W. B. and Daniels P. A. Jr. (1990) Structure, stratigraphy and petroleum geology of the Michigan Basin. In *Interior Cratonic Basins*, American Association of Petroleum Geologists, Memoir 51, 561-601.

Cercone K. R. (1988) Evaporative sea-level drawdown in the Silurian Michigan basin. *Geology* **16**, 387-389.

Chacko T., Cole D. R. and Horita, J. (2001) Equilibrium oxygen, hydrogen and carbon isotope fractionation factors applicable to geological systems. In *Stable Isotope Geochemistry* (eds. J. W. Valley and D. R. Cole) Review in Mineralogy 43, Mineralogical Society of America, 1-81.

Chambers L. A. and Trudinger P. A. (1978) Microbiological fractionation of stable sulfur isotopes: A review and critique. *Geomicrobiological Journal* **1**, 249–295.

Clark I. D. and Fritz P. (1997) *Environmental Isotopes in Hydrogeology*. CRC Press, USA.

Clark I., Mohapatra R., Mohammadzadeh H. and Kotzer T. (2010a) Porewater and Gas Analyses in DGR-1 and DGR-2 Core. *Technical Report TR-07-21*, Intera Engineering Ltd., Ottawa.

Clark I., Liu I., Mohammadzadeh H., Mohapatra R., Zhang P. and Wilk M. (2010b) Porewater and Gas Analyses in DGR-3 and DGR-4 Core. *Technical Report TR-08-19*, Intera Engineering Ltd., Ottawa.

Clark I., Scharf V., Zuliani J. and Herod M. (2011) Porewater and Gas Analyses in DGR-3 and DGR-4 Core. *Technical Report TR-09-04*, Intera Engineering Ltd., Ottawa.

Claypool G. E. and Caplan I. R. (1974) The origin and distribution of methane in marine sediments. In *Natural Gases in Marine Sediments* (ed. I. R. Kaplan). Plenum Press, New York, pp. 97-139.

Claypool G. E., Holser W. T., Kaplan I. R., Sakai H. and Zak I. (1980) The age curves of sulfur and oxygen isotopes in marine sulfate and their mutual interpretation. *Chemical Geology* **28**, 199-260.

Clayton R. N., Friedman I., Graf D. L., Mayeda T. K., Meents W. F. and Shimp N. F. (1966) The Origin of Saline Formation Waters - 1. Isotopic Composition. *Journal of Geophysical Research* **71**(16), 3869-3882.

Coleman M. L., Shepherd T. J., Durham J. J., Rouse J. E. and Moore G. R. (1982) Reduction of water with zinc for hydrogen isotope analysis. *Analytical Chemistry* **54**, 993-995.

Collins A.G. (1975) *Geochemistry of Oilfield Waters*. Elsevier, New York, p. 496.

Coniglio M., Williams-Jones A. E. (1992) Diagenesis of Ordovician carbonates from the northeast Michigan Basin, Manitoulin Island area, Ontario: evidence from petrography, stable isotopes and fluid inclusions. *Sedimentology* **39**, 813–36.

Coniglio M., Zheng Q. and Carter T. R. (2003) Dolomitization and recrystallization of middle Silurian reefs and platformal carbonates of the Guelph Formation, Michigan Basin, southwestern Ontario. *Bulletin of Canadian Petroleum Geology* **51**(2), 177-199.

Coplen T. B. and Hanshaw B. B. (1973) Ultrafiltration by a compacted clay membrane – I. Oxygen and hydrogen isotopic fractionation. *Geochimica et Cosmochimica Acta* **37**, 2295-2310.

Coplen T. B. (1994) Reporting of stable hydrogen, carbon, and oxygen isotopic abundances. *Pure and Applied Chemistry* **66**, 273-276.

Coplen T. B. (2011) Guidelines and recommended terms for expression of stable-isotope-ratio and gas-ratio measurement results. *Rapid Communications in Mass Spectrometry* **25**(17): 2538-2560.

Crowley D. J. (1973) Middle Silurian patch reefs in the Gasport Member (Lockport Formation), New York. *American Association of Petroleum Geologists Bulletin* **57**, 283-300.

Dansgaard W. (1964) Stable isotopes in precipitation. *Tellus* **16**(4), 436-468.

Das N., Horita J. and Holland H. D. (1990) Chemistry of fluid inclusions in halite from the Salina Group of the Michigan Basin: Implications for Late Silurian seawater and the origin of sedimentary brines. *Geochimica et Cosmochimica Acta* **54**, 319-327.

Davis S. N. (1964) The chemistry of saline waters by R. A. Krieger – Discussion. *Ground Water* **2**(1): 51.

Desaulniers D. E., Cherry J. A. and Fritz P. (1981) Origin, age and movement of pore water in argillaceous Quaternary deposits at four sites in southwestern Ontario. *Journal of Hydrology* **50**, 231–257.

Dollar P. S., Frape S. K. and McNutt R. H. (1991) Geochemistry of Formation Waters, Southwestern Ontario, Canada and Southern Michigan U.S.A.: Implications for Origin and Evolution. *Ontario Geological Survey,* Ontario Geoscience Research Grant Program, Grant No. 249, Open File Report 5743, 72p.

Donaldson W. S. (1989) The depositional environment of the Queenston shale, southwestern Ontario. In *Proceedings, Ontario Petroleum Institute, 28th Annual Conference*, London, Ontario, Technical Paper 16, 27p.

Dyer B. D. (2003) *A field guide to bacteria*. Cornell University Press, 355p.

Easton R. M. (1992) The Grenville Province and the Proterozoic history of central and southern Ontario. In *Geology of Ontario*, Ontario Geological Survey, Special Volume 4, Part 2, 714-904.

Easton R M and Carter T R (1991) Extension of Grenville basement beneath southwestern Ontario. *Ontario Geological Survey*, Open File Map 162, scale 1:1,013,760.

Eberts S. M. and George L. L. (2000) Regional groundwater flow and geochemistry in the Midwestern basins and arches aquifer system in parts of Indiana, Ohio, Michigan, and Illinois: *U.S. Geological Survey* Professional Paper 1423-C p. C1–C103.

Egeberg P. K. and Aagaard P. (1989) Origin and evolution of formation waters from oil fields on the Norwegian shelf. *Appl. Geochem*. **4**, 131–142.

Elliott W. C. and Aronson J. L. (1987) Alleghanian episode of K-bentonite illitization in the southern Appalachian Basin. *Geology* **15**, 735-739.

Epstein S. and Mayeda T. (1953) Variation of ^{18}O content of waters from natural sources. *Geochimica et Cosmochimica Acta* **4**, 213-224.

Farquhar R. M., Haynes S. J., Mostaghel M. A., Tworo A. G., Macqueen R. W. and Fletcher I. R. (1987) Lead isotope ratios in Niagara Escarpment rocks and galenas: implications for primary and secondary sulphide deposition. *Canadian Journal of Earth Sciences* **24**, 1625-1633.

Fontes, J.-C. and Gonfiantini, R. (1967) Comportement isotopique au cours de l'évaporation de deux bassins Sahariens. *Earth and Planetary Science Letters* **3**, 258-266.

Frape S. K., Fritz P. and McNutt R. H. (1984) Water-rock interaction and chemistry of groundwaters from the Canadian Shield. *Geochimica et Cosmochimica Acta* **48**, 1617-1627.

Freckelton C. N. (2013) A Physical and Geochemical Characterization of Southwestern Ontario's Breathing Well Region. M.Sc. thesis, The University of Western Ontario, London, Ontario, Canada.

Friedman I. (1953) Deuterium content of natural waters and other substances. *Geochimica et Cosmochimica Acta* **4**, 89-103.

Friedman G. M. and Kopaska-Merkel D. C. (1991) Late Silurian pinnacle reefs of the Michigan Basin. *Geological Society of America*, Special Paper 256, 89-100.

Fritz P. and Frape S. K. (1982) Saline groundwaters in the Canadian Shield – A first overview. *Chemical Geology* **36**(1-2), 179-190.

Fritz P., Frape S. K., Drimmie R. J. and Heemskerk A. R. (1986) Reply to comments by Grabczak et al. on "Water-rock interaction and chemistry of groundwaters from the Canadian Shield". *Geochimica et Cosmochimica Acta* **50**, 1561-1563.

Fritz P., Basharmal G. M., Drimmie R. J., Ibsen J. and Qureshi R. M. (1989) Oxygen isotope exchange between sulphate and water during bacterial reduction of sulphate. *Chemical Geology (Isotope Geoscience Section)* **79**, 99-105.

Frizzell R., Cotesta L. and Usher S. (2011) Regional Geology – Southern Ontario. *AECOM Canada Ltd. and Itasca Consulting Canada, Inc*. report for the Nuclear Waste Management Organization NWMO DGR-TR-2011-15 R000. Toronto, Canada.

Fry B., Gest R. and Hayes J. M. (1983). Sulfur isotopic composition of deep-sea hydrothermal vent animals. *Nature* **306**, 51-2.

Fry B., Ruf W., Gest H. and Hayes J. M. (1988) Sulphur isotope effects associated with oxidation of sulfide by O_2 in aqueous solution. *Isotope Geoscience* **73**, 205-210

Gao C., Shirota J., Kelly R. I., Brunton F. R. and van Haaften S. (2006) Bedrock topography and overburden thickness mapping, southern Ontario. *Ontario Geological Survey*, Miscellaneous Release – Data 207, 43p.

Gat J. R. (1984) The stable isotope composition of Dead Sea waters. *Earth and Planetary Science Letters* **71**, 361-376.

Gillespie R., Harrison W. B., and Grammer G. M. (2008) *Geology of Michigan and the Great Lakes*. Cengage Brooks/Cole, Canada.

Ging P. B., Long D. T. and Lee R. W. (1996) Selected geochemical characteristics of ground water from the Marshall aquifer in the central Lower Peninsula of Michigan, *U.S. Geological Survey, Water Resources Investigations*, Report 94-4220, 19p.

Graf D. L., I. Friedman and Meents, W. F. (1965) The origin of saline formation waters, II: Isotopic fractionation by shale micropore systems. *Illinois State Geological Survey*, Circular 393, 38p.

Grieve R.O. (1955) Leaching of Silurian slate beds in southwestern Ontario as evidenced in wells drilled for oil and gas. *Canadian Mining and Metallurgical Bulletin*, January 1955, pp. 12-18.

Haeri-Ardakani O., Al-Aasm I. and Coniglio M. (2013) Fracture mineralization and fluid flow evolution: an example from Ordovician–Devonian carbonates, southwestern Ontario, Canada. *Geofluids* **13**, 1-20.

Hamilton S. M. (2011) Ambient groundwater geochemistry data for southwestern Ontario 2007–2010. *Ontario Geological survey*, Miscellaneous Release – Data 283.

Hanor J. S. (1994) Origin of saline fluids in sedimentary basins. *Geological Society, London, Special Publications* **78**, 151-174.

Harper D. A., Longstaffe F. J., Wadleigh W. A. and McNutt R. H. (1995) Secondary K-feldspar at the Precambrian-Paleozoic unconformity, southwestern Ontario. Canadian Journal of Earth Sciences **32**, 1432-1450.

Harrison A.G. and Thode H.G. (1958) Mechanisms of the bacterial reduction of sulfate from isotope fractionation studies. *Transactions of the Faraday Society* **53**, 84-92.

Hay R. L., Lee M., Kolata D. R., Mathews J. C. and Morton J. P. (1988) Episodic potassic diagenesis of Ordovician tuffs in the Mississippi Valley area. *Geology* **16**, 743-747.

Haynes S. J. and Parkins W. G. (1992) Stratigraphy of the Cayugan Series: Lithofacies of the Bertie and Bass Islands formations, Onondaga Escarpment. In *Geoscience Research Grant Program, Summary of Research 1991-1992*, Ontario Geological Survey, Miscellaneous Paper 159, pp. 22-37.

Heagle D. and Pinder L. (2010) Opportunistic Groundwater Sampling in DGR-3 and DGR-4. *Technical Report TR-08-18,* Intera Engineering Ltd., Ottawa.

Hearn P. P. and Sutter J. K. (1985) Authigenic potassium feldspar in Cambrian carbonates: evidence of Alleghanian brine migration. *Science* **228**, 1529-1531.

Hearn P. P., Sutter J. F. and Belkin, H. F. 1987. Evidence for Late-Paleozoic brine migration in Cambrian carbonate rocks of the central and southern Appalachians: implications for Mississippi Valley-type sulfide mineralization. *Geochimica et Cosmochimica Acta* **51**, 1323-1334.

Henderson R. (2011) New TLV® exposure limit: Measuring hydrogen sulfide. ISHN - Environmental and Occupational Health. http://www.ishn.com/articles/91070-new-tlv-exposure-limit-measuring-hydrogen-sulfide.

Hitchon B. and Friedman I. (1969) Geochemistry and origin of formation waters in the western Canada sedimentary basins -1: Stable isotopes of hydrogen and oxygen. *Geochimica et Cosmochimica Acta* **33**, 1321-1349.

Hoaglund J. R., Kolak J. J., Long D. T. and Larson G. J. (2004) Analysis of modern and Pleistocene hydrologic exchange between Saginaw Bay (Lake Huron) and the Saginaw Lowlands area. *Geological Society of America Bulletin* **116**(1/2), 3-15.

Hobbs M. Y., Frape S. K., Shouakar-Stash O. and Kennel L. R. (2011) Regional Hydrogeochemistry – Southern Ontario. *Nuclear Waste Management Organization* Report NWMO DGR-TR-2011-12 R000. Toronto, Canada.

Holser W. (1979) Trace elements and isotopes in evaporites. In *Marine Minerals* (ed. R. G. Burns), *Reviews in Mineralogy* **6**, 295-346.

Holser W. and Kaplan I. R. (1966) Isotope geochemistry of sedimentary sulfates. *Chemical Geology* **1**, 93-135.

Horita J. (1988) Hydrogen isotope analysis of natural waters using an H_2-water equilibration method: A special implication to brines. *Chemical Geology (Isotope Geoscience Section)* **72**, 89-94.

Horita J. (1989) Analytical aspects of stable isotopes in brines. *Chemical Geology (Isotope Geoscience Section)* **79**, 107-112.

Horita J. (2005) Saline Waters. In *Isotopes in the Water Cycle: Past, Present and Future of a Developing Science* (eds. P. K. Aggarwal, J. R. Gat and K. F. O. Froehlich). IAE, the Netherlands.

Horita J. and Gat J. R. (1988) Procedure for the hydrogen isotope analysis of water from concentrated brines. *Chemical Geology (Isotope Geoscience Section)* **72**, 85-88.

Horita J. and Gat J. R. (1989) Deuterium in the Dead Sea: Remeasurement and implications for the isotope activity correction in brines. *Geochimica et Cosmochimica Acta* **53**, 131-133.

Horita J., David R. C. and Wesolowski D. J. (1993) The activity-composition relationship of oxygen and hydrogen isotopes in aqueous salt solutions: II. Vapor-liquid water equilibration of mixed salt solutions from 50 to 100°C and geochemical implications. *Geochimica et Cosmochimica Acta* **57**, 4703-4711.

Horowitz P., Chiarizia R. and Dietz M. (1992) A novel strontium selective extraction chromatographic resin. *Solvent Extraction Ion Exchange* **10**, 313–336.

Hower J., Eslinger E. V., Hower M. E. and Perry E. A. (1976) Mechanism of burial metamorphism of argillaceous sediments. 1: Mineralogical and chemical evidence. *Geological Society of America Bulletin* **87**, 725–737.

Howell P. D. and van der Pluijm B. A. (1999) Early history of the Michigan basin: Subsidence and Appalachian tectonics. *Geology* **18**, 1195-1198.

Husain M. M., Cherry J. A. and Frape S. K. (2004) The persistence of a large stagnation zone in a developed regional aquifer, southwestern Ontario. *Canadian Geotechnical Journal* **41**, 943-958.

IAEA/WMO (2014). Global Network of Isotopes in Precipitation. The GNIP Database. Accessible at: http://www.iaea.org/water.

Irwin H., Curtis C. and Coleman M. (1977) Isotopic evidence for source of diagenetic carbonates formed during burial of organic-rich sediments. *Nature* **269**, 209-213.

Jackson R. and Heagle D. (2010) Opportunistic Groundwater Sampling in DGR-1 & DGR-2. *Technical Report TR-07-11*, Intera Engineering Ltd., Ottawa.

Johnson M. D., Armstrong D. K., Sanford B. V., Telford P. G. and Rutka M. A. (1992) Paleozoic and Mesozoic geology of Ontario. In *Geology of Ontario*, Ontario Geological Survey, Special Volume 4, Part 2, 907-1008.

Kaplan I. R. and Rafter T. A. (1958) Fractionation of stable isotopes of sulfur by *Thiobacilli*. *Science* **127**, 517-518.

Karim A. and Veizer J. (2000) Weathering processes in the Indus River Basin: implications from riverine carbon, sulfur, oxygen, and strontium isotopes. *Chemical Geology*, **170**(1–4), 153-177.

Karrow P. F. (1974) Till Stratigraphy in Parts of Southwestern Ontario. *Geological Society of America Bulletin* **85**, 761-768.

Kazemi G. A., Lehr J. H. and Perrochet, P. (2005) Age-Dating Very Old Groundwaters. In *Groundwater Age*, John Wiley & Sons, Inc., Hoboken, NJ, USA.

Kerr M. and Eyles N. (1991) Storm-deposited sandstones (tempestites) and related ichnofossils of the Late Ordovician Georgian Bay Formation, southern Ontario, Canada. *Canadian Journal of Earth Sciences* **28**, 226-282.

Kendall C. and Caldwell E. (1998). Fundamentals of Isotope Geochemistry. In *Isotope Tracers in Catchment Hydrology* (eds. C. Kendall and J. J. McDonnell). Elsevier Science B.V., Amsterdam. pp. 51-86.

Kharaka Y. K., Maest A. S., Carothers W. W., Law L. M., Lamothe P. J. and Fries, T. L. (1987) Geochemistry of metal-rich brines from central Mississippi Salt Dome Basin, U.S.A. *Applied Geochemistry* **2**, 543-561.

Kharaka Y.K. and Hanor J.S. (2007) Deep fluids in the continents: I. Sedimentary basins. In *Surface and Ground Water, Weathering and Soils, Treatise on Geochemistry, vol. 5* (ed. J. I. Drever). Elsevier, pp. 1-48.

Knauth L. P. and Beeunas M. A. (1986) Isotope geochemistry of fluid inclusions in Permian halite with implications for the isotopic history of ocean water and the origin of saline formation. *Geochimica et Cosmochimica Acta* **50**, 419-433.

Kobluk D. R. and Brookfield M. E. (1982) Excursion 12A: Lower Paleozoic carbonate rocks and paleoenvironments in southern Ontario. *International Association of Sedimentologists, 11th International Congress on Sedimentology*, McMaster University, Hamilton, Ontario, Field Excursion Guidebook, 62p.

Kohn M. (2010) Carbon isotope compositions of terrestrial C3 plants as indicators of (paleo)ecology and (paleo)climate. *Proceedings of the National Academy of Sciences* **107**(46): 19691-19695.

Kolak J. J., Long D. T., Matty J. M., Larson G. J., Sibley D. F. and Councell T. B. (1999) Ground-water, large-lake interactions in Saginaw Bay, Lake Huron: A geochemical and isotopic approach. *Geological Society of America Bulletin* **111**(2), 177–188.

Kroopnick P. M. and Craig I. (1972) Isotopic composition of molecular oxygen in the atmosphere and the sea. *Transactions - American Geophysical Union* **52**, 255.

Krouse H. R. and Mayer B. (2000) Sulphur and oxygen isotopes in sulphate. In: *Environmental Tracers in Subsurface Hydrology* (eds. P. G. Cook and A. L. Herczeg). Kluwer Academic Press, Boston, pp. 195-231.

Land L. S. (1985) The origin of massive dolomite. *Journal of Geological Education* **33**, 112–25.

Land L. S. (1997) Mass transfer during burial diagenesis in the Gulf of Mexico sedimentary basin: An overview. In *Basinwide Fluids Flow and Associated Diagenetic Patterns, Special Publication 56* (eds. I. Montanez, J. M. Gregg and K. S. Shelton), (SEPM) Society for Sedimentary Geology, pp. 29–40.

Land L.S. and Prezbindowski D.R. (1981) The origin and evolution of saline formation water, Lower Cretaceous carbonates, south-central Texas, USA. *Journal of Hydrology* **54**, 51-74.

Lazorek L. and Carter T. R. (2008) *The Oil and Gas Plays of Ontario*. Ontario Petroleum Institute, 2008 Ontario Oil & Gas magazine.

Lee M. and Aronson J.L. (1991) Repetitive occurrence of potassic diagenesis in the region of the Upper Mississippi Valley (UMV) mineral district: implications for a persistent paleo-hydrological setting favorable for diagenesis. *Clay Minerals Society, 28th Annual Meeting*, Houston, Texas, 98p.

Leighton M. W. (1996) Interior cratonic basins: A record of regional tectonic influences. In *Basins and basement of eastern North America* (eds. B. A. van der Pluijm and P. A. Catacosinos) Geological Society of America Special Paper 308, 77–93, Boulder, Colorado.

Lesage S., Jackson R. E., Priddle M., Beck P. and Raven K. G. (1991) Investigation of possible contamination of shallow ground water by deeply injected liquid industrial wastes. *Groundwater Monitoring & Remediation* **11**(1), 151-159.

Liberty B. A. (1969) Paleozoic geology of the Lake Simcoe area, Ontario. *Geological Survey of Canada*, Paper 65-41, 8p.

Liberty B. A. and Bolton T. E. (1971) Paleozoic geology of the Bruce Peninsula area, Ontario. *Geological Survey of Canada*, Memoir 360, 163p.

Lilienthal R. T. (1978) Stratigraphic cross-sections of the Michigan Basin. *Michigan Department of Natural Resources, Geological Survey Division*, Report of Investigation 19, 36p.

Lin G. and Ehleringer J. R. (1997) Carbon isotopic fractionation does not occur during dark respiration in C3 and C4 plants. *Plant Physiology* **114**(1): 391–394.

Liu J., Hay R. L., Deino A. and Kyser T. K. (2003) Age and origin of authigenic K-feldspar in uppermost Precambrian rocks in the North American Midcontinent. *GSA Bulletin* **115**(4), 422–433.

Lloyd R. M. (1966) Oxygen isotope enrichment of sweater by evaporation. *Geochimica et Cosmochimica Acta* **30**, 801-819.

Long D. T., Wilson T. P., Takacs M. J. and Rezabek D. H. (1988) Stable-isotope geochemistry of saline near-surface ground water: East-central Michigan basin. *Geological Society of America Bulletin* **100**, 1568-1577.

Longstaffe F. J., Ayalon A., Bumstead N. L., Crowe A. S., Hladyniuk R., Hornibrook P. A., Hyodo A. and Macdonald R.A. (2011) The oxygen-isotope evolution of the North American Great Lakes. Northeastern (46th Annual) and North-Central (45th Annual) Joint Meeting of the Geological Society of America, Pittsburgh, Pennsylvania, USA, March 20-22, 2011, p. 57.

Lowry R. M., Faure G., Mullet D. I. and Jones L. M. (1988) Interpretation of chemical and isotopic compositions of brines based on mixing and dilution, "Clinton" sandstones, eastern Ohio, U.S.A. *Applied Geochemistry* **3**, 174-184.

Ma L., Castro M. C., Hall C. M. and Walter L. M. (2005) Cross-formational flow and salinity sources inferred from a combined study of helium concentrations, isotopic ratios, and major elements in the Marshall aquifer, southern Michigan. *Geochemistry, Geophysics, Geosystems* **6**(10), 1-21.

Machel H.G. (2001) Bacterial and thermochemical sulfate reduction in diagenetic settings – old and new insights. *Sedimentary Geology* **140**, 143-175.

Matheson E. (2012) Analysis of the anomalous groundwater geochemistry of the Niagara Peninsula, Ontario, Canada. B. Sc. thesis, Queen's University, Kingston, Ontario, Canada.

Martini A. M., Walter L. M., Budai J. M., Ku T. C. W., Kaiser C. J. and Schoell M. (1998) Genetic and temporal relations between formation waters and biogenic methane: Upper Devonian Antrim Shale, Michigan Basin, USA. *Geochimica et Cosmochimica Acta* **62**(10), 1699-1720.

Matray J.-M. (1988) Hydrochimie et géochime isotopiques des eaux de réservoir pétrolier du trias et du dogger dans le bassin de Paris. Thése, Université de Paris XI, Paris, 119p.

Mazurek M. (2004) Long-term used nuclear fuel waste management - Geoscientific review of the sedimentary sequence in southern Ontario. *University of Bern Technical Report TR 04-01*. Bern, Switzerland, 104p.

McCaffrey M. A., Lazar B. and Holland H. D. (1987) The evaporation path of seawater and the coprecipitation of Br^- and K^+ with halite. *Journal of Sedimentary Petrology* **57**(5), 928-937.

McIntosh J. C., Walter L.M. and Martini A. M. (2002) Pleistocene recharge to midcontinent basins: effects on salinity structure and microbial gas generation. *Geochimica et Cosmochimica Acta* **66**(10), 1681–1700.

McIntosh J. C. and Walter L. M. (2006) Paleowaters in Silurian-Devonian carbonate aquifers: Geochemical evolution of groundwater in the Great Lakes region since the late Pleistocene. *Geochimica et Cosmochimica Acta* **70**, 2454-2479.

McIntosh J. C., Walter L. M. and Martini A. M. (2004) Extensive microbial modification of formation water geochemistry: Case study from a Midcontinent sedimentary basin, United States. *Geological Society of America Bulletin* **116**(5/6), 749-759.

McIntosh J.C., Garven G. and Hanor J.S. (2011) Impacts of Pleistocene glaciation on large-scale groundwater flow and salinity in the Michigan Basin. *Geofluids* **11**, 18-33.

McNutt R. H., Frape S. K. and Dollar P. (1987) A strontium, oxygen and hydrogen isotopic composition of brines, Michigan and Appalachian Basins, Ontario and Michigan. *Applied Geochemistry* **2**, 495-505.

Melchin M. J., Brookfield M. E., Armstrong D. J. and Coniglio M. (1994) Stratigraphy, sedimentology and biostratigraphy of the Ordovician rocks of the Lake Simcoe area, south-central Ontario. *Geological Association of Canada – Mineralogical Association of Canada, Joint Annual Meeting*, Waterloo 1994, Field Trip A4 Guidebook, 101p.

Middleton K. (1991) Fracture-related diagenesis of Middle Ordovician carbonate reservoirs, southwestern Ontario. M.Sc. Thesis, University of Waterloo, Waterloo, Ontario, Canada.

Miles M. C., Appleyard E. C., Fritz P., Frape S. K., Lawson D. E., O'Shea K. and Lapcevic P. (1986) Geochemical Study of the Salina Group of Southern Ontario: Isotopes and Major and Minor Elements. *Ontario Geological Survey Open File Report 5619*, 93p.

Mizutani Y. and Rafter T. A. (1969) Oxygen isotopic composition of sulphates, Part 4. *New Zealand Journal of Science* **12**, 60-68.

Mook W. G. (2001) Environmental Isotopes in the Hydrological Cycle: Principles and Applications, Vol. I: Introduction - Theory, Methods, Review, 1 (2000). *International Atomic Energy Agency*.

Moore J. W. and Semmens B. X. (2008) Incorporating uncertainty and prior information into stable isotope mixing models. *Ecology Letters* **11**, 470-480.

Mostaghel M.A. (1983). Genesis of disseminated sulphide assemblages in Niagara Peninsula, Canada. *Geologische Rundschau* **72**, 353-375.

O'Neil J. R. and Kharaka Y. F. (1976) Oxygen isotope exchange reactions between clay minerals and water. *Geochimica et Cosmochimica Acta* **40**, 241-246.

OEB (2014) History of the OEB: 1907-1959. http://www.ontarioenergyboard.ca/OEB/Industry/ About+the+OEB/Legislation/History+of+the+OEB. Queens Printer for Ontario.

OGSR (2009) Summary of Oil and Natural Gas Exploration, Production and Underground Storage in Ontario. *Ontario Oil, Gas & Salt Resources Library*, London, Ontario.

OMFA (2011) Southern Ontario Region at a Glance – 2011 Census of Agriculture and Strategic Policy Branch, *Ontario Ministry of Food and Agriculture*.

OMNR (2013) The Abandoned Works Program. Ontario Ministry of Natural Resources. http://www.mnr.gov.on.ca/en/Business/OGSR/2ColumnSubPage/STEL02_167093.html

Park R. and Epstein S. (1961) Metabolic fractionation of C13 & C12 in plants. *Plant Physiology* **36**(2): 133–138.

Parnell A. C., Inger R., Bearhop S. and Jackson A. L. (2010) Source partitioning using stable isotopes: coping with too much variation. *PLoS ONE* **5**, 1-5.

Pearson F. J. (1987) Models of mineral controls on the composition of saline groundwaters of the Canadian Shield. In, *Saline water and gases in crystalline rocks* (eds, Fritz P. and Frape S. K.) Geological Association of Canada Special Paper 33, pp. 39-51.

Pemberton S. G. (1987) Ichnology of the Thorold Sandstone in the vicinity of Hamilton, Ontario: A Silurian storm-influenced deposit. In *Sedimentology, Stratigraphy and Ichnology of the Lower Silurian Medina Formation in New York and Ontario*, Guidebook for the 1987 Annual Field Trip of the Eastern Section of the Society of Economic Paleontologists and Mineralogists, pp. 66-80.

Person M., McIntosh J., Bense V. and Remenda V. H. (2007) Pleistocene hydrology of North America: The role of ice sheets in reorganizing groundwater flow systems. *Reviews of Geophysics* **45**(3), 1-28.

Peterman Z. E., Hedge C. E. and Tourtelot H. A. (1970) Isotopic composition of strontium in seawater throughout Phanerozoic time. *Geochimica et Cosmochimica Acta* **34**, 105-120.

Phillips, D. L. (2001) Mixing models in analyses of diet using multiple stable isotopes: a critique. *Oecologia* **127**, 166-170.

Phillips, D. L. and Gregg, J. W. (2003) Source partitioning using stable isotopes: coping with too many sources. *Oecologia* **136**, 261-269.

Piper A.M. (1944) A graphical procedure in the geochemical interpretation of water analyses. *American Geophysical Union Transactions* **25**, 914-923.

Qureshi R. M. (1986) The isotopic composition of aqueous sulphate - A laboratory investigation. Ph.D. thesis, University of Waterloo, Waterloo, Ontario, Canada.

Raiswell R. (1987) Non-steady state microbiological diagenesis and the origin of concretions and nodular limestones. In *Diagenesis of Sedimentary Sequences* (ed. J. D. Marshall), Geological Society Special Publication No. 36, pp. 41-54.

Rees C. E. (1973) A steady-state model for sulphur isotope fractionation in bacterial reduction processes. *Geochimica et Cosmochimica Acta* **37**, 1141–1162.

Révész K. and Coplen T. B. (2008) Determination of the $\delta(^2H/^1H)$ of Water: RSIL Lab Code 1574, In *Methods of the Reston Stable Isotope Laboratory: U.S. Geological Survey Techniques and Methods 10–C1* (eds. K. Révész and T. B. Coplen), 27p.

Rittenhouse G. (1967) Bromine in oil-field waters and its use in determining possibilities of origin of these waters. *American Association of Petroleum Geologists Bulletin* **51**, 2430–2440.

Russell D. J. (1993) Role of the Sylvania Formation in sinkhole development, Essex County. *Ontario Geological Survey*, Open File Report 5861, 122p.

Rutka M. A., Cheel R. J., Middleton G. V. and Salas C. J. (1991) The Lower Silurian Whirlpool Sandstone. In *Sedimentary and Depositional Environments of Silurian Strata of the Niagara Escarpment, Ontario and New York*. Geological Association of Canada – Mineralogical Association of Canada – Society of Economic Geologists, Joint Annual Meeting, Toronto 1991, Field trip B4 Guidebook, pp. 27-34.

Sanford B. V. (1961) Subsurface stratigraphy of Ordovician rocks in southwestern Ontario. *Geological Survey of Canada*, Paper 60-26, 54p.

Sanford B. V. (1968) Devonian of Ontario and Michigan. In *International Symposium of the Devonian System, Alberta Society of Petroleum Geologists*, v.1, 973-999.

Sanford B. V. (1969) Silurian of southwestern Ontario. In *Proceedings of the Ontario Petroleum Institute, 8th Annual Conference*, Toronto, Ontario, v.8, Technical Paper 5, 44p.

Sanford B. V. (1977) Distribution, thickness and three-dimensional geometry of salt deposits in southwestern Ontario. *Geological Survey of Canada*, Open File 401, 11 maps and section, scales 1:250 000 and 1:125 000.

Sanford B. V. and Quillian R. G. (1959) Subsurface stratigraphy of Upper Cambrian rocks in southwestern Ontario. *Geological Survey of Canada*, Paper 58-12, 33p.

Sharma S. and Dix G. R. (2004) Magnesian calcite and chamositic ooids forming shoals peripheral to Late Ordovician (Ashgill) muddy siliciclastic shores: southern Ontario. *Palaeogeography, Palaeoclimatology, Palaeoecology* **210**, 347-366.

Sharpe D. R., Piggott A., Carter T. R., Gerber R. E., MacRitchie S. M., de Loe R., Strynatka S. and Zwiers G. (2014) Southern Ontario hydrogeological region. In *Canada's Groundwater Resources* (ed. A. Rivera), Fitzhenry and Whiteside, Canada, pp. 444-499.

Sherwood Lollar B. and Frape S. K. (1989) Report on Hydrogeochemical and isotopic investigations at Ontario Hydro UN-2 and OHD-1 Boreholes. *Contract # GHED 88-1, Ontario Hydro Report*, 30p.

Shields, G. and Veizer, J. (2002) Precambrian marine carbonate isotope database: Version 1.1. *Geochemistry, Geophysics, Geosystems* **3**(6), pp. 1-12.

Shouakar-Stash O. (2008) Evaluation of stable chlorine and bromine isotopes in sedimentary formation fluids. Ph.D. thesis, University of Waterloo, Waterloo, Ontario, Canada.

Sidle W. C. (2002) $^{18}O_{SO4}$ and $^{18}O_{H2O}$ as prospective indicators of elevated arsenic in the Goose River ground-watershed, Maine. *Environmental Geology* **42**, 350–359.

Siegel D. I. and Mandle R. J. (1984) Isotopic evidence for glacial melt water recharge to the Cambrian-Ordovician Aquifer, northcentral United States. *Quaternary Research* **22**, 328–335.

Sima A., Paul A., Schulz M. and Oerlemans J. (2006) Modeling the oxygen-isotopic composition of the North American Ice Sheet and its effect on the isotopic composition of the ocean during the last glacial cycle. *Geophysical Research Letters* **33**, 1-5.

Sofer Z. and Gat J. R. (1972) Activities and concentrations of oxygen-18 in concentrated aqueous salt solutions: Analytical and geophysical implications. *Earth and Planetary Science Letters* **15**, 232-238.

Sofer Z. and Gat J. R. (1975) The isotopic composition of evaporating brines: Effects of the isotope activity ratio in saline solutions. *Earth and Planetary Science Letters* **26**, 179-186.

Stewart M. K. and Friedman I. (1975) Deuterium fractionation between aqueous salt solutions and water vapor. *Journal of Geophysical Research* **80**, 3812-3818.

Stoessell R.K. and Carpenter A.B. (1986) Stoichiometric saturation tests of $NaCl_{1-x}Br_x$ and $KCl_{1-x}Br_x$. *Geochimica et Cosmochimica Acta* **50**, 1465-1474

Stiller M., Rounick J. S., and Shasha, S. (1985) Extreme carbon-isotopic enrichments in evaporating brines. *Nature* **316**, 434-435.

Stueber A. M., Pushkar P. and Baldwin A. D. (1972) Survey of $^{87}Sr/^{86}Sr$ ratios and total strontium concentrations in Ohio stream and ground waters. *Ohio Journal of Science* **72**, 97-104.

Sykes J. F., Normani S. D. and Yin Y. (2011) Hydrogeologic Modelling. Nuclear Waste Management Organization Report NWMO DGR-TR-2011-16 R000. Toronto, Canada.

Taube H. (1954) Use of oxygen isotope effects in the study of hydration of ions. *Journal of Physical Chemistry* **58**, 523-528.

Taylor B. E. and Wheeler M. C. (1984) Isotope composition of sulphate in acid mine drainage as measure of bacterial oxidation. *Nature* **308**, 538-541.

Thode H.G. and Monster J. (1965) Sulfur-isotope geochemistry of petroleum, evaporites, and ancient seas. In *Fluids in subsurface environments* (eds. A. Young and J. E. Galley), American Association of Petroleum Geologists Memoir **4**, p. 367–377.

Thode H. G. (1991) Sulphur Isotopes in Nature and the Environment: An Overview. In *Stable Isotopes in the Assessment of Natural and Anthropogenic Sulphur in the Environment* (eds. H. R. Krouse and V. A.Grinenko). John Wiley & Sons Ltd., Chichester, New York, Brisbane, Toronto, Singapore, 26p.

Tieszen L. L. and Fagre T. (1993) Carbon isotopic variability in modern and archeological maize. *Journal of Archaeological Science* **20**, 25-40.

Tiller C. and Selleck B. (1992) Mineralogy and geochemistry of sub-potsdam sandstone Proterozoic gneisses, northern New York State. *Geological Society of America, Northeastern Section, Abstracts with Programs* **24**, 81.

Torres M. E., Mix A. C. and Rugh W. D. (2005) Precise δ13C analysis ofdissolved inorganic carbon in natural water using automatedheadspace sampling and continuous-flow mass spectrometry. *Limnology and Oceanography: Methods* **3**, 349-360.

Trevail R. A. (1990) Cambro-Ordovician shallow water sediments, London area, southwestern Ontario. In *Subsurface Geology of Southwestern Ontario: A Core Workshop, American Association of Petroleum Geologists, 1990 Eastern Section Meeting*, London, Ontario, pp. 29-50.

Trevail R. A., Carter T. R. and McFarland S. (2004) Trenton-Black River hydrothermal dolomite reservoirs in Ontario: An assessment of remaining potential after 100 years of production. In *Proceedings of the Ontario Petroleum Institute, 43rd Annual Conference*, Niagara Falls, Ontario, v.43, Technical paper 15, 36p.

Tsujita C. J., Tetreault D. K. and Jin J. (2001) Middle and Upper Devonian strata of southwestern Ontario. *Canadian Paleontology Conference*, Field Trip no.9, 57p.

Tworo A.G. (1985) The nature and origin of lead-zinc mineralization, Middle Silurian dolomites, southern Ontario. M.Sc. thesis, University of Waterloo, Waterloo, Ontario Canada.

Veizer J. and Compston W. (1974) ^{87}Sr/^{86}Sr composition of seawater during the Phanerozoic. *Geochimica et Cosmochimica Acta* **38**, 1461-1484.

Veizer J., Ala D., Azmy K., Bruckschen P., Buhl D., Bruhn F., Carden G., Diener A., Ebneth S., Godderis Y., Jasper T., Korte C., Pawellek F., Podlaha O. and Strauss H. (1999) ^{87}Sr/^{86}Sr, δ^{13}C and δ^{18}O evolution of Phanerozoic seawater. *Chemical Geology* **161**, 59-88.

Weaver T. R. (1994) Groundwater flow and solute transport in shallow Devonian bedrock formations and overlying Pleistocene units, Lambton County, southwetsern Ontario. Ph.D. thesis, University of Waterloo, Waterloo, Ontario, Canada.

Weaver T. R., Frape S. K. and Cherry J. A. (1995) Recent cross-formational fluid flow and mixing in the shallow Michigan Basin. *GSA Bulletin* **107**(6), 697-707.

Whiticar M. J. (1999) Carbon and hydrogen isotope systematics of bacterial formation and oxidation of methane. *Chemical Geology* **161**, 291-314.

Whitney G. and Northrop H. R. (1987) Diagenesis and fluid flow in the San Juan basin, New Mexico – regional zonation in the mineralogy and stable isotope composition of clay minerals in sandstone. *American Journal of Science* **287**, 353-382.

Wickman F. W. (1948) Isotope ratios – A clue to the age of certain marine sediments. *Journal of Geology* **56**, 61-66.

Wilson T. P. and Long D. T. (1993a) Geochemistry and isotope chemistry of Michigan Basin brines: Devonian formations. *Applied Geochemistry* **8**, 81-100.

Wilson T. P. and Long D. T. (1993b) Geochemistry and isotope chemistry of Ca-Na-Cl brines in Silurian strata, Michigan Basin, U.S.A. *Applied Geochemistry* **8**, 507-524.

Worden R. H., Coleman M. L., and Matray J. M. (1999) Basin scale evolution of formation waters: a diagenetic and formation water study of the Triassic Chaunoy Formation, Paris Basin. *Geochimica et Cosmochimica Acta* **63**, 2513-2528.

U.S. EPA (1994) Method 200.8: Determination of Trace Elements in Waters and Wastes by Inductively Coupled Plasma-Mass Spectrometry, Revision 5.4.

U.S. EPA (1997) Method 300.1: Determination of Inorganic Anions in Drinking Water by Ion Chromatography, Revision 1.0.

U.S. EPA (2001) Method 200.7: Determination of Metals and Trace Elements in Water and Wastes by Inductively Coupled Plasma-Atomic Emission Spectrometry, Revision 5.0.

Vugrinovich R. (1986) Patterns of Regional Subsurface Fluid Movement in the Michigan Basin. *Michigan Geological Survey Division*, Open File Report, OFR 86-6. Lansing, Michigan.

Vugrinovich R. (1987) Regional heat flow variations in the northern Michigan and Lake Superior region determined using the silica heat flow estimator. *Journal of Volcanology and Geothermal Research* **34**, 15-24.

Zheng Q. (1999) Carbonate diagenesis and porosity evolution in the Guelph Formation, southwestern Ontario. Ph.D. thesis, University of Waterloo, Waterloo, Ontario, 265p.

Ziegler K. and Longstaffe F. J. (2000) Clay mineral authigenesis along a mid-continent scale fluid conduit in Palaeozoic sedimentary rocks from southern Ontario, Canada. *Clay Minerals* **35**, 239-260.

Appendix A

Sample locations & δ^{18}O values* by formation

*on concentration scale

Shallow waters
$\delta^{18}O$ ‰ (VSMOW)

- ● -18 to -16
- ● -16 to -14
- ● -14 to -12
- ● -12 to -10
- ● -10 to -8
- ● -8 to -6

Bedrock Geology

- 33: Port Lambton Group
- 32: Kettle Point
- 31: Hamilton Group
- 30: Marcellus
- 29: Dundee
- 28: Lucas
- 27: Amherstburg
- 26: Onondaga
- 25: Bois Blanc
- 24: Oriskany
- 23: Bass Islands
- 22: Bertie
- 21: Salina
- 20: Guelph
- 19: Amabel
- 18: Lockport
- 17: Clinton-Cataract Group
- 16: Queenston

Salina-Guelph
$\delta^{18}O$ ‰ (VSMOW)
- -7 to -5
- -5 to -3
- -3 to -1
- -1 to +1
- +1 to +5
- +3 to +5

Bedrock Geology

33: Port Lambton Group	24: Oriskany
32: Kettle Point	23: Bass Islands
31: Hamilton Group	22: Bertie
30: Marcellus	21: Salina
29: Dundee	20: Guelph
28: Lucas	19: Amabel
27: Amherstburg	18: Lockport
26: Onondaga	17: Clinton-Cataract Group
25: Bois Blanc	16: Queenston

Appendix B

General Sample Information

Sample ID	Pool	Formation of origin	Estimated Depth (m)	Latitude	Longitude	Sampling date	Collection details
Port Dover Quarry 1	-	Dundee (subcrop)	~20	42.80996	-80.18800	26-Jun-12	quarry seep
Port Dover Quarry 2	-	Dundee (subcrop)	~20	42.80996	-80.18800	26-Jun-12	quarry seep
T012149 (D)	-	Dundee (subcrop)	43	43.29517	-81.71305	18-Jan-12	cable-tool rig bailer
T012101	Dunwich 4-24-A	Dundee	102-108	42.71166	-81.44440	08-Sep-11	cable-tool rig bailer
T011050	Oil Springs	Dundee	76	42.77627	-82.10537	18-Apr-12	well production line
T012150 (D)	-	Dundee	51	42.22711	-82.63942	03-Apr-12	cable-tool rig bailer
T009537	Bothwell-Thamesville	Dundee	67.4-110.3	42.60437	-81.89577	30-Aug-12	wellhead
T009536	Bothwell-Thamesville	Dundee	100	42.60383	-81.89622	30-Aug-12	wellhead
T008979	Bothwell-Thamesville	Dundee	100	42.60619	-81.87140	30-Aug-12	wellhead
F013661	-	Dundee	50	42.85697	-80.72996	28-Nov-12	abandoned well seep
T012111	Bayham	Dundee	80	42.66543	-80.79428	12-Jan-12	abandoned well seep†
T012111 (2)	Bayham	Dundee	80	42.66543	-80.79428	8-Aug-12	abandoned well seep†
T012111 (3)	Bayham	Dundee	80	42.66543	-80.79428	06-Sep-12	abandoned well seep
F005427	-	Dundee	47	42.73979	-80.51132	26-Jun-12	pipe from abandoned well discharging into a stream (underwater)
T010678	Aldborough 7-D-VII	Columbus	131	42.54237	-81.72623	16-Mar-11	brine separator
TAQA North battery	Rodney	Columbus	~120	42.58342	-81.74037	24-Aug-12	brine tank †
T009308	Rodney	Columbus	125.6-130.8	42.57047	-81.72586	24-Aug-12	wellhead †
T007578	Rodney	Columbus	113.4-117.7	42.57889	-81.73362	24-Aug-12	wellhead †
T012124(L)	Paton	Lucas	129-178	42.71146	-81.44415	08-Sep-11	cable-tool rig bailer
T012145 (L1)	(Tecusmeh-Seckerton)	Lucas	196-198	42.86135	-82.37386	24-Jan-12	cable-tool rig bailer
T012145 (L2)	(Tecusmeh-Seckerton)	Lucas	206	42.86135	-82.37386	25-Jan-12	cable-tool rig bailer
T012146	(Tecusmeh-Seckerton)	Lucas	194	42.86864	-82.37188	02-May-12	cable-tool rig bailer
Oil Springs 2	Oil Springs	Lucas	120	42.77164	-82.10936	18-Apr-12	brine tank
Oil Springs 3	Oil Springs	Lucas	120	42.77131	-82.11694	18-Apr-12	brine tank

Sample ID	Pool	Formation of origin	Estimated Depth (m)	Latitude	Longitude	Sampling date	Collection details
Oil Springs 4	Oil Springs	Lucas	120	42.76842	-82.11292	18-Apr-12	brine tank
T012152 (L)	Dunwich 4-24-A	Lucas	120	42.71160	-81.43761	23-Apr-12	cable-tool rig bailer
T009650	Petrolia (center)	Lucas	139.9	42.89075	-82.13469	30-Aug-12	wellhead †
T010111	Petrolia (NW)	Lucas	134.1-140.2	42.90093	-82.15177	30-Aug-12	wellhead
T005511	Petrolia (NW)	Lucas	134.1-140.2	42.90401	-82.15563	30-Aug-12	wellhead
LAI front battery	Petrolia (NW)	Lucas	140	42.90303	-82.15225	30-Aug-12	brine tank
T011355	Petrolia (SE)	Lucas	140	42.88017	-82.11078	30-Aug-12	wellhead
T011323	Petrolia (SE)	Lucas	140	42.87421	-82.11264	30-Aug-12	wellhead †
T012149 (L)	-	Lucas	88	43.29517	-81.71305	01-Feb-12	cable-tool rig bailer
McGregor Quarry	-	Lucas	21-27.5	42.16141	-83.01296	26-Apr-12	quarry seep
St Mary's Quarry	-	Lucas	20	43.24493	-81.16543	04-Oct-13	wellhead
Goderich harbour well	-	Lucas	50	43.74348	-81.72415	18-Oct-12	wellhead
T012135	-	Amherstberg	240	42.92330	-81.97176	23-Jan-12	cable-tool rig bailer
T012152 (DR)	Dunwich 4-24-A	Amherstberg	190	42.71160	-81.43761	10-May-12	cable-tool rig bailer
T002484	(subcrop)	Salina E-unit	50	43.20921	-80.62942	28-Mar-12	abandoned well seep
T012177	-	Bass Islands	198	43.74606	-81.726041	04-Sept-13	cable-tool rig bailer
T012177 (2)	-	Bass Islands		43.74606	-81.726041	11-Sept-13	cable-tool rig bailer
Sulphur Springs C.A.	(subcrop)	Salina E unit	~27	44.11880	-80.99969	18-Oct-12	artesian spring
Brantford spring	(subcrop)	Salina A-2 carbonate	~15	43.16876	-80.31190	25-Jul-12	artesian spring
Goderich salt mine N	-	Salina A-2 carbonate	510	43.76583	-81.76806	14-Mar-12	dewatering pipe
Goderich salt mine S	-	Salina A-2 carbonate	510	43.72694	-81.74750	14-Mar-12	dewatering pipe
T007498	Camden 6-10-IX Gore	Salina A-2 carbonate	450.5-457.5	42.62507	-82.09549	29-Mar-12	wellhead
T008641	Morpeth	Salina A-2 carbonate	495	42.36502	-81.84347	12-Feb-13	wellhead
T008633	Botany	Salina A-1 carbonate	509.9-512.4	42.50689	-81.99964	14-Feb-12	brine tank
T007583	Moore 5-50-Front	Salina A-1 carbonate	740.5-748.5	42.87128	-82.45181	29-Mar-12	brine tank
T001539	Brigden	Salina A-1 carbonate	647.4	42.81388	-82.31104	25-Jul-12	wellhead
T011888	Brigden	Salina A-1 carbonate	653-657	42.81135	-82.31423	25-Jul-12	brine tank
T008595	Becher West	Salina A-1 carbonate	579.4-580.6	42.64037	-82.41781	02-Oct-12	wellhead †
T008596	Becher West	Salina A-1 carbonate	579.7-582.2	42.63260	-82.41840	02-Oct-12	brine tank
T008592	Becher West	Salina A-1 carbonate	583.7	42.63567	-82.43857	02-Oct-12	wellhead †
T003536	Brooke	Salina A-1 carbonate	514-518	42.89243	-81.96937	02-Oct-12	wellhead
T011190	Aldborough 4-15-IV	Guelph/Salina A-1	450	42.62847	-81.69167	16-Mar-11	brine tank
T008657-1	Tuckersmith 30-III-SHR	Guelph	490-508	43.57030	-81.49271	30-Mar-12	brine tank
T008657-2	Tuckersmith 30-III-SHR	Guelph	490-508	43.57030	-81.49271	30-Mar-12	wellhead
T002235	Dungannon	Guelph	468.8-537.1	43.87826	-81.54383	05-Jun-12	wellhead †

Sample ID	Pool	Formation of origin	Estimated Depth (m)	Latitude	Longitude	Sampling date	Collection details
T012124(G) - A	Paton	Guelph	421	42.71146	-81.44415	07-Oct-11	cable-tool rig bailer
T012124(G) - B	Paton	Guelph	421	42.71146	-81.44415	07-Oct-11	cable-tool rig bailer
T012150 (G)	-	Guelph	428-430	42.22711	-82.63942	05-Jun-12	cable-tool rig bailer
North Seckerton battery	-	Guelph	~750	42.88408	-82.37664	02-Aug-12	brine separator †
Corunna battery	-	Guelph	~750	42.88380	-82.37689	02-Aug-12	brine separator †
Seckerton battery	-	Guelph	~750	42.86469	-82.38375	02-Aug-12	brine separator †
Ladysmith battery	Ladysmith	Guelph	684.9-688.9	42.81226	-82.38533	02-Aug-12	brine separator †
Moore Brine Facility	-	Guelph	657-687.8	42.83148	-82.26307	02-Aug-12	wellhead
Den-Mar Brine Facility	-	Guelph	~700	42.93242	-82.27225	09-Aug-12	brine tank
T004912	Euphemia 8-18-IV	Guelph	447-535	42.66339	-81.96018	09-Aug-12	wellhead
T004678	Warwick 6-17-IV SER	Guelph	609-619	42.95862	-81.89187	16-Aug-12	wellhead †
T005442	Plympton 5-19-VI	Guelph	723.8-734	43.00021	-82.08555	16-Aug-12	wellhead †
T006733	Dawn 28-II	Guelph	596-605	42.73098	-82.21804	02-Oct-12	wellhead
Lowrie Dawn battery	Dawn 28-II	Guelph	~600	42.72693	-82.20833	02-Oct-12	brine tank
T010097	Dashwood	Guelph	536-538	43.33074	-81.66485	30-Mar-12	brine tank
T001521	Brigden	Guelph	680.9	42.81129	-82.30689	25-Jul-12	brine tank
T008932	S. Walsingham 5-6-VI	Rochester-Irondequoit	401.5-409	42.68519	-80.58219	12-May-11	brine tank
T008812	S. Walsingham 5-6-VI	Grimsby-Thorold	410	42.65378	-80.57206	12-Mar-11	brine tank
T011830	Haldimand	Irondequoit	226	42.91034	-80.02034	28-Mar-13	wellhead
T010691	Bayham	Thorold	407.5-409	42.75433	-80.70935	12-May-11	brine tank
T011549	Houghton 5-8-ENR	Grimsby-Thorold	425	42.67023	-80.66431	12-May-11	brine tank
T005741	Venison Creek	Grimsby	422.7-425	42.62092	-80.55461	12-May-11	brine tank
T004185	Norfolk	Thorold	386.5-389.5	42.70463	-80.44191	12-May-11	brine tank
T003188	Norfolk	Grimsby	383.4	42.68878	-80.34892	12-Feb-13	wellhead
T011814	Norfolk	Grimsby	355-360	42.78318	-80.31921	12-Feb-13	wellhead
T009153	Gosfield North 2-21-VI	Cobourg	814-1750*	42.11673	-82.68906	26-Jun-12	wellhead
T010019	Gosfield North 2-21-VI	Sherman Fall	858-1875*	42.11881	-82.69263	04-Jul-12	wellhead
T007330	Mersea 6-23-VII	Cobourg-Sherman Fall	809.5-856	42.12463	-82.52717	26-Jun-12	wellhead
T007636	Mersea 6-23-VII	Sherman Fall	818.4-824.6	42.12393	-82.53037	26-Jun-12	wellhead
T008358	Mersea 3-6-V	Cobourg-Sherman Fall	782-796	42.09226	-82.60596	04-Jul-12	wellhead
T008358 (2)	Mersea 3-6-V	Cobourg-Sherman Fall	782-796	42.09226	-82.60596	07-Aug-12	wellhead
T009605	Mersea 3-4-IV	Cobourg-Sherman Fall	975-1427*	42.10944	-82.62874	07-Aug-12	wellhead
T007954	Rochester 1-17-II EBR	Cobourg-Sherman Fall	821-853	42.24130	-82.66632	07-Aug-12	wellhead
T008313	Rochester 7-17-IV EBR	Coboconk-Sherman Fall	847-936	42.25517	-82.67444	07-Aug-12	wellhead
T008057	Tilbury North 1-11-IV	Sherman Fall	866-878	42.26565	-82.51506	07-Aug-12	brine tank

Sample ID	Pool	Formation of origin	Estimated Depth (m)	Latitude	Longitude	Sampling date	Collection details
T009859	Mersea 2-12-I	Sherman Fall	991-1998*	42.04292	-82.56260	03-Jul-12	wellhead
T007240	Dover 7-5-V E	Coboconk	1015	42.37113	-82.34193	02-Aug-12	wellhead
T006658A	Dover 7-5-V E	Coboconk	1009-1034*	42.37277	-82.34058	14-Feb-12	brine tank
T007793	Dover 7-5-V E	Coboconk	988	42.36744	-82.35322	14-Feb-12	brine separator
T005912	Willey West	Cambrian	1095.1	42.72876	-81.54219	09-Aug-12	wellhead
T000947	Willey West	Cambrian	1100-1103	42.72597	-81.54772	09-Aug-12	brine tank
T001591	Willey West	Cambrian	1077.2	42.73858	-81.54594	09-Aug-12	brine tank
T001303	Clearville	Cambrian	1203-1233	42.47732	-81.69808	16-Aug-12	wellhead
T011362	Clearville	Cambrian	1207-1207	42.48535	-81.70888	16-Aug-12	wellhead
T001610	Clearville	Cambrian	1208-1209	42.48893	-81.69874	16-Aug-12	wellhead
T001343	Clearville	Cambrian	1204-1206	42.48452	-81.70052	16-Aug-12	wellhead
T008532	Innerkip	Cambrian	915-940	43.35257	-80.91059	16-Feb-12	brine tank
T008532 (2)	Innerkip	Cambrian	915-940	43.35257	-80.91059	08-Mar-13	wellhead
T007369	Raleigh 1-17-XIII	Cambrian	1151-1157	42.29331	-82.12810	14-Feb-12	brine separator
T007369 (2)	Raleigh 1-17-XIII	Cambrian	1151-1157	42.29331	-82.12810	26-Jun-12	wellhead
F014364	-	Unknown (drift?)	26?	42.94103	-81.78919	18-Apr-12	wellhead
F015549	Haldimand	Unknown (Silurian?)	-	43.06592	-79.79131	23-May-12	abandoned well seep
F020066 / T012165	Haldimand	Unknown (Salina?)	-	43.05703	-79.76583	8-May-12	abandoned well seep
Oil Springs 5	Oil Springs	Unknown (Dundee?)	-	42.77627	-82.10537	14-Aug-12	well production line
Oil Springs 6	Oil Springs	Unknown (Dundee?)	-	42.77627	-82.10537	14-Aug-12	well production line
T012116	Welland	Unknown (<Guelph)	39?	42.90600	-79.03748	24-May-12	cable-tool rig bailer
Hemlock Creek 1	-	Unkn. (Amherstberg?)	-	42.82046	-79.92927	28-Nov-12	artesian spring
Hemlock Creek 2	-	Unkn. (Amherstberg?)	-	42.82046	-79.92927	28-Nov-12	artesian spring
Ancaster sulphur spring	-	Unkn. (Lockport?)	20?	43.24218	-80.00137	28-Nov-12	artesian spring
T012062-1	-	Unkn. (Bass Islands?)	-	42.86367	-79.12498	4-Mar-11	abandoned well seep
T012062-2	-	Unkn. (Bass Islands?)	-	42.86367	-79.12498	30-Mar-11	abandoned well seep
Church Road Spring	-	Unknown (drift?)	shallow	43.02140	-79.61799	8-Mar-13	artesian spring
Twelve Mile Creek	-	Contact aquifer	shallow	43.08038	-79.30226	8-Mar-13	top of bedrock - seep
Niagara Gorge	-	Whirlpool (shallow)	60	43.12751	-79.05841	1-Aug-12	seep from cliff face
TAQA North flood water	-	Drift aquifer	~55-75	42.58342	-81.74037	24-Aug-12	wellhead
T0121355	-	Unknown (Dundee?)	~80	42.65844	-80.80316	20-Feb-14	abandoned well seep

* indicates a horizontal well (bottom of interval represents total well length, not true vertical depth)

† indicates a sample from a well that is noted by operators to have undergone production-related activities that might influence the water chemistry (such as injection of water or chemical treatments)

Appendix C

Isotopic Data

Sample ID	$\delta^{18}O$ (‰ VSMOW)	δ^2H (‰ VSMOW)	$\delta^{18}O$ (‰ VSMOW)	δ^2H (‰ VSMOW)	$\delta^{13}C_{DIC}$ (‰ VPDB)	$\delta^{34}S_{SO4}$ (‰ CDT)	$\delta^{18}O_{SO4}$ (‰ VSMOW)	$^{87}Sr/^{86}Sr$
	Activity scale		Concentration scale					
Port Dover Quarry 1	−7.5	−53	−7.5	−53	−14.1	−	−	0.70894
Port Dover Quarry 2	−8.2	−55	−8.2	−55	−14.4	−	−	−
T012149 (D)	−10.8	−74	−10.8	−74	−	+27.2	+15.4	0.70863
T012101	−15.7	−111	−15.7	−111	−	−	−	−
T011050	−10.4	−66	−10.4	−66	+20.0	−	−	0.70858
T012150 (D)	−13.4	−90	−13.4	−90	−15.2	+42.4	+12.4	0.70833
T009537	−8.5	−62	−8.5	−63	−6.2	+34.4	+15.2	0.70829
T009536	−8.8	−59	−8.7	−60	−4.1	−	−	−
T008979	−9.2	−65	−9.2	−65	−14.2	+53.9	+17.7	0.70842
F013661	−11.0	−74	−11.0	−75	+6.3	+27.4	−10.1	0.70851
T012111	−15.1	−105	−15.1	−105	−	−	−	−
T012111 (2)	−15.2	−107	−15.2	−107	+15.5	−	−	−
T012111 (3)	−14.0	−94	−14.0	−94	−4.0	+35.8	+12.3	0.70866
F005427	−10.1	−70	−10.1	−70	−13.5	+33.4	+8.7	0.70862
T010678	−10.7	−70	−10.7	−70	−	−	−	−
TAQA North battery	−15.7	−115	−15.7	−115	+11.8	+18.2	−1.3	0.70826
T009308	−14.3	−103	−14.2	−104	−5.3	−	−	0.70812
T007578	−15.9	−118	−15.8	−118	17.9	−	−	0.70830
T012124(L)	−13.7	−86	−13.7	−86	−	−	−	−
T012145 (L1)	−6.7	−42	−6.6	−43	−	+52.5	+20.2	0.70842
T012145 (L2)	−6.7	−38	−6.6	−39	−	+52.8	+19.6	0.70813
T012146	−6.8	−50	−6.8	−51	−	+44.8	+16.1	0.70809
Oil Springs 2	−7.3	−45	−7.2	−46	−3.7	+28.4	+16.4	0.70826
Oil Springs 3	−6.6	−43	−6.5	−44	−6.5	+27.9	+15.7	0.70823
Oil Springs 4	−7.0	−44	−6.8	−45	−3.8	+28.0	+16.5	0.70818
T012152 (L)	−15.5	−113	−15.5	−113	−	+12.2	−	0.70921
T009650	−7.1	−43	−7.0	−43	−13.8	+31.4	+16.6	0.70827

Sample ID	$\delta^{18}O$ (‰ VSMOW)	δ^2H (‰ VSMOW)	$\delta^{18}O$ (‰ VSMOW)	δ^2H (‰ VSMOW)	$\delta^{13}C_{DIC}$ (‰ VPDB)	$\delta^{34}S_{SO4}$ (‰ CDT)	$\delta^{18}O_{SO4}$ (‰ VSMOW)	$^{87}Sr/^{86}Sr$
	Activity scale		Concentration scale					
T010111	−8.1	−56	−8.0	−56	−10.8	−	−	−
T005511	−7.0	−44	−7.0	−45	−16.8	+33.1	+16.8	0.70824
LAI front battery	−6.6	−41	−6.5	−42	−15.9	+28.0	+14.0	0.70825
T011355	−6.5	−40	−6.5	−41	−16.7	−	−	−
T011323	−6.5	−40	−6.5	−41	−15	+27.2	+15.7	0.70823
T012149 (L)	−13.9	−95	−13.8	−95	−	+29.5	+12.9	0.70815
McGregor Quarry 1	−16.3	−118	−16.3	−118	−3.3	+29.7	+13.5	0.70836
McGregor Quarry 2-1	−16.2	−119	−16.2	−119	−0.3	+24.9	+12.6	0.70844
McGregor Quarry 2-2	−16.7	−122	−16.7	−122	−2.4	−	−	−
St Mary's Quarry	−10.5	−69	−10.5	−69	−	−	−	−
Goderich harbour well	−12.5	−83	−12.5	−83	−4.5	+27.1	+13.6	0.70807
T012135	−7.1	−48	−6.7	−53	−	+24.2	+14.9	0.70928
T012152 (DR)	−8.6	−62	−8.6	−63	−4.2	−	−	0.70925
T012177	−11.2	−74	−11.2	−74	−	−	+13.7	−
T012177 (2)	−10.5	−77	−10.5	−77	−	−	+14.3	−
T002484	−9.0	−62	−9.0	−62	−10.6	+33.5	+12.0	0.70868
Sulphur Springs C. A.	−11.7	−81	−11.7	−81	−7.9	+26.8	+13.3	0.70850
Brantford spring	−10.2	−69	−10.2	−69	−	+6.0	+2.9	0.70881
Goderich salt mine N	+2.1	−22	+4.0	−41	+14.8	+28.7	+13.9	0.70860
Goderich salt mine S	+2.2	−23	+4.1	−43	+12.5	−	−	−
T007498	−2.5	−26	−1.6	−37	−1.8	+27.1	+10.4	0.70887
T008641	−1.8	−22	−0.6	−37	−3.0	+26.4	+10.6	0.70856
T008633	−2.0	−23	−1.2	−32	−	+29.4	+12.6	0.70946
T007583	−1.8	−26	−0.7	−38	+2.4	+33.3	+15.4	0.70848
T001539	−0.7	−24	+1.5	−47	−	−	−	0.70850
T011888	−3.8	−38	−2.7	−49	−	+30.3	+14.8	0.70879
T008595	−6.3	−51	−5.3	−62	+3.3	+33.0	+16.0	−
T008596	−5.1	−39	−4.2	−50	+14.2	+27.3	+12.4	0.70839
T008592	−7.3	−43	−6.3	−53	+0.9	−	−	−
T003536	−2.1	−21	−0.8	−34	+7.2	+28.0	+13.5	0.70928
T008657-1	−4.3	−40	−4.1	−43	−5.9	+28.1	+13.1	−
T008657-2	−3.8	−34	−3.2	−41	−0.6	+28.3	+12.0	0.70877
T002235	−11.3	−73	−11.1	−77	+3.5	+27.6	+12.1	0.70880
T011190	−2.8	−36	−1.8	−47	−	−	−	−

Sample ID	$\delta^{18}O$	δ^2H	$\delta^{18}O$	δ^2H	$\delta^{13}C_{DIC}$	$\delta^{34}S_{SO4}$	$\delta^{18}O_{SO4}$	$^{87}Sr/^{86}Sr$
	(‰ VSMOW)	(‰ VSMOW)	(‰ VSMOW)	(‰ VSMOW)	(‰ VPDB)	(‰ CDT)	(‰ VSMOW)	
	Activity scale		Concentration scale					
T012124(G) - A	−3.4	−29	−2.6	−37	−	−	−	−
T012124(G) - B	−3.3	−27	−2.5	−36	−	−	−	−
T012150 (G)	−3.3	−26	−2.7	−33	−0.3	+27.6	+12.3	0.70920
North Seckerton battery	−2.1	−29	−1.2	−39	−	+27.6	+14.0	0.70928
Corunna battery	−2.1	−23	−1.3	−33	−	+27.2	+12.7	0.70928
Seckerton battery	−1.4	−25	−0.1	−41	−	+27.4	+13.4	0.70927
Ladysmith battery	−0.7	−22	+0.7	−38	−	+28.8	+11.5	0.70911
Moore Brine Facility	−0.04	−23	+2.4	−49	−	+28.2	+12.8	0.70920
Den-Mar Brine Facility	−0.2	−21	+1.9	−43	−	+28.5	+13.2	0.70937
T004912	−1.9	−18	−0.3	−38	−	+28.7	+12.1	0.71049
T004678	−5.9	−36	−5.6	−40	−6.5	+25.3	+12.3	0.70917
T005442	−3.5	−32	−2.8	−40	+1.9	+23.0	+10.5	0.70890
T006733	−5.4	−44	−5.0	−49	−	−	−	−
Lowrie Dawn battery	−7.1	−52	−6.6	−57	−	+32.2	+13.8	0.70915
T010097	−3.2	−33	−1.3	−52	−1.7	+24.5	+10.0	0.70880
T001521	−7.4	−57	−6.9	−63	−	+25.3	+12.2	0.70854
T008932	−3.8	−27	−3.0	−36	−	−	−	−
T008812	−3.8	−40	−3.2	−47	−	−	−	−
T011830	−4.8	−31	−4.1	−38	−3.0	+20.7	+10.1	−
T010691	−4.6	−32	−4.0	−39	−	−	−	−
T011549	−3.8	−41	−3.1	−48	−	−	−	−
T005741	−3.6	−28	−2.9	−36	−	−	−	−
T004185	−4.3	−46	−3.5	−54	−	−	−	−
T003188	−2.3	−25	−0.9	−39	−	+22.3	+10.8	0.71045
T011814	−3.4	−27	−1.9	−42	−	+22.0	+11.9	0.71036
T009153	−1.9	−12	−1.2	−20	+1.6	+43.0	+15.6	0.71035
T010019	−2.1	−14	−1.5	−22	−2.2	+39.7	+15.6	0.71030
T007330	−2.3	−12	−1.6	−20	+0.9	+33.9	+15.2	0.71055
T007636	−2.4	−16	−1.7	−24	+1.7	+43.3	+15.3	0.71042
T008358	−2.2	−14	−1.5	−22	+2.8	+34.8	+14.8	0.71040
T008358 (2)	−2.2	−17	−1.6	−25	−	−	−	−
T009605	−2.2	−13	−1.4	−23	+8.0	+36.9	+13.1	0.71038
T007954	−2.1	−13	−1.4	−21	−	−	−	0.71032
T008313	−2.3	−11	−1.6	−18	−	+36.6	+15.2	0.71034

Sample ID	$\delta^{18}O$ (‰ VSMOW)	$\delta^{2}H$ (‰ VSMOW)	$\delta^{18}O$ (‰ VSMOW)	$\delta^{2}H$ (‰ VSMOW)	$\delta^{13}C_{DIC}$ (‰ VPDB)	$\delta^{34}S_{SO4}$ (‰ CDT)	$\delta^{18}O_{SO4}$ (‰ VSMOW)	$^{87}Sr/^{86}Sr$
	Activity scale		*Concentration scale*					
T008057	−2.4	−12	−0.9	−31	–	+27.7	+12.3	0.71031
T009859	−2.7	−16	−1.8	−27	+7.3	+31.5	+13.2	0.71033
T007240	−2.2	−13	−1.2	−25	–	+26.6	+11.5	0.71011
T006658A	−2.4	−14	−1.5	−24	–	+27.0	+12.0	0.71008
T007793	−2.7	−10	−2.6	−11	–	–	–	0.70991
T005912	−3.7	−16	−2.0	−36	–	+26.4	+12.9	0.70988
T000947	−5.8	−23	−4.0	−44	–	–	–	–
T001591	−2.5	−17	−1.5	−28	–	–	–	0.70951
T001303	−4.4	−13	−3.4	−25	–	+27.5	+12.3	0.70980
T011362	−4.4	−13	−2.6	−34	–	+21.6	+10.5	0.70979
T001610	−4.6	−17	−2.7	−39	–	–	–	–
T001343	−4.4	−18	−3.6	−27	+7.4	+31.1	+13.5	0.70983
T008532	−5.4	−25	−4.3	−38	–	+25.0	+14.2	0.70930
T008532 (2)	−5.2	−26	−3.6	−44	–	+25.5	+13.9	0.70930
T007369	−2.9	−9	−2.0	−20	–	+26.8	+9.3	0.71033
T007369 (2)	−2.9	−12	−1.9	−24	+1.5	+23.5	+9.5	0.71027
F014364	−10.2	−70	−10.2	−70	−12.1	–	–	0.70919
F015549	−9.9	−65	−9.9	−65	−11.1	+28.8	+13.9	0.70888
F020066 / T012165	−10.7	−72	−10.7	−73	–	+27.5	+12.2	0.70895
Oil Springs 5	−9.9	−66	−9.9	−66	+16.5	–	–	–
Oil Springs 6	−9.4	−60	−9.4	−60	+10.2	–	–	–
T012116	−10.3	−70	−10.3	−70	−14.5	+27.4	+12.2	0.70843
Hemlock Creek 1	−9.8	−68	−9.8	−68	−11.2	–	+9.3	0.70894
Hemlock Creek 2	−9.3	−59	−9.3	−59	−11.7	+11.5	+11.0	–
Ancaster sulphur spring	−10.6	−69	−10.6	−69	−11.2	+27.8	+12.6	0.70995
T012062-1	−11.1	−76	−11.1	−76	–	–	–	–
T012062-2	−11.6	−77	−11.6	−77	–	–	–	–
Church Road Spring	−12.1	−90	−12.1	−90	−9.8	+26.7	+13.0	0.70881
Twelve Mile Creek	−10.5	−78	−10.5	−78	−12.1	+15.7	+5.5	0.71072
Niagara Gorge	−10.1	−63	−10.1	−63	−7.1	+10.6	+5.8	–
TAQA North flood water	−16.5	−121	−16.5	−121	+17.3	–	–	0.70876
T0121355	−14.2	−98	−14.2	−98	–	–	+14.1	–

Appendix D

Major ion chemistry

Sample ID	TDS	Ca^{2+} (mg/L)	Mg^{2+} (mg/L)	Na^{+} (mg/L)	K^{+} (mg/L)	Sr^{2+} (mg/L)	Cl^{-} (mg/L)	Br^{-} (mg/L)	SO$_4^{2-}$ (mg/L)	(HCO$_3^{-}$ + CO$_3^{2-}$) (mg/L)
Port Dover Quarry	901	190	26	227	7.5	2.3	230	<3	42.0	168
T012149 (D)	4678	487	155	846	33.1	30.3	2478	20	370.8	145
T012101	2518	149	99	627	20.3	–	1128	8.0	16.0	–
T011050	2356	140	51	587	55.8	2.7	910	3.3	79.5	522
T012150 (D)	6385	834	23	1160	101	28.8	3900	24	180.0	146
T009537	31260	2050	1460	6850	216	46.3	18000	130	2100.0	351
T008979	25952	1110	943	4830	129	29.3	18000	76	540.0	276
F013661	1453	255	59	290	10.8	6.8	450	<3	27.0	365
F005427	1963	649	49	202	8.5	4.5	580	3.0	320	141
T012111	1976	155	82	676	29	12.9	993	ND	18.9	–
T012111 (3)	3945	144	118	755	28.4	9.7	2600	13	260.0	3
TAQA North battery	3542	183	149	830	22.5	23.5	1900	13	13.0	379
T009308	9618	388	381	2410	62.3	36.5	5600	33	17.0	646
T007578	3133	212	150	833	16.7	16.2	1500	9.8	39.0	339
T012124(L)	2592	895	0.5	424	91.1	–	963	5.6	77.0	–
T012145 (L1)	35688	3060	1540	8312	454	67.1	20077	133	1352.1	159
T012145 (L2)	29278	1585	1185	7530	136	100	16378	86	1323.6	255
T012146	13696	641	459	3350	91.7	60.5	8300	31	640.0	101
Oil Springs 2	32142	2854	1674	6474	252	69.3	18680	137	937.2	217
Oil Springs 3	40156	3473	2071	8316	308	83.3	23556	158	994.9	201
Oil Springs 4	38663	3248	1890	7811	334	81.6	22938	321	948.0	210
T012152 (L)	5944	743	142	1247	78	18.7	3434	33	56.7	160
T009650	23328	1880	916	5080	198	30.3	13000	57	1900.0	241
T005511	23601	1440	928	5770	135	30.1	13000	64	1900.0	308
LAI front battery	20339	1490	876	4630	155	25.1	11000	57	1800.0	250
T011323	19929	1310	852	4290	122	31.5	11000	58	1900.0	344
T012149 (L)	4343	556	198	301	11	14.6	355	1.6	2000.0	270
McGregor Quarry 1	3769	467	225	204	16.6	12.6	380	<3	1690.1	125
McGregor Quarry 2-1a	2792	350	169	94	6.2	12.8	170	<3	1319.9	242

Sample ID	TDS	Ca^{2+} (mg/L)	Mg^{2+} (mg/L)	Na$^+$ (mg/L)	K$^+$ (mg/L)	Sr^{2+} (mg/L)	Cl$^-$ (mg/L)	Br$^-$ (mg/L)	SO$_4^{2-}$ (mg/L)	(HCO$_3^-$ + CO$_3^{2-}$) (mg/L)
McGregor Quarry 2-1b	2497	353	175	253	–	13.8	301	–	1401	–
St. Mary's Quarry	580	146	32	64	2.5	16.0	22	<3	210	85
Goderich harbour well	2474	519	114	102	1.9	14.9	230	3.0	1300	183
T012135	138066	15500	3890	36100	1240	226	80000	658	366	5
T012152 (DR)	15342	2520	1.1	2680	260	73.3	9700	85	13	50
T002484	6208	799	149	1320	80.7	17.0	3500	33	56	160
T012177	3241	629	20	370	10.6	12.20	870	< 3	1300	27
T012177 (2)	4382	543	45	836	33.8	16.30	1600	< 3	1300	21
Sulphur Springs C. A.	2070	567	52	7	2.1	12.6	8.6	3.0	1200	212
Brantford spring	1488	567	28	61	2.3	0.3	500	0.3	38	284
Goderich salt mine N	383732	84085	15177	31007	7431	1470	240000	3502	89	22
T007498	391550	38900	6050	91900	5690	747	245695	1936	200	38
T008641	374770	57700	8940	79300	5600	1070	220000	1800	230	5
T008633	303892	35982	7680	62939	2660	708	191512	1863	244	<2
T007583	330281	54222	8269	52336	3654	924	207443	2734	150	<2
T001539	518533	74600	14100	48300	7330	1240	370000	2700	110	<2
T011888	286440	42100	8300	46100	6910	839	180000	1800	250	84
T008596	325930	39900	9270	79200	4880	946	190000	1300	360	16
T003536	365643	35600	13500	99600	4130	780	210000	1700	250	5
T008657-1	154554	11886	2617	36917	697	185	100904	501	624	–
T008657-2	301858	26665	5874	85500	1623	408	180000	920	330	2
T002235-1	302015	6780	987	112000	600	143	180000	260	1200	4
T002235-2	313207	6800	1100	143300	605	161	160000	280	1400	4
T012124 (G) - A	265883	36432	7862	47580	2121	–	169944	1741	203	–
T012124 (G) - B	265039	35863	7707	46874	2033	–	170591	1769	201	–
T012150 (G)	288158	20100	4850	98000	2790	403	160000	1200	660	93
North Seckerton battery	283048	43200	6850	56100	3540	1140	170000	1800	340	16
Corunna battery	355477	44700	6700	76600	4100	943	220000	2100	250	<2
Seckerton battery	319540	69600	8210	52700	4810	1210	180000	2800	130	13
Ladysmith battery	385484	70300	10620	54896	5550	1310	240000	2600	130	<2
Moore Brine Facility	441259	102000	16800	72600	5420	1420	240000	2800	120	3
Den-Mar Brine Facility	415714	99500	13700	61700	6020	1550	230000	3000	130	26
T004912	364171	91900	5660	71000	1570	2030	190000	1800	100	<2
T004678	153210	13800	3120	38000	1190	294	95000	710	1000	70
T005442	348436	30700	5740	106000	3430	817	200000	1300	360	31

Sample ID	TDS	Ca^{2+} (mg/L)	Mg^{2+} (mg/L)	Na^+ (mg/L)	K^+ (mg/L)	Sr^{2+} (mg/L)	Cl^- (mg/L)	Br^- (mg/L)	SO_4^{2-} (mg/L)	$(HCO_3^- + CO_3^{2-})$ (mg/L)
Lowrie Dawn battery	188314	18700	4360	52000	1730	423	110000	890	140	5
T010097	358146	80825	13753	31308	3696	1306	222203	3853	95	<2
T001521	234622	21400	4950	83400	2670	415	120000	970	740	<2
T008932	251142	37804	6599	50782	1207	–	152763	1566	421	–
T008812	222989	31237	5679	47267	1086	–	135938	1324	458	–
T011830	236120	29300	5510	48200	765	543	150000	1100	560	<2
T010691	198714	27307	6138	40097	978	–	122542	1133	519	–
T011549	230220	30052	6326	45848	1070	–	145041	1408	475	–
T005741	241711	33932	5631	48770	1024	–	150503	1511	340	–
T004185	249215	35462	6416	50741	1177	–	153560	1562	297	–
T003188	383666	58000	10800	59300	1670	1220	250000	2400	180	<2
T011814	407661	53000	9920	59500	1700	1130	280000	1900	260	<2
T009153	275902	27300	5610	57400	3340	768	180000	1100	330	<2
T010019	268628	27800	6220	79000	3120	871	150000	1200	360	<2
T007330	267071	28500	5710	57500	3120	631	170000	1200	350	<2
T007636	263024	28950	5730	62900	3070	634	160000	1300	380	<2
T008358	288050	30100	6620	75700	3200	758	170000	1200	400	20
T009605	285523	32500	7360	89400	3730	965	150000	1200	300	<2
T007954	266940	27400	6067	58100	3100	806	170000	1200	210	3
T008313	260593	27900	6200	61100	3090	686	160000	1200	360	8
T008057	403179	70900	9180	85900	3940	1220	230000	1600	300	<2
T009859	306446	38900	8080	63100	3600	843	190000	1600	250	<2
T007240	358453	42700	7620	71900	2890	1070	230000	2000	200	<2
T006658A	302689	41335	7090	65700	2800	956	182278	1935	197	<2
T007793	7934	1360	321	1830	46	10.1	4143	22	7.2	<2
T005912	396232	85000	8440	86500	2490	1510	210000	2100	140	3
T001591	342669	37300	8220	90100	4000	766	200000	2000	220	8
T001303	323747	48800	6760	62000	2200	1420	200000	2300	220	<2
T011362	402027	94200	8540	72200	2780	1750	220000	2300	160	<2
T001343	269504	37600	6240	50400	1950	889	170000	1900	470	<2
T008532	309954	56634	6740	49690	1232	1385	191086	2390	120	<2
T008532 (2)	381499	78200	9590	47400	1760	1910	240000	2400	120	<2
T007369	288769	47535	5768	50228	1615	1131	180000	1800	200	<2
T007369 (2)	422936	46700	6250	64300	2390	1170	300000	1800	240	<2
F014364	419	17	9.0	80	3.2	0.6	20	<3	22	259

Sample ID	TDS	Ca^{2+} (mg/L)	Mg^{2+} (mg/L)	Na$^+$ (mg/L)	K$^+$ (mg/L)	Sr^{2+} (mg/L)	Cl$^-$ (mg/L)	Br$^-$ (mg/L)	SO$_4^{2-}$ (mg/L)	(HCO$_3^-$ + CO$_3^{2-}$) (mg/L)
F020066 / T012165	3814	615	182	330	18.2	12.0	760	8.7	1800	81
T012116	1602	637	37	30	3.9	8.1	80	0.7	640	163
Hemlock Creek 1	493	70	27	36	5.7	1.2	63	0.3	120	166
Ancaster sulphur spring	7130	750	182	1450	59	34.3	4000	43	420	181
Church Road Spring	4391	710	227	461	42.3	12.8	960	11	1800	160
Twelve Mile Creek	724	114	39	37	3.1	1.0	68	0.5	72	383
TAQA North flood water	1209	77	38	197	4.5	3.6	620	3.0	2.0	249
T0121355	3673	192	178	1320	30.3	11.1	1500	11	110	281

Appendix E

Minor and trace element chemistry

Table E1: Ag-Mn (mg/L)

Sample ID	Ag	Al	As	Ba	Be	B	Cd	Co	Cr	Cu	Fe	Li	Mn
Port Dover Quarry	0.0010	<0.1	<0.02	0.040	<0.002	0.08	<0.0003	0.00020	0.050	<0.05	<0.03	0.28	0.086
T012149 (D)	<0.0001	0.02	0.007	0.293	<0.0002	0.64	0.00009	<0.00002	<0.005	<0.005	<0.03	0.27	0.038
T011050	<0.0001	<0.01	0.019	0.213	<0.0002	1.29	<0.00003	0.00097	<0.005	<0.005	0.066	0.25	0.147
T012150 (D)	0.0010	<0.1	<0.02	0.942	<0.002	1.34	<0.0003	0.00020	0.050	<0.05	<0.03	1.71	0.024
T009537	0.0010	<0.1	0.060	0.033	<0.002	11.70	<0.0003	0.00020	0.050	<0.05	0.038	9.58	0.049
T008979	<0.0001	<0.01	0.200	0.298	<0.0002	7.57	<0.00003	0.00210	0.009	0.018	0.127	8.60	0.276
F013661	0.0010	<0.1	0.020	0.077	<0.002	1.25	<0.0003	0.00020	0.050	<0.05	0.038	0.54	0.091
F005427	<0.0001	<0.01	0.026	0.062	<0.0002	0.48	<0.00003	0.00090	<0.005	0.010	0.044	0.27	0.052
T012111 (3)	0.0010	<0.1	<0.02	0.113	<0.002	3.94	<0.0003	0.00020	0.050	<0.05	<0.03	2.63	0.063
TAQA North battery	<0.0001	0.09	0.018	3.260	<0.0002	2.22	<0.00003	0.00227	<0.005	<0.005	0.022	1.71	0.010
T009308	0.0010	<0.1	<0.02	0.256	<0.002	3.69	<0.0003	0.00020	0.080	<0.05	0.032	4.44	0.089
T007578	0.0050	<0.1	<0.02	4.400	<0.002	2.16	<0.0003	0.00020	0.050	<0.05	0.057	1.47	0.039
T012145 (L1)	<0.0001	0.18	0.052	0.263	<0.0002	8.11	0.00005	0.00130	<0.005	0.011	0.043	7.71	0.440
T012145 (L2)	<0.0001	0.03	0.044	0.120	<0.0002	8.69	0.00005	0.00080	<0.005	0.011	0.117	7.49	0.405
T012146	0.0010	<0.1	<0.02	0.121	<0.002	4.74	<0.0003	0.00020	0.050	<0.05	<0.03	2.96	0.080
Oil Springs 2	<0.0001	<0.01	0.089	0.113	<0.0002	8.46	<0.00003	0.00097	<0.005	0.015	0.109	8.77	0.063
Oil Springs 3	<0.0001	0.02	0.108	0.129	<0.0002	9.99	<0.00003	0.00129	0.006	0.018	0.127	11.10	0.119
Oil Springs 4	<0.0001	<0.01	0.104	0.143	<0.0002	11.80	0.00006	0.00317	<0.005	0.026	0.010	9.85	0.097
T012152 (L)	<0.0001	0.22	0.012	1.080	<0.0002	2.28	<0.00003	0.00033	<0.005	<0.005	0.635	1.45	0.102
T009650	<0.0001	0.04	0.099	0.035	<0.0002	6.07	<0.00003	0.01050	<0.005	0.020	0.023	6.09	0.042
T005511	0.0010	<0.1	0.040	0.032	<0.002	8.10	<0.0003	0.00020	0.050	<0.05	<0.03	6.19	0.081
LAI front battery	<0.0001	0.07	0.097	0.034	<0.0002	4.66	0.00004	0.00192	<0.005	<0.058	0.031	5.71	0.071
T011323	0.0010	<0.1	0.040	0.034	<0.002	5.94	<0.0003	0.00020	0.050	<0.05	0.040	6.13	0.194
T012149 (L)	<0.0001	<0.01	0.003	0.013	<0.0002	1.55	<0.00003	0.00019	<0.005	0.006	0.203	0.16	0.208
McGregor Quarry 1	<0.0001	0.03	0.005	0.061	<0.0002	1.08	0.00005	0.00017	<0.005	0.006	0.357	0.21	0.034
McGregor Quarry 2-1a	<0.0001	<0.01	0.003	0.014	<0.0002	0.61	<0.00003	<0.00002	<0.005	<0.005	0.065	0.06	0.064
St. Mary's Quarry	<0.00001	< 0.1	0.001	0.063	<0.00002	0.041	0.000041	0.000226	<0.0005	0.001	0.08	0.004	0.006
Goderich harbour well	0.0130	<0.1	<0.02	0.018	<0.002	0.07	<0.0003	0.00020	0.050	<0.05	0.179	0.03	0.042

Sample ID	Ag	Al	As	Ba	Be	B	Cd	Co	Cr	Cu	Fe	Li	Mn
T012135	<0.0001	<0.01	0.170	0.318	<0.0002	6.68	0.00015	0.01070	0.013	0.019	50.800	15.10	2.560
T012152 (DR)	0.0010	<0.1	<0.02	3.520	<0.002	0.02	<0.0003	0.00300	0.050	<0.05	0.049	1.51	0.011
T012177	0.00001	< 0.1	0.005	0.036	<0.00002	0.023	0.000028	0.000399	0.0032	0.0014	<0.02	0.028	0.0024
T012177 (2)	0.00003	< 0.1	0.004	0.052	<0.00002	0.057	0.000063	0.000434	0.0059	0.0025	<0.02	0.066	0.0003
T002484	<0.0001	0.22	0.012	1.080	<0.0002	2.28	<0.00003	0.00033	<0.005	<0.005	0.635	1.45	0.102
Sulphur Springs C. A.	<0.0001	0.06	0.005	0.031	<0.0002	0.26	<0.00003	0.00815	<0.005	<0.005	<0.003	0.04	0.006
Brantford spring	<0.0001	<0.01	0.015	0.098	<0.0002	0.23	<0.00003	0.00206	<0.005	<0.005	0.019	0.17	0.014
Goderich salt mine N	<0.0001	0.17	1.780	0.066	<0.0002	38.60	0.00060	0.03680	0.007	0.221	0.571	102.0	0.590
T007498	<0.0001	<0.01	0.749	0.037	<0.0002	23.40	0.00049	0.02550	0.009	0.098	8.960	35.90	0.324
T008641	0.0007	<0.01	0.316	0.131	<0.0002	46.50	0.00054	0.02400	0.024	0.061	30.400	33.40	11.90
T008633	0.0011	<0.01	0.818	0.108	<0.0002	5.79	0.00063	0.02920	0.007	0.141	21.000	29.30	1.150
T007583	<0.0001	0.12	1.220	0.161	<0.0002	5.36	0.00287	0.03070	0.007	0.153	117.00	43.60	3.410
T001539	0.0002	<0.01	1.230	0.349	<0.0002	12.90	0.00079	0.03300	0.008	0.208	84.500	41.20	3.010
T011888	0.0002	<0.01	0.774	0.631	<0.0002	6.92	0.00151	0.02940	0.038	0.181	15.500	23.90	2.640
T008596	0.0010	0.17	0.160	0.635	<0.002	23.70	<0.0003	0.01770	0.050	0.090	3.590	23.40	1.520
T003536	0.0430	<0.1	0.130	0.260	<0.002	20.60	<0.0003	0.01390	0.050	0.100	15.700	35.10	0.842
T008657-2	0.0004	<0.01	0.437	0.191	<0.0002	6.77	0.00095	0.02660	0.008	0.117	133.00	15.30	3.530
T002235-1	<0.0001	0.02	0.165	0.021	<0.0002	4.58	0.00066	0.01600	<0.005	0.028	11.500	7.58	0.437
T012150 (G)	0.0010	<0.1	0.180	0.037	<0.002	25.20	<0.0003	0.01130	0.050	<0.05	<0.03	30.70	0.419
North Seckerton battery	0.0010	<0.1	0.310	0.117	<0.002	10.50	<0.0003	0.02090	0.050	0.100	21.200	20.90	3.400
Corunna battery	0.0139	<0.01	0.920	0.184	<0.0002	4.44	0.00127	0.03290	0.010	0.124	38.600	21.40	3.040
Seckerton battery	0.0002	0.04	1.070	0.135	<0.0002	3.88	0.00085	0.02810	0.007	0.127	20.600	30.60	2.210
Ladysmith battery	0.0007	<0.01	1.210	0.145	<0.0002	4.26	0.00176	0.03210	0.007	0.177	38.200	23.00	2.840
Moore Brine Facility	0.0010	<0.1	0.150	0.091	<0.002	21.60	<0.0003	0.02190	0.050	0.120	30.200	36.10	1.880
Den-Mar Brine Facility	0.0010	<0.1	0.190	0.056	<0.002	30.10	<0.0003	0.02550	0.050	0.120	7.310	44.10	1.170
T004912	0.0030	<0.1	0.340	2.990	<0.002	4.21	<0.0003	0.01910	0.050	0.080	60.600	5.92	28.80
T004678	<0.0001	0.07	0.348	0.092	<0.0002	3.62	0.00037	0.01290	0.006	0.054	0.045	14.90	0.880
T005442	0.0010	<0.1	0.080	0.059	<0.002	26.00	<0.0003	0.01300	0.050	<0.05	0.400	24.40	0.841
Lowrie Dawn battery	0.0010	<0.1	0.200	0.942	<0.002	10.20	<0.0003	0.00860	0.050	<0.05	32.700	16.70	0.947
T010097	<0.0001	0.06	2.230	0.114	<0.0002	5.21	0.00089	0.04010	0.026	0.423	214.00	36.50	12.80
T001521	0.0010	<0.1	0.170	0.474	<0.002	20.00	<0.0003	0.00970	0.050	<0.05	28.200	19.00	1.110
T011830	0.0004	< 0.1	0.654	0.538	<0.00002	3.36	0.00047	0.0314	0.0237	0.162	81.1	34.3	20
T003188	0.0002	<0.01	0.376	0.950	<0.0002	4.38	<0.00003	0.01900	0.025	0.082	20.800	44.30	21.40
T011814	0.0002	<0.01	0.305	0.866	<0.0002	3.45	<0.00003	0.01610	0.025	0.064	176.00	40.80	21.20
T009153	0.0046	0.06	0.525	0.827	<0.0002	6.42	0.00053	0.01880	0.006	0.125	4.850	23.90	6.990
T010019	0.0020	0.13	0.160	0.895	<0.002	12.10	<0.0003	0.01330	0.050	0.080	3.930	25.90	6.600

Sample ID	Ag	Al	As	Ba	Be	B	Cd	Co	Cr	Cu	Fe	Li	Mn
T007330	0.0002	<0.01	0.532	0.867	<0.0002	5.92	0.00052	0.02250	0.006	0.110	10.200	25.10	7.650
T007636	<0.0001	<0.01	0.533	0.573	<0.0002	5.05	0.00050	0.02240	0.006	0.106	8.880	26.30	7.600
T008358	0.0280	<0.1	0.270	0.727	<0.002	11.50	<0.0003	0.01650	0.050	0.080	0.760	27.90	5.840
T009605	0.0010	<0.1	0.160	1.280	<0.002	13.30	<0.0003	0.01080	0.050	0.070	10.700	28.90	6.140
T007954	<0.0001	0.04	0.563	1.700	<0.0002	5.45	0.00100	0.02390	0.006	0.111	9.540	25.60	4.240
T008313	0.0002	<0.01	0.545	0.846	<0.0002	5.82	0.00107	0.02420	0.006	0.115	4.670	27.00	3.210
T008057	0.0010	<0.1	0.230	1.130	<0.002	11.40	<0.0003	0.02200	0.050	0.100	22.900	83.80	10.80
T009859	0.0003	<0.01	0.757	0.822	<0.0002	3.66	0.00083	0.02630	0.010	0.151	18.300	31.70	6.300
T007240	<0.0001	0.04	0.900	0.582	<0.0002	4.10	0.00523	0.02590	<0.005	0.118	27.100	24.30	6.320
T006658A	<0.0001	0.14	0.747	0.589	<0.0002	4.00	0.00070	0.02470	0.008	0.122	15.700	20.30	7.010
T007793	<0.0001	<0.01	0.038	0.024	<0.0002	0.40	0.00049	0.00687	0.009	0.038	74.000	0.37	4.620
T005912	0.0010	<0.1	0.290	1.810	<0.002	9.09	<0.0003	0.02440	0.050	0.110	4.810	17.00	12.10
T001591	<0.0001	0.02	0.652	0.259	<0.0002	5.73	0.00060	0.02390	<0.005	0.118	4.380	32.00	2.340
T001303	<0.0001	<0.11	0.980	1.820	<0.0002	2.60	0.00061	0.02670	0.006	0.110	5.550	13.60	11.50
T011362	0.0010	<0.1	0.360	2.350	<0.002	8.43	<0.0003	0.02470	0.050	0.110	51.300	12.30	13.70
T001343	<0.0001	<0.01	0.715	0.679	<0.0002	4.01	0.00047	0.02440	0.006	0.111	13.500	20.80	7.770
T008532	0.0002	<0.01	1.060	2.850	<0.0002	0.82	0.00090	0.03340	0.007	0.396	50.000	7.09	69.90
T008532 (2)	<0.0001	<0.01	0.416	2.780	<0.0002	2.01	<0.00003	0.02210	0.023	0.300	25.600	9.17	75.10
T007369	<0.0001	0.05	0.891	1.840	<0.0002	3.93	0.00063	0.04670	0.007	0.133	32.000	13.90	18.00
T007369 (2)	0.0012	<0.01	0.951	1.800	<0.0002	4.92	0.00064	0.02920	0.006	0.123	36.300	13.30	17.70
F014364	<0.0001	<0.01	0.002	0.058	<0.0002	1.12	<0.00003	<0.00002	<0.005	<0.005	0.104	0.03	0.006
F015549	<0.0001	<0.01	0.012	0.007	<0.0002	0.70	<0.00003	0.00249	<0.005	<0.005	<0.003	0.19	0.035
F020066 / T012165	<0.0001	<0.11	0.008	0.006	<0.0002	1.39	<0.00003	0.00521	<0.005	<0.005	0.055	0.32	0.030
T012116	<0.0001	0.03	0.029	0.049	<0.0002	0.46	<0.00003	0.00248	<0.005	<0.005	0.021	0.21	0.372
Hemlock Creek 1	<0.0001	0.20	0.004	0.040	<0.0002	0.25	<0.00003	0.00307	<0.005	<0.005	0.256	0.04	0.008
Ancaster sulphur spring	<0.0001	<0.01	0.024	0.040	<0.0002	1.48	<0.00003	0.00746	0.020	<0.005	0.005	1.41	0.115
Church Road Spring	<0.0001	0.05	0.006	0.024	<0.0002	2.04	<0.00003	<0.00002	<0.005	<0.005	0.052	0.43	0.043
Twelve Mile Creek	<0.0001	<0.01	0.008	0.058	<0.0002	0.17	<0.00003	<0.00002	<0.005	<0.005	0.043	0.30	0.153
TAQA North flood water	0.0010	<0.1	<0.02	1.520	<0.002	1.26	<0.0003	0.00020	0.050	<0.05	0.779	0.27	0.057
T012355	0.00005	0.3	0.011	0.765	<0.00002	2.81	0.000022	0.000401	0.0007	0.0027	0.25	1.6	0.0543

Table E2: Mo-Zn (mg/L)

Sample ID	Mo	Ni	Pb	Sb	Se	Si	Sn	Ti	Tl	U	V	Zn
Port Dover Quarry	<0.001	<0.01	0.0005	<0.002	0.10	1.94	<0.001	<0.01	<0.002	0.00080	<0.003	<0.02
T012149 (D)	0.1770	<0.01	0.0002	<0.002	0.02	2.04	0.0008	0.005	<0.002	0.00191	<0.0003	<0.002
T011050	<0.0001	0.005	0.0007	<0.002	0.04	2.16	<0.0001	0.002	<0.002	<0.00001	0.0009	<0.02
T012150 (D)	0.0200	0.030	0.0000	<0.002	0.10	3.79	<0.001	<0.01	<0.002	<0.0001	0.0060	<0.02
T009537	<0.001	0.020	0.0009	<0.002	0.10	3.43	<0.001	0.010	<0.002	<0.0001	<0.003	<0.02
T008979	0.0003	<0.019	0.0002	0.008	0.10	3.46	<0.0012	0.006	<0.002	<0.00001	0.0014	0.0100
F013661	<0.001	<0.01	0.0008	<0.002	0.10	4.08	<0.001	<0.01	<0.002	<0.0001	<0.003	<0.02
T012111 (3)	<0.001	<0.01	0.0006	<0.002	0.10	4.65	<0.001	<0.01	<0.002	<0.0001	<0.003	<0.02
TAQA North battery	<0.0001	0.004	0.0002	<0.002	0.02	6.54	<0.0001	0.003	<0.002	<0.00001	0.0006	<0.002
T009308	<0.001	<0.01	0.0006	<0.002	0.10	2.84	<0.001	<0.01	<0.002	<0.0001	<0.003	<0.02
T007578	0.0020	<0.01	0.0009	<0.002	0.10	6.84	0.0060	<0.01	<0.002	<0.0001	<0.003	<0.02
T012145 (L1)	0.0017	0.022	0.0002	<0.002	0.13	9.53	<0.0012	0.009	<0.002	0.00652	<0.0003	<0.002
T012145 (L2)	0.0007	0.016	0.0008	<0.002	0.09	3.10	<0.0019	0.009	<0.002	0.00096	<0.0003	0.0070
T012146	0.0280	0.020	0.0000	<0.002	0.10	10.90	<0.001	<0.01	<0.002	0.00300	<0.003	<0.02
Oil Springs 2	<0.0001	0.021	0.0002	<0.002	0.15	3.53	0.0003	0.008	<0.002	0.00005	<0.0003	<0.002
Oil Springs 3	<0.0001	0.022	0.0003	<0.002	0.15	3.56	0.0003	0.009	<0.002	<0.00001	<0.0003	<0.002
Oil Springs 4	<0.0001	0.026	0.0003	<0.002	0.04	3.49	<0.0001	<0.01	<0.002	0.00002	<0.0003	<0.002
T012152 (L)	<0.0019	0.008	0.0002	<0.002	0.04	5.54	0.0002	0.006	<0.002	0.00224	0.0005	0.1110
T009650	<0.0001	0.016	0.0004	<0.002	0.11	3.16	<0.0001	<0.011	<0.002	<0.00016	0.0006	<0.002
T005511	<0.001	<0.01	0.0003	<0.002	0.10	3.00	<0.001	<0.01	<0.002	<0.0001	<0.003	<0.02
LAI front battery	<0.0001	0.046	0.0003	<0.002	0.16	3.32	<0.0001	<0.01	<0.002	0.00002	0.0007	<0.029
T011323	<0.001	0.020	0.0004	<0.002	0.10	3.40	0.0040	0.010	<0.002	<0.0001	<0.003	<0.02
T012149 (L)	0.0090	0.007	0.0005	<0.002	0.01	6.50	0.0006	0.009	<0.002	0.00056	<0.0003	0.0110
McGregor Quarry 1	0.0002	0.005	0.0002	<0.002	0.02	5.58	0.0004	0.007	<0.002	<0.00018	<0.0003	0.0430
McGregor Quarry 2-1a	<0.0001	0.003	0.0002	<0.002	0.01	4.98	0.0002	0.005	<0.002	0.00035	<0.0003	0.0060
St. Mary's Quarry	0.0023	0.005	0.00007	<0.0002	0.003	2.50	0.00003	0.0002	0.0003	0.00163	0.00015	0.09
T012135	0.0318	0.098	0.0002	<0.002	0.19	5.35	<0.0001	0.020	<0.002	0.00033	<0.0003	0.0150
T012152 (DR)	0.1150	0.040	0.0002	<0.002	0.10	0.44	<0.001	<0.01	<0.002	<0.0001	0.0040	<0.02
T012177	0.0346	0.0111	0.00032	0.0038	0.004	1.50	0.0001	0.0009	<0.0002	0.00355	0.0025	< 0.02
T012177 (2)	0.146	0.0061	0.00008	0.0039	0.006	3.10	0.0001	0.0005	<0.0002	0.00264	0.00723	< 0.02
T002484	<0.0019	0.008	0.0002	<0.002	0.04	6.68	0.0002	0.006	<0.002	0.00224	0.0005	0.1110
Sulphur Springs C. A.	<0.0001	0.006	0.0002	<0.002	0.02	4.63	<0.0001	0.002	<0.002	0.00002	0.0006	<0.002
Brantford spring	0.0002	0.005	0.0015	<0.002	0.03	6.72	0.0003	0.003	<0.002	0.00052	0.0007	<0.002

Sample ID	Mo	Ni	Pb	Sb	Se	Si	Sn	Ti	Tl	U	V	Zn
Goderich salt mine N	0.0048	0.419	0.0007	0.008	0.09	3.50	0.0052	0.063	<0.002	<0.00001	<0.0003	0.1290
T007498	0.0047	0.235	0.0034	<0.002	0.06	8.29	0.0004	0.040	<0.002	<0.00001	<0.0003	<0.002
T008641	0.0054	0.252	0.1810	<0.002	0.20	0.83	<0.0011	0.041	<0.002	0.00040	<0.0003	0.0580
T008633	0.0038	0.187	0.0138	0.005	0.06	9.07	0.0009	0.045	<0.002	<0.00001	<0.0003	<0.002
T007583	0.0057	0.262	0.0384	0.004	0.10	9.74	<0.0015	0.055	<0.002	0.00090	<0.0003	1.0100
T001539	0.0039	0.322	0.0037	0.005	0.11	6.60	0.0021	0.055	<0.002	<0.00001	<0.0003	0.6570
T011888	0.0056	0.330	0.0949	0.004	0.10	4.96	0.0007	0.042	<0.002	0.02700	<0.0003	0.4260
T008596	<0.001	0.260	0.0012	<0.002	0.20	1.28	<0.001	0.030	<0.002	<0.0001	<0.003	0.0320
T003536	0.0040	0.200	0.0009	<0.002	0.50	2.01	0.0280	0.040	<0.002	<0.0001	<0.003	0.0470
T008657-2	0.0032	0.156	0.1180	<0.002	0.15	12.00	0.0004	0.054	<0.002	<0.00001	<0.0003	0.1920
T002235-1	0.0006	0.064	0.0059	<0.002	0.18	14.10	<0.0001	0.034	<0.002	<0.00001	<0.0003	0.0050
T012150 (G)	<0.001	0.140	0.0000	<0.002	0.20	2.61	<0.001	0.030	<0.002	<0.0001	<0.003	<0.02
North Seckerton battery	<0.001	0.330	0.1100	<0.002	0.30	1.96	0.0040	0.030	0.005	<0.0001	<0.003	0.2480
Corunna battery	0.0034	0.269	2.0600	0.004	0.12	8.31	0.0006	0.047	0.006	0.00009	<0.0003	1.4300
Seckerton battery	0.0068	0.292	0.2210	0.007	0.05	5.94	<0.0017	0.047	0.004	0.00004	<0.0003	1.1100
Ladysmith battery	0.0044	0.330	0.0355	0.005	0.09	5.17	<0.0015	0.052	0.004	<0.00001	<0.0003	0.0600
Moore Brine Facility	<0.001	0.380	0.0018	<0.002	0.20	1.61	0.0050	0.050	0.006	<0.0001	<0.003	<0.025
Den-Mar Brine Facility	<0.001	0.420	0.0043	<0.002	0.10	1.27	0.0030	0.050	0.004	<0.0001	<0.003	<0.02
T004912	<0.001	0.320	0.6020	<0.002	0.10	1.71	0.0120	<0.01	0.008	<0.0001	<0.003	0.3510
T004678	0.0015	0.092	0.0003	<0.002	0.11	5.62	<0.0001	0.024	<0.002	<0.00001	<0.0003	<0.002
T005442	<0.001	0.190	0.0022	<0.002	0.10	2.49	0.0130	0.030	<0.002	<0.0001	<0.003	<0.02
Lowrie Dawn battery	<0.001	0.140	0.0000	<0.002	0.20	1.77	0.0010	0.010	<0.002	<0.0001	<0.003	<0.024
T010097	0.0117	0.435	0.3010	0.009	0.09	9.30	0.0084	0.065	<0.002	<0.00001	<0.0003	1.4400
T001521	<0.001	0.180	0.0062	<0.002	0.10	2.57	0.0130	0.020	<0.002	<0.0001	<0.003	0.0440
T011830	0.0241	0.403	0.0019	0.0061	0.065	0.90	0.00989	0.078	<0.0002	0.00061	<0.00003	1.26
T003188	0.0007	0.229	0.0016	<0.002	0.21	0.73	<0.0001	0.044	0.004	0.00008	<0.0003	0.0160
T011814	0.0005	0.196	0.0002	<0.002	0.22	5.34	<0.0001	0.045	<0.002	0.00004	<0.0003	0.0070
T009153	0.0007	0.161	0.0745	<0.002	0.15	6.77	<0.0001	0.036	<0.002	<0.00001	<0.0003	<0.028
T010019	<0.001	0.210	0.0685	<0.002	0.30	2.40	0.0030	0.030	<0.002	<0.0001	<0.003	0.1430
T007330	0.0012	0.231	0.0004	<0.002	0.13	6.36	0.0006	0.040	<0.002	<0.00001	<0.0003	0.0190
T007636	<0.001	0.177	0.0022	<0.002	0.14	7.09	<0.0001	0.038	<0.002	<0.00001	<0.0003	<0.002
T008358	<0.001	0.290	0.0078	<0.002	0.10	1.65	0.0030	0.040	<0.002	<0.0001	<0.003	0.1530
T009605	<0.001	0.190	0.0307	<0.002	0.10	2.17	0.0100	0.030	<0.002	<0.0001	<0.003	0.0360
T007954	0.0009	0.168	0.0032	0.003	0.12	5.96	<0.0001	0.038	0.004	<0.00001	<0.0003	0.0400
T008313	0.0015	0.182	0.0042	0.003	0.12	5.75	0.0003	0.035	0.003	<0.00001	<0.0003	0.0680
T008057	<0.001	0.510	0.0066	<0.002	0.20	1.44	0.0080	0.110	0.004	<0.0001	<0.003	0.9880

Sample ID	Mo	Ni	Pb	Sb	Se	Si	Sn	Ti	Tl	U	V	Zn
T009859	0.0019	0.268	0.0083	0.003	0.12	7.56	0.0005	0.045	0.002	<0.00001	<0.0003	0.0410
T007240	0.0036	0.232	0.0165	0.004	0.06	6.53	0.0008	0.043	0.006	<0.00001	<0.0003	0.0990
T006658A	0.0030	0.286	0.0070	0.003	0.08	6.16	0.0007	0.043	<0.002	<0.00001	<0.0003	0.0110
T007793	0.0006	0.051	0.0952	<0.002	0.06	2.08	0.0004	0.002	<0.002	<0.00001	0.0017	0.0310
T005912	<0.001	0.370	0.0066	<0.002	0.20	0.64	0.0030	0.030	0.013	<0.0001	<0.003	0.0560
T001591	0.0042	0.194	0.0596	0.003	0.06	8.43	<0.0013	0.043	<0.002	<0.00001	<0.0003	<0.028
T001303	0.0041	0.270	0.0009	0.005	0.06	6.42	0.0008	0.046	<0.002	<0.00001	<0.0003	0.0770
T011362	<0.001	0.430	0.0043	<0.002	0.10	3.26	0.0130	0.020	0.014	<0.0001	<0.003	0.0470
T001343	0.0014	0.357	0.0003	<0.002	0.10	4.16	0.0002	0.038	<0.002	<0.00001	<0.0003	0.0170
T008532	0.0039	0.273	0.0176	0.004	0.09	6.44	0.0006	0.051	0.005	<0.00001	<0.0003	0.1590
T008532 (2)	<0.001	0.303	0.0105	<0.002	0.23	1.08	<0.0001	<0.017	0.007	0.00004	<0.0003	0.0770
T007369	0.0034	0.265	0.0110	0.004	0.09	6.79	0.0006	0.047	0.005	<0.00001	<0.0003	0.3890
T007369 (2)	0.0038	0.260	0.0019	0.006	0.10	7.72	<0.001	0.046	0.005	<0.00001	<0.0003	0.0610
F014364	0.0007	0.001	0.0002	<0.002	0.01	4.54	<0.0001	0.002	<0.002	<0.00001	<0.0003	<0.002
F015549	<0.0001	0.007	0.0002	<0.002	0.03	5.43	<0.0001	0.004	<0.002	0.00008	0.0006	<0.002
F020066 / T012165	<0.0001	<0.01	0.0012	<0.002	0.02	4.66	<0.0001	0.001	<0.002	<0.00017	0.0005	<0.002
T012116	0.0018	0.011	0.0002	<0.002	0.10	2.05	<0.0001	0.005	<0.002	<0.00018	0.0006	0.0610
Hemlock Creek 1	0.0003	0.003	0.0002	<0.002	0.01	2.20	<0.0001	0.008	<0.002	0.00050	0.0016	<0.002
Ancaster sulphur spring	<0.0001	0.007	0.0002	<0.002	0.03	7.52	<0.0001	0.003	<0.002	<0.00001	<0.0003	<0.002
F005427	0.0003	0.008	0.0007	<0.002	0.09	4.42	<0.0001	0.004	<0.002	0.00050	0.0011	<0.002
Goderich harbour well	0.0090	<0.01	0.0004	<0.002	0.10	3.40	0.0010	<0.01	<0.002	0.00030	<0.003	<0.02
Church Road Spring	<0.0001	0.005	0.0002	<0.002	0.02	4.13	<0.0011	0.007	<0.002	0.00004	<0.0003	0.0130
Twelve Mile Creek	<0.0001	0.004	0.0002	<0.002	0.02	5.58	0.0020	0.008	<0.002	0.00032	<0.0003	0.0030
TAQA North flood water	0.0190	<0.01	0.0004	<0.002	0.10	9.16	<0.001	<0.01	<0.002	<0.0001	0.0040	<0.02
T012355	0.00023	0.004	0.00013	0.0003	< 0.001	5.90	0.00019	0.011	<0.0002	0.000232	0.00102	< 0.02

Appendix F

Supplementary SIAR statistics and matrix plots

Dataset 2

Supplementary Material for Section 5.1.3.2

Summary statistics

Table F1-a

Mixture 1 Sources	Lower 95% CI	Upper 95% CI	Mode	Mean
Dev-low	0.48	0.64	0.57	0.56
Dev-high	0.02	0.45	0.24	0.25
Salina-Guelph	0.02	0.31	0.13	0.16
Trenton-Black River	0.00	0.07	0.01	0.02
Cambrian	0.00	0.05	0.00	0.02

Table F1-b

Mixture 2 Sources	Lower 95% CI	Upper 95% CI	Mode	Mean
Dev-low	0.19	0.35	0.28	0.27
Dev-high	0.00	0.37	0.20	0.18
Salina-Guelph	0.19	0.48	0.30	0.33
Trenton-Black River	0.00	0.27	0.03	0.12
Cambrian	0.00	0.23	0.03	0.10

Table F1-c

Mixture 3 Sources	Lower 95% CI	Upper 95% CI	Mode	Mean
Dev-low	0.42	0.59	0.50	0.51
Dev-high	0.05	0.49	0.28	0.28
Salina-Guelph	0.00	0.20	0.07	0.09
Trenton-Black River	0.00	0.16	0.02	0.06
Cambrian	0.00	0.17	0.02	0.06

Table F1-d

Mixture 3 Sources	Lower 95% CI	Upper 95% CI	Mode	Mean
Dev-low	0.00	0.05	0.01	0.02
Dev-high	0.00	0.14	0.01	0.05
Salina-Guelph	0.13	0.51	0.29	0.31
Trenton-Black River	0.06	0.58	0.33	0.32
Cambrian	0.03	0.52	0.30	0.29

Tables F1a-d: Summary statistical information about the predicted proportions (in decimal format) of the different sources contributing to Mixtures 1-4, respectively, for Dataset 2. All isotopes except $\delta^{37}Cl$ and $\delta^{81}Br$ are included, and the Clinton-Cataract end-member is excluded.
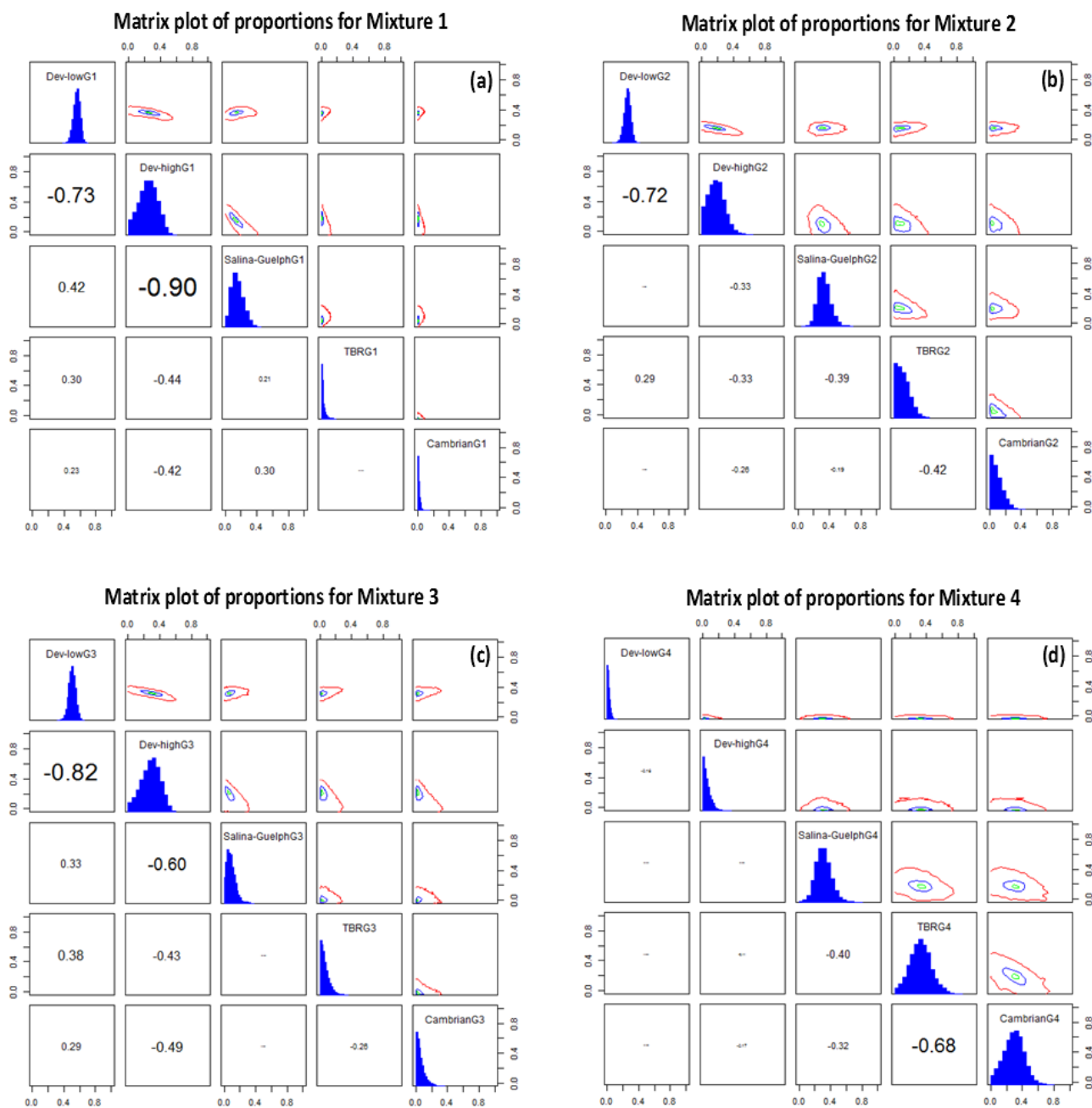
Matrix plots

Figures F1a-d: Matrix plots for Mixtures 1-4, respectively, for Dataset 2. All isotopes except $\delta^{37}Cl$ and $\delta^{81}Br$ are included, and the Clinton-Cataract end-member is excluded.

Dataset 2 with $\delta^{37}Cl$ and $\delta^{81}Br$

Supplementary Material for Section 5.1.3.3

Summary statistics

Table F2-a

Mixture 1 Sources	Lower 95% CI	Upper 95% CI	Mode	Mean
Dev-low	0.41	0.59	0.52	0.50
Dev-high	0.41	0.58	0.48	0.50
Salina-Guelph	0.00	0.00	0.00	0.00
Trenton-Black River	0.00	0.01	0.00	0.00
Cambrian	0.00	0.01	0.00	0.00

Table F2-b

Mixture 2 Sources	Lower 95% CI	Upper 95% CI	Mode	Mean
Dev-low	0.17	34.00	0.27	0.26
Dev-high	0.01	0.40	0.22	0.21
Salina-Guelph	0.30	0.61	0.44	0.45
Trenton-Black River	0.00	0.13	0.01	0.05
Cambrian	0.00	0.07	0.01	0.03

Table F2-c

Mixture 3 Sources	Lower 95% CI	Upper 95% CI	Mode	Mean
Dev-low	0.39	0.55	0.46	0.47
Dev-high	0.25	0.56	0.45	0.42
Salina-Guelph	0.00	0.03	0.01	0.01
Trenton-Black River	0.00	0.10	0.01	0.03
Cambrian	0.00	0.15	0.03	0.06

Table F2-d

Mixture 4 Sources	Lower 95% CI	Upper 95% CI	Mode	Mean
Dev-low	0.00	0.05	0.01	0.02
Dev-high	0.00	0.13	0.01	0.05
Salina-Guelph	0.20	0.41	0.31	0.31
Trenton-Black River	0.07	0.57	0.27	0.31
Cambrian	0.10	0.49	0.31	0.31

Tables F2a-d: Summary statistical information about the predicted proportions (in decimal format) of the different sources contributing to Mixtures 1-4, respectively, for Dataset 2. All isotopes are included, and the Clinton-Cataract end-member is excluded.
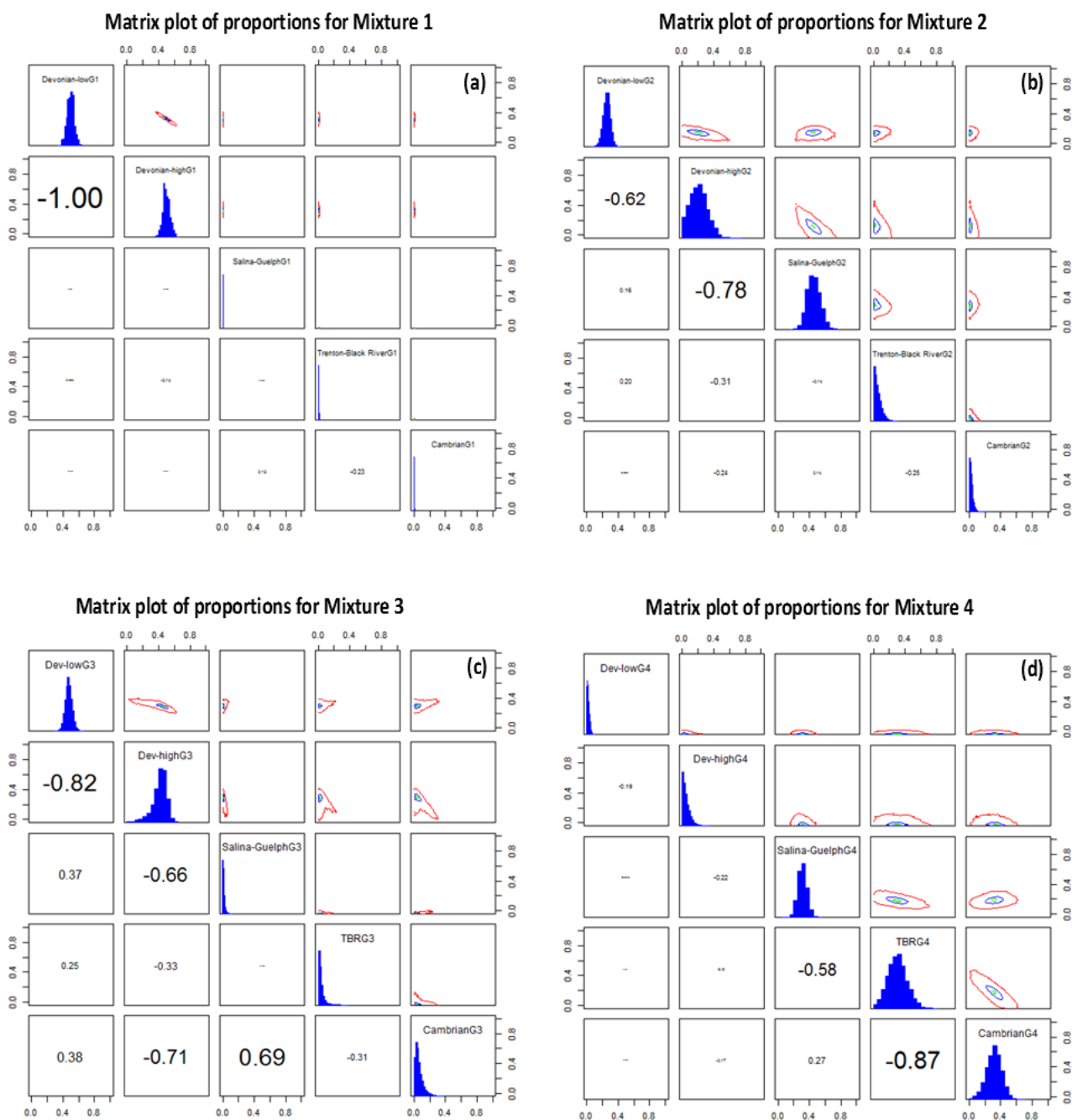
Matrix plots

Figures F2a-d: Matrix plots for Mixtures 1-4, respectively, for Dataset 2. All isotopes are included, and the Clinton-Cataract end-member is excluded.

Dataset 2 with Clinton-Cataract (no δ^{37}Cl and δ^{81}Br)

Supplementary Material for Section 5.1.3.4.1

Summary statistics

Table F3-a

Mixture 1 Sources	Lower 95% CI	Upper 95% CI	Mode	Mean
Dev-low	0.50	0.64	0.56	0.57
Dev-high	0.00	0.37	0.23	0.20
Salina-Guelph	0.00	0.04	0.16	0.17
Clinton-Cataract	0.00	0.10	0.01	0.03
Trenton-Black River	0.00	0.07	0.01	0.02
Cambrian	0.00	0.05	0.00	0.02

Table F3-b

Mixture 2 Sources	Lower 95% CI	Upper 95% CI	Mode	Mean
Dev-low	0.20	0.34	0.27	0.27
Dev-high	0.00	0.32	0.15	0.15
Salina-Guelph	0.16	0.47	0.29	0.31
Clinton-Cataract	0.00	0.27	0.03	0.10
Trenton-Black River	0.00	0.23	0.02	0.09
Cambrian	0.00	0.20	0.02	0.07

Table F3-c

Mixture 3 Sources	Lower 95% CI	Upper 95% CI	Mode	Mean
Dev-low	0.43	0.59	0.52	0.51
Dev-high	0.02	0.43	0.24	0.24
Salina-Guelph	0.00	0.20	0.07	0.10
Clinton-Cataract	0.00	0.14	0.01	0.05
Trenton-Black River	0.00	0.14	0.01	0.05
Cambrian	0.00	0.16	0.01	0.06

Table F3-d

Mixture 4 Sources	Lower 95% CI	Upper 95% CI	Mode	Mean
Dev-low	0.00	0.04	0.01	0.02
Dev-high	0.00	0.14	0.01	0.05
Salina-Guelph	0.11	0.45	0.27	0.28
Clinton-Cataract	0.00	0.29	0.06	0.13
Trenton-Black River	0.07	0.54	0.30	0.30
Cambrian	0.00	0.43	0.23	0.22

Tables F3a-d: Summary statistical information about the predicted proportions (in decimal format) of the different sources contributing to Mixtures 1-4, respectively, for Dataset 2. All end-members are included, and δ^{13}C$_{DIC}$, δ^{37}Cl and δ^{81}Br are excluded.

Matrix plots
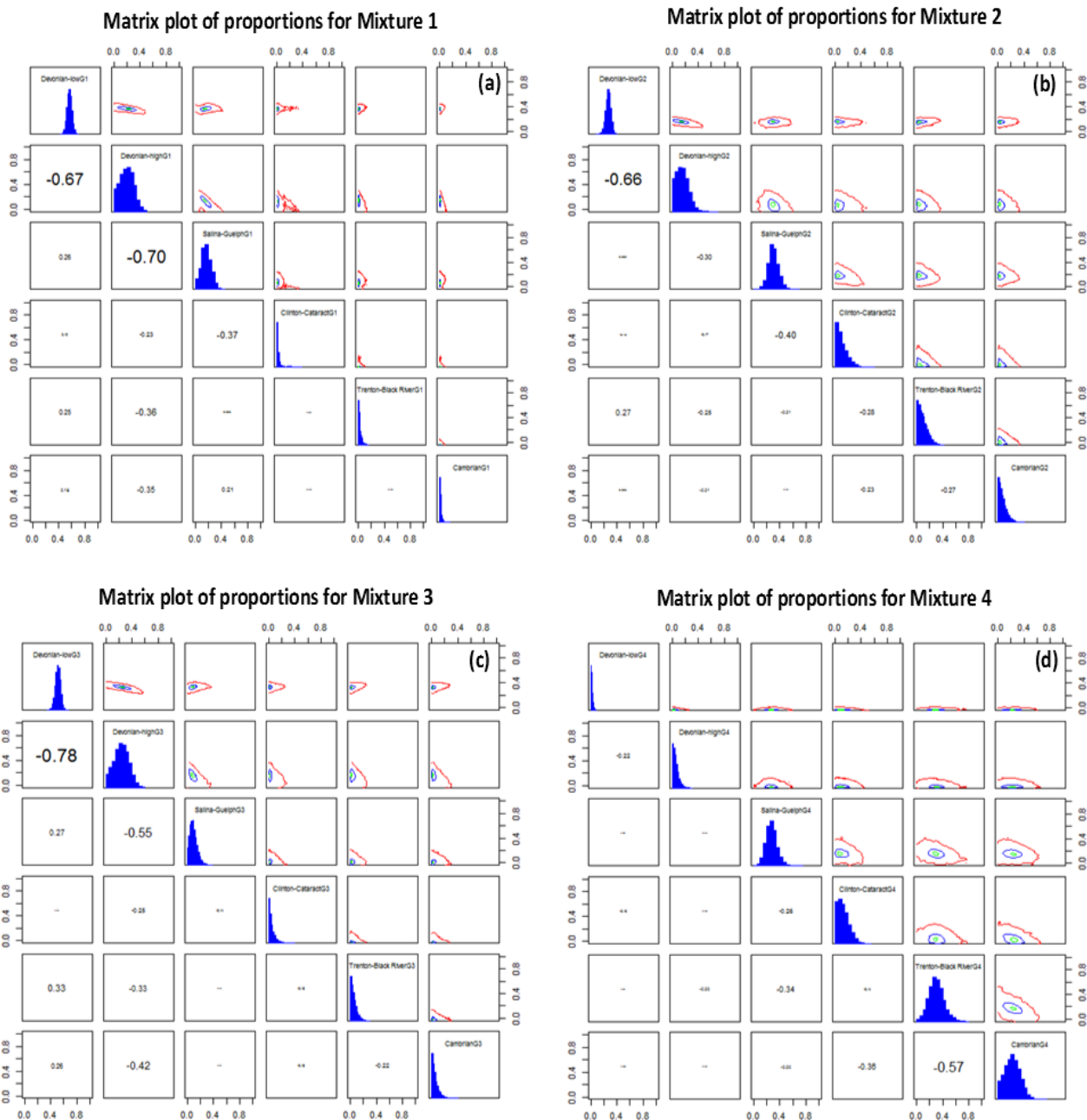
Figures F3a-d: Matrix plots for Mixtures 1-4, respectively, for Dataset 2. All end-members are included, and $\delta^{13}C_{DIC}$, $\delta^{37}Cl$ and $\delta^{81}Br$ are excluded.

Dataset 2 with Clinton-Cataract (plus δ^{37}Cl and δ^{81}Br)

Supplementary Material for Section 5.1.3.4.2

Summary statistics

Table F4-a

Mixture 1 Sources	Lower 95% CI	Upper 95% CI	Mode	Mean
Dev-low	0.45	0.57	0.51	0.51
Dev-high	0.23	0.24	0.49	0.46
Salina-Guelph	0.00	0.03	0.00	0.01
Clinton-Cataract	0.00	0.08	0.00	0.02
Trenton-Black River	0.00	0.01	0.00	0.00
Cambrian	0.00	0.01	0.00	0.00

Table F4-b

Mixture 2 Sources	Lower 95% CI	Upper 95% CI	Mode	Mean
Dev-low	0.17	0.34	0.26	0.26
Dev-high	0.00	0.36	0.15	0.18
Salina-Guelph	0.31	0.62	0.48	0.47
Clinton-Cataract	0.00	0.06	0.01	0.02
Trenton-Black River	0.00	0.12	0.01	0.05
Cambrian	0.00	0.07	0.01	0.02

Table F4-c

Mixture 3 Sources	Lower 95% CI	Upper 95% CI	Mode	Mean
Dev-low	0.43	0.57	0.50	0.50
Dev-high	0.06	0.59	0.26	0.28
Salina-Guelph	0.00	0.09	0.04	0.05
Clinton-Cataract	0.00	0.19	0.10	0.09
Trenton-Black River	0.00	0.10	0.01	0.04
Cambrian	0.00	0.12	0.01	0.04

Table F4-d

Mixture 4 Sources	Lower 95% CI	Upper 95% CI	Mode	Mean
Dev-low	0.00	0.04	0.01	0.02
Dev-high	0.00	0.13	0.01	0.05
Salina-Guelph	0.21	0.41	0.32	0.32
Clinton-Cataract	0.00	0.21	0.03	0.09
Trenton-Black River	0.08	0.52	0.28	0.30
Cambrian	0.01	0.41	0.23	0.22

Tables F4a-d: Summary statistical information about the predicted proportions (in decimal format) of the different sources contributing to Mixtures 1-4, respectively, for Dataset 2. All end-members and isotopes are included, except δ^{13}C$_{DIC}$.

Matrix plots
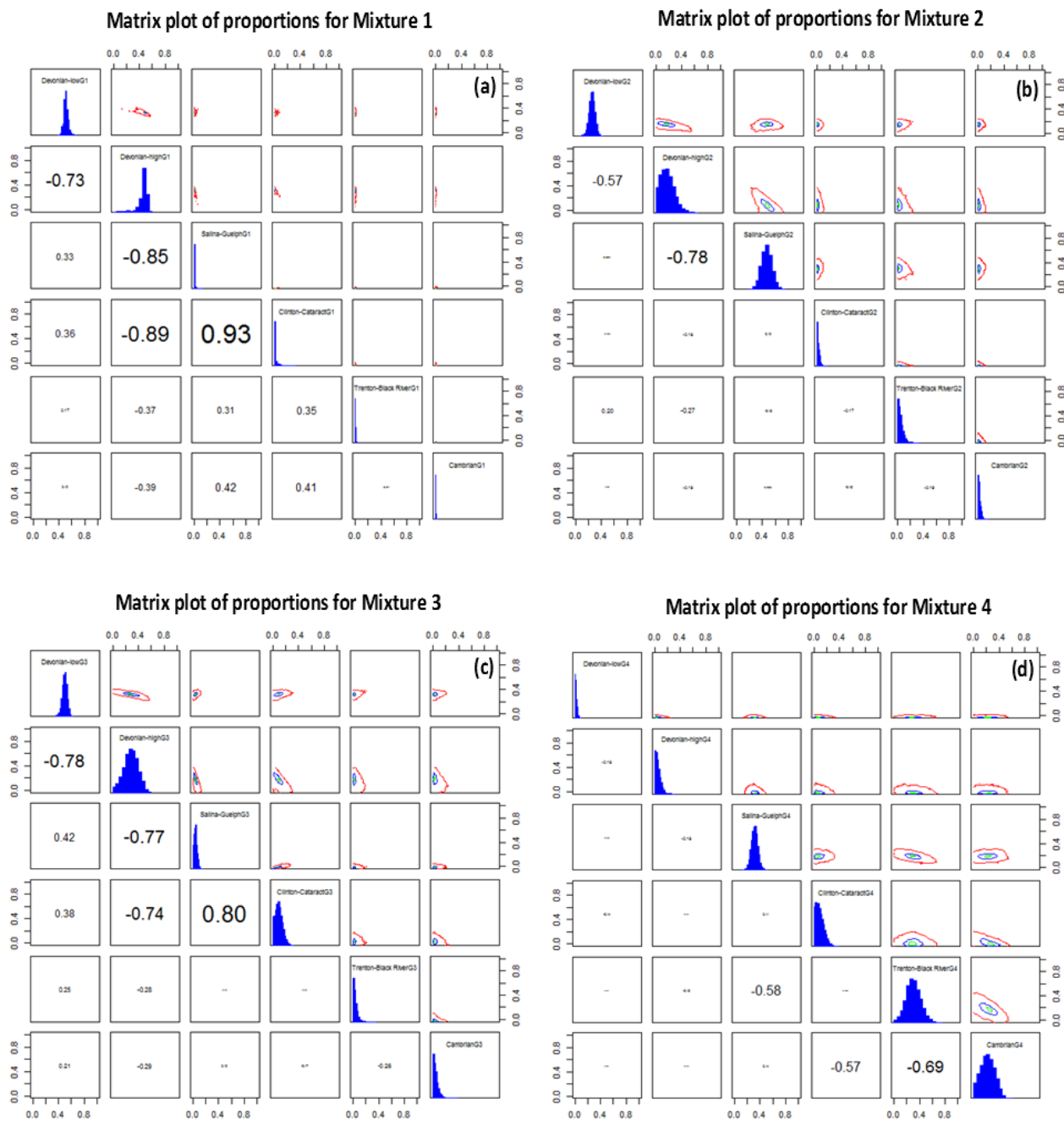
Figures F4a-d: Matrix plots for Mixtures 1-4, respectively, for Dataset 2. All end-members and isotopes are included, except $\delta^{13}C_{DIC}$.

Appendix G

Distillation experiments

Questions are commonly raised concerning the comparability of isotopic results obtained for brines using equilibration methods (corrected for salt effects) versus distillation methods. Azeotropic distillation experiments for several samples were therefore conducted to measure their hydrogen isotopic concentrations and compare those results with concentration values calculated using the salt effect correction from the activity values measured by Gas Bench equilibration (Section 3.2.1.2).

Aliquots of samples that had already been analysed using the equilibration method were distilled using a method similar to that described by Horita and Gat (1988). The apparatus is illustrated in Figure F1. Ten (10) mL of sample were measured into a 100 mL round flask, together with fifteen (15) mL of petroleum ether and an amount of Na_2CO_3 equivalent to the combined molalities of the cations that cause the salt effect (Ca^{2+}, Mg^{2+}, K^+). The Na_2CO_3 reacts with these cations, trapping them as carbonates and replacing the ions in solution with Na^{2+}. The flask was then attached to sample arm of the distillation column, which consists of a tube, closed at the top using a balloon, around which cold water is circulated. Vapour generated in the sample flask travels up into this tube, condenses, and drips down into the catchment arm below. Once the apparatus was assembled, the mixture was stirred with a magnetic stir bar for at least 2 hours to allow the reaction between the ions and the Na_2CO_3 to finish. The solution was then heated to boiling, while being stirred. The vapour cooled in the condensation column and the condensate was collected in the catchment arm, which has a spigot. A heat gun or heating tape was used to prevent condensation in parts of the apparatus other than the condensation column. Once all liquid had been distilled, the water and petroleum ether were then allowed to separate in the catchment arm, with the ether floating on top. The water was then decanted and analyzed in the same manner as the other samples.

Average δ^2H concentration values measured by this method are compared in Table F1 to those calculated from activity values. Overall, the results show very good agreement between the two methods, although variability between duplicates (having been distilled separately) is higher than the analytical error. This likely reflects difficulties with the distillation technique employed, such as incomplete extraction of water from the carbonate material in the sample flask, or failure to ensure complete recovery of water vapour or condensation from all parts of the apparatus.

Sample ID	Calculated $\delta^2H_{conc.}$	Measured $\delta^2H_{conc.}$	n
T012150(D)	−90.0	−92.0 ± 4.3	3
T012150(G)	−33.5	−31.1 ± 5.5	4
T007369(2)	−24.0	−25.0 ± 6.2	4
T007330	−19.9	−22.5 ± 3.2	2
T007583	−38.3	−40.5 ± 2.0	2
T009859	−26.8	−24.5	1

Table G1: Hydrogen isotope concentration values calculated from activity values using the salt effect correction, compared with the average isotopic compositions measured for distilled samples (n = number of duplicates). All values are in ‰ VSMOW.
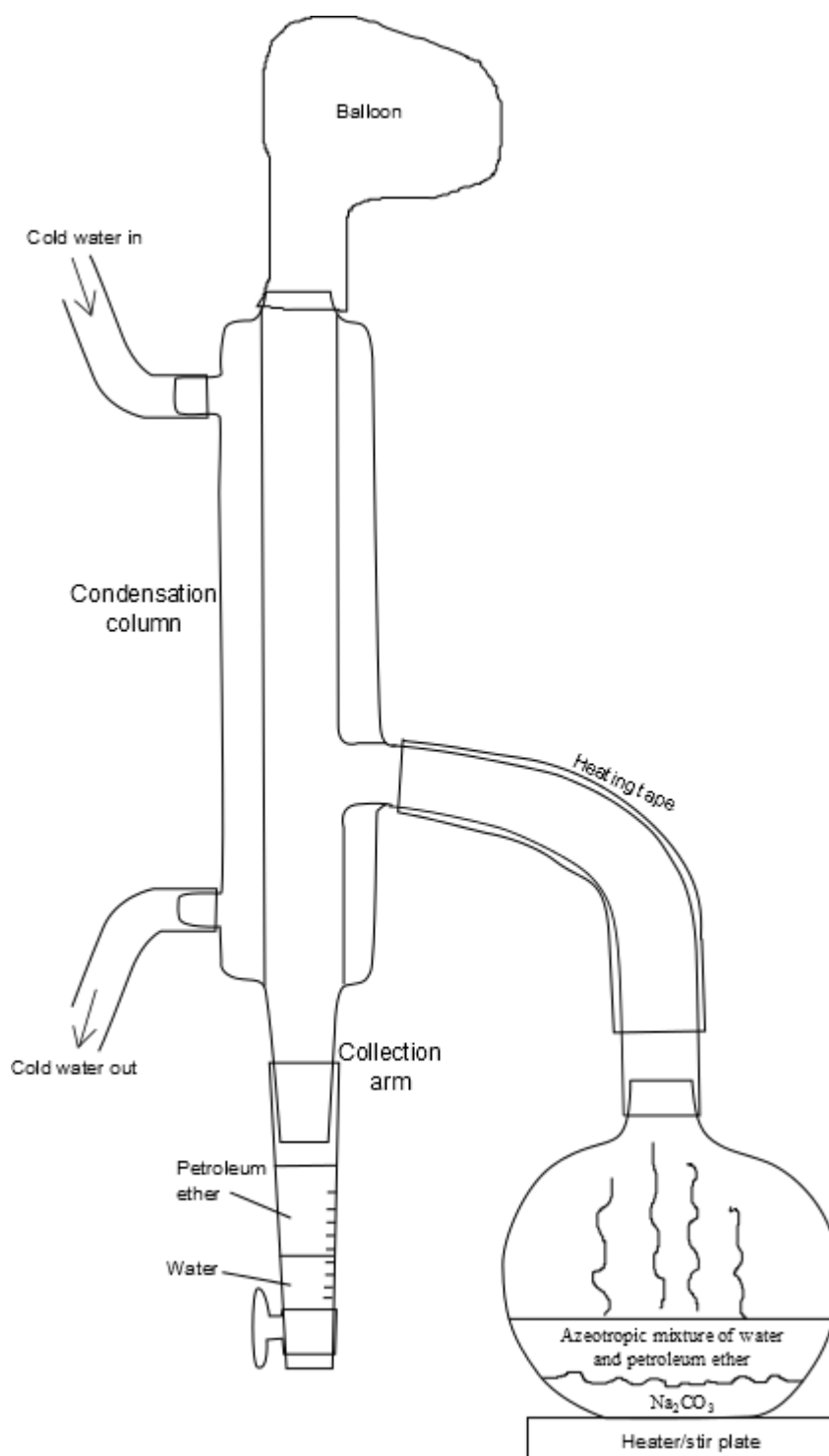
Figure F1: Distillation apparatus.

Curriculum Vitae

Name: Mitchell Skuce

Post-secondary Education and Degrees: Queen's University
Kingston, Ontario, Canada
2007-2011 H.B.Sc. in Environmental Geology

The University of Western Ontario
London, Ontario, Canada
2011-2014 M.Sc. in Geology

Honours and Awards: Queen Elizabeth II Graduate Scholarship in Science and Technology (QEIIGSST)
2012-2013

Related Work Experience   Geology Summer Student
Oil, Gas, Salt Resources Library
2012

Teaching Assistant
The University of Western Ontario
2011-2012

Research Assistant
Queen's Facility for Isotope Research
2010-2011

Publications & Abstracts

Skuce M., Longstaffe F., Potter J., Carter T. (2014) Development of a geochemical tool for sourcing leaking well fluids in southwestern Ontario. Canadian Society of Petroleum Geologists, Geoconvention 2014: Focus, Calgary, Alberta, Canada.

Skuce M., Longstaffe F., Potter J., Carter T. (2013) Identification of leaking wellbore fluids from the geochemistry of deep formation waters and natural gases, southwestern Ontario. Advances in Earth Sciences Research Conference, London, Ontario, Canada.

Skuce M., Longstaffe F., Potter J., Carter T. (2012) Identification of leaking wellbore fluids from the geochemistry of deep formation waters and natural gases, southwestern Ontario. International Association of Hydrogeologists, Niagara Falls, Ontario, Canada.

Skuce M. (2011) Characterization of nickel speciation in soils near Kalgoorlie, Australia. B.Sc. thesis, Queen's University, Kingston, Ontario, Canada.